Expansion Microscopy for the Interrogation of Nanoscale Features in Complex Biological Systems

Tyler Joseph Chozinski

A dissertation
submitted in partial fulfillment of the
requirements for the degree of

Doctor of Philosophy

University of Washington
2018

Reading Committee:
Dr. Joshua C. Vaughan, Chair
Dr. Bo Zhang
Dr. Dan Fu

Program Authorized to Offer Degree:
Chemistry

University of Washington

Abstract

Expansion Microscopy for the Interrogation of Nanoscale Features in Complex Biological Systems

Tyler Joseph Chozinski

Chair of the Supervisory Committee:
Professor Joshua C. Vaughan
Departments of Chemistry and Physiology & Biophysics

Super-resolution fluorescence microscopy enables researchers to directly observe details of biological systems on the nanoscale. However, current methods are often costly, require considerable skill, and necessitate the use of specialized instrumentation, all of which have limited the widespread use of super-resolution techniques. Expansion microscopy, which physically enlarges the specimen and enables ~65 nm resolution using standard confocal microscopy, is an inexpensive and easy-to-implement compliment to current super-resolution imaging modalities. Due to its low barrier of entry and ability to resolve nanoscale features with standard microscopes, it has the potential to find use in a broad range of biological research areas. Here, I discuss the development, validation, and optimization of new expansion microscopy protocols for various biological specimens including those which have previously been incompatible with this method. Additionally, I demonstrate applications in *Drosophila* neurobiology as well as mouse and human nephrology.

Table of Contents

List of Figures, Tables, and Video Captions

Acknowledgements

Over the last five years here at UW, I've experienced many of the highs and lows of scientific research. I know the unique feeling of accomplishment gained after taking an idea from a crude drawing on a white board to being featured on the cover of a major research journal. I also know the frustration of being unable to get a crucial set of experiments to work for weeks on end. Outside of lab I've also experienced major rearrangements in my personal life, both good and bad. Regardless of where any of these events have taken place, I've been fortunate enough to have a fantastic group of friends and family to support me in tough times and to share my joy when things work out. I'd like to take the next few paragraphs to recognize and thank some of the individuals who have helped shape me into the person and scientist that I am today.

Josh Vaughan is a fantastic mentor and a tremendous scientist. I don't think I've ever met someone with his breadth of knowledge. When looking for graduate programs and visiting UW, I spoke with Josh about some of my undergraduate research and within five minutes I think he knew more about what I was doing than I did. He is incredibly involved in the lab, extremely patient, and an amazing teacher. Josh's dedication to his students is unmatched. Not only does he give us every opportunity to succeed, he offers help wherever he can and pushes us to be our best to ensure that we *do* succeed. I recall speaking to my undergraduate professors about the possibility of joining a first-year professor and hearing their concerns: "Your success will be tied to his! You'll have a great deal more responsibility as his first student! You'll be his guinea pig!" Well, they were right. My success was tied to his and Josh has been *extremely* successful here at UW. I did have much more responsibility than I would have if I had joined a more established lab and I'm a better scientist for it. And I'm glad I was a guinea pig because I got to help launch a fantastic research laboratory while learning directly from an expert. Josh, I'm proud to be the first student to graduate from your lab and I can't wait to see what the Vaughan lab accomplishes in the future.

Aaron Halpern is a postdoctoral researcher that joined the group soon after it started and has been a fantastic mentor to everyone in the Vaughan lab. I've learned a tremendous amount from Aaron and I can say with 100% certainty that I would not be where I am today without him. For the last 5 years, I've had the pleasure of collaborating on projects with him, sharing ideas for future work, and—on Fridays—watching YouTube videos about bootleg fireworks and leprechauns in Mobile, Alabama. Aaron is like a big brother to everyone in the lab and is indispensable in keeping the lab up and running, both in terms of research and in day-to-day operation. Aaron, I sincerely thank you for your help and I hope that all of your future jobs will meet your one requirement of work attire being a t-shirt and jeans.

Lauren Gagnon is another graduate student who joined Josh in his first year at UW and has been a great friend and coworker over the years. On our first day of setting up the lab, Josh had Lauren and I step into an empty shipping container so that he could take a photo captioned, "My graduate students have arrived!" I'm very thankful I wasn't alone for that picture and that I haven't been alone in being an "old" student in the lab. I vividly remember working with Lauren to order lab equipment and supplies, learning about aligning lasers, and assembling a step stool that Josh fell from after stepping on it before it was complete (we tried to warn him, but he was too fast). Lauren was also instrumental in both super-resolution microscopy workshops we

hosted and they would not have been remotely possible without her efforts and organizational skills.

I'd also like to thank the other current and former members of the Vaughan lab: Marco Howard, Min Yen Lee, Honglin Lee, Danying Lin, Hyeon-Jin Kim, Jonathan Perr, Ethan Vo, Sarah Parkhurst, Grant Tremel, Marcus Woodworth, and Chenyi Mao. I would be remiss if I did not recognize the labs of Dr. Rachel Wong, Dr. Stuart Shankland, Dr. Behzad Najafian, Dr. Charles Alpers, Dr. Linda Wordeman, and Dr. Jay Parrish for their help in various research projects. Additionally, I'd like to thank the staff of the Chemistry Department as well as Dr. Wai Pang Chan at the UW Biology Imaging Facility. My research would not have been possible without any of you and I thank you for all your help!

To Mark and Ricky: Hello there! These two have been some of my best friends since we were all in kindergarten. Although we all moved away from one another after high school and haven't been able to get together much in person, being able to talk with them each week, play games online, and forget about everything else has been incredibly therapeutic. Being able to find mutual free time to play games together was a surprise to be sure, but a welcome one. I look forward to many more years of friendship (and stupid jokes) with both of you.

My big sister Brittany is one of the smartest people I know and I'm finally ready to admit it. I honestly don't know how many degrees she has at this point, but I know she's been outsmarting me ever since I came home from the hospital 26 years ago. Although we fought a lot when we were younger, we've since grown much closer and have been through quite a bit together. Britt, from now on, I insist that we only greet each other with "Doctor". Thank you for all your help throughout the years. I love you!

Mom and Dad, there aren't enough pages for me to write how thankful I am to the both of you. You worked your hardest to ensure that Brittany and I grew up to be the best possible version of ourselves and I hope I can use the lessons you've taught me and give the same to my children (no grandkids yet, Mom, calm down). You're both always there when we need you most and I really don't know how you were able to raise both me and Brittany and stay sane. I love you both and I owe everything to you two. Thank you and I love you both!

I'd also like to thank Caitlin Eichberg for her patience as well as everything else she has done for me. I never imagined that I'd be lucky enough to be with someone so beautiful, loving, funny, and kind as you. Caitlin, I don't think either of us expected to come into each other's lives and make such a big impact so suddenly, but I'm incredibly happy we met when we did. I tried to hide my weirdness from you at first, but I quickly found out that 1) I couldn't and 2) I didn't need to because you appreciate the same odd things in life that I do (except Star Wars, but that's okay, I still love you). I can't thank you enough for all you've done for me. I love you and I look forward to the coming years I get to spend with you.

Last but not least, I'd like to thank all scientists that have come before me. My work would not be possible without theirs and I am surely standing on their shoulders today.

Chapter 1

Introduction

1.1 Thesis Structure

This thesis is organized into 4 major chapters. The first of these is a brief introduction to super-resolution microscopy followed by a general overview of expansion microscopy, the main subject of this work, as well as considerations for the development of new expansion procedures. Chapters 2-4 are composed of my major research publications along with detailed protocols at the end of each chapter. Not included in this thesis are a review I co-authored at the start of my graduate research (which has been cited 40 times as of May 16, 2018)[1] as well as a research article in which I played a relatively minor role.[2]

1.2 A Brief Overview of Super-Resolution Microscopy

When speaking about the mysteries of life such as the central dogma of biology and the workings of the cellular machinery involved, world-renowned physicist Richard Feynman was quoted as saying, *"It is very easy to answer many of these fundamental biological questions; you just look at the thing!"* Dr. Feynman's assessment has since held true and is evident in many facets of biological research. Optical microscopy has allowed researchers to directly observe structural organization and processes inside fixed and living specimens, and with the ability to specifically label molecules of interest, fluorescence microscopy has become a workhorse tool in the life sciences. Although extremely powerful, optical microscopy is limited to a resolution of ~250 nm laterally and ~500 nm axially due to the diffraction of light, and structures that are spaced closer than these distances appear blurred together. Because many interesting and important biological processes take place below these length scales, there is a considerable effort to circumvent this so-called diffraction limit. Techniques such as electron microscopy (EM) and atomic force microscopy (AFM) are not beholden to the diffraction limits of light and can achieve <10 nm resolution. However, these methods are rarely compatible with living specimens, are primarily limited to imaging surface features or extremely thin sample sections, and have a poor

ability to report on spatial distributions of molecules of interest. Recently, several super-resolution fluorescence microscopy methods (the subject of the 2014 Nobel Prize in Chemistry[3–5]) have been developed and combine the best of both imaging worlds: molecular specificity and nanoscale resolution.

1.2.1 Stimulated Emission Depletion (STED) Microscopy

STED microscopy is a point-scanning super-resolution imaging method that uses non-linear optical processes for resolution enhancement. Similar to confocal microscopy, an excitation beam is focused to a diffraction limited volume to excite fluorophores decorating the sample. An additional beam shaped like an annulus, called the depletion or STED beam, encircles the excitation beam and is red-shifted with respect to the fluorescence detection band. This beam stimulates the emission of light from excited state molecules in a diffraction limited volume and at saturating intensities only allows fluorophores near the center of the annulus (which has an intensity of zero) to emit at the fluorescence detection wavelength. This process effectively shrinks the excitation point spread function (PSF) to a size well below the diffraction limit and routinely enables 30-70 nm resolution (**Figure 1.1**).[6–8]

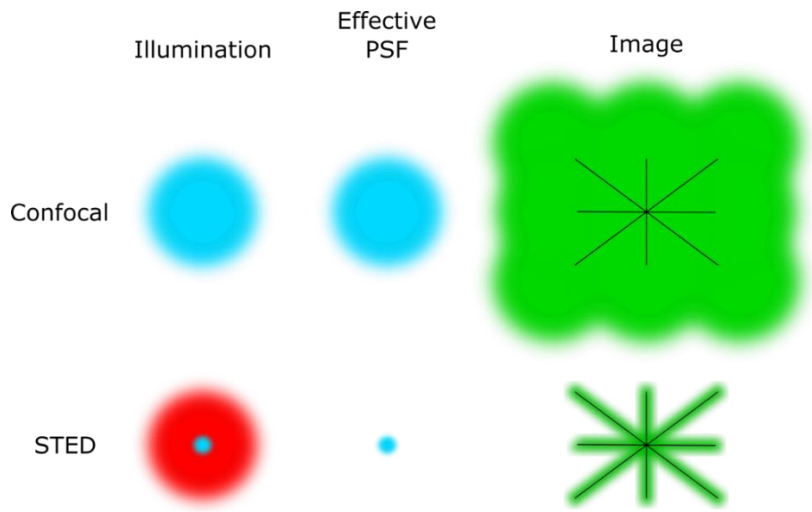

Figure 1.1 | Stimulated Emission Depletion (STED) microscopy is a point scanning imaging method analogous to confocal microscopy. However, unlike confocal microscopy, whose resolution is limited to ~250 nm, STED microscopy uses a depletion beam (red) that surrounds the excitation beam (blue) to shrink the effective excitation PSF and achieve 30-70 nm resolution.

In the initial reports, multicolor STED imaging used multiple pairs of excitation and depletions lasers, which added to the technique's complexity and sometimes caused color channel misalignment due to the slight spatial variations in the STED beams.[9,10] However, by using two dyes with partially overlapping emission spectra (emission maxima at 620 nm and 670 nm) combined with 50 ns time-gated detection in each channel, Göttfert *et al.*[9] were able to achieve two-color, offset-free STED imaging with one depletion laser (775 nm) and resolved the eightfold symmetry of the xenopus nuclear pore complex, which is composed of a ring of eight 20-40 nm homodimers and an 80 nm central nucleoporin. Additionally, because the effective PSF size shrinks as the depletion beam intensity is raised, the researchers were also able to monitor the diffusion of a single fluorescently labeled lipid through a living cell's membrane with 20 nm resolution.[9]

1.2.2 Single Molecule Localization Microscopy (SMLM)

SMLM, sometimes referred to as stochastic optical reconstruction microscopy (STORM) or photoactivated localization microscopy (PALM), uses extremely sensitive cameras to detect the positions of individual fluorophores decorating a sample with an uncertainty 1-2 orders of magnitude smaller than the diffraction limit. Subsets of fluorophores are continuously and stochastically cycled between "on" and "off" states using photochemistry[11–13] until all probes have been imaged or bleached. The precisely determined locations of each molecule (often obtained by fitting single-molecule images with multidimensional Gaussian functions) are then used to reconstruct a super-resolution image (similar to pointillism) with a typical resolution of ~20-50 nm (**Figure 1.2**).[14–17]

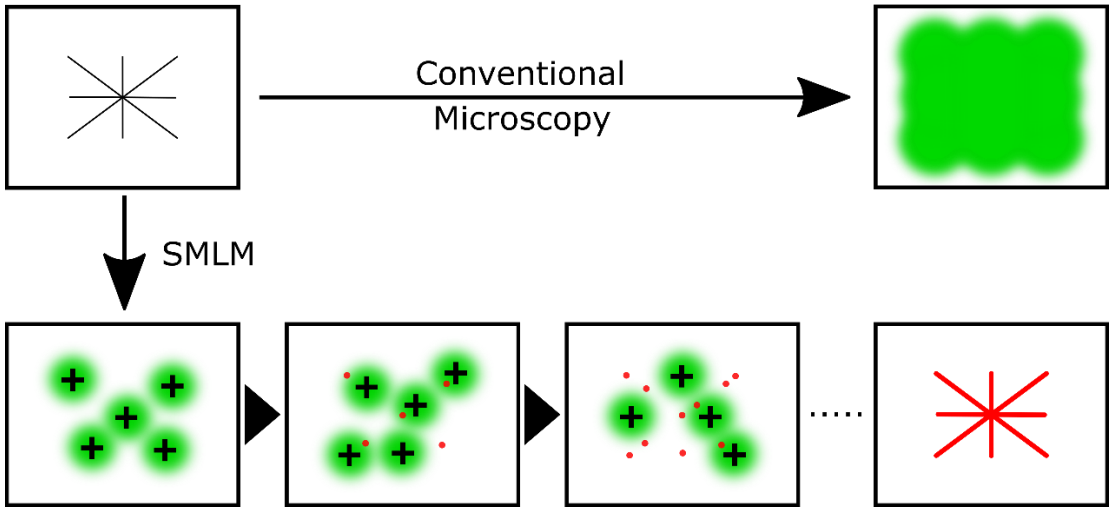

Figure 1.2 | Single Molecule Localization Microscopy (SMLM) uses sequential activation, detection, localization, and deactivation of individual fluorophores in a stochastic manner to achieve ~20 nm resolution. Molecules are localized (black crosses), compiled (red dots), and used to reconstruct a final super-resolution image (red asterisk).

SMLM is typically limited to imaging thin sections because it often uses total internal reflection (TIR) illumination to reduce background fluorescence and increase the signal-to-noise ratio. However, large volumetric images can be obtained by physically sectioning the specimen and imaging thin slices sequentially. Sigal *et al.*[18] employed this method in visualizing mouse retinal neurons with image volumes on the order of 10^5 μm^3 and ~20 nm lateral resolution. Furthermore, by sequentially imaging ultrathin (70 nm thick) tissue sections, they achieved a consistent axial resolution of 140 nm (twice the section thickness due to Nyquist sampling) throughout the reconstructed sample volume. The researchers then leveraged the molecular specificity afforded by multicolor fluorescence imaging to computationally segment image volumes to identify neurons as well as pre- and postsynaptic markers. This allowed them to map the spatial organization of neurons including the molecular identity of their synaptic connections on the nanoscale. The use of SMLM and ultrathin sectioning enabled more accurate assignment of synapses to the correct neurons compared to conventional diffraction-limited imaging, which was shown to often misidentify neuron-synapse relationships due to its lack of spatial resolution. This work demonstrates of the power of SMLM to interrogate the nanoscale, volumetric organization of biological specimens; however, with the technical challenges of SMLM, as well as

an image acquisition time of ~3 weeks (under constant imaging), this method is clearly limited to specialists in the super-resolution microscopy field.[18]

1.2.3 Structured Illumination Microscopy (SIM)

Although not included as part of the 2014 Nobel Prize in Chemistry, SIM has become a popular technique in the field of super-resolution imaging. In SIM, a fluorescently labeled sample is illuminated with a sinusoidal striped pattern of light that resembles a barcode with lines spaced ~230 nm apart. The phase and angle of the pattern are then varied and interference patterns, or moiré fringes, caused by the superposition of the illumination pattern with the sample are observed and recorded. Because the illumination pattern is known, previously unobservable frequencies can be extracted from the computational analysis of moiré fringes in a series of images in order to achieve a two-fold increase in spatial resolution (**Figure 1.3**).[19–21] Since SIM relies on illumination patterns for resolution enhancement as opposed to dye photophysics, multicolor imaging is straightforward and essentially the only limitation regarding fluorescent labels is that they are photostable. However, by incorporating photoswitching probes[22] or non-linear saturated excitation[23], SIM can theoretically achieve diffraction-unlimited resolution.

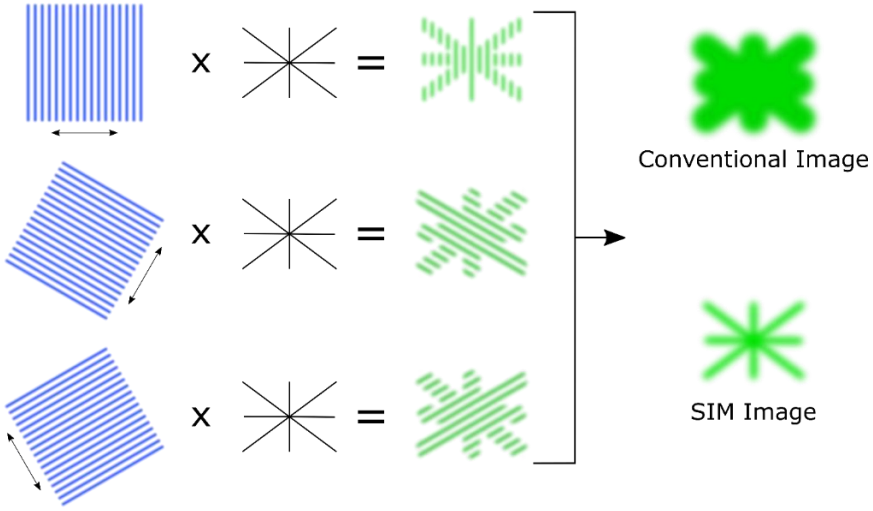

Figure 1.3 | Structured Illumination Microscopy (SIM) uses striped patterned illumination that is rotated and phase-shifted such that the convolution of the illumination pattern (blue lines) with the fluorescently labeled sample (black asterisk) creates moiré fringes that contain high

frequency information that is used to algorithmically double the resolution of an optical microscope.

Because SIM does not require the use of high-intensity illumination and is relatively non-invasive, it is well-suited for imaging fast biological processes in living specimens. For instance, Nixon-Abell *et al.*[24] imaged endoplasmic reticulum (ER) dynamics in COS-7 cells at 40 Hz with ~100 nm resolution and found that the sheet-like structures that appeared continuous in standard microscopy images actually contained many small, highly dynamic holes. Using other super-resolution techniques in addition to SIM, they found that the peripheral ER, which also appears to contain numerous sheet-like domains in diffraction-limited imaging, is actually composed of dense tubular ER matrices. The authors were also able to localize ER-shaping proteins to these areas of dense tubular networks and confirmed that these nanoscale phenotypes were present in a range of different cell types.[24]

1.2.4 Challenges with Current Methodologies

Although extremely powerful, each of the above methods suffers from certain limitations. Multicolor imaging with both SMLM and STED, while possible, is difficult due to the stringent requirements of the dyes used in each technique.[25–28] The high light intensities used in SMLM and STED also hamper their applicability to live cell imaging due to phototoxicity, although it has been successfully demonstrated.[29,30] Additionally, SMLM typically requires TIR, or near TIR, illumination which makes large-scale volumetric imaging problematic.[31,32] Both STED and SIM are in principle capable of imaging at large depths, but often suffer from spherical aberrations that arise from refractive index mismatch (due to the use of oil immersion objectives with water-based samples)[33] and subsequent reconstruction artifacts[34] if the point spread functions are not well-preserved throughout the sample. Perhaps the greatest limitation of these techniques, however, is their limited accessibility to users. Commercial super-resolution instruments, which are unavailable at many research institutions, often exceed hundreds of thousands of dollars in cost, and although homebuilt microscopes can be constructed for 25-50% of the cost of commercial microscopes, the option is not viable for most potential users. Beyond gaining access, the use of these instruments requires a considerable amount of training for successful operation,

which further alienates non-specialists. With the popularity of super-resolution microscopy steadily growing faster, there is a strong unmet need for simple, cost-effective nanoscale imaging.

1.3 Expansion Microscopy (ExM)

1.3.1 A Brief Summary of ExM

In 2015, the Boyden lab at MIT published a method called expansion microscopy (ExM) capable of achieving ~65 nm lateral resolution using standard confocal microscopy by physically expanding a biological specimen isotropically in all dimensions.[35] In this initial version of ExM, a sample is first immunostained with antibodies conjugated to DNA molecules which are doubly modified with a fluorophore and an acrydite group (**Figure 1.4**). The sample is then embedded in an acrylamide-based hydrogel (which covalently incorporates the fluorescently modified DNA molecules into the polymer through the acrydite moiety) and then homogenized via enzymatic digestion with a broad-spectrum protease to degrade rigid structures that would otherwise resist expansion. The polymer is then expanded four-fold in each dimension via dialysis in deionized water and the effect is an effective shrinking of the PSF of a conventional microscope relative to the sample size which thereby enables features that were once smaller than the diffraction limit to be resolved in the post-expansion state (**Figure 1.4**). Additionally, the expanded sample is rendered optically transparent with a refractive index nearly identical to that of water, and with the use of water immersion objectives, aberrations due to refractive index mismatch are easily avoided. Because it made sub-diffraction-limit resolution attainable with microscopes that most researchers readily have access to (i.e. confocal and epifluorescence microscopes), this work represents a forward leap in making super-resolution fluorescence microscopy a standard technique available to a broad range of researchers.

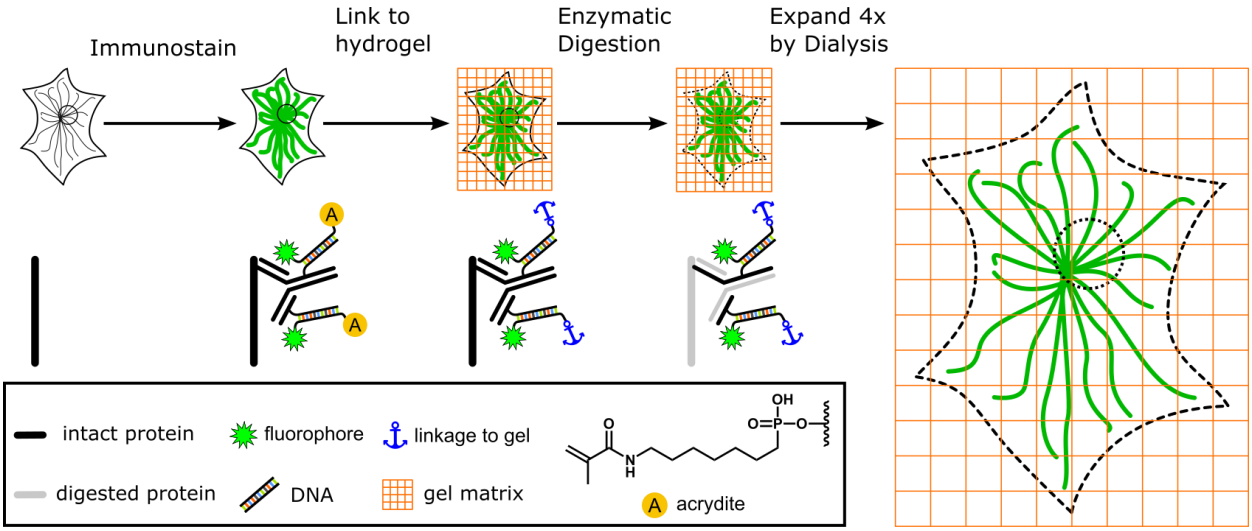

Figure 1.4 | Expansion Microscopy (ExM), in its initial form, used antibodies modified with DNA strands labeled at opposite ends with an acrydite moiety and a fluorophore. After immunostaining, a swellable acrylamide-based hydrogel is grown throughout the sample which covalently links the fluorophores to the hydrogel through the acrydite moiety (which resembles acrylamide). The sample is then enzymatically digested with proteinase K in order to degrade rigid structures that resist expansion. Four-fold expansion in each dimension is then achieved by dialysis in deionized water.

1.3.2 Mechanism of Hydrogel Expansion

The power of ExM comes from the swellable nature of the hydrogel polymer, which has been extensively studied. It has been shown that polymers containing ionically charged monomer subunits can swell and contract in a controllable manner with the addition of water and salt, respectively.[36,37] Additionally, the amount of expansion can be controlled by the amount of salt or water in the solvent as well as the degree of cross-linking inside the polymer network. The mechanism by which ionic hydrogels expand is complex, but the simplest theory is via osmotic pressure.[38] In ExM, the hydrogel is composed of the monomers acrylamide and sodium acrylate as well as a bis-acrylamide crosslinker. In the unexpanded state, the salt concentration inside the gel is high due to the gel's small volume and sodium acrylate residues. When placed in deionized water, the osmotic pressure due to the salt concentration difference between the polymer network and the solvent causes an influx of water into the gel. The ion-dipole interactions between the water molecules and the acrylate monomers further facilitates water absorption.

As water is absorbed, the polymer chains reorient themselves, their random coiled configurations are disrupted, and as the gel gets larger, the osmotic pressure decreases. The gel reaches equilibrium (and maximum expansion) once the force of extension from osmotic pressure is equal to the force of retraction exhibited by the cross-linkers (which prevent infinite expansion). It is important to note that the gel remains electrically neutral and sodium cations freely diffuse throughout the gel. Because of this, repelling forces from adjacent acrylate monomers can slightly contribute to the force of extension; however, osmotic pressure is the key driving force for expansion (**Figure 1.5**).

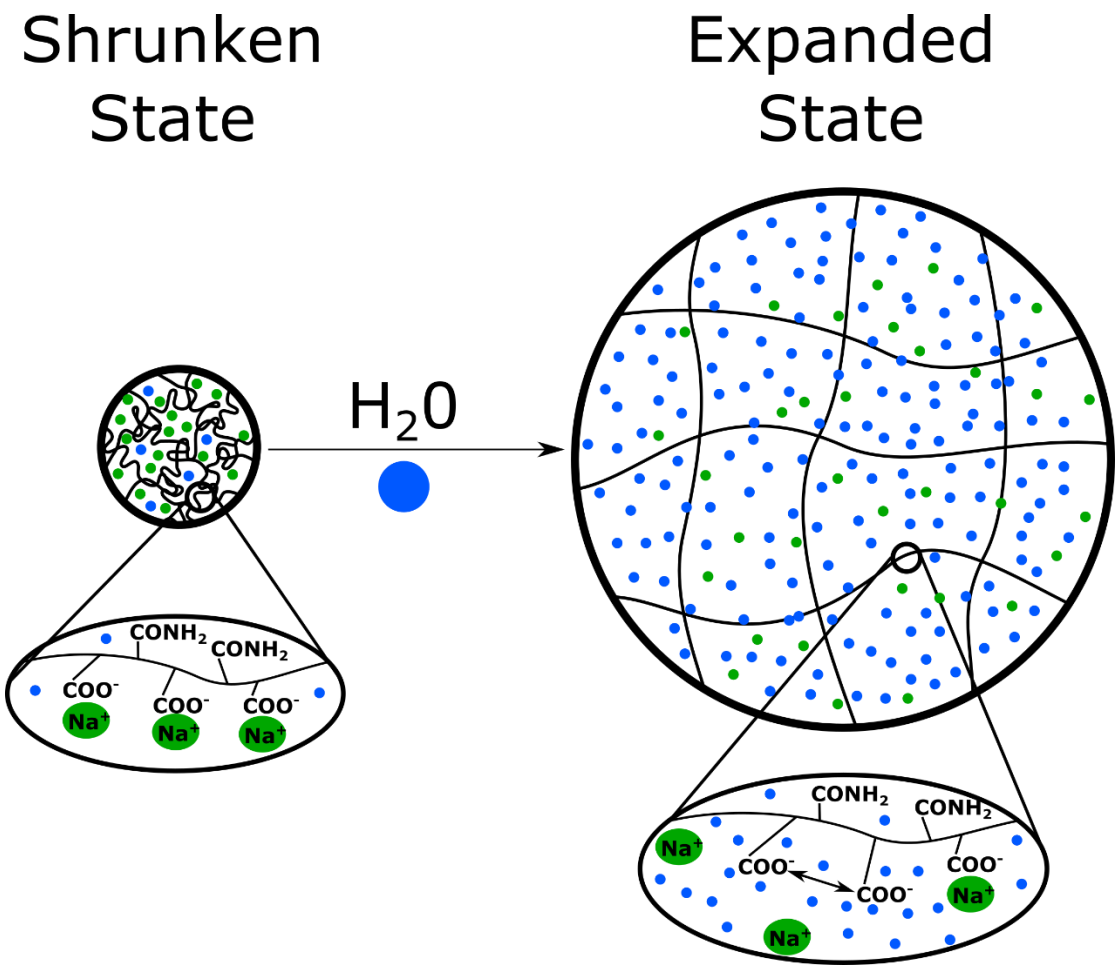

Figure 1.5 | A highly coiled and contracted polymer network composed of acrylamide and sodium acrylate monomers expands when exposed to water due to osmotic pressure and to a lesser extent, repulsive forces between adjacent anionic residues (double-headed arrow in second zoom).

1.3.3 Challenges with the Initial ExM Method

Although revolutionary in the field of super-resolution microscopy due to its unique approach to resolving nanoscale features, the first iteration of ExM faced several technical challenges. First, the custom DNA-modified antibodies used for immunostaining biological samples are not commercially available, which requires researchers to synthesize their own using a multistep protocol and expensive reagents.[35] Additionally, due to the substantial charge and large size of the DNA molecules (~6,000 g mol^{-1}), a limited number of oligonucleotides can be conjugated to an antibody before it loses its capacity to bind antigens. These DNA-modified antibodies produce considerably dimmer stains compared to standard fluorescently labeled antibodies modified with small molecule organic dyes (~600 g mol^{-1}) which can accommodate more fluorophores per protein before having their binding ability compromised. This lack of fluorescence signal is further exacerbated by the dilution of fluorescence signal caused by expansion (see **Chapter 2**).

The initial expansion protocol was also limited to a subset of fluorophores due to chemical bleaching caused by radicals produced during hydrogel polymerization. For example, cyanine dyes such as Alexa 647, a common choice in fluorescence microscopy, are non-fluorescent after polymerization and are incompatible with the original expansion protocol.[35] Furthermore, genetically expressed fluorescent proteins, which offer an advantage when labeling targets that are challenging to immunostain, are not retained in the expanded sample using the DNA method discussed above (see **Chapter 2**).

Additionally, the digestion step of the original protocol, which uses proteinase K as the only digestion enzyme, limits its application to a small number of sample types.[35] This first iteration of ExM demonstrated robust expansion of cultured cells and brain tissue, specimens that were sufficiently digested using only proteinase K. Although proteinase K is a broad-spectrum protease, it is ineffective at digesting extracellular matrix proteins (e.g. collagen, elastin, etc.) and has no effect on polysaccharides such as chitin.[39–41] Therefore, enzymatic digestion of specimens with a high abundance of these materials[41,42] using only proteinase K is insufficient and causes large structural distortions upon expansion (see **Chapters 3** and **4**).

1.3.4 Parallel Development of ExM and Recent Advances

Since the initial ExM publication, several significant advancements in specimen expansion have been developed (in addition to the methods developed by our own lab which are discussed in the following chapters) and their utility in solving various biological problems has been demonstrated. An alternative protocol termed magnified analysis of the proteome (MAP) leverages the effects of high concentrations of acrylamide monomer in the sample fixation solution as well as heat and detergent in place of the enzymatic digestion to isotropically expand specimens while preserving most antigenicity in the sample, thereby enabling multiple rounds of immunostaining even after expansion.[43] The resolution of ExM has also been enhanced by increasing the expansion factor of the hydrogel. The most extreme instance, iterative ExM (iExM), involves first embedding the sample in a swellable polyelectrolyte hydrogel that contains chemically cleavable crosslinkers. The sample is then homogenized and expanded, a new polymer network is formed throughout the first, the initial gel is dissolved, and the newly formed polymer is expanded for an overall expansion of ~16-22× to achieve ~25 nm resolution.[44] Hardware-based super-resolution imaging methods can also be combined with ExM for increased resolution and has been implemented using SIM (due to its compatibility with a broad range of fluorophores) to achieve ~35 nm resolution.[2,45] Spatial transcriptomics has also benefited from ExM by enabling the detection of RNAs clustered in high densities at nanoscale resolution.[46,47] From this partial review of recent developments in ExM, it is evident that this field of study is advancing at a considerable pace, and it is thus necessary to clearly define metrics and considerations that will enable successful, widespread dissemination of reliable techniques.

1.4 Considerations for Expansion Microscopy Development

Because ExM is a newly introduced technique that will continue to rapidly evolve in the coming years, it is important for researchers to keep in mind certain considerations to ensure the development and implementation of robust new protocols. Careful characterization of expansion-induced distortions, thorough protocol optimization for new sample types, and assessments of cost and difficulty will play a key role in convincing a broad range of scientists of ExM's utility.

1.4.1 Distortion Analysis

When presenting ExM to a new audience, one particular line of questioning arises quickly: "Does this process cause distortions in the sample? How do you know expansion is isotropic and that structures are preserved?" These questions are expected because the protocol entails homogenizing biological samples either by protein denaturation or enzymatic digestion, which may lead one to believe that catastrophic distortions are inevitable. In the initial report by Chen *et al.*, structural distortions were quantified by comparing images of the same area within a sample before and after expansion and determining the non-linear warping patterns need to make post-expansion images align with pre-expansion images, which are considered to be ground truth data.[35] Additionally, SIM was used for pre-expansion imaging and confocal for post-expansion imaging so that spatial resolutions before and after expansion were better matched (~110 nm and ~65 nm, respectively). As will be discussed in the next chapter, higher resolution techniques such as SMLM can be performed for pre-expansion imaging to ensure that ground truth images possess higher resolution (~25 nm) than post-expansion images obtained with a confocal microscope, thus enabling a more rigorous distortion analysis. In place of correlative imaging, approaches that analyze the size and shape of well-defined features have been used for expansion validation[45]; however, while this method is capable of detecting gross distortions in the sample, it fails to account for expansion-induced variations that may have affected the structure of interest. In order for researchers to trust the results of ExM, validation of each new method must be rigorously performed. The details of the distortion analysis can be found in each of the subsequent chapters of this dissertation.

1.4.2 Homogenization of Different Tissue Types and Method Optimization

A key step in ExM which allows expansion of biological specimens without structural distortion is sample homogenization, which disrupts the rigid components of samples that resist expansion. As discussed above and in the following chapters, samples containing large amounts of chitin (**Chapter 3**) and/or collagen (**Chapter 4**) are not compatible with the initial expansion protocol because they are resistant to proteinase K digestion. In these cases, additional enzymes or different digestion procedures must be incorporated so that low-distortion, isotropic sample

expansion is achieved. Additionally, the order with which the enzymes are introduced may affect digestion efficiency due to limited access to substrates (see **Chapters 3** and **4**). With each new sample type encountered, it is important to carefully adapt and optimize expansion procedures to ensure the development of robust methods.

In addition to choosing the proper digestion enzymes, other factors such as sample fixation and the concentration of the protein/hydrogel linker can affect the quality of expansion. These aspects of method optimization are thoroughly explored in **Chapter 2**. For example, when treated with the same concentration of protein/hydrogel linker, tissue sections fixed in paraformaldehyde (PFA) overnight expand isotropically while sections fixed in PFA for one hour exhibit gross structural distortions. However, using lower concentrations of linker allow both tissues to expand uniformly. As another example, glutaraldehyde (a common fixation agent) can be used as both a fixative and a linkage to the hydrogel when expanding cultured cells, which allows flexibility when fixation conditions are important for preserving certain epitopes for immunohistochemistry (e.g. when PFA cannot be used). With so many possibilities, it is important for researchers to perform initial quality control checks before moving on to quantitative distortion analysis. Simply by evaluating the shape of the hydrogel after expansion or by imaging simple structures such as nuclei with a low magnification objective, users can quickly and efficiently determine if their samples were expanded without obvious distortion.

1.4.3 Cost and Accessibility

In order to make ExM an attractive option for non-specialist users, the barrier to entry must be kept low, which can be done in a number of ways. By avoiding the use of specialized reagents, the financial cost of ExM can be minimized. As shown in the next chapter, off the shelf reagents and standard fluorescent probes can be used in place of the expensive and commercially unavailable DNA-modified antibodies used in the initial expansion report. In fact, by doing this, the cost per sample was reduced from ~$40[48] to ~$1.50. Other reports, such as protein-retention ExM (proExM)[49] and MAP[43], have also successfully reduced the cost per sample by a similar amount using off-the-shelf reagents and have found wide use throughout the scientific community. Although it is important, the financial cost of reagents and kits may not be the chief

concern for those considering implementing ExM in their research. The time that researchers spend familiarizing themselves with the technique is perhaps the most important expense that must be evaluated. To ensure that this cost is minimized, the ease of implementation must be taken into account when developing new variations of ExM, and by providing detailed protocols with the publication of new methods, researchers not familiar with super-resolution fluorescence microscopy will be able to quickly apply ExM to broad range of complex biological problems. Fortunately, recent publications have followed this trend with additional resources in the form of websites[48,50] and workshops[51–53].

1.5 Summary

Because of its growing popularity throughout the biological imaging community, ExM has rapidly undergone numerous modifications that have improved its performance and extended its applicability to a broad range of sample types. In the following chapters, this thesis specifically addresses the challenges and pitfalls associated with ExM that were briefly discussed above by detailing my contributions to the field through advancements in specimen/hydrogel linking strategies for improved sample brightness and inclusion of previously incompatible fluorescent probes (**Chapter 2**), protocol modification and quantitative characterization for expansion of new tissue types (**Chapters 3** and **4**), applications in biological research and clinical pathology (**Chapters 3** and **4**), and overall method simplification to promote rapid dissemination of this revolutionary new technique.

Chapter 2

Expansion Microscopy with Conventional Antibodies and Fluorescent Proteins

2.1 Preface

As discussed above, the initial report of ExM by Chen *et al.*[35] was revolutionary in the field of biological imaging because it allowed a broad range of researchers to visually interrogate nanoscale structures without the use of specialized super-resolution microscopes. However, although it obviated the need for super-resolution instrumentation and specialized training, the method possessed several issues in terms of performance and accessibility that had the potential to limit the number of users. First, the custom DNA-modified antibodies used in the study are not commercially available and are expensive and challenging to synthesize with high yield. Second, the brightness of these custom antibodies is limited due to the small number of fluorescent probes that can be conjugated to each before binding ability is lost. Third, certain small organic dyes as well as fluorescent proteins are incompatible with the initial protocol.

With these issues in mind, we set out to simplify and improve the method by finding ways to allow for the use of standard fluorescently labeled antibodies and inexpensive reagents that are commercially available to allow ExM to reach a larger number of researchers. As I will show in the following sections, two new methods of linking biological structures to the expansion hydrogel were carefully optimized and quantitatively characterized in both cultured cells and mouse brain tissue. Additionally, previously incompatible organic dyes and fluorescent proteins were successfully incorporated into the procedure with further method optimization.

I was highly involved with and contributed to all aspects of this project. A larger portion of my contribution, however, was to the optimization and characterization of the method using mouse brain tissue. The protocol for the quantitative distortion analysis of pre- and post-expansion images (**section 2.8.1**) was authored by Dr. Aaron R. Halpern, I authored the protocols

for expansion of both cultured cells (**section 2.8.2**) and brain tissue (**section 2.8.3**), and all protocols were reviewed and edited by all manuscript authors. This work was carried out in collaboration with Dr. Haruhisa Okawa (from the laboratory of Dr. Rachel O.L. Wong), who imaged a subset of expanded brain tissue samples. Supplemental figures as well as several supplemental protocols are provided in addition to the main text. This was the first research publication to come from the Vaughan lab and earned the honor of being featured on the cover of the June 2016 issue of *Nature Methods* (**section 2.2**).

This article has been cited 23 times as of May 16, 2018, was the topic of a *Nature Methods News and Views* article[54] as well as many other secondary articles in the scientific press, and was featured on the cover of the June 2016 issue of *Nature Methods*.

All material in this chapter has been reformatted to conform with the style of this thesis.

2.2 *Nature Methods* Cover (June 2016 Issue)

June 2016 | volume 13 | number 6

nature methods
www.nature.com/naturemethods
Techniques for life scientists and chemists

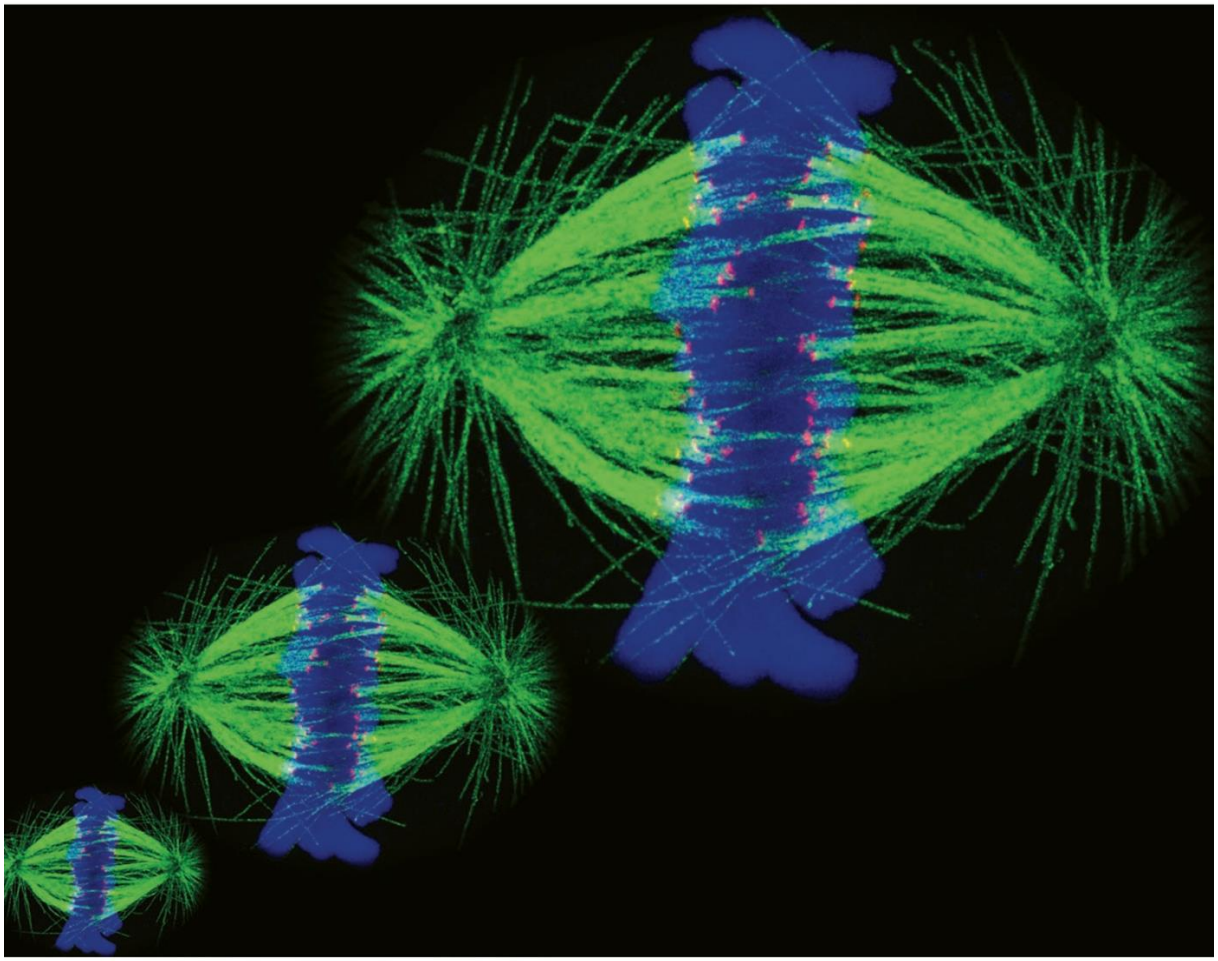

- Expansion microscopy with conventional labels
- Faster fluorescence lifetime imaging
- Efficient glycan release with bleach
- Improving CLIP
- Automated clustering of high-dimensional data

2.3 Abstract

Expansion microscopy is a technique in which fluorophores on fixed specimens are linked to a swellable polymer that is physically expanded to enable super-resolution microscopy with ordinary microscopes. We have developed and characterized new methods for linking fluorophores to the polymer that now enable expansion microscopy with conventional fluorescently-labeled antibodies and fluorescent proteins. Our methods simplify the procedure and expand the palette of compatible labels, allowing rapid dissemination of the technique.

2.4 Introduction

Boyden and coworkers recently introduced Expansion Microscopy (ExM) as a super-resolution microscopy technique that uses physical expansion of fixed specimens to allow features closer than the diffraction limit of light (~250 nm) to become resolvable in the expanded specimen.[35] Unlike other super-resolution techniques which rely on specialized instruments,[55,56] ExM is compatible with standard microscopes (e.g., widefield, confocal, etc.) and is poised to make a significant impact based on its accessibility and on its strong performance in thick specimens.

In the initial report on ExM, imaging with ~65 nm resolution was demonstrated in cultured cells and in brain tissue using a procedure entailing: staining of a specimen with polymer-linkable probes, growth of a swellable polymer within the specimen which links to the probes, protease digestion of the specimen, and expansion of the polymer through dialysis.[35] The polymer-linkable probes consisted of antibodies labeled with doubly-modified DNA oligonucleotides containing a fluorophore and a methacryloyl group designed to become covalently incorporated into the polymer. As these DNA-labeled antibodies are custom-made and require a 1-2 day multi-step protocol to prepare with expensive reagents, we sought to develop methods which would allow ExM to use standard fluorophore-labeled secondary antibodies lacking DNA. We refer to these antibodies as conventional secondary antibodies, and to their use as conventional immunostaining. We also extended our approach to allow the direct imaging of intrinsic fluorescent protein signal in ExM.

2.5 Results

2.5.1 Expansion of Cultured Cells

We initially reasoned that conventional fluorescently-labeled antibodies could potentially be used in ExM if a sufficient number of linkages could be formed between the antibodies and hydrogel so that protease-digested antibody fragments would remain linked to the hydrogel (**Fig. 2.1**). Indeed, we found that 60 min treatment of a fixed and conventionally immunostained cultured cells with a 25 mM solution of the amine-reactive small molecule MA-NHS (methacrylic acid *N*-hydroxy succinimidyl ester) conferred excellent retention of fluorescent signal after digestion and expansion (**Fig. 2.2 a-d**). Omission of the MA-NHS treatment resulted in distorted images with poor retention of fluorescence (**Supplementary Fig. 2.1**). MA-NHS was chosen here due to its resemblance to the methacryloyl group originally used in the DNA-labeled antibody probes; similar reactive groups are also established for linking of peptides or proteins to hydrogels.[57]

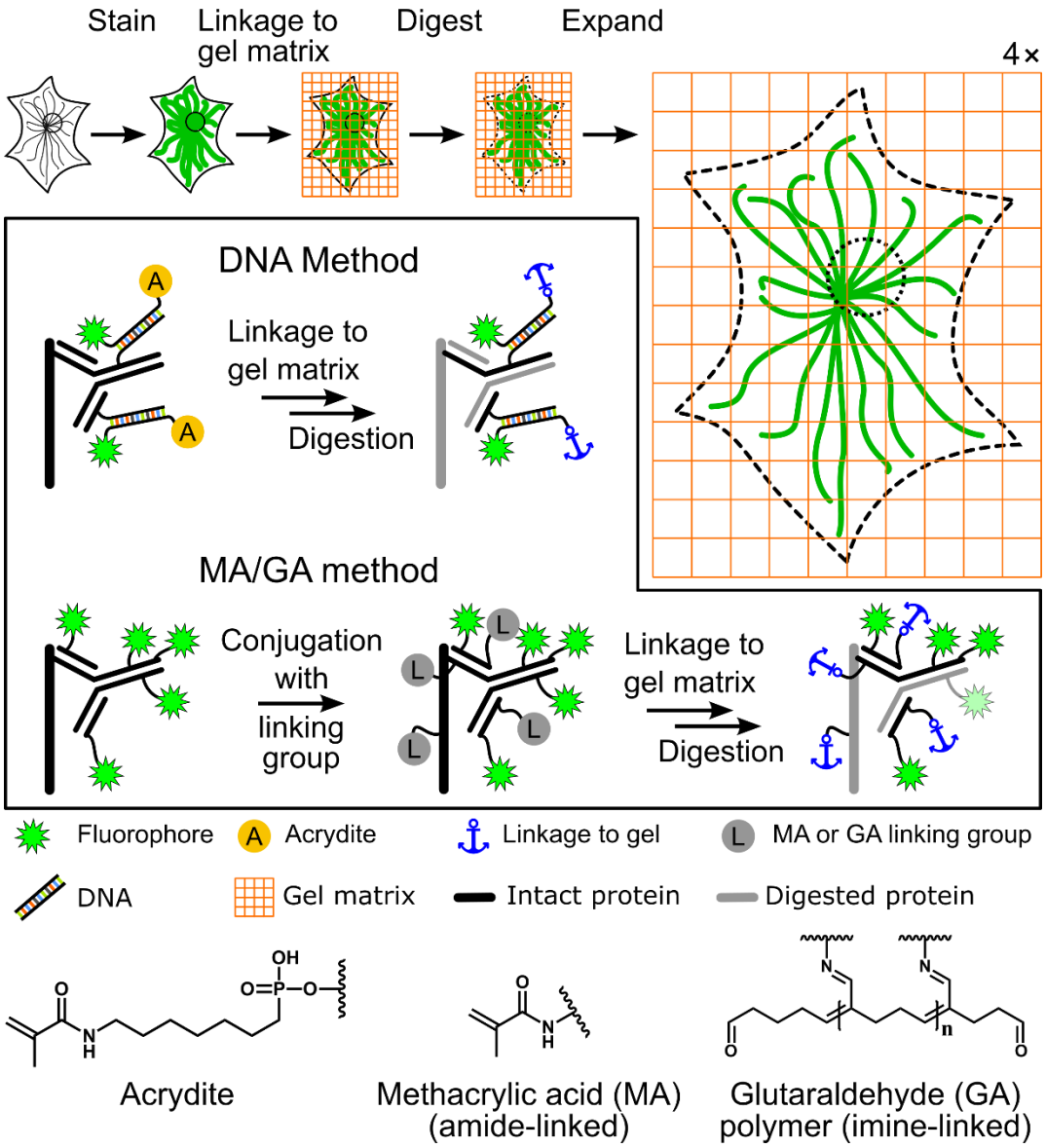

Figure 2.1 | Schematic illustration of expansion microscopy and label retention strategies. The boxed region highlights the difference between the original DNA method[35] and the post-stain linker-group functionalization method ("MA/GA method") presented in this work. In the DNA method, the specimen is immunostained with a custom-prepared antibody bearing doubly-modified DNA linked to a fluorophore and an acrydite moiety (A). In contrast, with the MA/GA method, methacrylic acid *N*-hydroxy succinimidyl ester (MA-NHS) or glutaraldehyde (GA) are used to label the entire sample with polymer-linking groups after conventional immunostaining with fluorophore-labeled antibodies (only secondary antibodies are shown). Fluorescent proteins are also retained using the MA/GA method but are not shown here for the sake of clarity.

As with the original ExM report, we observed fine details in the images of expanded specimens which were hidden in images of the unexpanded specimens (**Fig. 2.2 a-d**). The cross-sectional profile of expanded microtubules yields an average Gaussian-fitted full width at half maximum (FWHM) of 79 ± 9 nm (mean ± SD (standard deviation), **Supplementary Fig. 2.2**). This 79 nm width is consistent with a convolution of the double-peaked cross-sectional profile of indirectly immunolabeled microtubules[58,59] measured by localization microscopy (i.e., STORM, PALM, etc.)[55,56] and an estimated ~65 nm expansion-corrected lateral spatial resolution. The uniformity of expansion is remarkably good across the sample, and an analysis of distortions between corresponding pre-expansion and post-expansion images recorded by confocal microscopy showed that distortions were generally below 100 nm (root mean square distance) over length scales of up to 30 μm (**Supplementary Fig. 2.3**). A comparison of expansion fidelity using DNA-labeled secondary antibodies also yielded similar results (**Supplementary Fig. 2.4**). Note that all distances and scale bars for expanded specimens in this report have been divided by their respective, measured expansion factors of 4-4.2 and that all distances and scale bars therefore refer to pre-expansion dimensions.

In a second approach, we found that treatment of conventionally immunostained cultured cells with glutaraldehyde (GA) also yielded excellent fluorescence retention after digestion (**Supplementary Fig. 2.1**). Although GA post-fixation is a commonly used procedure in immunofluorescence assays, GA crosslinking is also well-known for use in linking proteins or enzymes to polyacrylamide gels.[60] Correlated pre-expansion localization microscopy and post-expansion confocal microscopy measurements using GA treatment of immunostained cells revealed that distortions were generally below 25 nm (root mean square distance) over length scales of up to 20 μm (**Supplementary Fig. 2.5**). Microtubule cross sectional profiles had an average Gaussian-fitted FWHM of 80 ± 7 nm (mean ± SD, **Supplementary Fig. 2.2**), indicating a spatial resolution of ~65 nm as before. A three-color stain of an early anaphase PtK1 cell produced clear images of the mitotic spindle and distinctly resolved attachments between kinetochore-fiber microtubule bundles and chromosomes with good expansion fidelity (**Fig. 2.2 e-j**, **Supplementary Figs. 2.6-2.8**). Although the DNA stain TO-PRO-3 is quenched by the polymerization reaction, we were able to stain DNA after expansion through a brief incubation

step with the dye (see **section 2.6**). A panel of GA-treated immunostained cells for a variety of cytoskeletal structures and sub-cellular organelles are shown in **Supplementary Fig. 2.9**.

Conventionally immunostained cells treated with either MA-NHS or GA showed 3-4× brighter signal after expansion compared to untreated cells using DNA-labeled antibodies (**Supplementary Fig. 2.10**). Although fluorescence retention post-expansion was somewhat better using DNA-labeled antibodies than with MA-NHS or GA treatment of conventional antibodies (~90% compared to ~70%, **Supplementary Fig. 2.11**), we found that pre-expansion specimens were ~4× brighter with conventional antibodies than with DNA-antibodies (data not shown). We believe the higher brightness likely results from the ability to conjugate more of the small fluorophore molecules (~600 g mol^{-1}) to an antibody than the comparably large single-stranded oligonucleotides (~6,000 g mol^{-1}) before compromising the antibody's binding ability.

In cultured cells, we observed that GA-treated specimens tolerated short digestion times (~30 minutes) with low distortion, while MA-treated specimens required longer digestion times to avoid distortion (~12-18 hours, **Supplementary Figs. 2.13**, **2.14**). This observation led us to ask whether fluorescent protein signals could be retained for imaging after digestion and expansion. Gratifyingly, we found that cells treated with GA retained intrinsic fluorescence signal from fluorescent proteins (GFP, DsRed) targeted to various structures when using a ~30 min digestion time (**Fig. 2.2 k-m**, **Supplementary Fig. 2.11**). The use of long digestion times (>12 hours), or the omission of GA treatment, resulted in little retained fluorescent protein (FP) signal (**Supplementary Figs. 2.15, 2.16**). Hybrid experiments using a mixture of FP and antibody stains are straightforward (**Fig. 2.2 k-m**).

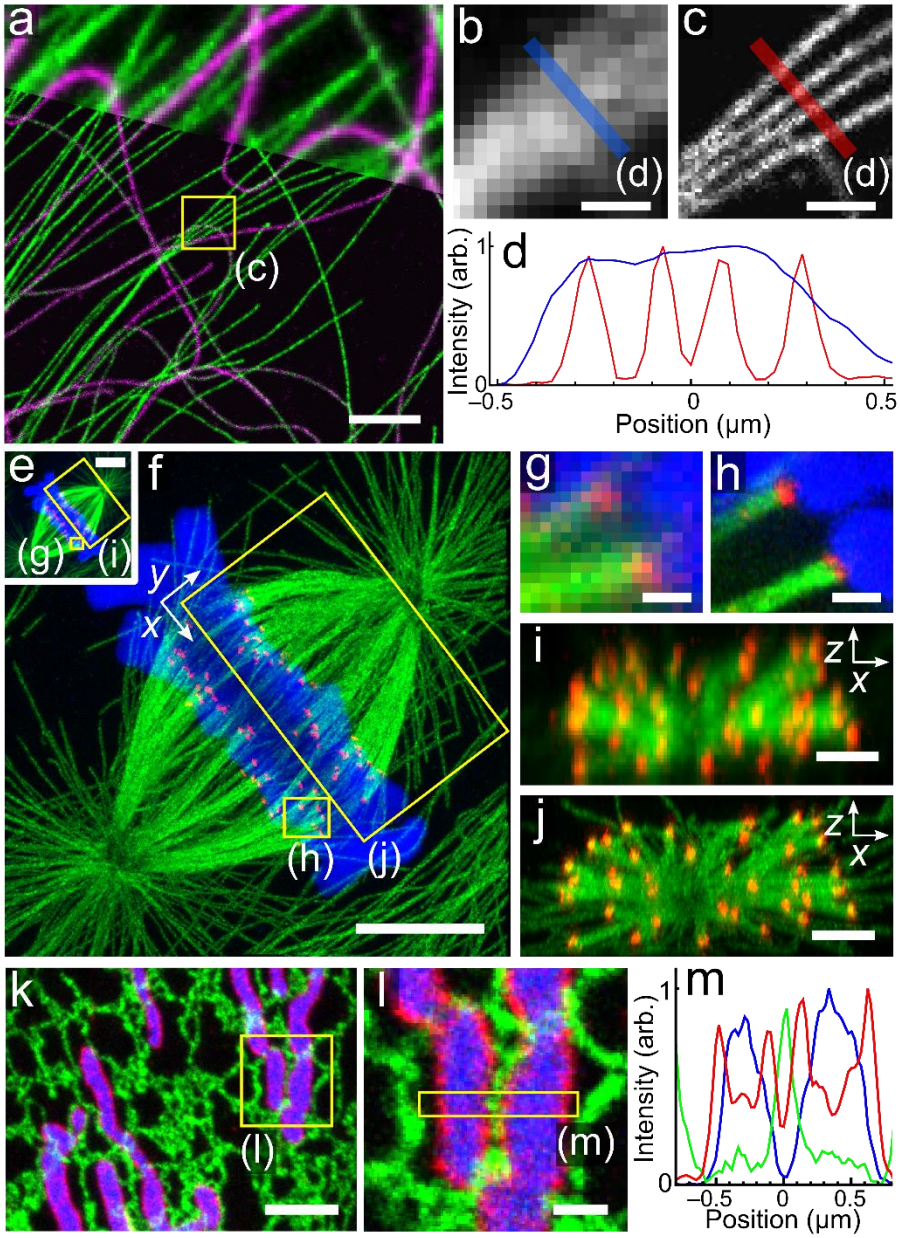

Figure 2.2 | Confocal fluorescence images of expanded cultured cells. (**a**) BS-C-1 cell immunostained for tyrosinated tubulin (green) and detyrosinated tubulin (magenta) using conventional secondary antibodies and partially overlaid with corresponding pre-expansion image (top). Specimen was treated with MA-NHS after immunostain. Zoom-in of boxed region in **a** showing corresponding pre-expansion (**b**) and post-expansion (**c**) images of tyrosinated tubulin signal along with corresponding line profiles (**d**). Pre-expansion (**e**) and post-expansion (**f**) images of a dividing PtK1 cell immunostained for tubulin (green) and the kinetochore protein HEC1 (red) using conventional secondary antibodies and also stained for DNA (blue) using TO-PRO-3. Specimen was treated with GA after immunostain. (**g-h**) Zoom-in of microtubule-kinetochore attachments from boxed regions in **e** and **f**. End-on views of boxed regions in **e**, **f** before (**i**) and after (**j**) expansion (DNA channel omitted for clarity). (**k**) Maximum intensity projection of a fixed

BS-C-1 cell expressing the endoplasmic reticulum (ER) tag Sec61B-GFP (green) and the inner mitochondrial membrane tag mito-DsRed (blue) and immunostained against the outer mitochondrial membrane protein TOM20 using a conventional secondary antibody (red). Specimen was treated with GA after immunostain. (**l**) Zoom-in of boxed region in **k** showing close apposition of an ER tubule with two mitochondria. (**m**) Cross-sectional profile of boxed region in **l**. All distances and scale bars are in pre-expansion units. Scale bars, (**a, i, j, k**) 2 μm, (**b, c, g, h, l**) 500 nm, (**e, f**) 5 μm.

2.5.2 Expansion of Mouse Brain Tissue

The above methods extended well to brain tissue. The treatment of conventionally immunostained 100 μm-thick THY1-YFP-H mouse brain slices with MA-NHS (**Fig. 2.3**) or GA retained antibody fluorescence, although we prefer the MA-NHS treatment because treatment with GA leads to high levels of background fluorescence (**Supplementary Fig. 2.17**).[61] Complete, high-fidelity expansion in tissue required a lower MA-NHS concentration than in cultured cells (1 mM for 60 min), presumably due to physical differences between the specimens. We therefore advise validation (through correlative imaging pre- and post-expansion) and possible optimization of these procedures or their variations before applying them to uncharacterized specimens which may have different properties.

We immunostained THY1-YFP-H brain slices for YFP-expressing neurons and the pre- and postsynaptic markers Bassoon and Homer using conventional secondary antibodies (**Fig. 3 a-f**) and treated with MA-NHS before gelation, digestion, and expansion. Presynaptic and postsynaptic densities were well-resolved and junctions between synapses and dendritic spines were clearly observable (**Fig. 2.3 a-f**, **Supplementary Fig. 2.18, Supplementary Video 2.1**). Over length scales of up to 30 μm we observed distortions generally below 0.2 μm (**Supplementary Fig. 2.19**). By decreasing the digestion time for MA-treated mouse brain tissue to 1 h (rather than 12-18 hours), we were able to preserve intrinsic YFP fluorescence in expanded brain tissue and we were easily able to observe dendritic spines on a neurite even using a rudimentary epifluorescence microscope equipped with a 20× 0.45 NA air objective lens (**Fig. 2.3 i-j**). Omission of MA-NHS treatment results in very weak intrinsic YFP fluorescence levels (**Supplementary Fig. 2.20**) as also pointed out by Boyden and coworkers.[35]

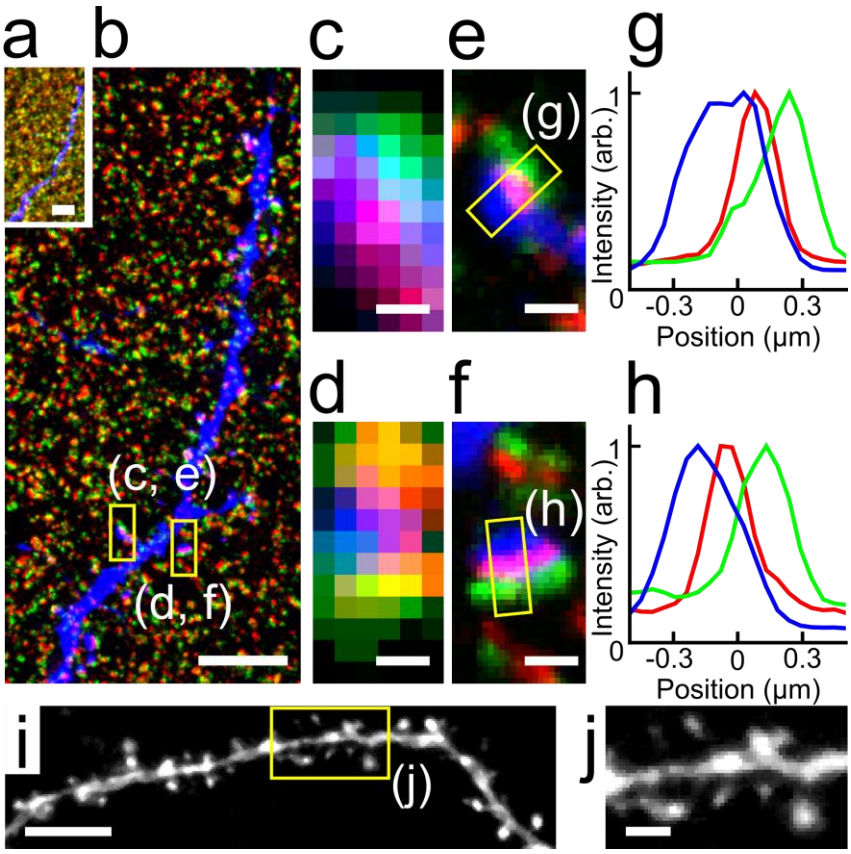

Figure 2.3 | Confocal (**a**-**f**) and epifluorescence (**i**, **j**) images of expanded mouse brain tissue using the MA-NHS treatment method. (**a**) Single pre-expansion focal plane of a THY1-YFP-H mouse brain slice indirectly immunostained for YFP (blue), the presynaptic marker Bassoon (green), and the postsynaptic marker Homer (red) using conventional secondary antibodies. (**b**) The same area in **a** after expansion, displayed with the relative size compared to **a**, in order to show the relative amount of physical expansion. Zoom-in of the boxed regions in **b** before expansion (**c, d**) and after expansion (**e, f**), revealing that the presynaptic and postsynaptic markers are well-resolved and aligned with dendritic spines. (**g**, **h**) Cross-sectional profiles of the boxed regions in **e**, **f**. (**i**) Epifluorescence image of a neuron in an expanded THY1-YFP-H mouse brain slice using YFP itself as the fluorescence reporter. (**j**) Zoom in of the boxed region in **i** showing clearly resolved dendritic spines. All distances and scale bars correspond to pre-expansion dimensions. Scale bars, (**a**, **b**) 5 μm, (**c, d, f, g**) 500 nm**,** (**i**) 4 μm**,** (**f**) 1 μm.

2.6 Discussion

The MA-NHS and GA polymer-linking steps resemble the formaldehyde-acrylamide linking strategy used in the CLARITY tissue clearing procedure to link protein amines to a polyacrylamide gel, although labeling of amines on the specimen with MA-NHS and GA is over an

order of magnitude faster, requiring an incubation of 60 minutes (or less) as opposed to one or more days in CLARITY.[62,63] While MA is almost certainly being incorporated covalently into the polymer, the linking mechanism of GA-treated specimens is less obvious. GA exists in aqueous solution as a complex equilibrium distribution of monomeric and polymeric forms which contain aldehyde and alkene groups.[64] Both aldehydes and alkene groups on GA could in principle become covalently linked to the acrylamide polymer. Additionally, the GA polymer could become linked to the gel by entanglement with the acrylamide polymer,[65] or a combination of covalent and entanglement mechanisms. Overall, we favor MA-NHS treatment for brain tissue due to its lower background signal and GA treatment for cultured cells due to its generality with both immunolabeled specimens and fluorescent proteins. **Supplementary Table 2.1** summarizes all stain procedures and imaging conditions used in this report.

Boyden and coworkers pointed out that not all organic fluorophores survive the polymerization step (e.g., several cyanine fluorophores do not survive) and they recommended use of Alexa Fluor 488, TAMRA or Atto 565, and Atto 647N.[35] To these we add that Alexa Fluor 405, Atto 488, Alexa Fluor 532, Alexa Fluor 546, Alexa Fluor 568, GFP, YFP, DsRed, Hoechst 33342, and SYBR Gold also survive polymerization (**Fig. 2.2**, **Supplementary Fig. 2.21**). Additionally, fluorophores may be introduced post-digestion to avoid quenching or bleaching by the polymerization reaction, such as by incubating the gel with labeled streptavidin for a specimen that has been labeled with a biotin-labeled secondary antibody, or through incubation with DNA-binding fluorophores such as TO-PRO-3, etc. (**Fig. 2.2 e-j**, **Supplementary Fig. 2.21**).

We have introduced and characterized new polymer-linking methods for expansion microscopy which now enable the use of conventional fluorophore-labeled antibodies and FPs. These methods should make ExM more accessible to a large and growing community of researchers applying super-resolution techniques to a wide range of biological questions. The methods improve the brightness of immunostained specimens compared to DNA-conjugated antibodies while making use of conventional secondary antibodies that are in many cases already available in research laboratories. Given the choice, we generally prefer immunostaining of FPs due to its enhancement of signal brightness. However, the use of intrinsic FP signals with ExM creates flexibility in multi-channel situations when compatible antibody species may not be

available or when FPs are separable spectrally, but not antigenically (e.g., CFP-YFP). The use of intrinsic FP signals may also provide advantages when antibody penetration into thick samples is limited.

Expansion microscopy is a highly attractive imaging modality owing to its compatibility with conventional microscopes and conventional probes, its robust multicolor and 3D capabilities, and its optical clearing properties for thick tissues.[35] While the method is limited to fixed specimens whose mechanical properties do not prevent expansion, the currently achieved ~65 nm resolution is sufficient to answer a wide range of biological questions and is likely to improve with further development.

2.7 Materials and Methods

2.7.1 Reagents and Reagent Preparation

Unconjugated secondary antibodies were purchased from Jackson Immunoresearch (West Grove, PA, USA) including donkey anti-rat (712-005-151), donkey anti-rabbit (711-005-152), donkey anti-mouse (715-005-151), and donkey anti-chicken (703-005-155). An Alexa Fluor 488 conjugated donkey anti-rat antibody (712-545-150) was purchased from Jackson Immunoresearch. Primary antibodies are listed as follows: Rat anti-alpha tubulin (MA1-80017, Thermo Fisher Scientific, Waltham, MA, USA), Rabbit anti-detyrosinated tubulin (ab48389, Abcam, Cambridge, MA, USA), Mouse anti-HEC1 (ab3613, Abcam), Rabbit anti-TOM20 (sc-11415, Santa Cruz Biotechnology, Santa Cruz, CA, USA), Rabbit anti-GFP (A31857, Life Technologies, Carlsbad, CA, USA), Chicken anti-GFP (A10262, Thermo Fisher Scientific), Rabbit anti-Homer1 (160003, Synaptic Systems, Goettingen, Germany), Mouse anti-Bassoon (ab82958, Abcam). Bovine serum albumin (BSA) was purchased from Santa Cruz Biotechnology. NHS-functionalized (amine-reactive) dyes and biotin were obtained from Sigma-Aldrich, (Atto 488, Atto 565, Atto 647N, St. Louis, MO, USA) or Thermo Fisher Scientific (Alexa Fluor 405, Alexa Fluor 488, Alexa Fluor 532, Alexa Fluor 546, Alexa Fluor 647, EZ-link NHS-PEG-4-Biotin). Dyes were obtained in 1 mg aliquots from the suppliers, dissolved at a concentration of ~100 mg mL^{-1} in anhydrous DMSO, sub-aliquoted into anhydrous DMSO at 1 and 10 mg mL^{-1}, and stored at -20 °C. NAP-5 size-exclusion chromatography columns were obtained from GE Healthcare (Little Chalfont,

Buckinghamshire, United Kingdom) and were reused ten or more times by washing with 5 mL aqueous 1 M sodium hydroxide between uses and storage at 4 °C in phosphate-buffered saline (PBS) containing 2 mM sodium azide for up to several months. Methacrylic acid N-hydroxy succinimidyl ester (MA-NHS), anhydrous dimethyl sulfoxide (DMSO), sodium bicarbonate, PIPES salt (for buffer), ethylene diamine tetraacetic acid (EDTA), magnesium chloride, Triton X-100, and sodium borohydride were obtained from Sigma-Aldrich. MA-NHS was dissolved in anhydrous DMSO at a concentration of 1 M and stored at -20 °C until used. Paraformaldehyde (32%) and glutaraldehyde (50%) were obtained from Electron Microscopy Sciences (Hatfield, PA, USA). All DNA was purchased from Integrated DNA Technologies (Coralville, IA, USA). DNA stains including Hoescht 33342 (NucBlue Live), SYBR Gold, and TO-PRO-3 were purchased from Life Technologies. Tetramethylethylenediamine (TEMED, 17919) and ammonium persulfate (APS, 17874) were purchased from Thermo Fisher Scientific. 4-hydroxy-TEMPO (97%, 176141), and sodium acrylate (97%, 408220) were purchased from Sigma-Aldrich. 40% acrylamide (1610140) and 2% bis bis-acrylamide (1410142) solutions were purchased from Bio-Rad Laboratories (Hercules, CA, USA).

2.7.2 Preparation of Fluorophore-Labeled Antibodies and Streptavidin

Fluorophore-conjugated antibodies or streptavidin were prepared as follows. To 40 µL of unconjugated protein (~1.3 mg mL^{-1} IgG, or 1 mg mL^{-1} streptavidin) was added 5 µL of aqueous 1 M sodium bicarbonate (pH ~8.3) and 1 µL of NHS-dye stock in DMSO. These reagents were allowed to react at room temperature (22 °C) for ~30 minutes. During the reaction, a NAP-5 size-exclusion chromatography column, for purification of labeled antibody from free dye, was equilibrated by flowing ~10 mL of PBS through each column. The ~50 µL reaction was loaded onto the column followed by flowing through and discarding 650 µL of PBS and flowing through and keeping 300 µL eluate. The eluate was characterized by absorption spectroscopy by measuring the average concentration of dye and average concentration of antibody according to the instructions provided by the dye manufacturers. Care was taken to avoid adding more than ~5 % DMSO to the antibody solution to avoid disturbing the antibody in all antibody-labeling reactions. The obtained dye to protein ratios are listed in **Supplementary Table 2.1**. The DNA-antibody conjugate was prepared using 5' amine modified DNA (TAC GCC CTA AGA ATC CGA ACT TTA CGC CCT AAG AAT CCG AAC) according to the protocol described previously[35] (updated protocols

available at expansionmicroscopy.org). The tri-functional linker was prepared from 5' acrydite and 3' amine modified DNA (GTT CGG ATT CTT AGG GCG TA), reacted with a tenfold molar excess of Atto 488 NHS for 1 h at pH 8.3, and purified by cold ethanol precipitation.

2.7.3 Fluorescence Microscopes

Confocal microscopy was performed on a Leica SP5 inverted confocal scanning microscope at the UW Biology Imaging Core (**Fig. 2.2**, **Supplementary Figs. 2.2-2.8, 2.21**) using a 63× 1.2 NA water lens (Leica, Nussloch, Germany), or an Olympus upright FV1000 (**Fig. 2.3**, **Supplementary Figs. 2.18, 2.19**) with a 25× 1.0 NA SCALE objective. Conventional widefield epifluorescence imaging was performed on an inverted Nikon Ti-S microscope configured with a 10× 0.25 NA air objective lens (Nikon, Melville, NY, USA), 20× 0.45 NA air objective lens (Nikon), or a 60× 1.2 NA water-immersion objective lens (Nikon). The widefield microscope was illuminated using a four-channel light emitting diode source (LED4D120, Thorlabs, Newton, NJ, USA) using a multiband filter set (LF405/488/532/635-A-000, Semrock, Rochester, NY, USA) and images were captured with a Zyla 5.5 sCMOS camera (Andor, Windsor, CT, USA) (**Supplementary Figs. 2.1, 2.9-2.17, 2.20**). Localization microscopy (**Supplementary Fig. 2.5**) was performed on a homebuilt Nikon Ti-U system configured for total internal reflection fluorescence using a Nikon CFI Plan Apo Lambda 100× 1.45 NA objective and a 647-nm diode-pumped solid-state laser source (MPB Communications, Pointe-Claire, QC, Canada). A 405-nm solid state laser (Obis, Coherent) was used for activation to increase the rate of fluorophore blinking. Localization images were acquired on an EMCCD (iXon Ultra 897, Andor) operating at 200 frames per second. A custom-built focus lock using an objective nanopositioner (Nano F-100S, Mad City Labs, Madison, WI, USA) and a 940-nm diode laser (LP-940, Thorlabs) was used to control axial drift.

2.7.4 Cell Culture

BS-C-1 and Ptk1 cells were obtained from ATCC and both tested negative for mycoplasma using 4',6-diamidino-2-phenylindole dihydrochloride. Cell lines obtained from ATCC were used without additional authentication. BS-C-1 cells were cultured in EMEM (ATCC, 30-2003, Manassas, VA, USA) containing penicillin and streptomycin (PS, 15140-122, Life Tech.), 10 % FBS (FB22-500, Serum Source International, Charlotte, NC, USA), and non-essential amino acids

(NEAA, 11140-050, Life Tech.). PtK1 cells were cultured in RPMI (11875-093, Life Tech.) containing PS, 10 % FBS and NEAA. Cells were maintained at 37 °C environment with 5 % CO_2.

2.7.5 Immunostaining of Cultured Cells

See also Supplementary Table 1 for a summary and detailed list of concentrations and reagents for the preparation of all imaged specimens.

Immunostaining of BS-C-1 cells was conducted as follows. Cells were seeded at a density of ~50,000 cells per well of a 24-well plate containing a 12 mm #1.5 coverglass and incubated overnight. Cells were optionally extracted for 30s with PEM (0.1 M PIPES pH 7, 1 mM EDTA, 1 mM $MgCl_2$) containing 0.5 % Triton-X-100 immediately prior to fixation. The extraction step is important for high-quality stains of cytoskeletal structures, but was not used on stains of organelle structures where treatment with detergent would likely destroy the structure (see Supplementary Table 1). Specimens were fixed for 10 minutes in a solution containing 3.2 % paraformaldehyde and 0.1 % glutaraldehyde in PEM (for microtubules) or PBS (for organelles), followed by brief washing in PBS and reduction in an aqueous solution of 10 mM sodium borohydride for 5 minutes. After reduction, samples were washed three times with PBS and then incubated with blocking/permeabilization buffer (PBS with 3 % BSA and 0.5 % Triton X-100) for 30 minutes. Specimens were then incubated with primary antibodies in blocking/permeabilization buffer for 45 minutes, washed three times with PBS, and incubated for 45 minutes with secondary antibodies in blocking/permeabilization buffer. After three more washes with PBS, cells were treated with either GA or MA-NHS. GA-treatment consisted of a 10 minute, room-temperature incubation with 0.25% GA in PBS followed by washing three times with PBS. MA-NHS-treatment consisted of a 60 minute, room-temperature incubation with 25 mM MA-NHS in PBS followed by washing three times with PBS. For correlative pre-expansion localization microscopy and post-expansion widefield imaging of fixed BS-C-1 cells in **Supplementary Fig. 2.5**, a tertiary antibody immunostain was performed including steps for: primary rat anti-tubulin, secondary Alexa Fluor 647 mouse anti-rat, tertiary Atto 488 donkey anti-mouse antibody and finally GA treatment.

Immunostaining of PtK1 cells was conducted using a variation of the above protocol for BS-C-1 cells, but with the following differences. Cells were incubated with rat anti-tubulin and mouse anti-HEC1 primary antibodies overnight at 4 °C. After washing, cells were incubated at room temperature for 45 minutes with secondary antibodies consisting of donkey anti-rat secondary antibody labeled with Atto 488 and a donkey anti-mouse secondary antibody that was dually labeled Alexa Fluor 546 and biotin. After secondary labeling, samples were treated with GA as described above for BS-C-1 cells. Prior to post-ExM imaging, the expanded samples were incubated with 2 μg mL^{-1} Alexa Fluor 546 labeled streptavidin in PBS containing 3% BSA for one hour. After contracting during this incubation, the gel was allowed to re-expand to full size in DI water. Additionally, immediately prior to pre- and post-ExM imaging, cells were incubated with 1 μM TO-PRO-3 in water for 15 minutes.

2.7.6 Transfection of Cultured Cells

BS-C-1 cells were dissociated and concentrated to ~10^6 cells mL^{-1} by centrifugation at 90 *g* for 10 min and resuspended in Solution SF (Lonza, Basel, Switzerland). A 100 μL volume of cells was mixed with 5 μg of plasmid: pAcGFP1-Mito (Clontech, Mountain View, CA, USA) in **Supplementary Figs. 2.9 e** and **2.16**, or pAc-GFPC1-Sec61β[13] (a gift from Tom Rapoport (Harvard Medical School), Addgene plasmid# 15108) in **Supplementary Figs. 2.9 f** and **2.15**, or Sec61Bβ and pDsRed2-Mito (BD Biosciences, Franklin Lakes, NJ, USA) in **Fig. 2.2 k, l**. The cells were then electroporated in an electrode cuvette with pulse code X-001 in a Lonza Amaxa nucleofector, immediately resuspended in warm media, and plated in a 24-well plate as described above. After 24-48 hours, the cells were fixed with paraformaldehyde and glutaraldehyde (**Supplementary Figs. 2.15, 2.16 a**, or paraformaldehyde only in **2.16 b-c**), or fixed and immunostained for outer mitochondrial membrane (**Fig. 2.2 k, l**) or with anti-GFP (**Supplementary Fig. 2.9 e-f**) as described above.

2.7.7 Mouse Brain Tissue Dissection and Preparation

All animal experiments were carried out in accordance with the Institutional Animal Care and Use Committee at the University of Washington. Mice (strain C57BL/6) were anesthetized with isoflurane and perfused transcardially with PBS, followed by paraformaldehyde (PFA, 4%

wt/vol in PBS). Brains were dissected out, postfixed in 4% PFA in PBS at 4 °C for one hour and washed in PBS. Then, the brains were sliced to 100 µm thickness using a vibratome. All mice used in this work were between the ages of 1 and 4 months at the time of dissection. Both male and female mice were used.

2.7.8 Immunostaining of Tissue Slices

100 µm thick mouse brain slices were first incubated in blocking/permeabilization buffer (3% BSA and 0.1% Triton X-100 in PBS) for 6-12 h at 4 °C. The tissue was then incubated in primary antibody diluted into blocking/permeabilization buffer for at least 24 h at 4 °C and was then washed three times in blocking/permeabilization buffer (20 min each). Tissues were then incubated with secondary antibody diluted into blocking/permeabilization buffer for 24 h at 4 °C and afterwards were washed three times with PBS (20 min each). The brain slices were then either treated with 0.1% GA in PBS or 1 mM MA-NHS in PBS for 1 h at room temperature followed by three washes with PBS. Tissue slices that were not immunostained (samples with fluorescent protein signal preserved) were simply treated with GA or MA-NHS. See also Supplementary Table 1 for a summary and detailed list of concentrations and reagents for the preparation of all imaged specimens.

2.7.9 Gelation, Digestion, and Expansion of Cultured Cell Specimens

Fixed cell samples on 12 mm round coverglass were incubated in monomer solution (1× PBS, 2 M NaCl, 2.5% (wt/wt) acrylamide, 0.15% (wt/wt) N,N'-methylenebisacrylamide, 8.625% (wt/wt) sodium acrylate) for ~1 minute at room temperature prior to gelation. Concentrated stocks of ammonium persulfate (APS) and tetramethylethylenediamine (TEMED) at 10% (wt/wt) in water were diluted in monomer solution to concentrations of 0.2% (wt/wt) for gelation, with the initiator (APS) added last. The gelation solution (~70 µl) was placed in a 1 mm deep, 1 cm diameter Teflon well and the coverglass was placed on top of the solution with cells face down. Gelation was allowed to proceed at room temperature for 30 min. The coverglass and gel were removed with tweezers and placed in digestion buffer (1× TAE buffer, 0.5% Triton X-100, 0.8 M guanidine HCl) containing 8 units mL^{-1} Proteinase K (EO0491, Thermo or P8107S, New England BioLabs, Ipswich, MA, USA) added freshly. Unless otherwise indicated, gels were digested at 37

°C for various amounts of time as follows: MA-treated cells were digested overnight, GA-treated cells were digested for 30 min to 1 h, and fluorescent protein samples were digested for 30 min maximum. The gels (sometimes still attached to the coverglass) were removed from digestion buffer and placed in ~50 mL DI water to expand. Water was exchanged every 30 min until expansion was complete (typically 3-4 exchanges).

2.7.10 Post-Expansion Labeling of Expanded Cultured Cell Specimens with Streptavidin

Expanded cultured cell specimens initially immunostained with biotin-modified antibodies were submerged in a streptavidin solution (2 μg mL^{-1}) in PBS containing 3% BSA for 45 min. The contracted gels were then washed and re-expanded in DI water.

2.7.11 Gelation, Digestion, and Expansion of Mouse Tissue Specimens

Tissue samples were incubated in monomer solution at 4 °C for 45 min prior to gelation. Tissue was gelled with the same solution as cells but with the addition of 4-hydroxy-2,2,6,6-tetramethylpiperidin-1-oxyl (4-hydroxy-TEMPO) at a concentration of 0.01% (wt/wt) from a 1% (wt/wt) stock as an inhibitor to allow complete diffusion of the monomers throughout the tissue. The glass slide with the sample and a #1.5 coverglass on top separated by spacers (one #1 coverglass) on either side of the tissue was used as a gelation chamber. The samples were allowed to gel for 2-2.5 h at 37 °C. Excess gel around the samples was removed, the glass around the samples was cut to leave the tissue on a small glass square, and the samples were placed in digestion buffer with 8 units mL^{-1} and were allowed to digest at 37 °C for various amounts of time: stained samples were digested overnight and fluorescent protein samples were digested for 1 h. The gels were removed from the digestion solution (using the glass square to support the gel) and placed in DI water to expand. Gradually increasing the amount of water helped prevent the gels from folding.

2.7.12 Expanded Specimen Handling

Expanded gels were cut to fit on coverglass (2-4 cm edge-length rectangles) excess water was removed and then gently placed on coverglass substrates for imaging. When possible, gels

were immobilized using a small amount of cyanoacrylate glue on the periphery after wicking away excess water from the edges.

2.7.13 Correlative Localization Microscopy and ExM

Pre-expansion localization microscopy images of Alexa Fluor 647 labeled microtubules were acquired at 200 Hz for ~80,000 frames at ~2 kW cm^{-2} in an oxygen scavenging switching buffer (100 mM Tris pH 8, 10 % glucose (wt/wt), 0.5 mg mL^{-1} glucose oxidase, 40 µg mL^{-1} catalase, and 143 mM 2-mercaptoethanol). After localization microscopy, samples were washed to remove the switching buffer, gelled, digested, and expanded as described above. During gelation, the Alexa Fluor 647 signal was destroyed, however the Atto 488 from the tertiary antibody remained fluorescent for widefield epifluorescence imaging.

2.7.14 Image Processing

Expanded cell culture confocal z-stacks were aligned frame by frame using an automated rigid registration routine in Mathematica in order to correct for minor lateral drift during acquisition. Mitotic spindle confocal z-stacks of PtK1 cells were processed to remove peripheral non-specific adsorption of the HEC1 antibody as follows: A binary 3D mask of the kinetochore attachments was generated by binarizing the kinetochore channel and retaining connected-component features larger than 100 voxels and within 1 µm of the outer surface of the chromosomes. The kinetochore binary mask was then dilated by three pixels and multiplied by the original channel data. The processing was performed to clarify the maximum intensity projections in **Fig. 2.2 f, i, j**, but had little effect on the individual z-sections as shown in detail in **Supplementary Fig. 2.7**. Localization microscopy images were analyzed as described previously.[58] Registration of pre- and post-expansion correlative images were carried out in the open-source software Elastix, using rigid (similarity) and non-rigid (B-spline) transformations to determine the expansion factor and quantify distortions. Details, including example data and processing scripts, are included in the Supplemental Protocol.

2.7.15 Reproducibility

All experiments were carried out ≥3 times including all sample preparation and analysis, except as noted below. Representative data for each experiment are shown. Experiments for **Supplementary Figs. 2.5**, **2.10c**, **2.11**, **2.12**, **and 2.16b** were performed only once.

2.8 Acknowledgements

This work is supported by the University of Washington (J.C.V.), a Burroughs-Wellcome Career Award at the Scientific Interface (J.C.V.), an NSF Graduate Research Fellowship DGE-1256082 (T.J.C.), and by NIH grants EY10699 and EY17101 (R.O.L.W.). The authors would like to thank L. Wordeman (University of Washington, Seattle, WA) for providing the PtK1 cell line and anti-HEC1 antibody, for access to an electroporator, and for helpful discussions; K. Oda (University of Washington, Seattle, WA) for performing the cardiac perfusion of mice; and T. Rapoport (Harvard Medical School, Boston, MA) for the Sec61β-GFP plasmid.

2.9 Supplementary Information

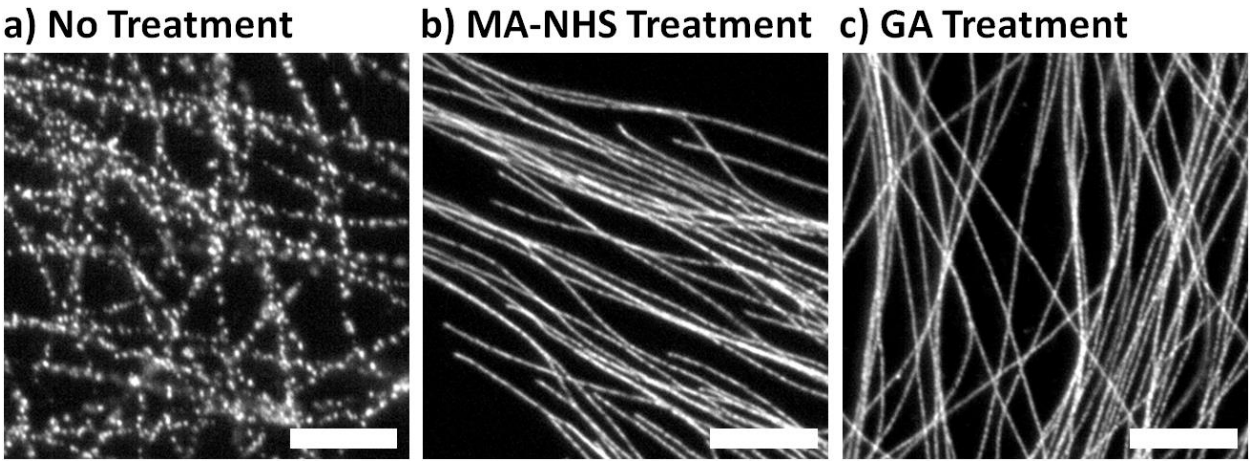

Supplementary Figure 2.1 | Epifluorescence images of expanded BS-C-1 cells that were immunostained against tubulin using conventional fluorophore-labeled antibodies and then treated as indicated prior to gelation, digestion, and expansion. (**a**) Omission of post-stain treatment leads to heavy distortion due to lack of retention along the original structure. Post-stain treatment of immunostained cells with (**b**) MA-NHS (methacrylic acid *N*-hydroxyl succinimidyl ester) or (**c**) GA (glutaraldehyde) both conferred excellent retention of fluorescence and structure. Scale bars are 2.4 µm and are all in pre-expansion dimensions.

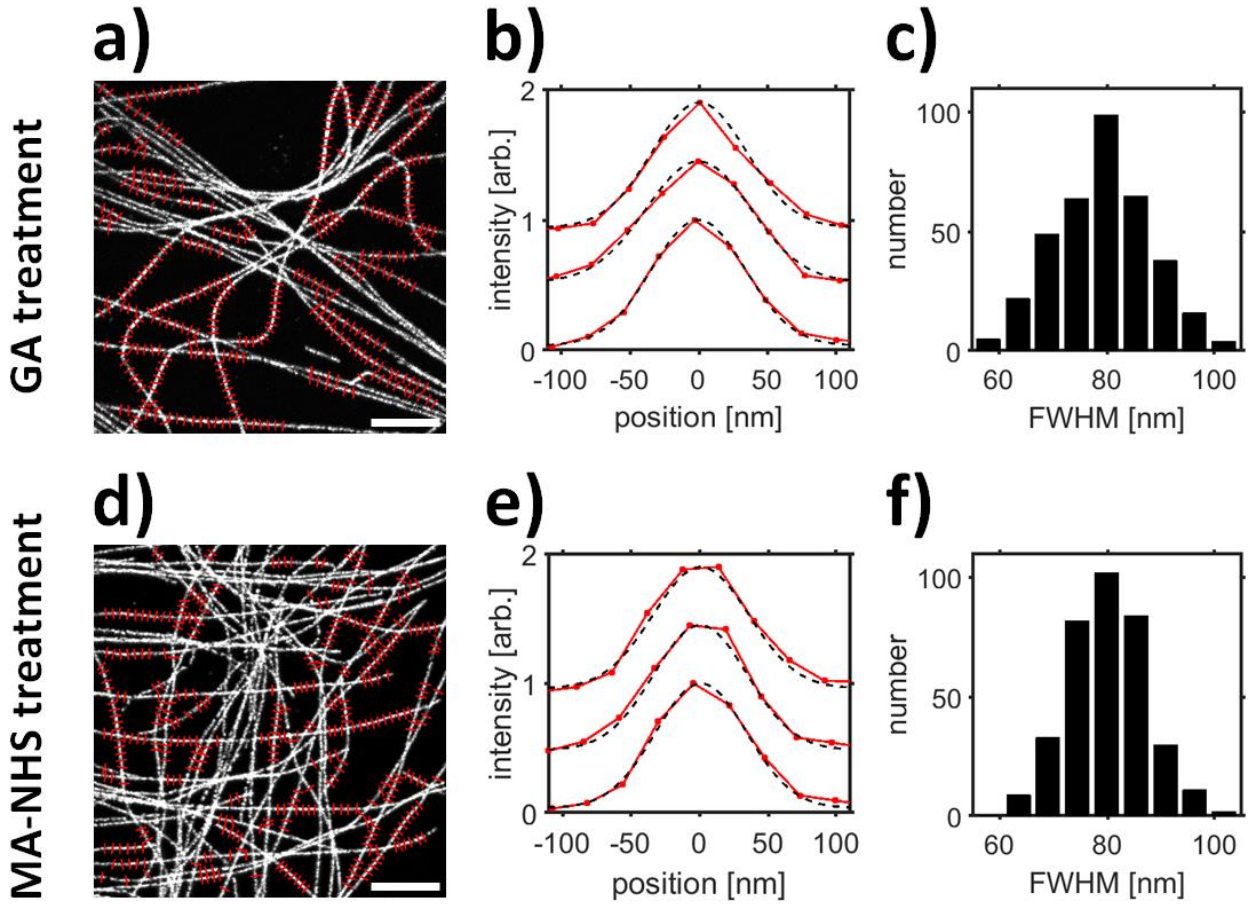

Supplementary Figure 2.2 | Confocal fluorescence measurement of microtubule cross-sectional profile for 4.15× expanded specimens and estimate of spatial resolution. (**a**) Confocal fluorescence image of an expanded BS-C-1 cell conventionally immunostained for tyrosinated tubulin and treated with GA prior to gelation. Red dashes are positions at which cross-sectional profiles were measured. (**b**) Representative cross-sectional profiles of microtubules (red lines) and Gaussian fits (dashed black lines). (**c**) Analysis of microtubule profiles (red lines in **a**) yielded an average Gaussian-fitted full width at half maximum (FWHM) of 79 ± 9 nm (mean ± SD, 362 microtubule profiles). (**d-f**) Cross-sectional profile analysis for an expanded, MA-NHS treated, conventionally immunostained BS-C-1 cell showing an average FWHM of 80 ± 7 nm (mean ± SD, 353 microtubule profiles). All distances and scale bars correspond to pre-expansion dimensions. Scale bars are 5 µm.

Resolution estimate: The observed ~80 nm FWHM profile of microtubules is consistent with the convolution of the double-peaked spatial profile of indirectly immunostained microtubules (measured by localization microscopy at ~20 nm resolution, **Supplementary Fig. 2.5**) with an effective ~65 nm Gaussian point spread function (PSF) for expansion microscopy. The value of 65 nm is also approximately equal to the physical PSF of our microscope (~265 nm FWHM, when configured with the 63× 1.2NA water-immersion lens used here) divided by the measured expansion factor of 4.15.

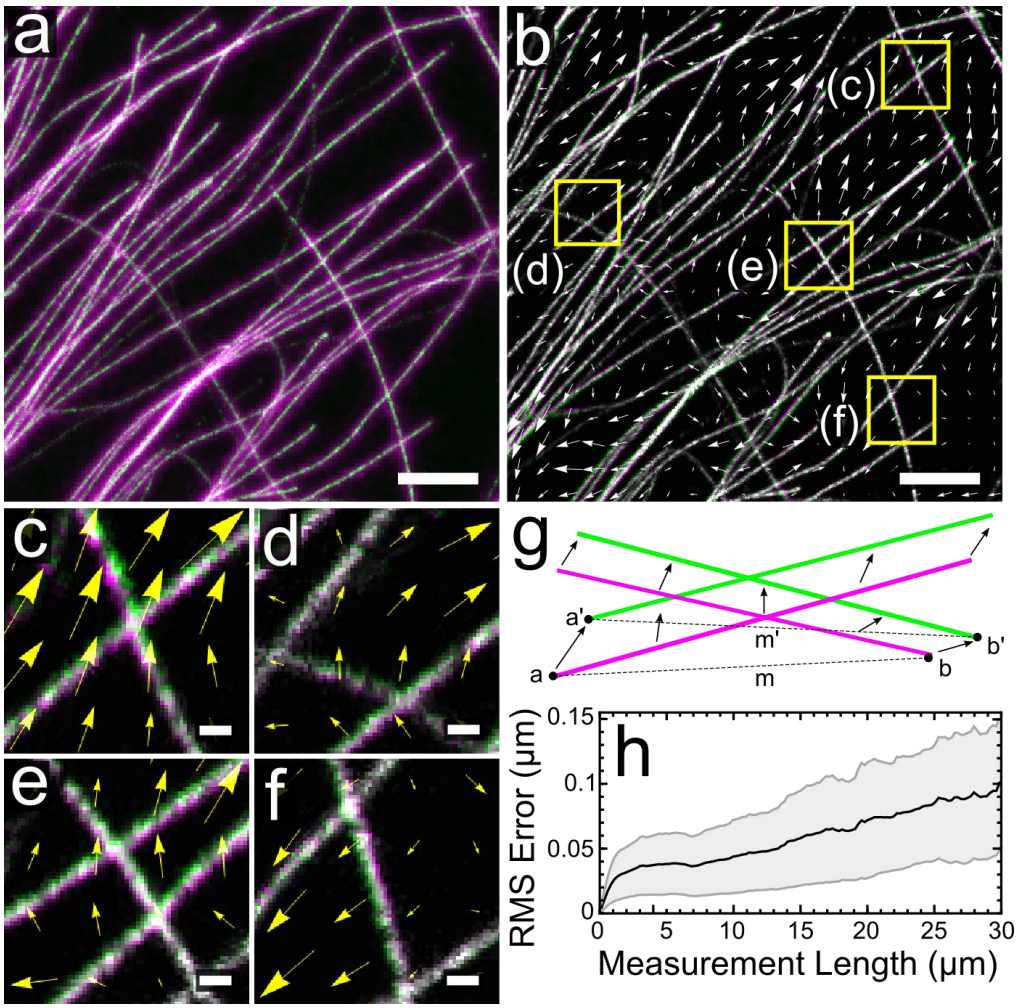

Supplementary Figure 2.3 | Comparison of pre-expansion and post-expansion images recorded by confocal fluorescence microscopy for a region of a BS-C-1 cell immunostained for tyrosinated tubulin with a conventional Atto 488 secondary antibody and treated with MA-NHS before gelation (data from **Fig. 2.2**). (**a**) Overlay of pre-expansion image (magenta) and post-expansion image (green) after alignment of the post-expansion image using similarity registration (i.e., translation, rotation, and magnification—see methods for further details). (**b**) Overlay of post-expansion image before (magenta) and after (green) a non-rigid transformation procedure that uses B-spline registration to "warp" the post-expansion image to optimally fit the pre-expansion image. Arrows indicate the direction and relative magnitude (scaled 8×) of the transformation required to optimally align the post-expansion to the pre-expansion image. (**c**-**f**) Zoom-in images of boxed regions in **b** showing that distortions are generally very small. (**g**) Schematic of procedure used to measure distances *m* and *m'* between features *a* and *b* in the post-B-spline-registration (green) and corresponding features *a'* and *b'* in pre-B-spline-registration (magenta). (**h**) Quantification of root mean square (RMS) error of *m*-*m'* as a function of distance *m* for matching image features (black line) with plus or minus standard deviation. The plot in **h** was calculated from a 20 µm × 20 µm data set; the image in **a** shows a 12 µm × 12 µm zoom-in of the data set. All distances and scale bars correspond to pre-expansion dimensions. Scale bars (**a**, **b**) 2 µm, (**c**-**f**) 200 nm.

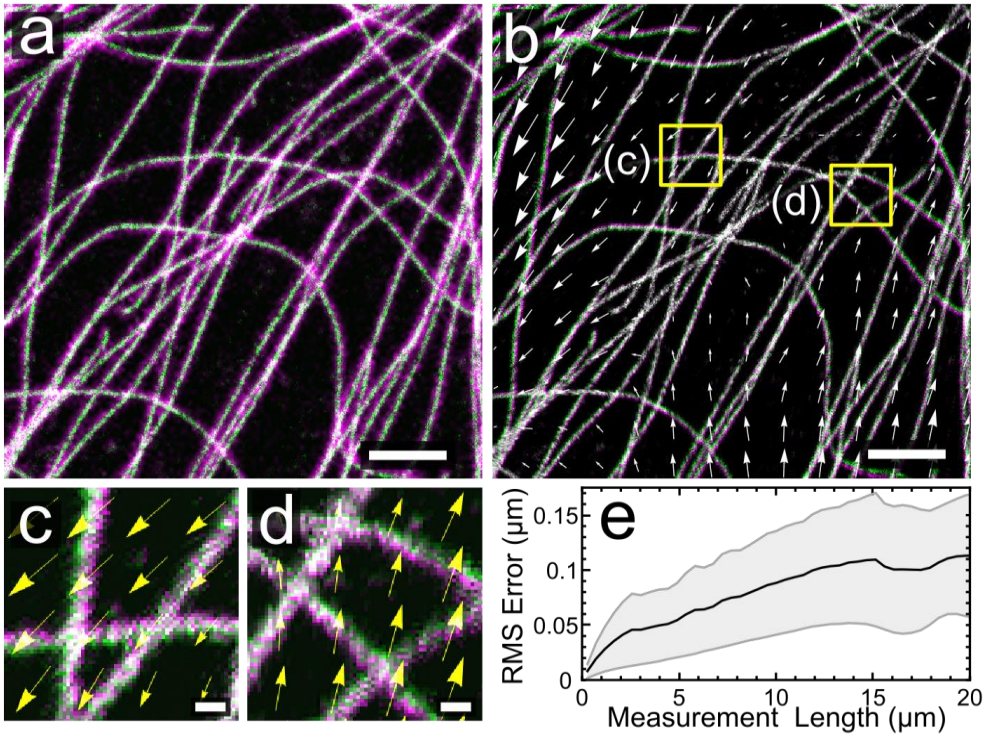

Supplementary Figure 2.4 | Comparison of pre-expansion and post-expansion images recorded by confocal fluorescence microscopy for a region of a BS-C-1 cell immunostained for tubulin with DNA-labeled secondary antibodies and hybridized with a modified complementary strand (5' acrydite and 3' Atto 488) prior to gelation. (**a**) Overlay of pre-expansion image (magenta) and post-expansion image (green) after alignment of the post-expansion image using similarity registration. (**b**) Overlay of post-expansion image before (magenta) and after (green) using a non-rigid B-spline registration. Arrows indicate the direction and relative magnitude (scaled 8x) of the transformation required to optimally align the images. (**c,d**) Zoom-in images of boxed regions in **b** showing that distortions are generally very small. (**e**) RMS error vs length distortion analysis for data in **a** (see **Supplementary Fig. 2.3**). The plot in **e** was calculated from a 20 µm × 20 µm data set; the image in **a** shows a 12 µm × 12 µm zoom-in of the data set. All distances and scale bars correspond to pre-expansion dimensions. Scale bars (**a**, **b**) 2 µm, (**c**,**d**) 200 nm.

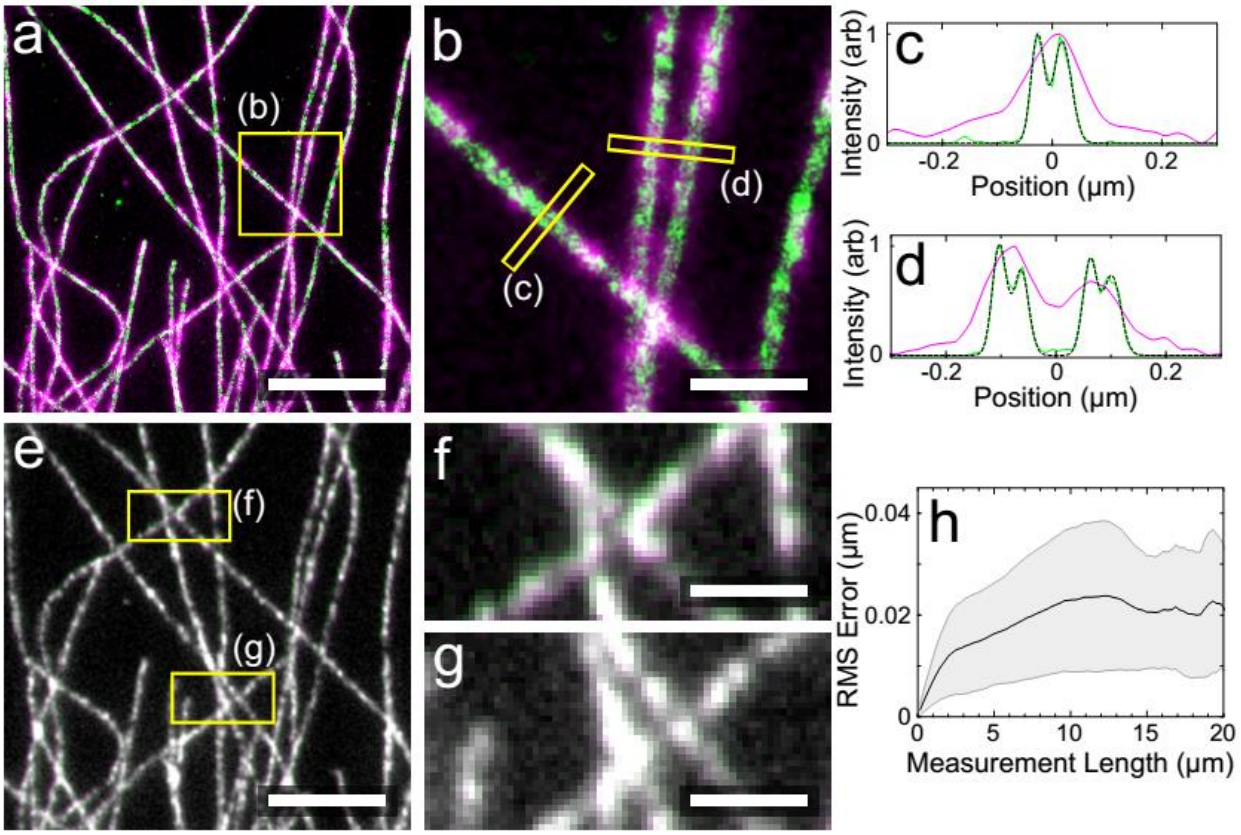

Supplementary Figure 2.5 | Comparison of pre-expansion image measured by localization microscopy and post-expansion image measured by epifluorescence microscopy for a BS-C-1 cell immunostained with conventional antibodies and treated with GA prior to gelation. (**a**) Overlay of pre-expansion image (green) and post-expansion image (magenta) after alignment of the post-expansion image using similarity registration. (**b**) Zoom-in of boxed region in **a** showing close agreement between localization microscopy image and expansion microscopy image. (**c**, **d**) Line profiles of the boxed regions in **b**. (**e**) Overlay of post-expansion image before (magenta) and after (green) B-spline registration as described in **Supplementary Fig. 2.3**. (**f**-**g**) Zoom-in images from boxed regions in **e** showing that distortions are generally very small. (**h**) RMS error vs length distortion analysis for data in **a** (see **Supplementary Fig. 2.3**). The plot in **h** was calculated from a 20 μm × 20 μm data set; the image in **a** shows an 8 μm × 8 μm zoom-in of the data set. All distances and scale bars correspond to pre-expansion dimensions. Scale bars, (**a**, **e**) 2 μm, (**b**) 500 nm, (**f**, **g**) 250 nm.

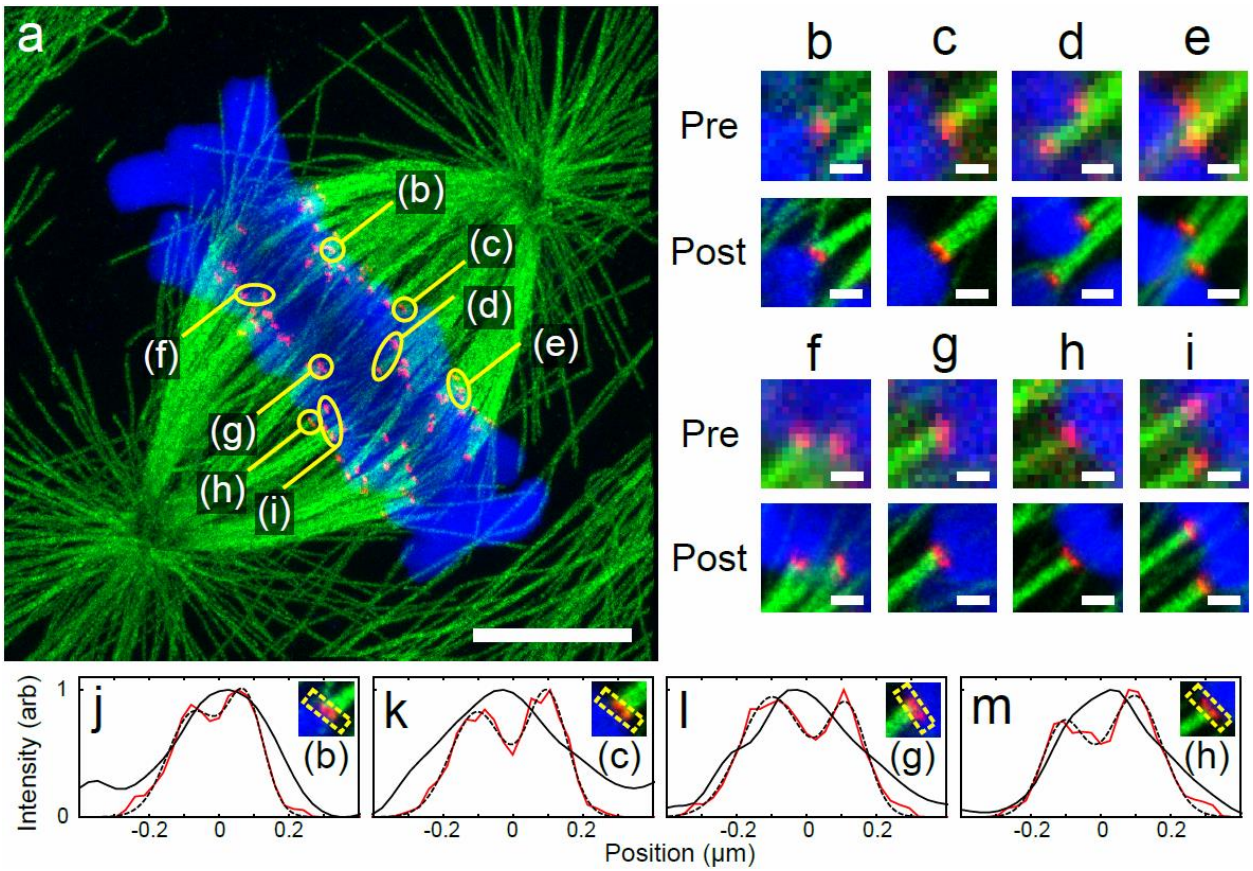

Supplementary Figure 2.6 | Comparison of attachments of kinetochore fibers (K-fibers) and chromosomes for mitotic cell from **Fig. 2.2 e**-**j**. (**a**) Maximum intensity projection of a post-expansion image of a dividing PtK1 cell that was immunostained against tyrosinated tubulin (green) and HEC1 (red) using conventional Atto 488 and dually labeled Alexa Fluor 546 and biotin secondary antibodies, respectively, and stained for DNA using TO-PRO-3 (blue). (**b**-**i**) Comparison of pre-expansion images of kinetochore attachments with corresponding post-expansion images, both imaged by confocal microscopy in z-sections from 400-800 nm thickness. (**j**-**m**) A subset of attachments showed double-peaked signals that were not resolvable in the pre-expansion images. Cross-sectional profiles of HEC1 signal from **b**, **c**, **g**, and **h**, for pre-expansion images (solid black), post-expansion images (red), and a double-Gaussian fit to the post-expansion signals (dashed black lines). Double peaks are separated by 149 nm, 201 nm, 214 nm, and 204 nm, respectively. All distances and scale bars correspond to pre-expansion dimensions. Scale bars, (**a**) 5 μm, (**b**-**i**) 500 nm.

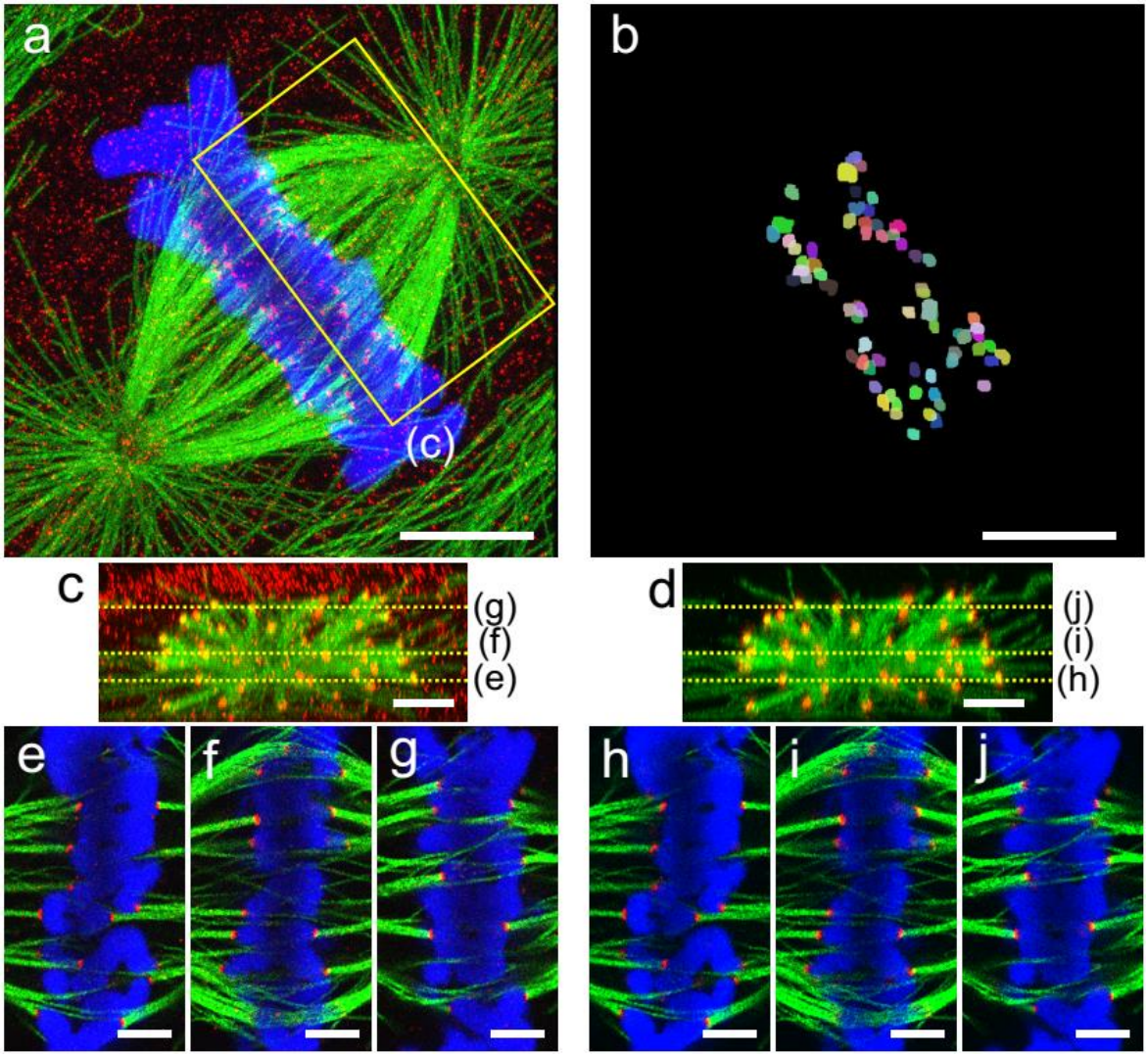

Supplementary Figure 2.7 | Image processing on post-expansion mitotic spindle data. Unprocessed confocal maximum intensity projection (**a**) of mitotic cell from **Fig. 2.2** and binarized kinetochore mask (**b**) resulting from image filtering (see **section 2.6** for additional details). Cross-sectional maximum intensity projection of boxed area in **a** showing non-specific adsorption of the HEC1 antibody (red) to the cell periphery (**c**) and processed cross-section (**d**). Unprocessed (**e-g**) versus processed (**h-j**) single z-section (~225 nm thickness) showing that kinetochore attachments are retained after processing. All distances and scale bars correspond to pre-expansion dimensions. Scale bars, (**a, b**) 5 µm, (**c**-**j**) 2 µm.

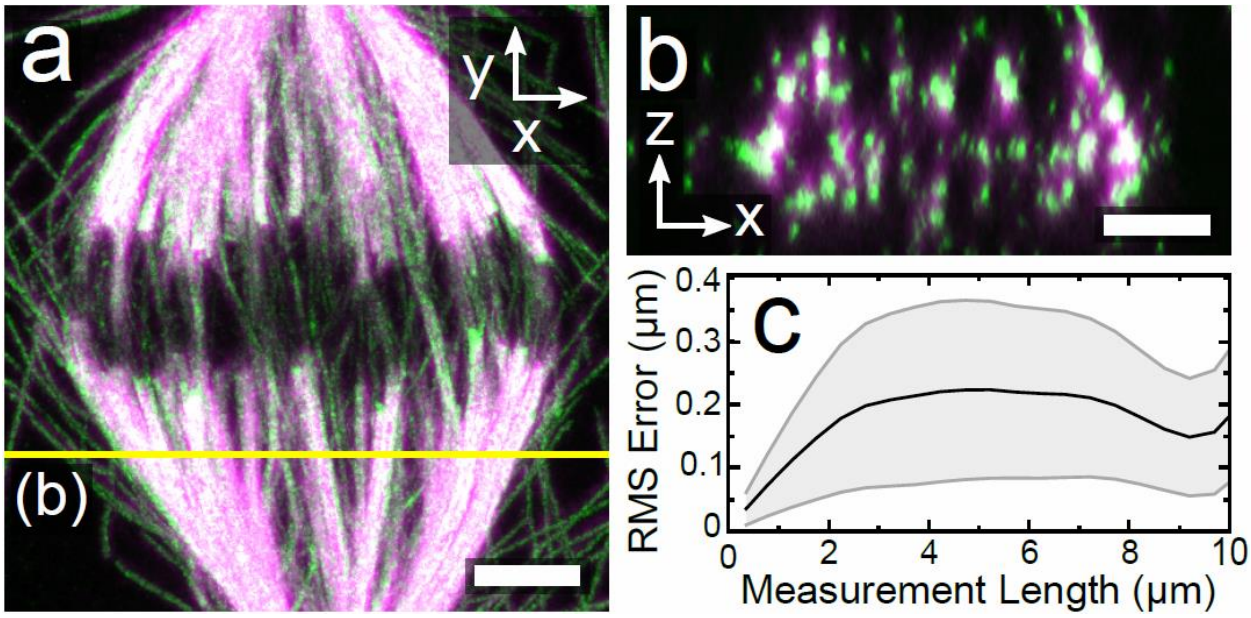

Supplementary Figure 2.8 | Comparison of pre-expansion and post-expansion images recorded by confocal fluorescence microscopy for immunostained mitotic PtK1 cell (data from **Fig. 2.2**, only tubulin channel). (**a**) XY maximum intensity projection overlay of pre-expansion (magenta) and post-expansion (green) images after alignment using three-dimensional similarity registration. (**b**) XZ maximum intensity projection along yellow line in **a**. (**c**) RMS error vs length distortion analysis in three dimensions (see **Supplementary Fig. 2.3**). Scale bars 2 µm. All distances and scale bars correspond to pre-expansion dimensions.

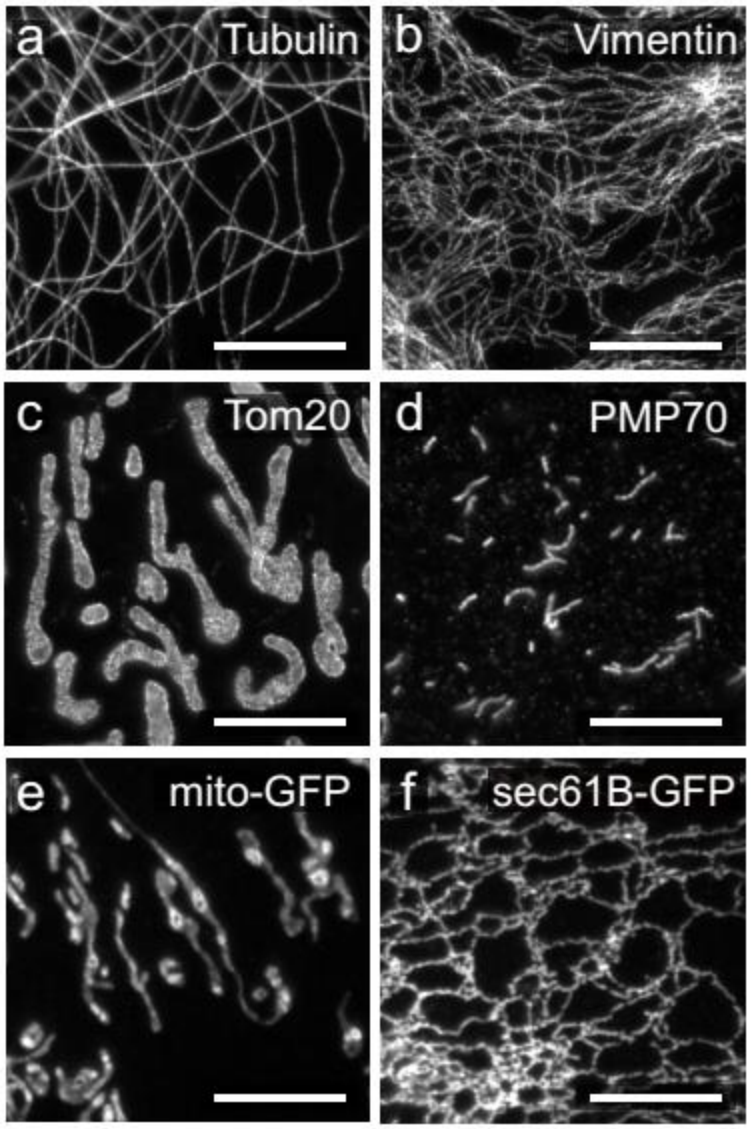

Supplementary Figure 2.9 | Gallery of expanded cellular structures. Epifluorescence images of expanded BS-C-1 cells indirectly immunostained with Atto 488 against (**a**) tyrosinated tubulin, (**b**) vimentin, (**c**) TOM20 (outer mitochondrial membrane), (**d**) PMP70 (peroxisomal membrane protein), (**e**) mito-GFP (inner mitochondrial membrane marker) and (**f**) Sec61β-GFP (endoplasmic reticulum marker) and treated with GA. Scale bars are 4.8 µm and are all in pre-expansion dimensions.

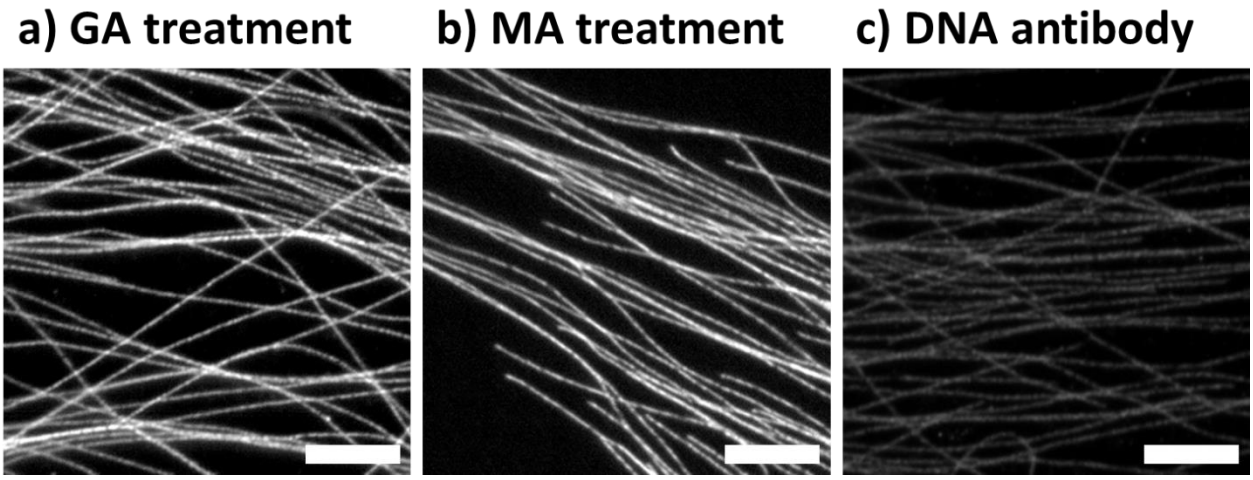

Supplementary Figure 2.10 | Epifluorescence images of expanded BS-C-1 cells stained for tyrosinated tubulin using different procedures. In (**a**), fixed cells were immunostained using conventional fluorescently-labeled antibodies and then treated with GA. In (**b**), fixed cells were immunostained using conventional fluorescently-labeled antibodies and then treated MA-NHS prior to gelation. In (**c**), fixed cells were immunostained using DNA-labeled antibodies which we prepared according to the protocol published by Boyden and coworkers.[35] Image contrasts have been matched to show the relative brightness of the stain achieved in each case; the specimens treated with MA-NHS or GA were both approximately 3-4 times brighter than that of the specimen stained using the DNA-labeled antibody. We note that the number of fluorophores per antibody with the DNA-labeled antibodies was not reported in the original expansion publication and it is possible that an optimized DNA-labeled antibody could be brighter than the one we prepared here.[35] However, we believe the DNA-labeled antibodies would be unlikely to achieve brighter stains than conventional (directly) fluorescently-labeled antibodies due to the more than ten-fold difference in molecular weight between an individual fluorophore and a 20-mer single-stranded oligonucleotide. Scale bars are 2.4 μm and are all in pre-expansion dimensions.

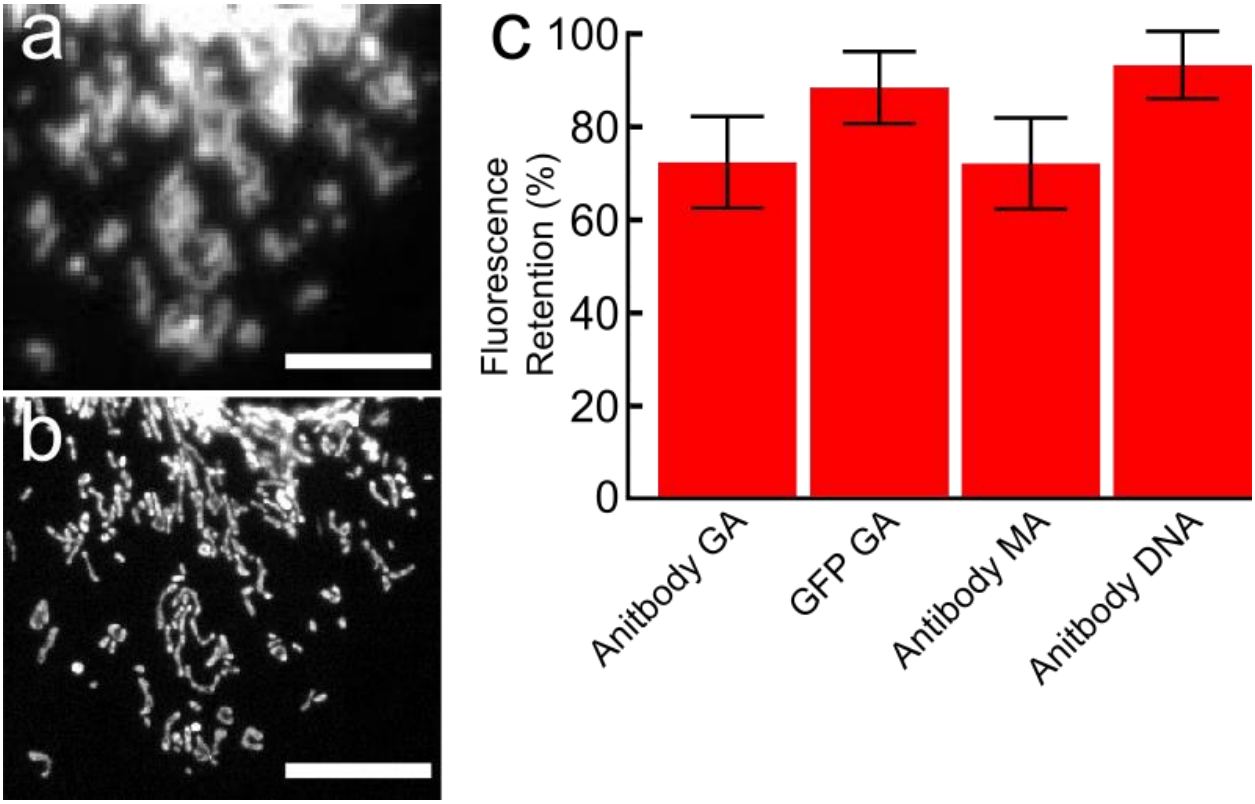

Supplementary Figure 2.11 | Determination of fluorescence retention for each method performed in this work using epifluorescence imaging. In each case, the total fluorescence of individual mitochondria was measured before and after expansion using a 20× 0.45 NA air objective. Fluorescence retention of GFP was measured using the inner mitochondrial membrane tag mito-GFP while all other methods used an outer mitochondria immunostain for TOM20 using Atto 488. (**a**) Pre-expansion image of a representative area used in the determination of GFP fluorescence retention. (**b**) Corresponding area in **a** after expansion. Scale bars are 10 µm in pre-expansion dimensions. (**c**) Bar graph of fluorescence retention for each method used in this work. Error bars represent the standard deviation in measured fluorescence retention (n=20).

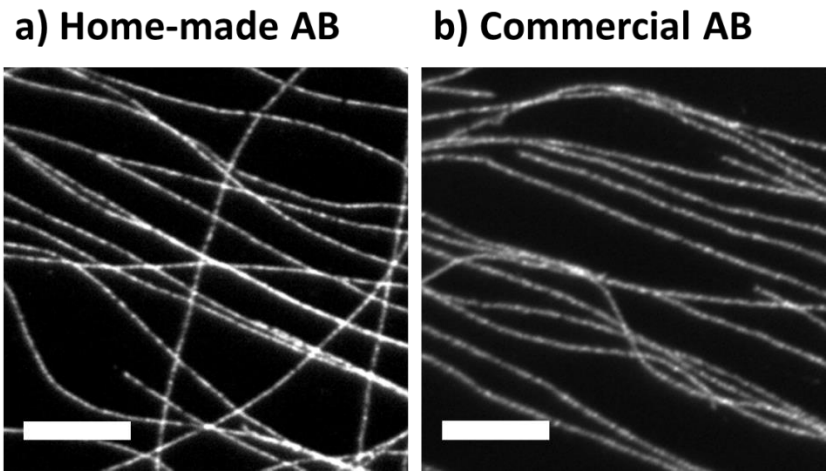

Supplementary Figure 2.12 | Epifluorescence images of expanded BS-C-1 cells prepared using the GA treatment method. Cells were indirectly immunostained for tyrosinated tubulin using either a homemade Atto 488 donkey anti-rat secondary antibody (**a**) or a commercially available Alexa Fluor 488 donkey anti-rat secondary antibody (**b**). Image contrasts were adjusted to be proportional to exposure time in order to show that the two stains are comparable in brightness. Scale bars are 2.4 µm and are all in pre-expansion dimensions.

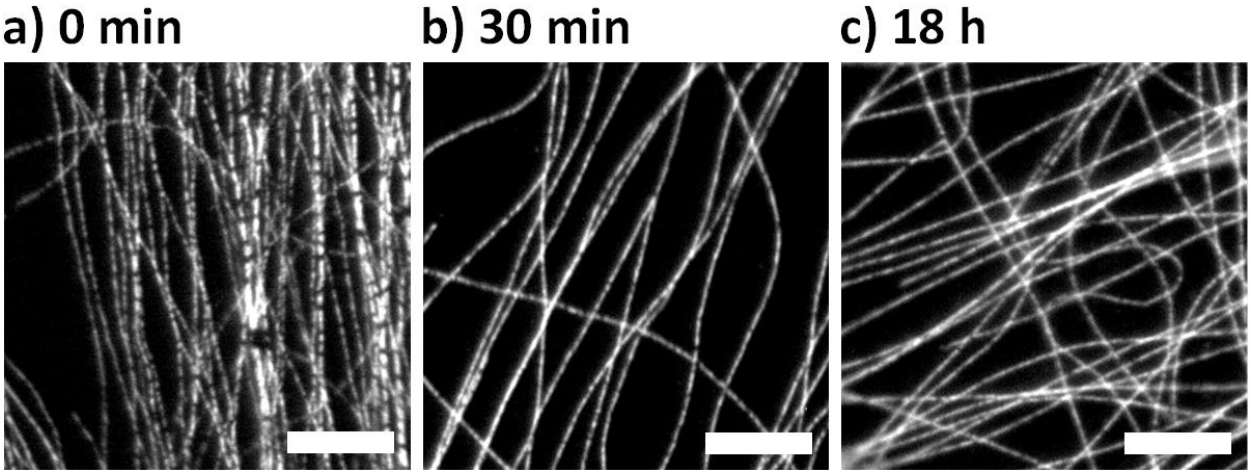

Supplementary Figure 2.13 | (**a-c**) Epifluorescence images of expanded BS-C-1 cells stained for tyrosinated tubulin, treated with GA, and digested for the period indicated. Digestion times shorter than 30 minutes show prominent distortions while these are largely absent for digestion times of 30 minutes or longer. Scale bars are 2.4 μm and are all in pre-expansion dimensions.

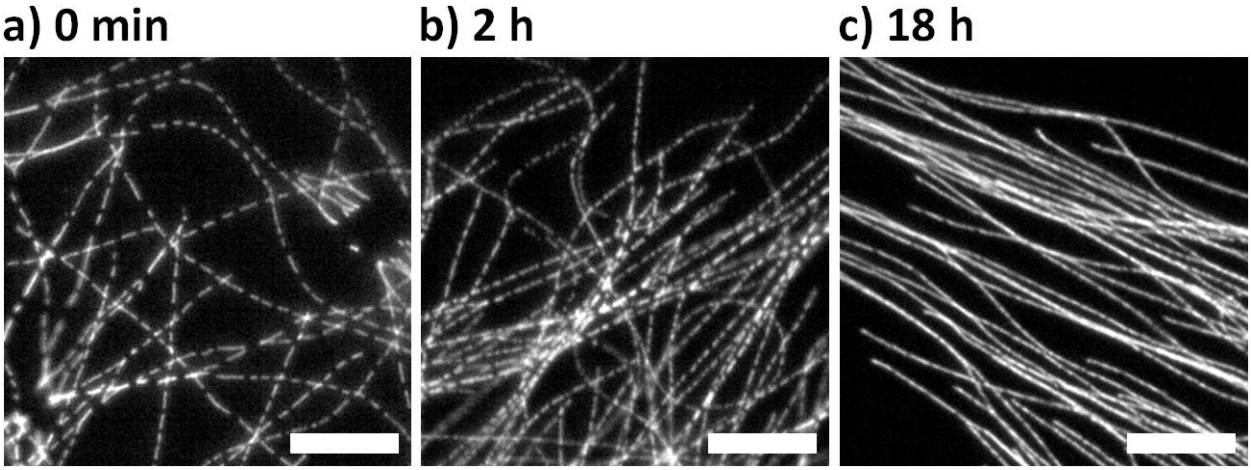

Supplementary Figure 2.14 | (**a-c**) Epifluorescence images of expanded BS-C-1 cells stained for tyrosinated tubulin, treated with MA-NHS, and digested for the period indicated. Digestion times of many hours were required to avoid prominent distortions. Scale bars are 2.4 μm and are all in pre-expansion dimensions.

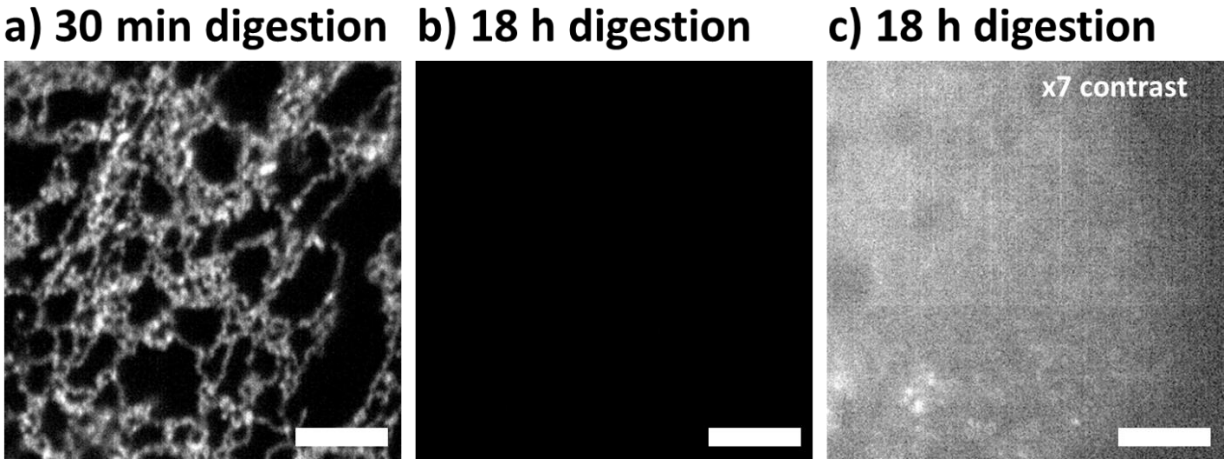

Supplementary Figure 2.15 | Epifluorescence images of expanded BS-C-1 cells expressing Sec61β-GFP and treated with GA during fixation; intrinsic GFP signal is only retained for short digestion times in cultured cells. In (**a**), the sample was digested for 30 min. In (**b**), the sample was digested for 18 h. The images in **a** and **b** were acquired under identical illumination conditions, exposure durations, and are displayed with the same contrast. Panel (**c**) is the same image as in **b** but with 7× contrast to show weak residual fluorescence. Scale bars are 2.4 μm and are all in pre-expansion dimensions.

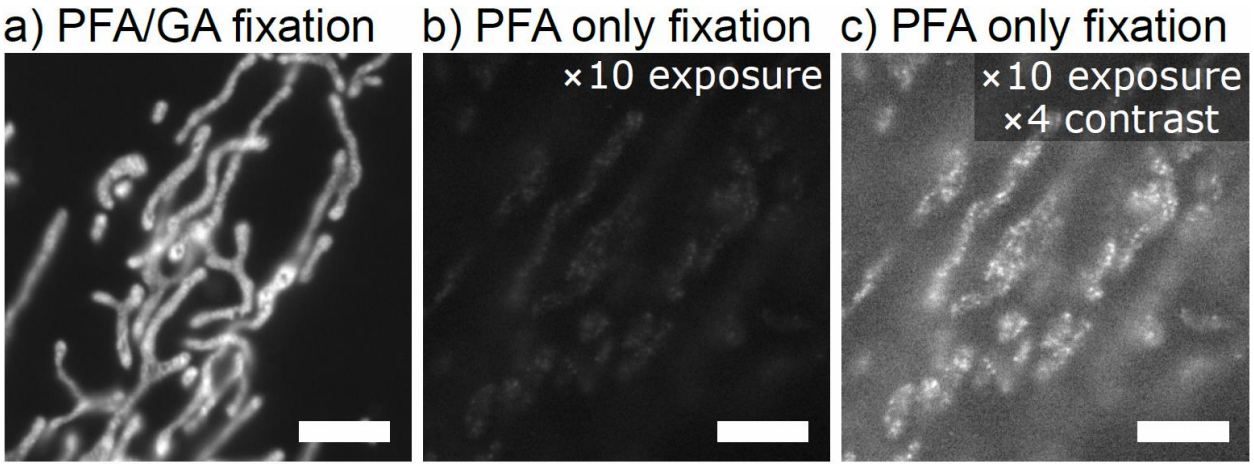

Supplementary Figure 2.16 | Epifluorescence images of expanded BS-C-1 cells expressing mito-GFP and digested for 30 minutes; intrinsic GFP signal is only retained for GA-treated cells. **a**) Treatment with a mixture of PFA/GA (paraformaldehyde and glutaraldehyde) during fixation retains intrinsic fluorescence from mito-GFP, whereas **b**) treatment with only PFA does not. Both specimens were subjected to a digestion time of 30 min. Panels **a** and **b** are displayed at the same contrast although panel **b** was recorded with ten times the exposure duration. **c**) Adjustment of the contrast of the image in **b** allows observation of dim residual signal. Scale bars are 2.4 µm and are all in pre-expansion dimensions.

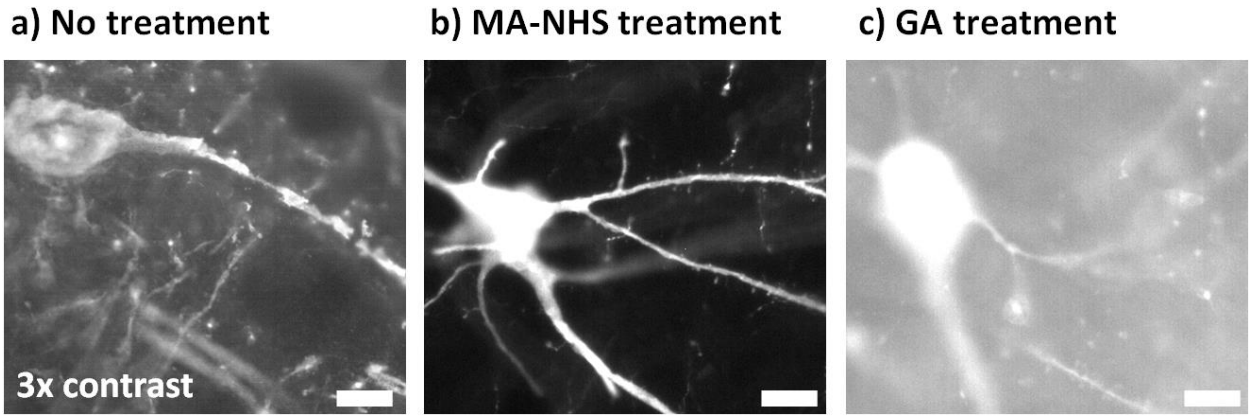

Supplementary Figure 2.17 | Epifluorescence images of expanded 100 µm thick THY1-YFP-H mouse brain slices immunostained for YFP and subjected to various post-stain treatments. (**a**) No treatment leads to low signal intensity and patchy preservation of signal along structure. (**b**) Treatment with MA-NHS after immunostaining led to higher signal levels with good retention along the original structures. (**c**) Treatment with GA after immunostaining resulted in high background signal. The three images were acquired using identical illumination and exposure; the images in **b** and **c** are displayed at the same contrast, while **a** is displayed with 3× contrast to show details within the comparably dim image. Due to the comparably long (~12 hour) digestion used here, there should be a negligibly small amount of intrinsic YFP signal remaining, in comparison to the data in **Supplementary Fig. 2.20** which show weak residual YFP signal after a 60 min digestion. Scale bars are 12 µm and are all in pre-expansion dimensions.

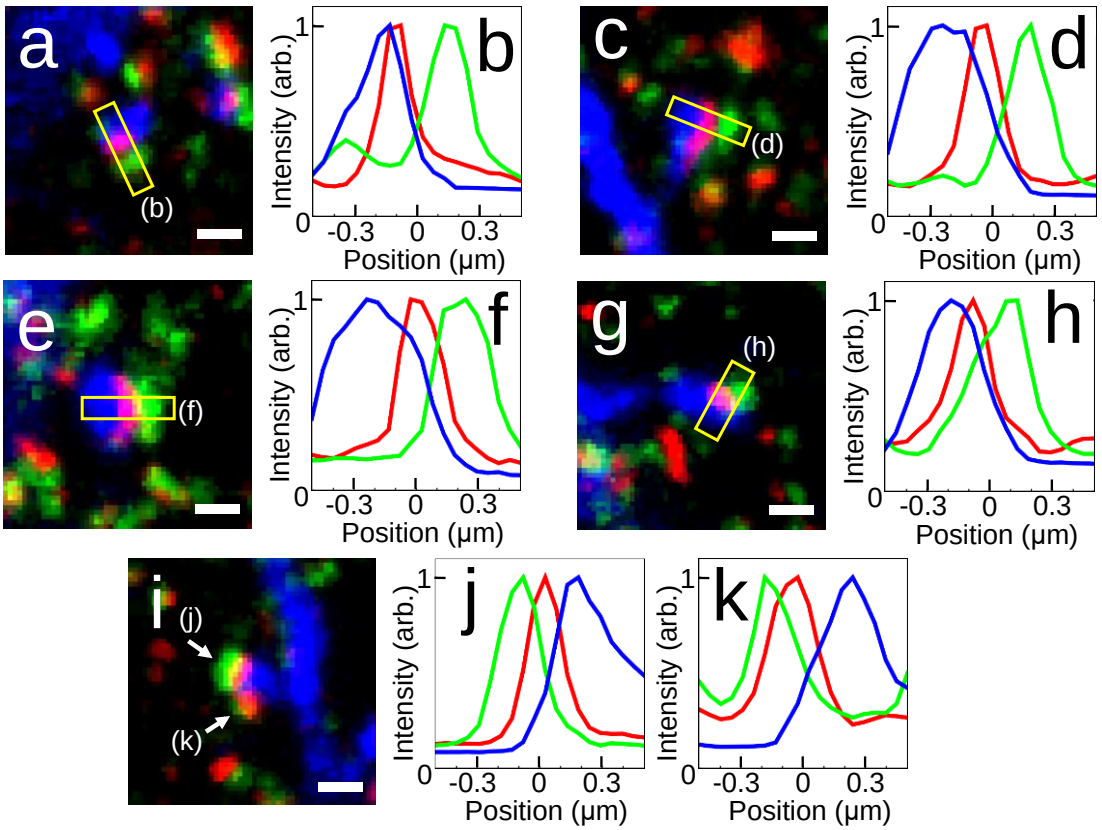

Supplementary Figure 2.18 | Gallery of expanded synapses in mouse brain tissue. Maximum intensity projections (**a, c, e, g, i**) of expanded THY1-YFP-H mouse brain tissue indirectly immunostained for YFP (blue, Atto 488), Bassoon (green, Atto 565), and Homer (red, Atto 647N) along with corresponding cross-sectional profiles of the indicated individual synapses (**b**, **d**, **f**, **h**, **j**, **k**). In each case, the pre- and postsynaptic densities are clearly resolvable and align well with dendritic spines. In **i**, two separate synapses are shown connecting to a single dendritic spine (cross-sectional profiles indicated with arrows). All distances and scale bars correspond to pre-expansion dimensions. Scale bars are 500 nm.

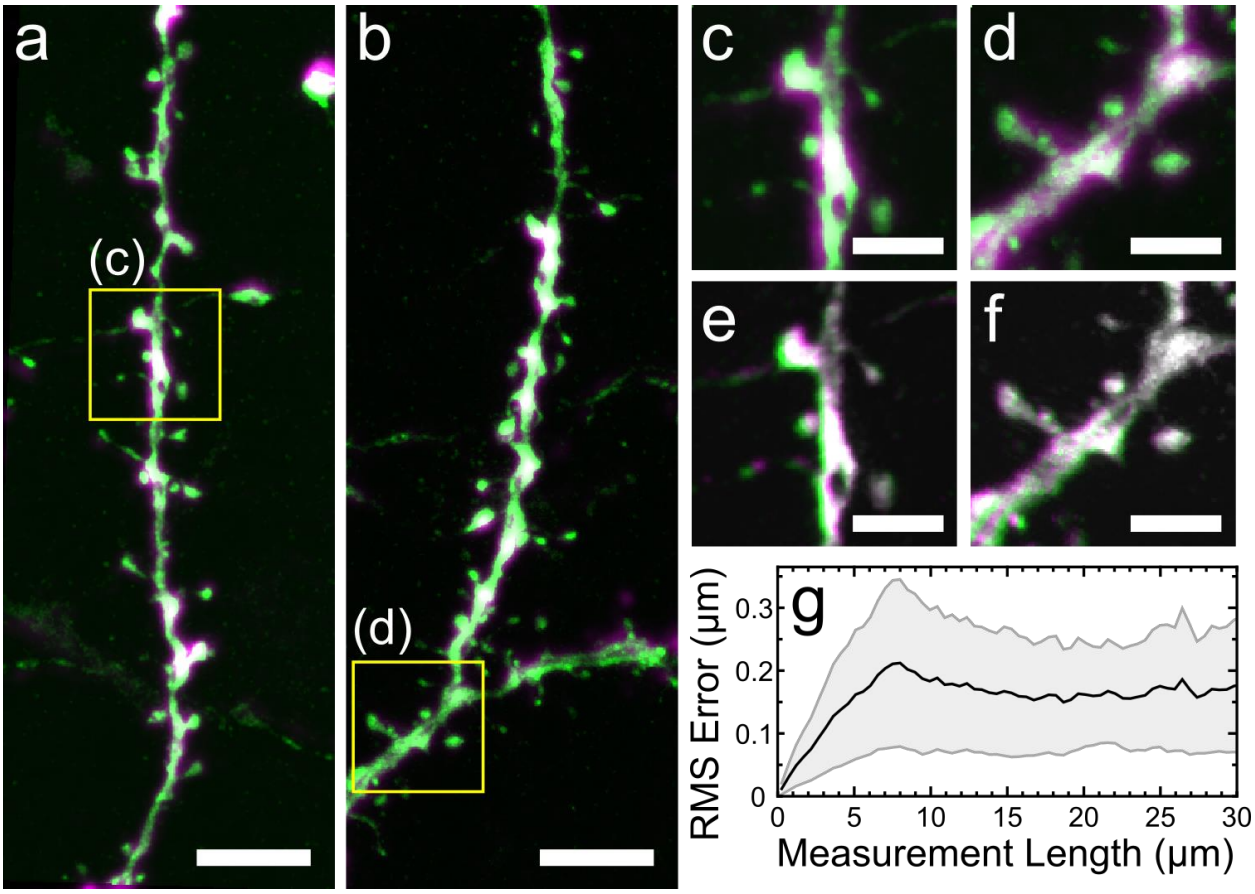

Supplementary Figure 2.19 | Comparison of pre-expansion and post-expansion images recorded by confocal fluorescence microscopy for a 100 µm thick THY1-YFP-H mouse brain slices immunostained for YFP. (**a, b**) Large area overlay of pre-expansion image (magenta) and post-expansion image (green) after alignment of the post-expansion image using similarity registration. (**c, d**) Overlay pre-expansion image (magenta) and post-expansion image (green) using similarity transformation in a local region. (**e**, **f**) Overlay of post-expansion images from before (magenta) and after (green) B-spline registration as described in **Supplementary Fig. 2.3**. (**g**) RMS error vs length distortion analysis for data in **a** and **b** (see **Supplementary Fig. 2.3**). All distances and scale bars correspond to pre-expansion dimensions. Scale bars (**a, b**) 10 µm, (**c, d, e, f**) 5 µm.

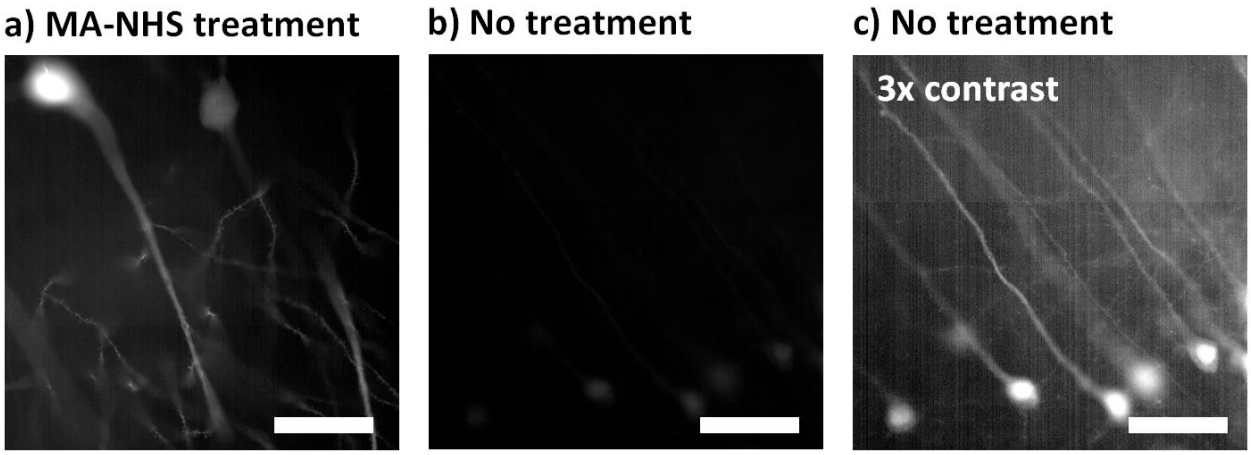

Supplementary Figure 2.20 | Epifluorescence images of 100 µm thick THY1-YFP-H mouse brain slices treated with either MA-NHS or nothing prior to gelation, a brief (60 min) digestion, and expansion. While both specimens expanded well, the MA-NHS treated brain slice in (**a**) showed much higher intrinsic YFP signal than the non-treated brain slice shown in (**b**). The images in **a** and **b** were acquired with identical illumination and exposure and are displayed with the same contrast settings. The image in (**c**) is a duplicate of that in **b** but is displayed with 3x contrast. Note that use of a long digestion time (>12 hours) led to essentially zero detectable signal (data not shown). Scale bars are 30 µm (pre-expansion dimensions).

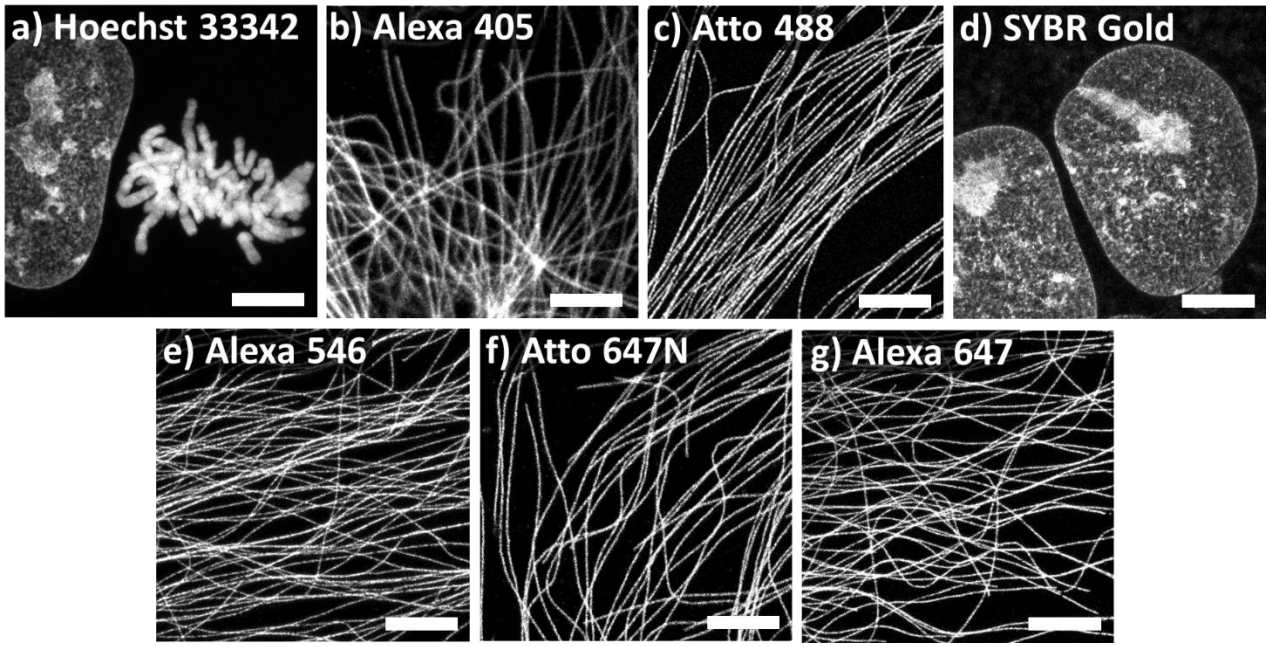

Supplementary Figure 2.21 | Confocal fluorescence maximum intensity projections of expanded BS-C-1 cells stained for DNA or immunostained against tyrosinated tubulin using various secondary antibodies and treated with GA prior to gelation. In panels **b**, **c**, **e**, and **f**, conventional secondary antibodies were used that were directly labeled with the indicated fluorophore. Panels **a** and **d** were stained for nuclear DNA using the corresponding dye without subsequent GA treatment. In **g**, a biotinylated secondary antibody was used prior to treatment with GA; after expansion the sample was incubated with Alexa Fluor 647 labeled streptavidin. Post-expansion labeling offers a way to introduce fluorophores to the sample that would otherwise not survive the polymerization step such as Alexa Fluor 647 and other cyanines.[35] Scale bars are 3.75 µm and are all in pre-expansion dimensions.

Supplementary Video 2.1 | 3D animation of expanded brain slice shown in **Fig. 2.3**. The animation begins as 29 × 13 µm and then zooms to show a view of 4.6 × 2.7 µm (all distances are in pre-expansion dimensions)**.**

Supplementary Table 2.1 | Summary of sample preparation and imaging conditions.

Figure	Specimen	Fixation	1° Ab all 1-2 µg/mL	2° Ab, etc., & dyes/protein 1-2.5 µg/mL, except as indicated	Polymer-linking	Digestion time & other notes	Imaging Image thicknesses in pre-expansion dimensions
2.2 a-c	BS-C-1 cell, wildtype	Extracted, then PFA/GA	Rat × Tub & Rb × dTub	D × Rat Atto 488 (~5.6 d/p) & D × Rb Alexa 546 (~12 d/p)	25 mM MA-NHS, 60 min	Overnight	Confocal, 63× 1.2NA water lens Image thicknesses: **a**) 900/200 nm; **b**) 900 nm; **c**) 225 nm
2.2 e-j, Supp. Fig. 2.6, 2.7, 2.8	PtK1 cell, wildtype	Extracted, then PFA/GA	Rat × Tub & Ms × HEC1	D × Rat Atto 488 (~7.1 d/p) & D × Ms Alexa 546 (~5 d/p) +biotin	0.25% GA 10 min	Overnight digestion; post-expansion incubation with streptavidin Alexa 546 (2 µg/mL, ~7 d/p) and TO-PRO-3 (1 µM)	Confocal, 63× 1.2NA water lens. Image thicknesses: **2.2e**,**f**) 5.6 µm; **2.2g**) 900 nm; **2.2h**) 420 nm; **S2.6**) ~800 nm; **S2.7a**) 5.6 µm; **S2.7e-j**) 225 nm; **S2.8a**) 5.6 µm; **S2.8b**) 130 nm.
2.2 k-l	BS-C-1 cell expressing Sec61β-GFP & mito-DsRed	PFA/GA, 37 °C	Rb × TOM20	D × Rb Atto 647 N (~2.7 d/p)	0.25% GA 10 min	30 min	Confocal, 63× 1.2NA water lens. Detected intrinsic GFP & YFP signal as well as signal from Atto 647N stain. Image thicknesses: **k**) 1 µm; **l**) 225 nm
Supp. Fig. 2.1	BS-C-1 cells, wildtype	Extracted, then PFA/GA	Rat × Tub	D × Rb Atto 488 (9-12 d/p)	**a**) no treatment **b**)25 mM MA-NHS 60 min **c**) 0.25% GA 10 min	Overnight	Epifluorescence, 60× 1.2NA water lens
Supp. Fig. 2.2	BS-C-1 cells, wildtype	Extracted, then PFA/GA	Rat × Tub	D × Rat Atto 488 (~5.6 d/p)	**a**) 0.25% GA 10 min **c**) 25 mM MA-NHS 60 min	Overnight	Confocal, 63× 1.2NA water lens. Image thickness ~225 nm
Supp. Fig. 2.3	BS-C-1 cell, wildtype	Extracted, then PFA/GA	Rat × Tub	D × Rat Atto 488 (~5.6 d/p)	25 mM MA-NHS, 60 min	Overnight	Confocal, 63× 1.2 NA water lens. Image thickness ~225 nm
Supp. Fig. 2.4	BS-C-1 cell, wildtype	Extracted, then PFA/GA	Rat × Tub	D × Rat DNA		Overnight	
Supp. Fig. 2.5	BS-C-1 cell, wildtype	Extracted, then PFA/GA	Rat × Tub	Ms × Rat Alexa 647 (~5.3 d/p) 3° Ab D × Ms Atto 488 (~6 d/p)	0.25% GA 10 min	Overnight	Pre-expansion localization microscopy with 100× 1.45NA TIRF lens; post-expansion imaging by epifluorescence with 60× 1.2NA water lens
Supp. Fig. 2.9	BS-C-1 cells: **a-d**) wildtype; expressing **e**) mito-GFP or **f**) Sec61β-GFP	**a-b**) extracted, fixed with PFA/GA **c-f**) not extracted, fixed with PFA/GA	**a**) Rat × Tub **b**) Ms × Vim **c**) Rb × TOM20 **d**) Rb × PMP70 **e,f**) Rb × GFP	**a**) D × Rat Atto 488 (4-6 d/p) **b**) D × Ms Atto 488 (4-6 d/p) **c**) D × Rb Atto 488 (4-6 d/p) **d**) D × Rb Atto 488 (4-6 d/p) **e,f**) D × Rb Atto 488 (4-6 d/p)	0.25% GA 10 min	Overnight	Epifluorescence, 60× 1.2NA water lens
Supp. Fig. 2.10	BS-C-1 cells, wildtype	Extracted, then PFA/GA	Rat × Tub	**a-b**) D × Rat Atto 488 (~8 d/p) **c**) D x Rat DNA (2.25 µg/mL) + 1 µM acrydite-DNA-Atto 488	**a**) 0.25% GA 10 min **b**)25 mM MA-NHS 60 min **c**) no post-stain linking	Overnight	Epifluorescence, 60× 1.2NA water lens
Supp. Fig. 2.11	BS-C-1 cells, wildtype and expressing mito-GFP	Not extracted, fixed with PFA/GA	Rb × TOM20 for antibody measurements	D × Rb Atto 488 (~8 d/p) D × Rb DNA (2.25 µg/mL) + 1 µM acrydite-DNA-Atto 488	Either 0.25% GA 10 min, 25 mM MA-NHS 60 min, or no post-stain linking (DNA)	Both GA: 30 min Antibody MA and DNA: overnight	Epifluorescence, 20× 0.45 NA air lens. Detected antibody or intrinsic GFP signal as indicated.
Supp. Fig. 2.12	BS-C-1 cells, wildtype	Extracted, then PFA/GA	Rat × Tub	**a**) D × Rat Atto 488 (~8 d/p) **b**) D × Rat Alexa 488 (~8 d/p, commercial)	0.25% GA 10 min	Overnight	Epifluorescence, 60× 1.2NA water lens
Supp. Fig. 2.13	BS-C-1 cells, wildtype	Extracted, then PFA/GA	Rat × Tub	D × Rat Atto 488 (~8 d/p)	0.25% GA 10 min	**a**) No digestion, **b**) 30 min, **c**) 18 h	Epifluorescence, 60× 1.2NA water lens
Supp. Fig. 2.14	BS-C-1 cells, wildtype	Extracted, then PFA/GA	Rat × Tub	D × Rat Atto 488 (~8 d/p)	25 mM MA-NHS 60 min	**a**) No digestion, **b**) 2h, **c**) 18 h	Epifluorescence, 60× 1.2NA water lens
Supp. Fig. 2.15	BS-C-1 cells expressing Sec61β-GFP	PFA/GA, 37 °C	--	--	Initial fixation included 0.1% GA for 10 min	**a**) 30 min, **b**,**c**) 18 h	Epifluorescence, 60× 1.2NA water lens. Detected intrinsic GFP signal.
Supp. Fig. 2.16	BS-C-1 cells expressing mito-GFP	**a**) PFA/GA **b,c**) PFA	--	--	Initial fixation included 0.1% GA for 10 min	30 min	Epifluorescence, 60× 1.2NA water lens. Detected intrinsic GFP signal.
2.3 a-f	THY1-YFP-H mouse brain, 100 µm slice	Cardiac perfusion with PFA, then 1 h PFA after slicing	Ch × GFP Rb × Homer Ms × Bassoon	**a**) D × Ch Atto 488 (~6 d/p) **b**) D × Rb Atto 647N (~2.7 d/p) **c**) D × Ms Atto 565 (~5.2 d/p)	1 mM MA-NHS 60 min	Digestion: overnight	Confocal, 25× 1.0 NA water SCALE lens. Image thicknesses: **a**) ~1.2 µm (single z-plane); **b**) ~3.8 µm; **c**-**d**) ~1.2 µm (single z-plane); **e**, **f**) 1.4 µm.
2.3 i-j	THY1-YFP-H mouse brain, 100 µm slice	Cardiac perfusion with PFA, then 1 h PFA after slicing	--	--	1 mM MA-NHS 60 min	60 min	Epifluorescence, 20× 0.45NA air lens
Supp. Fig. 2.17	THY1-YFP-H mouse	Cardiac perfusion with PFA, then 1 h PFA after slicing	Rb × GFP	D × Rb Atto 488 (~9 d/p)	**a**) 1 mM MA-NHS 60 min **b**) 0.1% GA 10 min	Overnight	Epifluorescence, 10× 0.25 NA air lens
Supp. Fig. 2.18, Supp. Vid. 2.1	THY1-YFP-H mouse	Cardiac perfusion with PFA, then 1 h PFA after slicing	Ch × GFP Rb × Homer Ms × Bassoon	**a**) D × Ch Atto 488 (~6 d/p) **b**) D × Rb Atto 647N (~2.7 d/p) **c**) D × Ms Atto 565 (~5.2 d/p)	1 mM MA-NHS 60 min	Digestion: overnight	Confocal, 25 × 1.0 NA water lens. Image thicknesses: **a**) 0.8 µm; **c**) 1.6 µm; **e**) 1.8 µm; **g**) 2 µm; **i**) 2.2 µm.
Supp. Fig. 2.19	THY1-YFP-H mouse	Cardiac perfusion with PFA, then 1 h PFA after slicing	Ch × GFP Rb × Homer Ms × Bassoon	**a**) D × Ch Atto 488 (~6 d/p) **b**) D × Rb Atto 647N (~2.7 d/p) **c**) D × Ms Atto 565 (~5.2 d/p)	1 mM MA-NHS 60 min	Digestion: overnight	Confocal, 25 × 1.0 NA water lens. Image thicknesses: 13.2 µm
Supp. Fig. 2.20	THY1-YFP-H mouse	Cardiac perfusion with PFA, then 1 h PFA after slicing	--	--	**a)** 1 mM MA-NHS 60 min **b)** No treatment	Digestion: overnight	Epifluorescence, 20× 0.45 NA air lens. Detected intrinsic YFP signal.
Supp. Fig. 2.21	BS-C-1 cells, wildtype	Extracted, then PFA/GA	Rat × Tub for tubulin stains only	**a**) Hoechst (2 drops/mL) **b**) D × Rat Alexa 405 (~3 d/p) **c**) D ×Rat Atto 488 (~10 d/p) **d**) SYBR Gold (10×) **e**) D × Rat Alexa 546 (~10 d/p) **f**) D × Rat Atto 647N (~5.5 d/p) **g**) D × Rat Biotin	**a-e**) 0.25% GA 10 min	**a-f**) Overnight digestion **g**) 1 h digestion. Post-expansion with streptavidin Alexa 647 (3 dyes/SA, 2 µg/mL)	Confocal, 63× 1.2 NA water lens. Image thicknesses: tubulin, 225 nm; nuclei, 7 µm.

2.10 Supplementary Protocols

2.10.1 Quantitative Distortion Analysis of Pre- and Post-Expansion Images

In this manuscript we used the open-source software *Elastix* for analysis of correlated pre- and post-expansion images in order to calculate the physical magnification (referred to as the expansion factor in the main text) and to perform analysis of expansion-related distortions.[66] The output from *Elastix* was further processed using custom-written Mathematica scripts. In this supplementary protocol we provide detailed instructions on how to perform these analyses for a computer based on a Microsoft Windows operating system. This protocol also makes use of the widely used open-source ImageJ-based software package *Fiji.*

This supplementary protocol is accompanied by the file "SupplementaryAnalysis.zip". The .zip file contains three subfolders: "original_data" contains original confocal data files for corresponding pre-expansion and post-expansion images; "similarity_example" contains input files for rigid registration analysis using *Elastix*; "spline_example" contains input files for distortion analysis with *Elastix* that are derived from the output of the similarity analysis. The spline_example folder also contains a Mathematica script file (.nb) for processing of the *Elastix* B-spline output file for distortion analysis.

Elastix Installation

The open-source software *Elastix* was used for rigid (similarity) and nonrigid (B-spline) registration of correlated pre- and post-expansion images. *Elastix* may be downloaded from the program's website at http://elastix.isi.uu.nl. Once installed, add the installed *Elastix* directory to the system's PATH variable. *Elastix* is controlled through the Command Prompt, and the following font and gray background will be used to denote command line inputs: `command line inputs`. To check whether the installation was successful, open a Command Prompt and enter `elastix -help` to see the version and command options (an error is returned if the installation was unsuccessful or if *Elastix directory* has not been added to the PATH variable). For more detailed information on installation, information about image registration, and all further procedures, consult the *Elastix* manual found on the homepage. The *Elastix* parameter database also has helpful example parameter files for analysis (http://elastix.bigr.nl/wiki/index.php/Parameter_file_database).

Image Data Formatting Preparation

Elastix is based on the Image Registration and Segmentation Toolkit (ITK), and therefore all input/output image files must be compatible with ITK, such as .mhd or .mha files that store image data in uncompressed binary format. It is convenient to use other imaging applications such as *Fiji* (http://fiji.sc/Fiji)[67] to create or view these binary image files. To create binary image files for our sample pre-expansion data located in the original_data folder, perform the following

steps: 1) Load the example pre-expansion data file “Pre_ExM.tif” (a 128 × 128 pixel 16 bit TIFF) into *Fiji*; 2) Use bicubic interpolation to resample the image with 4× smaller pixels (Image → Scale… → X Scale = 4, Y Scale = 4), resulting in a 512 × 512 image, so that the pre-expansion data will have approximately the same scale as the post-expansion data; 3) Save the image as a binary file by selecting (File → Save As… → Raw Data…), and name it “fixed.raw”; 4) Manually create a “.mhd” metadata file (MetaImage medical data) that contains the information shown below. The binary image file and metadata files generated according to this procedure are included in the similarity_example folder as “fixed.raw” and “fixed.mdh”, respectively.

ObjectType = Image
NDims = 2
BinaryData = True
BinaryDataByteOrderMSB = True
ElementSpacing = 1 1
DimSize = 512 512
ElementType = MET_USHORT
ElementDataFile = fixed.raw

Follow a similar procedure to create a binary image file and metadata file for the example post-expansion image “Post_ExM.tif” (a 512 × 512 pixel 16 bit TIFF), but omitting the bicubic interpolation step. These binary image and metadata files are included in the similarity_example folder as “moving.raw” and “moving.mdh”, respectively.

Troubleshooting note regarding file formats: Depending on the software and/or computer preferences for byte order (i.e., “endianness”), the .mdh metadata parameter BinaryDataByteOrderMSB may need to be changed to either True or False in order to be loaded properly by *Elastix*. In *ImageJ* and *Fiji*, “Raw Data…” export should default to big-endian byte order and the BinaryDataByteOrderMSB option should be set to True in the .mhd file. Validate the byte ordering is correct by loading the “.mhd” file into *Fiji*; when correctly formatted, the original images should appear normally as shown in Appendix Figure 1a and b (i.e., not scrambled). The initial overlay should be roughly the same region and scaling as in Appendix Figure 1c).

General *Elastix* Usage: Similarity Transform

Elastix compares two input images, denoted the fixed image and the moving image, and will attempt to rigidly or nonrigidly transform the moving image so that it matches the fixed image file. Example files are provided in the similarity_example and spline_example folders. The example files in each folder include a fixed image, a moving image, the corresponding .mhd metadata files, and an *Elastix* parameter files.

In this example, we will use the parameter file "Parameters_Similarity.txt" provided in the example files. To run *Elastix*, open a Command Prompt inside the "similarity_example" folder by pressing together *Shift* + *Right Click,* selecting "*Open command window here*", and entering:

```
elastix -f fixed.mhd -m moving.mhd -p Parameters_Similarity.txt -out .
```

The *–f* and *–m* indicate the fixed and moving image ".mhd" input files, the *–p* indicates the parameters input file, and *–out* indicates where the output files will be written. The period (.) after *-out* is shorthand for the current directory of the command prompt, however any valid path will work. In general, use file names that do not contain spaces (underscores are acceptable), or alternatively enclose names or full file paths with quotation marks. After *Elastix* finishes running, an output binary image file "*result.0*" and its corresponding "*result.0.mhd*" file should be generated. Check the output image by dragging the "*result.0.mhd*" file into *Fiji*. Overlay the fixed and result.0 images to display the registration result, as displayed in Appendix Figure 1d. Note that signedness of the output (MET_SHORT) is different from the input (MET_USHORT) and is specified in corresponding .mhd files; however the output will be displayed correctly when opened with *FIJI.*

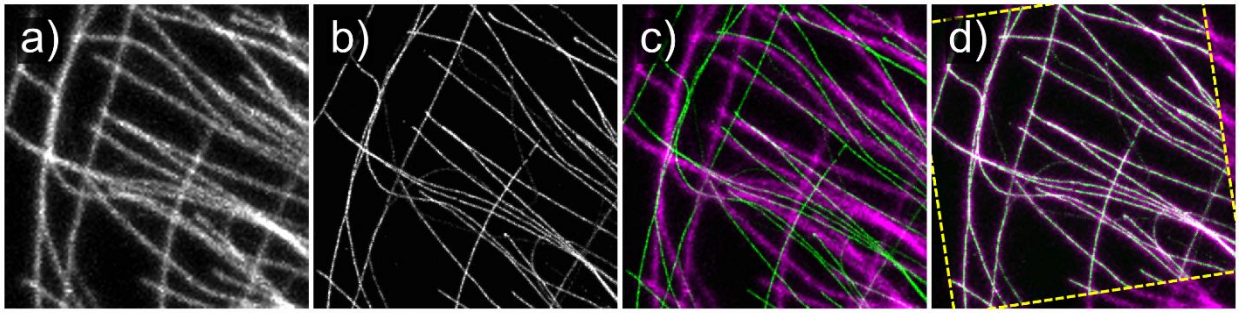

The "fixed" pre-expansion (**a**) and "moving" post-expansion (**b**) images to be registered by *Elastix*. The initial unregistered overlay (**c**) and overlay after *Elastix* similarity registration (**d**). The pre-expansion images are displayed in magenta and the post-expansion images in green. The dotted yellow lines in (**d**) outline the edges of the post-expansion image and have been added to emphasize the transformation.

Troubleshooting notes regarding Elastix command line usage. If *Elastix* does not run, observe the error output in the command window, or look for the "elastix.txt" output file, which should also contain the error. Common errors include incorrect input of file names into the command line, file names containing spaces, or an incorrect "ElementDataFile" name referencing the binary data in the .mhd file. Additionally, be wary of extra file extensions that may become appended (particularly in Windows), but appear hidden on the .raw and .mhd files, which will cause *Elastix* to respond with an error.

Expansion Factor Determination with *Elastix*

The similarity transformation (used in the previous example) attempts to match the moving image to the fixed image using only rotation, translation and isotropic scaling; and can therefore be used to calculate the isotropic expansion factor. In the previous example, the pre-expansion image was interpolated by a factor of 4; this factor was the estimated expansion factor determined macroscopically with a ruler (by measuring the size of the gel in millimeters before and after expansion). All ExM samples in this work had expansion factors ranging from 4.0-4.3, so a flat factor of 4 is a good initial guess for the similarity transform. Even this type of rough macroscopic measurement can yield results accurate to within 5-10% of the true expansion factor. Note, if the images were acquired with different pixel sizes (such as on a confocal microscope with adjustable magnification), it is convenient to first interpolate one of the images to match the smaller pixel size of the two; this is unnecessary if images were acquired with the same pixel size, such as on a CCD/CMOS array using the same objective lens. After successfully performing the similarity transform and ensuring proper registration of the two images, as in Appendix Figure 1d, look for the output text file named "TransformParameters.0.txt" which contains the following parameters of the similarity transform at the top of the document:

(Transform "SimilarityTransform")
(NumberOfParameters 4)
(TransformParameters 1.029177 0.163145 13.092766 17.873457)
(InitialTransformParametersFileName "NoInitialTransform")
(HowToCombineTransforms "Compose")

The key numbers are the TransformParameters, which represent the image scaling factor, rotation, translation in X, and translation in Y, respectively. The transformation is applied to the moving image (post-expansion image) and since the pre-expansion image was previously interpolated by the estimated factor of 4, this factor is multiplied by the scaling factor to get the true expansion factor: 4 × 1.03 = 4.12.

Troubleshooting Similarity Transform. If the similarity transformation does not return acceptable registration, it is useful to first try and select corresponding areas of the input pre-expansion and post-expansion images to be as close as possible by eye before running *Elastix*. This includes scaling by the estimated expansion factor (as described previously), as well matching the image orientations by rotating one of the images (In *Fiji,* Image → Transform → Rotate…). Additionally it is possible to tune the input parameter file "Parameters_Similarity.txt". Some useful parameters to consider are the (NumberofResolutions 8) or (MaximumNumberOfIterations 1000). *Elastix* will begin initial registration at a reduced image resolutions and increasing to full resolution, (by default each resolution to run is decreased by factor of 2), unless otherwise specified in the parameters file, and the

MaximumNumberOfIterations will allow for convergence during each resolution. These parameters are set initially at higher values for more robust registrion, however often times if the initial input images are similar, the number of resolutions and max iterations can be decreased to save computation time. Note that the similarity transform is a rigid transform, and only performs uniform scaling in X and Y, rotation and translation. If the scaling in X and Y are not uniform, which is typically not the case for ExM (unless for example, the gel is being stretched or imaging during pre- and post-expansion imaging was not performed on the same axis), it may be necessary to use an affine registration by changing the (Transform "Similarity") to (Transform "AffineTransform") in the parameters file.

Nonrigid B-spline Registration with *Elastix*

The similarity transform is a rigid registration and attempts to make a global best match, but correct for local deviations from the fixed image, making it necessary to apply a nonrigid bspline registration. Essentially, the output of the similarity transform is plugged back into *Elastix* as the moving image, and a second registration using B-spline parameters is used to correct for nonrigid deformations that may be present between the pre-expansion and post-expansion, similarity transformed output image. The data for this example is in the “spline_example” folder, and should contain a fixed and moving binary data files and corresponding .mhd files, as well as a “Parameters_BSpline.txt” file. Although the files are already included, the “moving” and “moving.mhd” are simply copies of “result.0” and “result.0.mhd” from the “similarity_example” folder, and renamed accordingly (it is important to change the ElementDataFile name in the .mhd as well). The Command Prompt input to run this parameter set in the spline_example folder is:

```
elastix -f fixed.mhd -m moving.mhd -p Parameters_BSpline.txt -out .
```

The resulting image “result.0” should show only minor deformation when overlayed with the input “moving” image. Further processing to create the deformation vector field plot and measurement RMS error plot using the output B-spline transformation parameters is possible using another program included in the *Elastix* installation called *Transformix*.

Vector Fields and RMS error Error using *Transformix* Output

Transformix is a complementary program to *Elastix* that is used to apply a deformation to an image, or a list of XY coordinates. The deformation information is contained within the “TransformParameters.0.txt” files. Here, *Transformix* is used to apply a deformation to a set of input points (an example of using *Transformix* on an image file is provided later). Due to the more advanced formatting, parsing and plotting requirements of the input and output data with *Transformix*, an example *Mathematica* notebook “Vector and RMS plot.nb” is included to

generate the deformation vector field plots, as well as measure the RMS error (as in **Supplemental Fig. 3**). The script is commented to contain instructions.

Briefly described here, to create the vector plot, the deformation field is applied to an input array of points sampled at a set interval, in this case every 10 pixels. *Transformix* is used deform these input points, and the deformation vector at each point is then used to make a plot of the deformation field. The Command Prompt input to run *Transformix* on set of input points is:

```
transformix -def inputPoints.txt -out . -tp TransformParameters.0.txt
```

The input points should be formatted as follows (see "inputPoints.txt" file in the spline_example folder):

Index
Total # of points
X1 Y1
X2 Y2
… …

To generate the measurement RMS error plots, a similar procedure to the vector plot is used, however the input points are the coordinates of a binary skeleton of the fixed image. In the script, the distance between a pair of points is calculated (m), as is the distance between the deformed coordinates (m', see **Supplemental Fig. 2.3**). The absolute value of the difference is the error. This is performed for all combinations of input coordinates in the image skeleton, and RMS error is calculated and plotted.

Gaussian Blurring of Post-ExM Images

For the sake of simplicity in the previous examples, the following steps on Gaussian blurring of the initial moving image were excluded from this protocol, but were carried out in analysis in the Supplemental Figures. When comparing the pre-expansion and post-expansion example images (in these examples, microtubules), there is a disparity in the microtubule width between the two, due to the increase in resolution in post-expansion space. To ensure that this width disparity does not affect the similarity or Bspline registration process, we first apply a Gaussian blur to the post-expansion image in *Fiji* (Process → Filters → Gaussian Blur… → Radius = 4) to make the microtubule widths roughly equivalent, then proceed with this blurred image as the moving image in similarity registration and subsequently, the blurred similarity output in the Bspline registration. Once the transformation parameters have been determined, the deformations can be applied to the original, unblurred image using *Transformix*. By using the following command:

```
transformix -in unblurred.mhd -out . -tp TransformParameters.0.txt
```

where the unblurred.mhd file corresponds to the original unblurred moving image, and "TransformParameters.0.txt" correspond to the similarity transform parameters output in the "similarity_example" folder. The *Transformix* output will be called "result" and "result.mhd"; these images are then plugged back into *Transformix* using the Bspline output parameters in the "spline_example" folder likewise.

3D Registration in *Elastix*

Rigid and nonrigid registration is easily extended into three dimensions using the earlier procedures with minor changes. Beginning from an image stack (assume a 512 × 512 × 128 pixel image) in *Fiji,* save the data as "Raw Data…" as done previously. The corresponding metadata .mhd must be modified to contain:

```
ObjectType = Image
NDims = 3
BinaryData = True
BinaryDataByteOrderMSB = True
ElementSpacing = 1 1 1
DimSize = 512 512 128
ElementType = MET_SHORT
ElementDataFile = moving.raw
```

The important fields to update are the NDims = 3, to denote three dimensional data, and DimSize with the appropriate image dimensions (in this case, the 128 refers to the number of z-planes). Again, it is helpful to check that the metadata file is correct by dragging it into *Fiji* and checking if the image opens correctly. Finally, change the *Elastix* parameter files ("Parameters_Similarity.txt" or "Parameters_Spline.txt") FixedImageDimension and MovingImageDimension fields to read:

```
(FixedImageDimension 3)
(MovingImageDimension 3)
```

Once these changes to the metadata and parameters files are made, *Elastix* can be called from the command line in the familiar manner.

Concluding Remarks

In general, due to the large amount of book-keeping involved for image, metadata and *Elastix* outputs files, we recommend running *Elastix* using a user preferred scripting language to automate the process, such as *Mathematica*, *MATLAB*, *Python*, etc. Many of these tools are already in existence, refer to Additional Tools on the Elastix Wiki (http://elastix.isi.uu.nl/wiki.php) or SimpleElastix (http://simpleelastix.github.io). This protocol and basic command line usage is meant to serve as a primer for using *Elastix* with correlative expansion microscopy.

2.10.2 ExM Protocol: Cultured Cells

BACKGROUND: This protocol is based off of methods used in the publication "Expansion microscopy with conventional antibodies and fluorescent proteins" (DOI: 10.1030/nmeth.3833) and is similar to the protocol[48] originally published by the group of Prof. Edward Boyden. **The following is meant for cultured cell expansion only.** Cells are assumed to be adhered to surface of #1.5 12 mm or 18 mm round coverslips.

REAGENTS:

1. Ammonium Persulfate (APS is a salt and initiates polymerization)
    a. Store at 4 °C
2. Tetramethylethylenediamine (TEMED is a liquid and catalyzes polymerization)
    a. Store at 4 °C
3. Methacrylic Acid-NHS (MA-NHS is a solid and is used to link proteins to the gel)
    a. Store the powder at 4 °C, KEEP AWAY FROM WATER
    b. Allow to warm to room temperature before opening to avoid condensation.
4. Glutaraldehyde (GA, a 50% solution, used to link proteins to the gel)
    a. Store aliquots at -20 °C
5. 40% Acrylamide (w/v) (Acrylamide is a liquid solution and is a monomer of the hydrogel)
    a. Store at 4 °C
6. 2% Bisacrylamide (w/v) (Bisacrylamide is a liquid solution and is a hydrogel crosslinker)
    a. Store at 4 °C
7. Sodium Acrylate (SA is an ionic monomer for the hydrogel)
    a. Store at room temperature, dry
8. Sodium Chloride (Salt)
9. 10x PBS Buffer
10. 10x TAE Buffer (Tris base, acetic acid, and EDTA)
11. 8 M Guanidine-HCl (component of digestion buffer)
12. Proteinase K (Digestion enzyme, 600-800 Units/mL in glycerol. We typically purchase stocks from NEB.)
    a. Store at -20 °C

STOCKS

1. APS: 10% (w/w) in water
    a. Store at -20 °C for up to 1 week
2. TEMED: 10% (v/v) in water
    a. Store at -20 °C for up to 1 week
3. MA-NHS: 1 M in anhydrous DMSO
    a. Store at -20 °C
    b. Keep away from water
4. Monomer Solution. Final concentrations are listed. Recipe achieves ~4x expansion. Bolded quantities in brackets, below, are for 10 mL of monomer solution.

a. 1x PBS **[1 mL]**
b. 2 M NaCl **[1.17 g]**
c. 8.625% (w/v) Sodium Acrylate **[0.863 g]**
d. 2.5% (w/v) Acrylamide **[0.625 mL]**
e. 0.15% (w/v) Bisacrylamide **[0.75 mL]**
f. Store at 4 °C for up to 1 month

5. Digestion Buffer. Bolded quantities in brackets, below, are for 10 mL of solution.
    a. 1x TAE Buffer **[1 mL]**
    b. 0.8 M Guanidine-HCl **[1 mL]**
    c. 0.5% Triton **[0.25 mL]**
    d. Store at 4 °C. Solution should be stable but we usually consume within a week.

POST-STAIN TREATMENT

1. After immunostaining the sample (or after expression of FP), treat with either 0.25% GA in PBS or 25 mM MA-NHS in PBS (diluted immediately before use from your concentrated DMSO stock). Because NHS compounds rapidly hydrolyze in water, do not make the NHS solution in PBS until you are ready to treat your sample.
    a. Note that if you want to preserve FP signal, you should use GA and NOT MA-NHS.
2. Allow the sample to react for ~30 min at room temperature (10 min is sufficient if using GA).
3. Wash the sample 2-3 times with several volumes of PBS.

GELATION

1. Incubate the samples in monomer solution ONLY for ~1 min (while you prepare the gelation solution).
2. Prepare the gelation solution. Quantities in brackets, below, are for a 100 µL volume. Note that APS should always be added last, right before adding to the specimen.
    a. 0.2% TEMED **[2 µL of 10% solution]**
    b. 96% monomer solution **[96 µL of monomer stock]**
    c. 0.2% APS **[2 µL of 10% solution]**
        i. This step may be sensitive to temperature. If gelation proceeds too quickly, drop to 0.1 % APS.
3. Quickly place 70-100 µL of the gelation solution on a hydrophobic surface (Teflon block or flat piece of parafilm) and place an inverted coverslip on top of the droplet (<u>cell side contacting the solution</u>).
    a. Polymerization occurs quickly so don't try to do all of your samples at the same time.
4. Allow polymerization reaction to proceed for ~30 min at room temperature.

DIGESTION

1. Gently remove the coverslip and gel from the hydrophobic surface.
2. Place the gel in a suitable container for digestion, e.g., a well of a 12-well plate.
    a. Keep in mind that the gels will expand slightly (~1.5x) during digestion so make sure the well is a bit larger than the gel.
3. Add digestion buffer with ~8 Units/mL of proteinase K to the sample. Make sure to cover the sample completely and allow to digest at 37 °C.
    a. Digest overnight if you used the MA-NHS method.
    b. Digest for 30 min or more if you used the GA method (for FPs, max 30 min).

EXPANSION

1. Remove gels from digestion buffer and place in DI water to expand. Anticipate the size of the expanded gel and use a suitably sized container (we often use a 3.5” petri dish).
2. Exchange water as needed until fully expanded (typically 2-3 exchanges). The refractive index of the gel is nearly identical to that of water so you will not easily see the gel. Be careful not to pour out or aspirate the gel. Typical expansion times are 1-2 hours, total, with exchanges every 30 min.
3. Thinner gels will expand relatively quickly and may only need one water exchange.

SAMPLE HANDLING TIPS

- Removing expanded gels from petri dishes (or handling them in general) can be difficult. A large rectangular coverglass (~1” x 2”) is probably the best tool to use but other flat objects or spatulas may also work well. Place the coverglass short edge against the petri dish surface and tilt the dish to allow the gel to gently slide onto the coverglass.
- Try to gently wick away excess water before imaging using a Kim wipe. The gels will otherwise slide around during imaging.

2.10.3 ExM Protocol: Brain Tissue

BACKGROUND: This protocol is based off of methods used in the publication "Expansion microscopy with conventional antibodies and fluorescent proteins" (DOI: 10.1030/nmeth.3833) and is similar to the protocol[48] originally published by Prof. Edward Boyden. **The following is meant for tissue expansion only.** Different tissues will require slightly different conditions, so it is best to start with simple, bright stains to assess effectiveness on a broader range of sample conditions. Try to keep samples small to start with (1-2 mm^2 and a few hundred microns thick or less). Optimization and validation are key when expanding new tissues. In the publication listed above, there is a correlative imaging procedure that is useful when assessing structure preservation after expansion. Keep in mind that this protocol was based on expansion of mouse brain (fixed for 1 h in 4% PFA) and may require modification for new tissue types or different methods of fixation.

REAGENTS:

1. Ammonium Persulfate (APS is a salt and initiates polymerization)
    a. Store at 4 °C
2. Tetramethylethylenediamine (TEMED is a liquid and catalyzes polymerization)
    a. Store at 4 °C
3. 2,2,6,6-tetramethylpiperidine 1-oxyl (TEMPO is a solid and inhibits polymerization so that gelation starts after reagents permeate sample)
    a. Store at 4 ^{0}C
4. Methacrylic Acid-NHS (MA-NHS is a solid and is used to link proteins to the gel)
    a. Store the powder at 4 °C, KEEP AWAY FROM WATER
    b. Allow to warm to room temperature before opening to avoid condensation.
5. 40% Acrylamide (w/v) (Acrylamide is a liquid solution and is a monomer of the hydrogel)
    a. Store at 4 °C
6. 2% Bisacrylamide (w/v) (Bisacrylamide is a liquid solution and is a hydrogel crosslinker)
    a. Store at 4 °C
7. Sodium Acrylate (SA is an ionic monomer for the hydrogel)
    a. Store at room temperature, dry
8. Sodium Chloride (Salt)
9. 10x PBS Buffer
10. 10x TAE Buffer (Tris base, acetic acid, and EDTA)
11. 8 M Guanidine-HCl (component of digestion buffer)
12. Proteinase K (Digestion enzyme, 600-800 Units/mL in glycerol. We typically purchase stocks from NEB.)
    a. Store at -20 °C

STOCKS

1. APS: 10% (w/w) in water
    a. Store at -20 °C for up to 1 week
2. TEMED: 10% (v/v) in water
    a. Store at -20 °C for up to 1 week
3. TEMPO: 1% (w/w) in water
    a. Prepare freshly, within a few hours of use
4. MA-NHS: 1 M in anhydrous DMSO
    a. Store at -20 °C
    b. Keep away from water
5. Monomer Solution. Final concentrations are listed. Recipe achieves ~4x expansion. Bolded quantities in brackets, below, are for 10 mL of monomer solution.
    a. 1x PBS **[1 mL]**
    b. 2 M NaCl **[1.17 g]**
    c. 8.625% (w/v) Sodium Acrylate **[0.863 g]**
    d. 2.5% (w/v) Acrylamide **[0.625 mL]**
    e. 0.15% (w/v) Bisacrylamide **[0.75 mL]**
    f. Store at 4 °C for up to 1 month
6. Digestion Buffer. Bolded quantities in brackets, below, are for 10 mL of solution.
    a. 1x TAE Buffer **[1 mL]**
    b. 0.8 M Guanidine-HCl **[1 mL]**
    c. 0.5% Triton **[0.25 mL]**
    d. Store at 4 °C. Solution should be stable but we usually consume within a week.

POST-STAIN TREATMENT

1. After immunostaining the sample (or after expression of FP), treat with 1 mM MA-NHS in PBS (diluted from your DMSO stock). Because NHS compounds rapidly hydrolyze in water, do not make the NHS solution in PBS until you are ready to treat your sample.
    a. Depending on how your tissue was fixed, you may need to alter the concentration of MA-NHS.
2. Allow the sample to react for 1 h at room temperature.
3. Wash the sample 2-3 times with several volumes of PBS.

GELATION

1. Incubate the tissue in monomer solution for 30-45 min at 4 °C prior to gelation to allow monomer to penetrate the whole tissue. **NOTE: the monomer here DOES NOT contain APS, TEMED, or TEMPO.**
2. Place tissue on #1.5 coverglass and remove excess monomer (wick away with Kim wipe). Ensure tissue is flat against the glass.
3. Prepare the gelation solution. Quantities in brackets, below, are for a 100 µL volume. Note that APS should always be added last, right before adding to the specimen.

a. 0.2% TEMED **[2 µL of 10% solution]**
b. 0.01% TEMPO **[1 µL of 1% solution]**
c. 95% monomer solution **[95 µL of monomer stock]**
d. 0.2% APS **[2 µL of 10% solution]**

4. Cover the tissue with the gelation solution without disturbing it. Avoid letting the tissue fold over or float up into the gel.
5. Place two pieces of #1.5 coverglass stacked on either side of the tissue and cover with another #1.5 coverglass. Place a drop of leftover gelation solution on top of the coverglass as a "tester" gel to see when the polymerization is complete.
    a. We use 2 pieces of coverglass to make the resulting gel thicker so it's easier to handle. You can alter the number of pieces or use thinner glass for thinner gels. You'll figure out what works best when you try to image the expanded sample and find out your needs based on the working distance of your objective lens.
    b. If you're using a thick piece of tissue you may need to use thicker coverglass spacers to ensure the whole sample is incorporated into the gel.
6. Allow the sample to gel at 37 °C for 1.5-2 h.

DIGESTION

1. Remove top piece of coverglass as well as spacers. Cut away excess gel from around the tissue (Your sample will be cleared after expansion and will be difficult to find in a lot of excess gel.) Use a diamond knife or razor blade to score the bottom coverglass near to the tissue and then break away excess coverglass so that the coverglass and gel will fit into the digestion buffer well. Do not try to remove the gels from the coverglass because they may tear.
2. Place the gel sitting on the coverglass in a suitably sized well, e.g., a well of a 12-well plate.
    a. Keep in mind that the gels will expand slightly (~1.5x) during digestion so make sure the well is a bit larger than the gel.
3. Add digestion buffer with ~8 Units/mL of proteinase K to the sample. Make sure to cover the sample completely and allow to digest at 37 °C
    a. Digest for 12-18 hours (typically done overnight).
    b. Digest for 1 h if you want to preserve FP signal.

EXPANSION

1. Remove gels from digestion buffer and place in DI water to expand. Anticipate the size of the expanded gel and use a suitably sized container (we often use a 3.5" petri dish).
2. Exchange water as needed until fully expanded (typically 2-3 exchanges). The refractive index of the gel is nearly identical to that of water so you will not easily see the gel. Be careful not to pour out or aspirate the gel. Typical expansion times are 1-2 hours, total, with exchanges every 30 min.
3. Thinner gels will expand relatively quickly and may only need one water exchange.

SAMPLE HANDLING TIPS

- Removing expanded gels from petri dishes (or handling them in general) can be difficult. A large rectangular coverglass (~1” x 2”) is probably the best tool to use but other flat objects or spatulas may also work well. Place the coverglass short edge against the petri dish surface and tilt the dish to allow the gel to gently slide onto the coverglass.
- Try to gently wick away excess water before imaging using a Kim wipe. The gels will otherwise slide around during imaging.
- If the gels fold over onto themselves after removing excess water, try to use a fine tip paintbrush and gently poke the edges of the gel back until the sample is back in its original shape.
- A flashlight (illuminating from below) and a dark background are helpful when trying to locate your tissue within the gel. Look for a small amount of scattering.

Chapter 3

Super-resolution Imaging of *Drosophila* Tissues Using Expansion Microscopy

3.1 Preface

After establishing the protocol described in **Chapter 2**, we next sought to extend the utility of ExM to a wider range of tissue types. As discussed previously (**sections 1.3.3** and **1.4.2**), tissues that contain large quantities of protease-resistant materials[39–41] can resist expansion due to a lack of homogenization and lead to gross structural distortions in the expanded state. Certain *Drosophila* tissues are a particularly challenging sample type for ExM due to their rigid exoskeleton, which is composed of a cuticle containing large amounts chitin. Chitin, a polysaccharide composed of *N*-acetylglucosamine monomers, is not digested by proteinase K[41] and is thus incompatible with the ExM protocol described in **Chapter 2**. In this chapter, it is shown that although proteinase K digestion enables robust expansion of *Drosophila* embyros and larval brain dissections (which lack a tough, chitin-rich cuticle), faithful expansion of *Drosophila* body walls requires that the enzymes chitinase and collagenase be incorporated into the digestion step. This careful method adaptation enabled the discovery of age-dependent structural variations on the nanoscale in *Drosophila* presynaptic active zones. Additionally, by taking advantage of the high axial resolution afforded by ExM, it was revealed that a larger number of somatosensory neuron dendrites are inserted into the epithelial layer of the *Drosophila* body wall than reported in previous works which used standard (diffraction-limited) fluorescence microscopy techniques.

In **section 1.4.1**, I discussed the importance of quantitative method validation for each new variation of ExM that is developed; that sentiment certainly holds true in this instance where *Drosophila* tissues were rendered ExM-compatible by altering digestion conditions. However, due to the large number of combinations of fixation, staining, mounting, and digestion conditions

involved with the expansion of each *Drosophila* tissue in this study, it became evident that an initial, qualitative evaluation of expansion fidelity was required. After selecting a small subset of conditions that produced satisfactory expanded specimens (those lacking obvious distortions), the quantitative analysis of structural distortions on the micro- and nanoscale (described in detail in **Chapter 2**) was performed with each type of *Drosophila* tissue. This method of narrowing down experimental conditions before performing a detailed evaluation of new ExM protocols, a non-trivial task, is highly advised for all ExM users. This maximizes the efficient use of a researcher's time as well as the range of possible sample conditions that lead to robust sample expansion (see **section 1.4**).

My contribution to this work was primarily focused on the evaluation of structural distortions in each tissue type. I performed all correlative data analyses quantifying structural distortions, aided in confocal imaging of specimens before and after expansion, and provided experimental advice to those optimizing digestion procedures. Additionally, Hyeon-Jin Kim and I co-authored and edited the expansion protocol in **section 3.8**, which was adapted from my protocols presented in **section 2.10**. I also directly contributed to **Figures 3.1A**, **3.2A-D**, **3.3A-B'**, **3.3E**, as well as **Supplementary Figures 3.1**, and **3.2**. Supplementary figures as well as a supplementary protocol are provided in addition to the main text.

The following material in this chapter is reproduced with permission from:

Molecular Biology of the Cell, In Press.[68] Jiang, N; Kim, H. J.; **Chozinski, T. C.**; Azpurua, J. E.; Eaton, B. A.; Vaughan, J. C.; and Parrish, J. Z.; "Super-resolution Imaging of *Drosophila* Tissues using Expansion Microscopy", Advanced Online Publication.

All material in this chapter has been reformatted to conform with the style of this thesis.

3.2 Abstract

The limited resolving power of conventional diffraction-limited microscopy hinders analysis of small, densely packed structural elements in cells. Expansion Microscopy (ExM) provides an elegant solution to this problem, allowing for increased resolution with standard microscopes via physical expansion of the specimen in a swellable polymer hydrogel. Here, we apply, validate, and optimize ExM protocols that enable the study of *Drosophila* embryos, larval brains, and larval and adult body walls. We achieve a lateral resolution of ~70 nm in *Drosophila* tissues using a standard confocal microscope, and we use ExM to analyze fine intracellular structures and intercellular interactions. First, we find that ExM reveals features of presynaptic active zone (AZ) structure that are observable with other super-resolution imaging techniques but not with standard confocal microscopy. We further show that synapses known to exhibit age-dependent changes in activity also exhibit age-dependent changes in AZ structure. Second, we use the significantly improved axial resolution of ExM to show that dendrites of somatosensory neurons are inserted into epithelial cells at a higher frequency than previously reported in confocal microscopy studies. Altogether, our study provides a foundation for the application of ExM to *Drosophila* tissues and underscores the importance of tissue-specific optimization of ExM procedures.

3.3 Introduction

Analysis of intercellular interactions and intracellular structures often requires optical resolution below the diffraction limit of light (~250 nm). While several methods have been developed for super-resolution imaging of biological samples using specialized microscopes[69], expansion microscopy (ExM) is compatible with standard optical microscopes that are already widely available, requires no specialized computational processing, can be used with a wide range of fluorophores, and is suitable for multicolor imaging at substantial depth. In ExM, a swellable hydrogel polymer is grown within a fixed specimen that is treated with proteolytic enzymes to soften the tissue and then expanded through dialysis in distilled water, yielding a ~4-fold increase in lateral resolution.[70–73] ExM is therefore dependent on the ability of the specimen to be successfully embedded in the swellable polymer hydrogel and to be rendered compliant to

expansion through proteolytic digestion. However, many invertebrates, fungi, and plants are covered with a rigid exoskeleton important for maintaining organismal integrity. In some of these organisms, including *Drosophila*, this exoskeleton is comprised of a lipid and polysaccharide-rich cuticle that resists conventional proteolytic digestion, presenting a major impediment to implementation of ExM.

Here, we set out to extend the utility of ExM by adapting it for use in *Drosophila*. We find that some *Drosophila* tissues lacking a rigid cuticle are compatible with established ExM protocols as has been also shown in two recent reports.[74,75] We also find that addition of a single step to established ExM protocols, treatment with cuticle-digesting enzymes, renders larval and adult body wall specimens compatible with ExM. Using our optimized ExM protocol, we achieve a lateral resolution of ~70 nm in various *Drosophila* tissues, facilitating analysis of structural elements that cannot be accurately studied with conventional optical microscopy, and we demonstrate the utility of this approach in three experimental contexts. First, we show that ExM allows for high-resolution analysis of presynaptic active zone (AZ) structure at the larval neuromuscular junction (NMJ) and that analysis of these structures with conventional confocal microscopy leads to systematic sampling errors. Second, we identify age-dependent changes in adult AZ structure using ExM. Finally, we analyzed cell-cell interactions in the larval peripheral nervous system using ExM and found that epithelial ensheathment of somatosensory dendrites is more prevalent than previously reported, underscoring the likely importance of this intercellular interaction. Altogether, these studies establish ExM as an accessible super-resolution imaging platform amenable to analysis of diverse *Drosophila* tissues.

3.4 Results

3.4.1 Expansion of Drosophila Tissues with Minimal Distortion

Prior studies demonstrated several specimens that are amenable to ExM[70–72], including various cultured cells and brain tissue. Given the prevalence of whole-mount imaging in analysis of *Drosophila* development, we first examined whether ExM could be applied to intact *Drosophila* embryos. To this end, we fixed embryos using a heptane/formaldehyde fixative and processed them for ExM, which includes gelation, digestion, and expansion steps (**Fig. 3.1A**). Using this

approach, *Drosophila* embryos were readily expanded ~4x without obvious tearing or distortion (**Fig. 3.1B**). To assess the fidelity of expansion, we recorded images of embryos before and after expansion. We then quantified distortion in X, Y, and Z dimensions by comparing post-expansion images to digitally expanded pre-expansion images with a non-rigid deformation algorithm (**Supplementary Figs. 3.1** and **3.2**). We found that lateral distortion was generally below 1-2% over a range of length scales.

Next, we examined the compatibility of isolated *Drosophila* tissue with ExM. Similar to embryos, formaldehyde-fixed larval brains were readily expanded without gross distortion (**Fig. 3.1C**). Staining larval brains with anti-Fas II antibody[76] provided feature-rich labeling in X, Y, and Z dimensions (**Supplementary Fig. 3.1**), allowing us to generate robust measures of lateral and axial distortion. As in embryo preps, distortion in expanded larval brains was generally low (<3%) over length scales of up to 30 µm (**Supplementary Fig. 3.1**), comparable to results reported for ExM of other tissue samples.[70–73]

Unlike embryo and larval brain samples, larval body wall samples failed to expand, instead detaching from the swellable hydrogel and becoming somewhat torn and distorted (**Supplementary Fig. 3.1**), likely the result of incomplete digestion of the polysaccharide-rich cuticle by the standard proteinase K digestion in ExM. Indeed, treatment with chitinase enzymes after gelation, but before proteolytic digestion with proteinase K, allowed for isotropic body wall expansion in larval (**Fig. 3.1D**) and adult body wall samples (see below, **Fig. 3.4**), suggesting that this approach may be broadly useful for ExM on samples with a chitin-rich exoskeleton, including other arthropods and fungi. Altogether, these results demonstrate that ExM is applicable to different types of *Drosophila* tissues and that fine structural elements are preserved during expansion of complex cellular assemblies including whole embryo preparations.

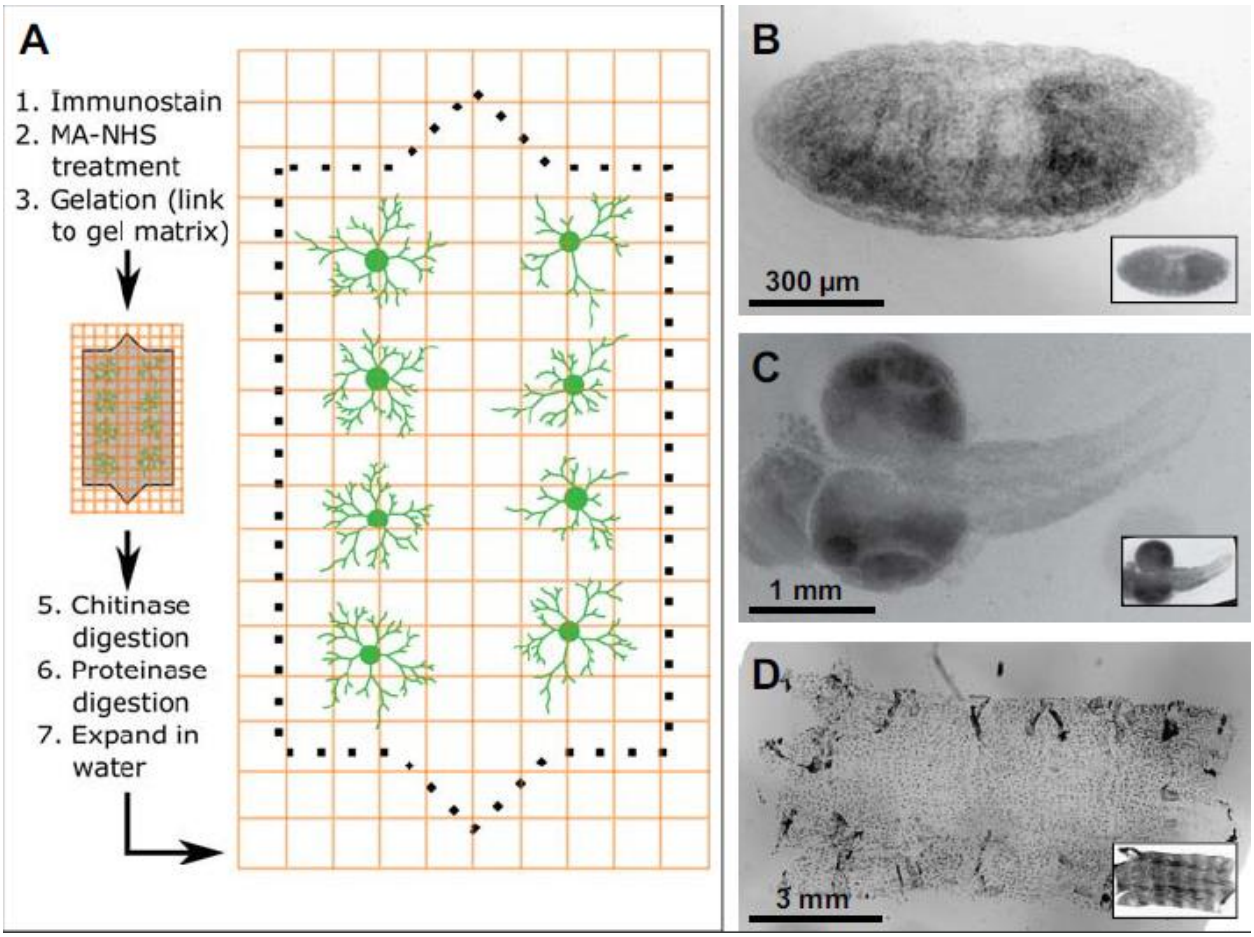

Figure 3.1 | Isotropic expansion of *Drosophila* tissues for fluorescence microscopy. (**A**) ExM workflow. (**B-D**) Correlative pre- and post-expansion imaging of Drosophila tissue. Drosophila embryos (**B**), larval brains (**C**), and larval body walls (**D**) stained with DAPI and imaged both before and after expansion. Pre-expansion (inset) and post-expansion images are shown at the same magnification such that post-expansion images are ~4× larger than the corresponding pre-expansion images (insets).

3.4.2 Super-resolution Imaging of Subcellular Structures with ExM

We next examined whether ExM would facilitate identification of fine structural details in *Drosophila* tissue that were not observable with standard confocal microscopy. We first focused on the imaging of mitochondria because mitochondrial morphology is dynamic during development, altered in a broad range of disease states[77] and is commonly studied with conventional fluorescence microscopy methods. We expressed a form of GFP that is targeted to the mitochondrial matrix (*UAS-mitoGFP*) in *Drosophila* class IV dendrite arborization (C4da)

neurons, which innervate the body wall, fixed and immunostained larval body wall fillets with anti-GFP antibodies, and processed the specimens for ExM. Confocal imaging of mitochondria in a cell before and after expansion (**Fig. 3.2A-D**) revealed much greater detail in the post-expansion state, with numerous loops, branches, and swellings that were visible after expansion but were difficult or impossible to detect before expansion. The pre-expansion images correspond excellently with post-expansion images of the same region (2-6% distortion over a range of length scales, ~4.08× expansion factor, **Supplementary Fig. 3.2**), Thus, ExM allows for visualization of fine structural elements in organelles and should prove to be a valuable tool in studying organelle morphogenesis.

Second, we used ExM to visualize the microtubule cytoskeleton by immunostaining for acetylated tubulin. Prior to expansion, individual microtubules in epithelial cells were difficult to detect due to their high density (**Supplementary Fig. 3.3**), however, expansion of specimens clearly revealed an intricate network of well-resolved microtubules (**Fig. 3.2, E-F**). The cross-sectional profile of expanded microtubules had an average Gaussian-fitted full width at half maximum of 83 ± 9 nm (mean ± SD); given that indirect immunofluorescence leads to specimen broadening due to the non-negligible size of primary and secondary antibodies, we estimate a spatial resolution of ~70 nm which is consistent with earlier work on other specimens.[70,71]

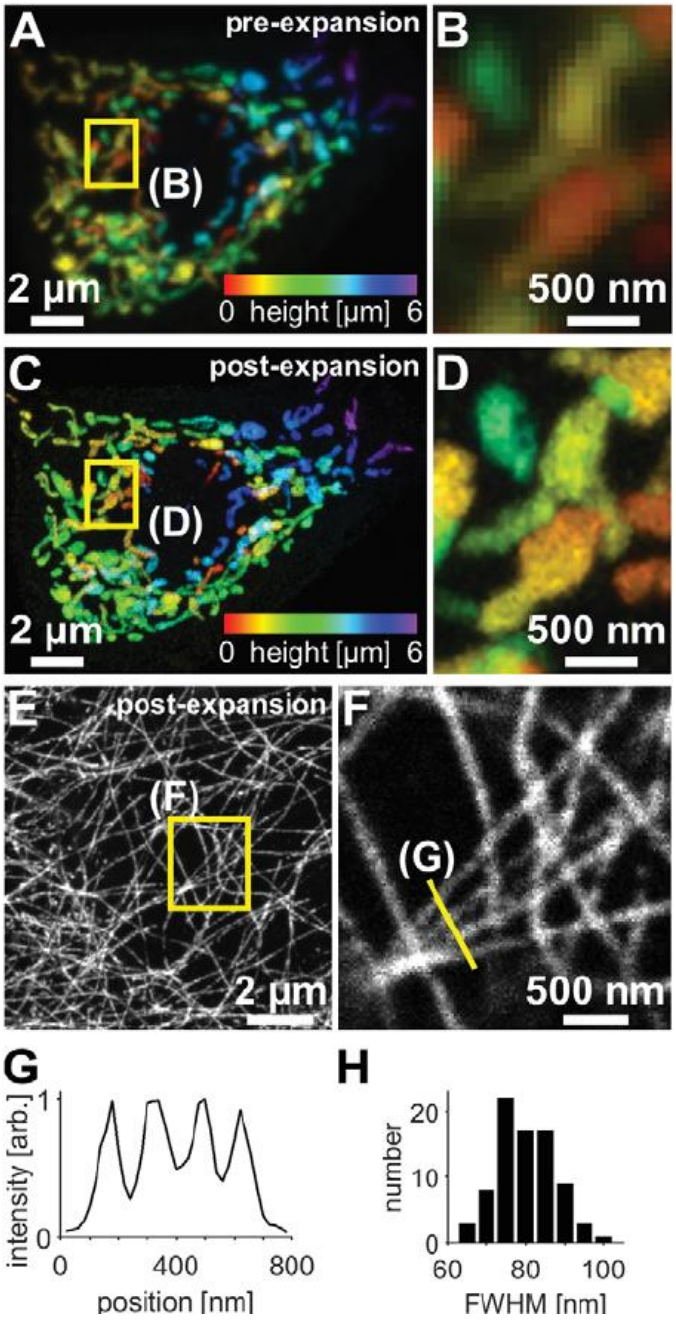

Figure 3.2 | Confocal imaging of sub-cellular structures in expanded *Drosophila* tissue samples. (**A-D**) Maximum intensity projections of C4da neurons expressing mito-GFP (*ppk-Gal4*, *UAS-Mito-GFP*) and immunostained for GFP, where color indicates height within the specimen. The same field of view is shown before expansion (**A** and **B**) and after expansion (**C** and **D**). (**E**) Maximum intensity projections of epithelial cells immunostained for acetylated tubulin in expanded third instar larval body walls. (**F**) Zoomed-in views of single focal plane image corresponding to boxed regions in (**E**). Images of epithelial acetylated tubulin in unexpanded body walls are shown in **Supplementary Fig. 3.3**. (**G**) Line profile from **F** (arb., arbitrary units). (**H**) Analysis of microtubule widths yielded average Gaussian-fitted full width at half maximum (FWHM) of 83 nm ± 9 nm

(mean ± standard deviation, 80 microtubule profiles). Here and in all subsequent figures containing ExM data, distances and scale bars have been divided by their respective measured expansion factors of ~4× and therefore correspond to pre-expansion dimensions.

3.4.3 Super-resolution Imaging of Presynaptic Active Zones with ExM

The high density and small size of *Drosophila* synapses prevent accurate assessment of synapse number and structure with conventional light microscopy. In particular, features of AZs, which serve as sites of neurotransmitter release, are obscured with conventional light microscopy. With super-resolution microscopy, AZs appear as hollow ring-like structures ~200-400 nm in diameter.[78–80] We reasoned that the increased lateral resolution provided by ExM, compared to conventional microscopy, should facilitate analysis of NMJ synapse number and structure while providing an opportunity to benchmark ExM against other super-resolution imaging platforms such as SIM, STORM and STED that have been successfully applied to NMJ analysis.[78,80–84]

To examine the utility of ExM in analysis of AZ structure, we conducted correlative pre- and post-expansion analysis of the third instar NMJ immunostained for the structural component Bruchpilot (Brp). Prior to expansion, a Brp immunostain revealed numerous solid structures ~300-500 nm in diameter and ~0.1-0.3 μm^2 in area (**Fig. 3.3, A and C**). These structures exhibited either uniform signal intensity or a central maximum. Expanded specimens showed excellent correspondence with pre-expansion images of the same region (<2% distortion, **Supplementary Fig. 3.2**), indicating a smooth and overall isotropic expansion, and we were able to observe fine details of AZs that were not evident in unexpanded specimens, as described below. First, AZs were less regularly shaped; whereas pre-expansion AZs were largely spherical, many post-expansion AZs were elliptical, elongated, and/or contained multiple lobes (**Fig. 3.3B**). Second, AZs appeared uniformly smaller (**Fig. 3.3C**). Third, many sites that appeared as individual structures prior to expansion were resolved into multiple independent structures (**Fig. 3.3, A'** and **B'**), and ratiometric analysis of pre- and post-expansion AZ counts revealed that ExM consistently facilitated identification of larger numbers of AZs (**Fig. 3.3D**). Fourth, many Brp puncta in expanded samples exhibited hollow ring-like structures (**Fig. 3.3, B, E-H**) with a maximum

intensity in the periphery. While we were able to resolve these hollow ring-like structures with structured illumination microscopy (SIM) analysis (**Supplementary Fig. 3.4**), we found that SIM images were intermediate in resolution between our pre- and post-ExM confocal images as assessed by apparent AZ area (**Fig. 3.3I**). In contrast, prior reports using STED imaging yielded measured sizes of AZs comparable to our findings using ExM.[80,81,85]

Thus, ExM allowed for visualization of AZ substructure at the larval NMJ, including the hollow ring-like structures previously revealed by super-resolution imaging using the same anti-Brp antibody[80,81], and more accurate scoring of AZ number than conventional fluorescence microscopy.

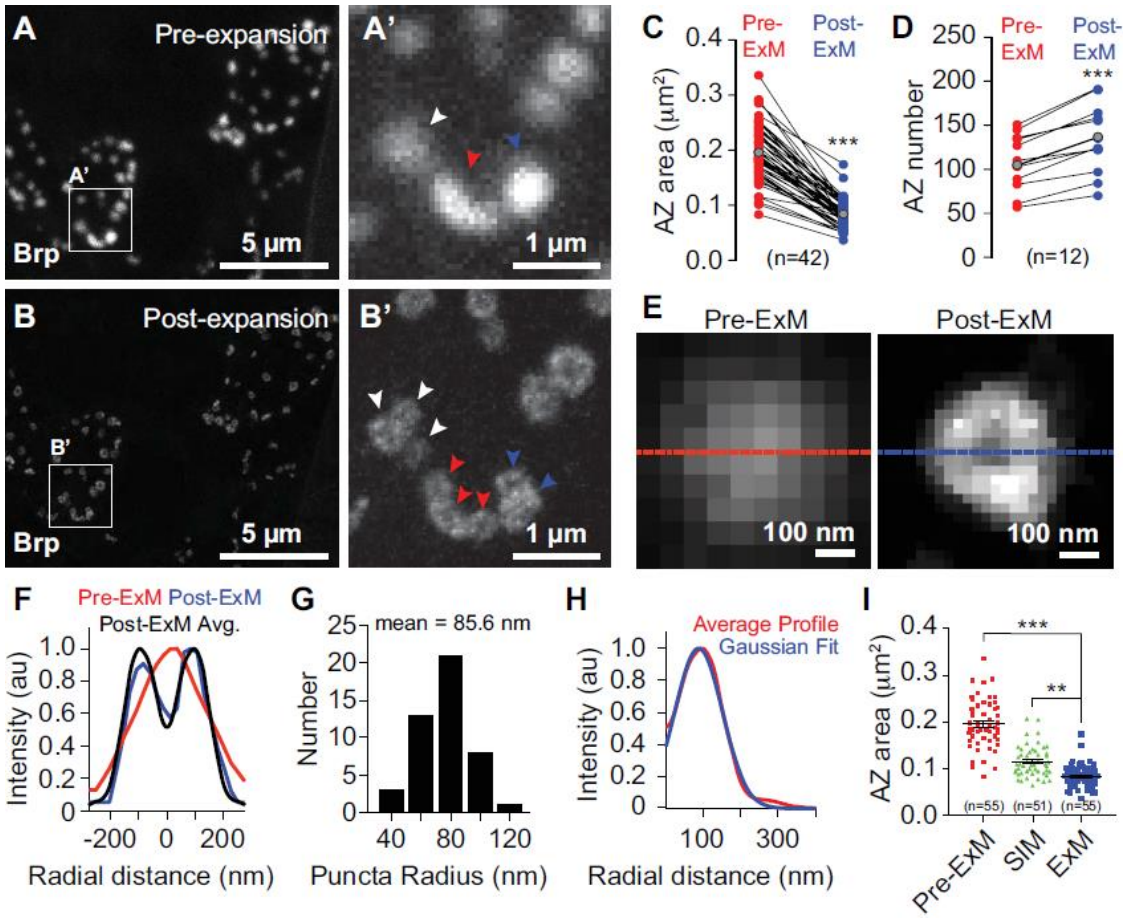

Figure 3.3 | Super-resolution imaging of synapses with ExM. Correlative confocal microscopy imaging of Brp staining (**A**) pre-expansion and (**B**) post-expansion in third instar larvae. (**A'-B'**) Zoomed view of boxed regions in **A** and **B** showing AZ features resolved by ExM but not

conventional confocal microscopy. Arrowheads mark individual AZs that can be resolved in correlated pre- and post-expansion samples. (**C**) AZ area and (**D**) AZ number in correlated pre- and post-expansion images. Red and blue points represent individual measurements from Pre- and Post-expansion samples, respectively, and lines connect paired measurements. Gray points mark mean values. ***P < 0.001, unpaired t-test with Welch's correction. (**E**) Pre- and post-expansion images of a single AZ. (**F**) Cross-sectional profile of pre- and post-expansion images of puncta in (**E**) and average cross-sectional profile of 46 individual post-expansion AZs. (**G**) Distribution of puncta radii and (**H**) average radial Brp intensity profile of 46 individual AZs aligned according to their centers of mass. (**I**) AZ area measurements from Brp-stained third instar larvae imaged using a conventional confocal microscope (pre-expansion and post-expansion) or using structured illumination microscopy (SIM). Note that SIM imaging was performed on unexpanded tissue (see **Supplementary Fig. 3.4**). Number of AZs measured for each imaging modality is shown. **P<0.01, ***P<0.001 compared to ExM, one-way ANOVA with a post-hoc Dunnett's test. All distances, areas, and scale bars correspond to pre-expansion dimensions.

3.4.4 Age-dependent Changes in Active Zone Structure

In adult flies, the CM9 NMJs experience an increase in neurotransmitter release during aging, but the cellular mechanisms underlying this potentiation of release are unclear.[86] The size of vesicle release events scale with presynaptic AZ size at numerous synapses including small glutamatergic synapses of the CNS and large synapses like the NMJ.[85,87–90] This includes changes in Brp levels at larval AZs during homeostatic plasticity.[85] We therefore used ExM to investigate whether changes in Brp staining patterns at the AZ could explain the age-dependent potentiation of neurotransmission at the CM9 NMJ.

In unexpanded tissue, Brp immunoreactivity at the CM9 NMJ appeared as regularly shaped spherical structures (**Fig. 3.4, A and A'**) as well as larger structures possibly representing clusters of AZs (**Fig. 3.4A"**). As in unexpanded larval samples, Brp immunoreactivity in unexpanded CM9 NMJs appeared as solid structures with uniform signal intensity or a central maximum, though the average apparent size of the adult AZs was increased ~20% (mean AZ area, $0.240 \pm 0.099\ \mu m^2$, n = 100). In contrast, imaging these tissues with ExM revealed Brp puncta with hollow ring-like structures that were less regularly shaped and smaller than unexpanded samples (**Fig. 3.4, B and C**). We therefore used ExM to examine AZ morphology in aging flies and found a significant increase in the 2D area of AZs across age (**Fig. 3.4D**) as well as a significant increase with age in the presence of AZs containing multiple Brp rings (**Fig. 3.4E**, **Supplementary Fig. 3.4**).

Notably, the AZs containing multiple Brp rings were larger than AZs harboring only a single Brp ring (**Fig. 3.4F**), although the size of individual rings in multiple Brp ring-containing AZs was significantly smaller than Brp rings in singlet AZs (**Supplementary Fig. 3.4**). Thus, it is possible that the AZs containing multiple Brp rings arise from fusion of singlet AZs. If this is indeed the case, these AZs could have enhanced release given the likely increased abundance of voltage-gated calcium channels and larger pools of synaptic vesicles (SVs).[88,91] Altogether, these results document an age-dependent change in AZ structure consistent with the fusion of neighboring AZs during aging that could not be resolved using conventional confocal microscopy.

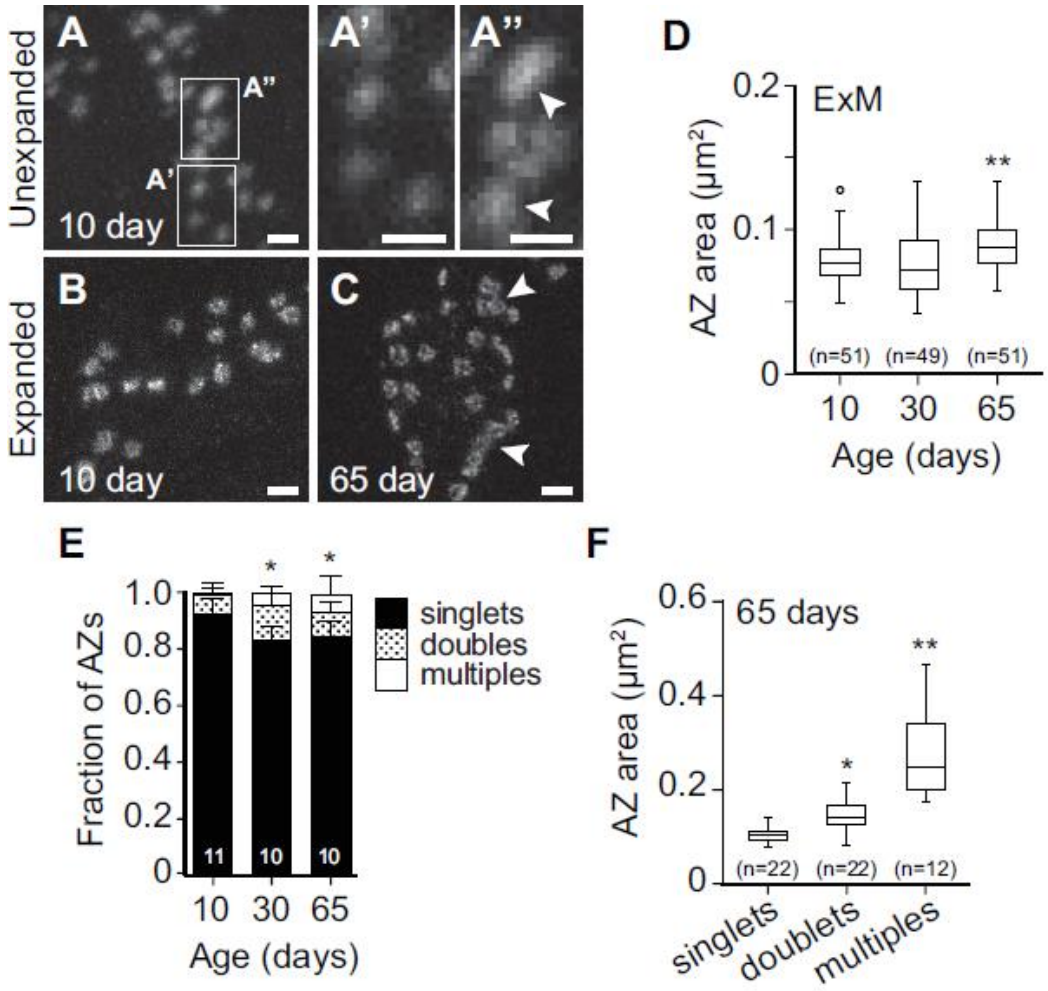

Figure 3.4 | ExM analysis of age-related changes in AZ structure. Brp staining at the CM9 NMJ in unexpanded (**A**) and expanded (**B**, **C**) tissue of 10 or 65-day adult flies. In unexpanded samples Brp immunoreactivity appeared as regularly shaped spherical structures (**A'**) as well as larger

structures possibly representing clusters of AZs (**A”**). Arrowheads mark elongated puncta that likely represent clusters of joined AZs that cannot be resolved in unexpanded tissue (**A”**) and clusters of joined AZs resolved by ExM (**C**). (**D**) Boxplots depicting AZ area measurements using ExM. In this and subsequent panels, boxes mark 1st and 3rd quartiles, bands mark medians, whiskers mark 1.5 x IQR, and outliers are shown as points. **P<0.01 compared to 10-day adults, one-way ANOVA with a post-hoc Dunnett’s test. (**E**) The proportion of AZs with individual (singlets) or multiple Brp rings is shown for the indicated time points. Error bars correspond to standard deviation and *P<0.05 compared to 10-day adults (Fisher’s exact test). Measurements in (**D**) and (**E**) were performed blind to specimen age. (**F**) Boxplots depicting area measurements for single, double and multiple Brp ring containing AZs in 65-day adults. *P<0.05, **P<0.01 compared to singlets, one-way ANOVA with a post-hoc Dunnett’s test. The number of NMJs analyzed for each time point is indicated. Scale bars, 1 μm. All areas and scale bars refer to pre-expansion dimensions.

3.4.5 Improved Axial Resolution with ExM

We next explored the utility of ExM for studying features of cell-cell interactions that are not observable with conventional confocal microscopy. Portions of *Drosophila* larval class IV da neuron (C4da) dendrite arbors, like peripheral arbors of other nociceptive sensory neurons, are ensheathed by the epidermis.[92–95] The extent of epidermal dendrite ensheathment has been difficult to ascertain, in part because the size and spacing of sensory dendrites and epithelial membranes cannot be accurately measured using diffraction-limited microscopy. Although transmission electron microscopy (TEM) analysis suggests that ~30% of C4da dendrites are ensheathed by the epidermis[96], the difficulty identifying terminal dendrites that are largely devoid of electron-dense material and the small cross-sectional area sampled by TEM limit the utility of TEM in a systematic analysis of epidermal ensheathment. We reasoned that the increased resolution afforded by ExM would allow for the most accurate analysis of C4da dendrite embedding to date. We therefore double-labeled the extracellular matrix (ECM) and C4da dendritic membranes and used confocal microscopy of unexpanded and expanded tissue to monitor apical displacement of dendrites from the ECM as a proxy for epithelial dendrite ensheathment.[93,96]

In unexpanded tissues, dendrites appeared elongated in cross-section, with splayed features and axial lengths ranging from 1 to 4 μm, substantially higher than dendrite diameters

observed by TEM (**Fig. 3.5**, **A** and **D**). The vast majority of these dendrites appeared to be in contact with the ECM (**Fig. 3.5**, **A** and **F**). However, the diameter of higher order dendrite branches (~150 nm) and the ECM thickness are smaller than the axial resolution of the confocal[93,96], precluding accurate assessment of the relative position of these structures.

In expanded tissue, we identified several differences in the apparent size and orientation of dendrites and ECM. First, dendrites appeared spherical with defined margins (**Fig. 3.5B**). Second, dendrite diameter was significantly reduced compared to pre-expansion images and comparable to values from TEM (**Fig. 3.5D**). Third, expansion allowed for identification of ECM detachment of dendrites over shorter length scales (**Fig. 3.5E**). Finally, ExM revealed that a significantly larger proportion of dendrites was detached from the ECM and ensheathed by epithelial cells in third instar larvae (**Fig. 3.5F**), comparable to estimates from TEM analysis.[96] By contrast, we observed significantly less dendrite detachment in second instar larvae, when epithelial ensheathment is initiated.[96] Taken together, these results strongly suggest that ExM sample processing does not induce significant levels of spurious ECM detachment of dendrites (**Fig. .35G**).

We noted a "dry lakebed" effect in ECM staining following expansion ECM with antibodies to Perlecan (**Fig. 3.5B**) or collagen (data not shown), likely the result of incomplete ECM proteolysis in conventional ExM. To ascertain whether the lakebed effect caused distortion in measurements of dendrite-ECM interactions we conducted ExM that included both chitinase treatment and a collagenase-mediated enzymatic ECM digestion step (ExM+chit+col). This collagenase treatment remedied the lakebed effect (**Fig. 3.5C**), and although signal intensity for ECM staining was attenuated by this treatment, dendrite-ECM interactions with ExM+chit+col mirrored results from ExM with chitinase.

Epithelial dendrite ensheathment is thought to modulate somatosensation[92–94] by reducing the distance between nerve endings and the skin surface or by some other means. If ensheathment acts primarily to increase dendrite proximity to the skin surface, we reasoned that ensheathed dendrites might be progressively displaced towards the body wall surface. This is not what we found. Using ExM we found that apical dendrite displacement was not increased

between the 2nd larval instar, when ensheathment is initiated, and the end of the 3rd larval instar, when >30% of the dendrite arbor is ensheathed (**Fig. 3.5**, **G** and **H**).

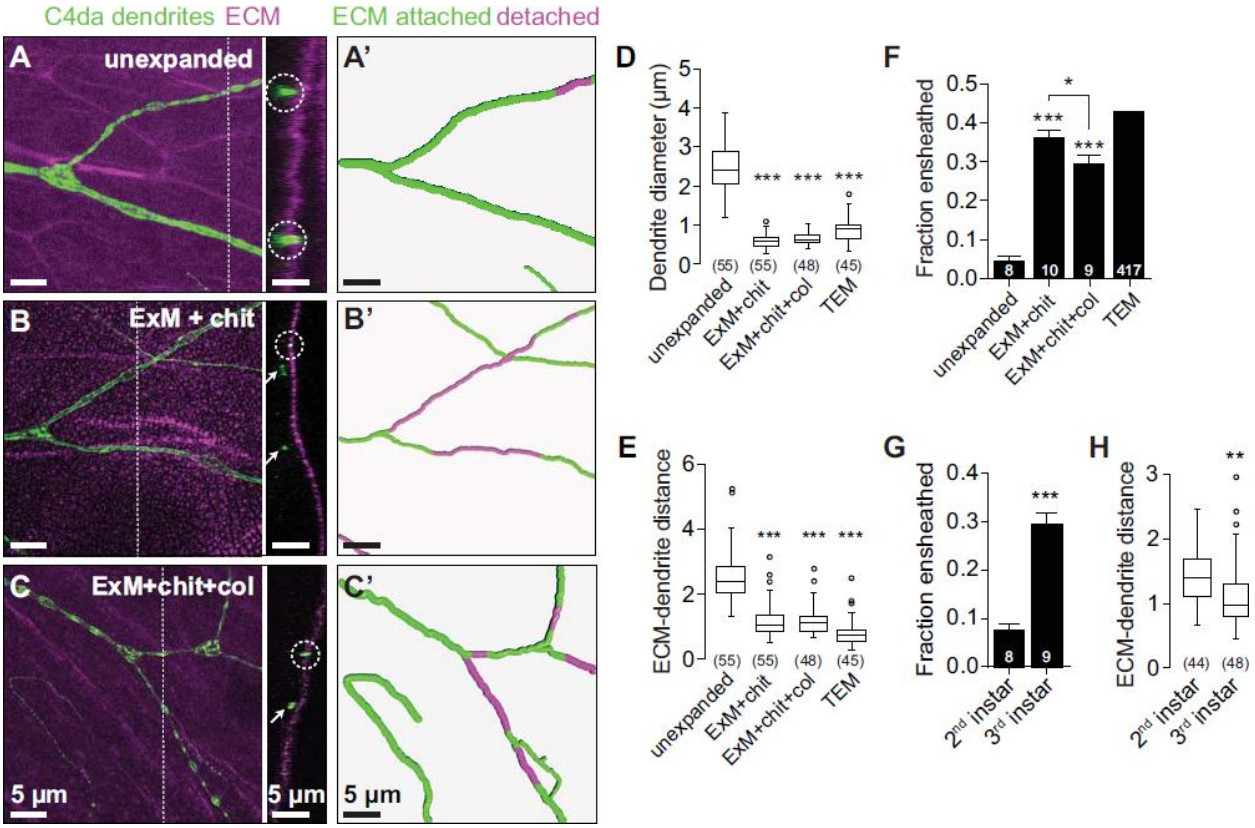

Figure 3.5 | Improved axial resolution facilitates analysis of cell-cell interactions. (**A-C**) Axial position of dendrites and ECM. Maximum intensity projections are shown for the following fillet preparations of larvae expressing the C4da-specific marker ppk-CD4-tdTomato: (**A**) unexpanded body walls, (**B**) expanded body walls of larvae treated with chitinase (ExM + chit), and (**C**) expanded body walls of larvae treated with chitinase and collagenase (ExM+chit+col), each stained with antibodies to Perlecan to label the ECM and to DsRed to label C4da dendrites. Dashed lines mark YZ cross-sectional positions shown to the right of each image. Circles mark ECM-contacting dendrites and arrows mark ECM-detached dendrites. (**A'-C'**) Traces depict ECM-contacting dendrites in green and ECM-detached dendrites in magenta. Plots depict (**D**) dendrite diameter, (**E**) the distance between detached dendrites and the ECM, and (**F**) the fraction of dendrites detached from the ECM measured using the indicated imaging approaches. (**G**) The fraction of dendrites detached from the ECM and (**H**) distance between detached dendrites and the ECM are shown for the indicated stages. Lines depict mean and standard deviation in (**F**) and (**G**). *P <0.05, ***P <0.005 compared to unexpanded samples unless otherwise indicated; one-way ANOVA with a post-hoc Dunnett's test in (**D**, **E**, and **F**). TEM samples were excluded from statistical analysis in (**E**) because the number of neurons sampled by TEM is not known. **P <0.01, ***P <0.005 compared to 2nd instar samples, unpaired t-test with Welch's correction in (**G** and **H**). n values represent the number of dendrites scored (**D**, **F**, and **H**; TEM values in **E**) or neurons

analyzed (**F** and **G**). Scale bars, 5 μm. All distances and scale bars refer to pre-expansion dimensions.

3.5 Discussion

In this work, we have optimized, validated, and applied ExM methods to interrogate *Drosophila* tissues at a spatial resolution of ~70 nm using a standard confocal microscope. Using ExM, we demonstrated that optical diffraction-limited microscopy, which is frequently used to analyze NMJ structure and function, leads to systematic errors in AZ quantification; ExM provides a solution to this problem. We also documented changes in AZ structure that provide a plausible cellular mechanism to account for age-dependent changes in neurotransmitter release at CM9 NMJs. Finally, our analysis of sensory neuron-epidermis interactions revealed that peripheral arbors of nociceptive neurons are extensively embedded in epithelial cells. Taken together with findings that *C. elegans* and *D. rario* nociceptive neurons and some mammalian unmyelinated intraepidermal nerve fibers are similarly ensheathed in the epidermis[92,95,97], our finding that large portions of nociceptive dendrite arbors are ensheathed by epithelial cells underscores the likelihood that epithelial ensheathment may contribute to nociceptor function. Intriguingly, some forms of peripheral neuropathy exhibit loss of unmyelinated intraepidermal nerves[98,99]; whether epithelial ensheathment plays a role in these neuropathies remains to be determined.

Two recent studies pointed towards the utility of ExM in super-resolution imaging of *Drosophila*. One study used a version of ExM together with the optical super-resolution microscopy method structured illumination microscopy (SIM) to study organization of synaptonemal complexes in *Drosophila* ovaries at relatively high resolution[74], and another demonstrated the compatibility of expansion microscopy for imaging of *Drosophila* brain dissection.[75] While these studies demonstrated applications and potential advantages of ExM, both lacked validation through correlative imaging of specimens before/after expansion applied ExM to only a single tissue, and one of the studies exhibited somewhat high variability in expansion factors. By contrast, we provide a thorough analysis of ExM applied to a variety of tissues.

We found that some *Drosophila* preparations including whole-mount embryos and larval brains expanded robustly with low distortion (<4%) using previously developed procedures based on digestion with the broad-specificity protease proteinase K to soften the specimen.[70] *Drosophila* larvae, on the other hand, required an additional enzymatic treatment step with chitinase to soften the tough, polysaccharide-based chitin-rich cuticle, and we found that robust expansion of the larval extracellular matrix required further treatment with collagenase. Our optimized procedures are detailed in a step-by-step protocol to aid others in evaluating or adopting the methodology (**Supplementary Protocol**, **section 3.9**).

In its current form, ExM will allow interrogation of numerous cellular structures that cannot be resolved with conventional diffraction-limited microscopy. We have demonstrated the utility of ExM in analysis of synapse structure and cell-cell interactions, and a natural extension of our results is the use of ExM to study neural circuits in *Drosophila*. We have shown that resolution limits lead to systematic undersampling of synapse number at the NMJ using conventional diffraction-limited microscopy, and the problem is likely worse in the neuropil where synapses are both more tightly packed and distributed over a larger volume. One elegant solution to this problem has been to use GFP reconstitution as a proximity sensor.[100] Splitting the GFP beta barrel yields two fragments that reassemble when stably juxtaposed within 7-10nm of one another.[101] Fusing these GFP fragments to inert membrane tethers, such as human CD4 lacking interaction domains, produces a sensor that yields GFP fluorescence when cells approach inside of ~30nm. While this tool has been useful in identifying synaptic partners, the technique is limited by spurious reassembly and the irreversibility of the reaction. ExM provides a complimentary tool, and should allow researchers to visualize juxtaposition of pre- and post-synaptic partners at sufficient resolution to map and count synapses, especially when used in combination with the recently completed EM connectivity maps.[102]

The vast number of epitope-tagged transgenes available for use in *Drosophila*, together with emerging techniques for tagging endogenous loci, provide numerous potential applications of ExM in super-resolution imaging of these transgenes. For example, we have demonstrated the utility of ExM in visualization of fine structural elements of GFP-labeled mitochondria. In another application, we anticipate that ExM will facilitate mapping of protein sub-cellular localizations,

for example the asymmetric distribution of polarity determinants. The potential future applications of ExM to *Drosophila* and other model organisms will grow with further development of the methodology. For instance, recent technical advances by other researchers include expansion of large intact specimens[72], interrogation of mRNA species[103], and the development of iterative expansion microscopy to achieve higher spatial resolution by means of larger (multi-step) hydrogel expansion.[104] While ExM is a particularly exciting methodology owing to its accessibility and strong performance with multicolor and volumetric imaging, the potential for artifacts is high, and we believe that it is important to carefully validate and optimize ExM for individual specimens as we have done here.

3.6 Materials and Methods

3.6.1 Fly Stocks

Flies were maintained on standard cornmeal-molasses-agar media and reared at 25° C under 12 h alternating light-dark cycles. The following fly lines were used in this study: *w^{1118}* (BL6326); *w^{1118}; ppk-Gal4* (BL32079); *w^{1118}; ; UAS-mito-GFP (BL8443); w^{1118}, ppk-mCD8-GFP.*[96]

3.6.2 Antibody Staining

A detailed list of antibodies and dilutions is presented in **Supplementary Table 1** (**section 3.9**). Details on fixation/staining are outlined in the following sections.

3.6.3 Larval Ventral Nerve Cord Staining

3rd instar larvae were pinned dorsal side up on a sylgard plate (Dow Corning) and filleted along the dorsal midline. Brains were carefully removed using forceps, fixed in EM-grade paraformaldehyde (PFA; Electron Microscopy Sciences) freshly diluted to 4% final concentration in PBS for 30min at room temperature and washed 5x 5 min in PBSTx (PBS with 0.2% Triton X-100) before being blocked in blocking/permeabilization buffer (PBS with 5% BSA and 0.2% Triton X-100) for 30min. Samples were incubated with primary antibodies in blocking/permeabilization buffer overnight at 4 °C, washed three times for 15 min each in PBST, and incubated for 6 h with secondary antibodies in blocking/ permeabilization buffer. After three 20 min washes in PBST,

samples were treated with the amine-reactive small molecule MA-NHS (methacrylic acid N-hydroxy succinimidyl ester) to preserve fluorescence signal[71] at room-temperature for 1 h followed by washing three times for 20 min each with PBS.

3.6.4 Whole Mount Embryo Staining

Embryos were collected on yeasted grape juice agar plates for 4 h and aged at 25° C in a moist chamber for 10-14 h. Embryos were dechorionated in 50% bleach for 4 min and rinsed in water. Embryos were then fixed in a 1:1 suspension of heptane and 4% formaldehyde (in PBS) for 15 min with vigorous shaking. The formaldehyde was removed and 1 volume of methanol added and the heptane:methanol suspension was vigorously shaken to devitellinize the embryos. After fixation, embryos were recovered and processed as described above for the nerve cord samples.

3.6.5 Larval Body Wall Fillets

3rd instar larvae were pinned on a sylgard plate, filleted along the ventral midline, and pinned open. After removing the intestines, fat bodies, imaginal discs and ventral nerve cord, fillets were fixed in PBS with 4% PFA for 15 min (for anti-brp staining) or 30 min (for anti-GFP staining). For microtubule staining, we extracted the tissue with PEM (0.1M PIPES ph7, 1mM EDTA, 1mM MgCl2) containing 0.5% Triton-X-100 for 30s immediately before fixation. Samples were then fixed for 15 min in a solution containing 3.2% paraformaldehyde and 0.1% glutaraldehyde or 3.2% paraformaldehyde alone in PEM, followed by a 30-sec wash with extraction buffer. After fixation, samples were processed as above for staining.

3.6.6 Gelation, Digestion, and Expansion of Nerve Cord and Embryo Samples

Samples were incubated in monomer solution (2 M NaCl, 8.625% Sodium Acrylate, 2.5% Acrylamide, 0.15% Bisacrylamide in PBS) for 1 h at 4° C prior to gelation. A stock of 4-hydroxy-2,2,6,6-tetramenthylpiperidin-1-oxyl (4-hydroxy-TEMPO) at 1% (wt/wt) in water was added to the incubation solution and diluted to concentration of 0.01%. Concentrated stocks of tetramethylethylenediamine (TEMED) and ammonium persulfate (APS) at 10% (wt/wt) in water were added sequentially to the incubation solution and diluted to concentrations of 0.2%

(wt/wt). The tissues were then incubated at 37 °C for 2-2.5 h. After the samples were gelled, the gels were cut and placed in a small 12-well chamber and were digested in 8 units/ml proteinase K solution in digestion buffer (40 mM Tris pH 8, 1 mM EDTA, 0.5% Triton, 0.8 M Guanidine HCl) for 1 h at 37 °C. Subsequently, samples were removed from the digestion solution and were allowed to expand in excess water overnight.

3.6.7 Gelation, Digestion, and Expansion of **Drosophila** *Body Wall Samples*

Samples were incubated in monomer solution for 1 h at 4 °C prior to gelation. Larva fillets were gelled with the same solution as above, but were incubated at 37 °C for 3-4 h. After gelation, the gels were cut and placed in a small 12-well chamber and 1mg/ml of Chitinase in PBS (pH6.0) was used to digest the cuticles for ~4 d at 37 °C. Samples were then rinsed 2x with PBS for 5 min each, digested with proteinase K solution, and expanded as described, above.

Prior to expansion, chitinase-treated samples were incubated with 1000 units/ml collagenase solution (prepared with buffer 1x HBSS lacking calcium, magnesium, and phenol red) with 0.01 M $CaCl_2$ and 0.01 M $MgCl_2$ overnight in a 37 °C shaking incubation chamber. Samples were then rinsed with PBS twice for 5 min and digested in 8 units/ml proteinase K solution in digestion buffer for 1 hour at 37 °C.

3.6.8 Mounting and Imaging

Before expansion, samples were mounted on lysine-coated #1.5 cover glass in wells made of polydimethylsiloxane. PBS was added to the well submerging the tissue to prevent it from drying out. After expansion, the expanded gel was trimmed to fit onto the coverglass, excess water was removed, and the gel was mounted on a lysine coated cover glass for imaging. Confocal microscopy was performed on a Leica SP5 inverted confocal scanning microscope using a 63× 1.2 NA water lens (**Figs. 3.1-3.5**) or a 20× 0.7 NA air lens (**Supplementary Fig. 3.1**).

3.6.9 Transmission Electron Microscopy

TEM was as previously described.[96] Briefly, larvae were perforated with insect pins, fixed in 2.5 % glutaraldehyde/0.1M sodium cacodylate buffer, washed in PBS and post-fixed in 2%

osmium tetroxide. Samples were embedded in epon-araldite and 70nm sections were stained with lead citrate and viewed on a JEOL-1230 microscope with an AMT XR80 camera.

3.6.10 Distortion Analysis

Distortion analysis of expanded specimens was performed as previously described.[71] Briefly, post-expansion images were aligned with corresponding pre-expansion images using only linear transformations (rotation, scaling, and translation). The linearly transformed post-expansion images were then non-linearly deformed to match the pre-expansion images. Quantitative comparison of the linearly and non-linearly transformed post-expansion images produced values for root-mean-square (RMS) deviation over a range of length scales. All analyses were performed in 3 dimensions and each RMS plot is generated with one set of corresponding (pre/post) images.

3.6.11 Active Zones

AZ numbers were scored as the number of discrete Brp positive structures in 2D projections of confocal stacks from corresponding areas of pre- and post-expansion tissue using the cell counting function of ImageJ. AZ area was measured by computer-assisted tracing of the perimeter of Brp positive structures in 2D projections of confocal stacks, and density measurements represent the number of Brp positive structures per unit area (in 2D projections of confocal stacks). AZ area and density measurements were taken from at least 5 independent samples. AZ architecture (singlets, doublets, multiples) represents the proportion of Brp positive structures with the respective number distinct ring-like structures.

3.6.12 Dendrite-Epithelia Interactions

Epithelial enclosure of somatosensory dendrites was measured in confocal image stacks as previously described.[105] Briefly, image stacks were captured at a Z-depth of 0.15 microns, and where indicated, image stacks were deconvolved using the Leica LAS deconvolution plugin set to adaptive PSF for 10 iterations. 3D reconstruction was performed with Imaris and co-localization was measured between fluorescent signals labeling dendrites (GFP immunoreactivity) and ECM (Perlecan immunoreactivity) using the Imaris Coloc module. The dendrites were traced in Imaris,

portions of the arbor that failed to co-localize with the ECM (apically detached dendrites) were pseudocolored in traces, and the proportion of the arbor that was detached from the ECM was measured in these traces. Dendrites were identified in TEM images as processes near the basal epithelial surface containing arrays of parallel microtubules. 417 total dendrites were scored (in sections of 4 larvae) as ECM attached (in direct contact with the basement membrane) or detached (internalized in the epidermis).

3.7 Acknowledgments

This work was supported by a National Institutes of Health grant (NINDS R01 NS076614), a UW Research Innovation award, and startup funds from UW (J.Z.P.); by a National Institutes of Health grant (NIMH R01 MH115767), a Burroughs-Wellcome Career Award at the Scientific Interface, and startup funds from UW (J.C.V.); and by NSF Graduate Research Fellowship DGE-1256082 (T.J.C.). We thank the CHDD for assistance with TEM sample preparation. Anti-Perlecan antibodies were provided by Stefan Baumgartner, and the Brp antibody was obtained from the Developmental Studies Hybridoma Bank, created by the NICHD of the NIH and maintained at The University of Iowa. Stocks obtained from the Bloomington *Drosophila* Stock Center (NIH P40OD018537) were used in this study.

3.8 Supplementary Information

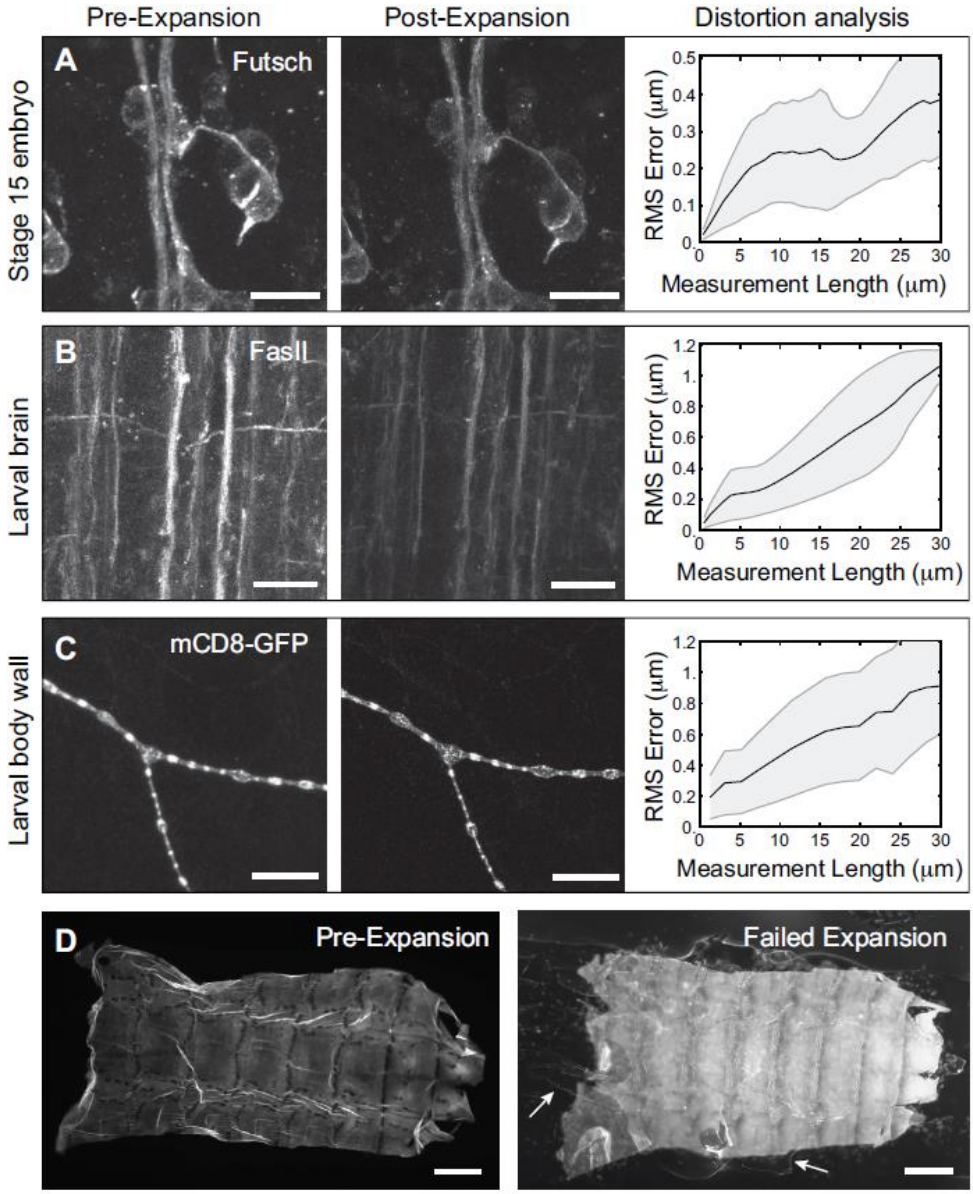

Supplementary Figure 3.1 | (**A-C**) Correlative imaging and distortion analysis of *Drosophila* tissues imaged by confocal microscopy before and after expansion. *Drosophila* (**A**) embryo immunostained for Futsch, (**B**) larval brain immunostained for FasII, and (**C**) larval body wall expressing C4da neuron-specific marker ppk-mCD8-GFP (labeling C4da dendrites) and immunostained for GFP. Distortion analyses (right panels of **A-C**) show root mean-squared error (RMSE, black line) plus or minus standard deviation (gray lines) over a range of length scales. (**D**) DAPI-stained *Drosophila* larval body wall imaged by widefield microscopy before and after attempted expansion; without chitinase treatment, the body wall specimen detached from the hydrogel, showing substantial distortion and tearing (arrows). Scale bars, 10 μm (**A-C**), 500 μm (**D**). All distances and scale bars refer to pre-expansion dimensions.

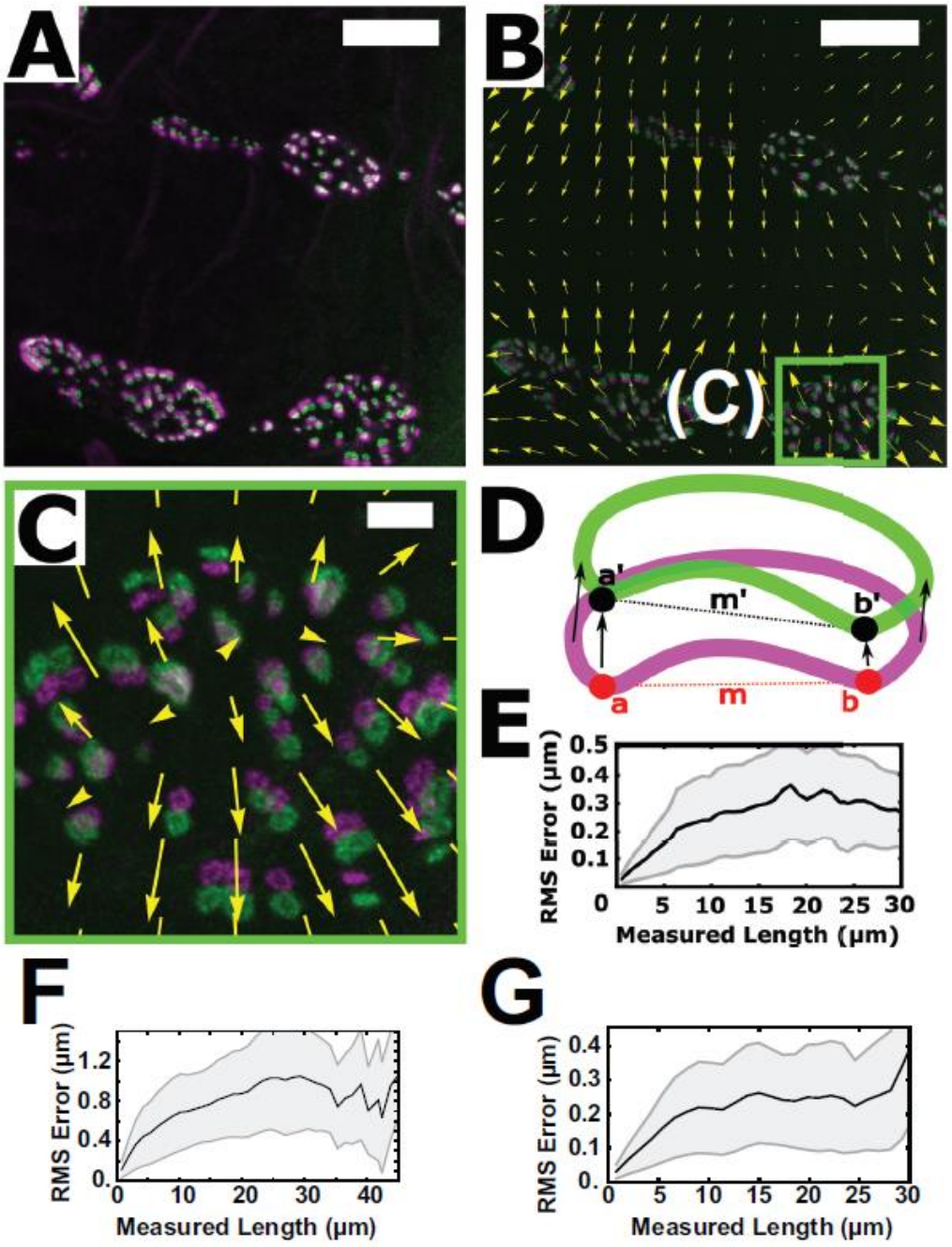

Supplementary Figure 3.2 | Distortion analysis. (**A-E**) Comparison of pre- and post-expansion confocal images of larval body wall fillets immunostained for Bruchpilot. (**A**) Overlay of pre-expansion (magenta) and post-expansion (green) images after registration by similarity transform (a rigid transformation including scaling, rotation, and translation). (**B**) Overlay of post-expansion image before (magenta) and after (green) application of a B-spline registration (non-rigid transformation) to warp the post-expansion image to optimally align it with the pre-expansion data. Yellow arrows show the direction of the relative magnitude (scaled up by a factor of 3.5 for visibility) of the local deformation applied to align the pre- and post-expansion images.

(**C**) Zoomed-in view of the boxed region in (**B**). (**D**) Schematic of correlation analysis procedure. The value *m* represents the distance between points a and b in the pre-B-spline registration image (magenta) while *m'* is the distance between points a' and b' in the post-B-spline-registration image (green). Root mean-square (RMS) error plots were generated by calculating the difference between *m* and *m'* as a function of distance *m* for many sets of points throughout the image (shaded areas represent standard deviation). Note that (**E**) was calculated by performing distortion analysis in three dimensions. Scale bars: 5 µm (**A**,**B**) and 1 µm (**C**). (**F-G**) Distortion measurements for correlative image analysis of (**F**) a mitochondria immunostain from **Fig. 3.2** and (**G**) a Bruchpilot immunostain from **Fig. 3.3**.

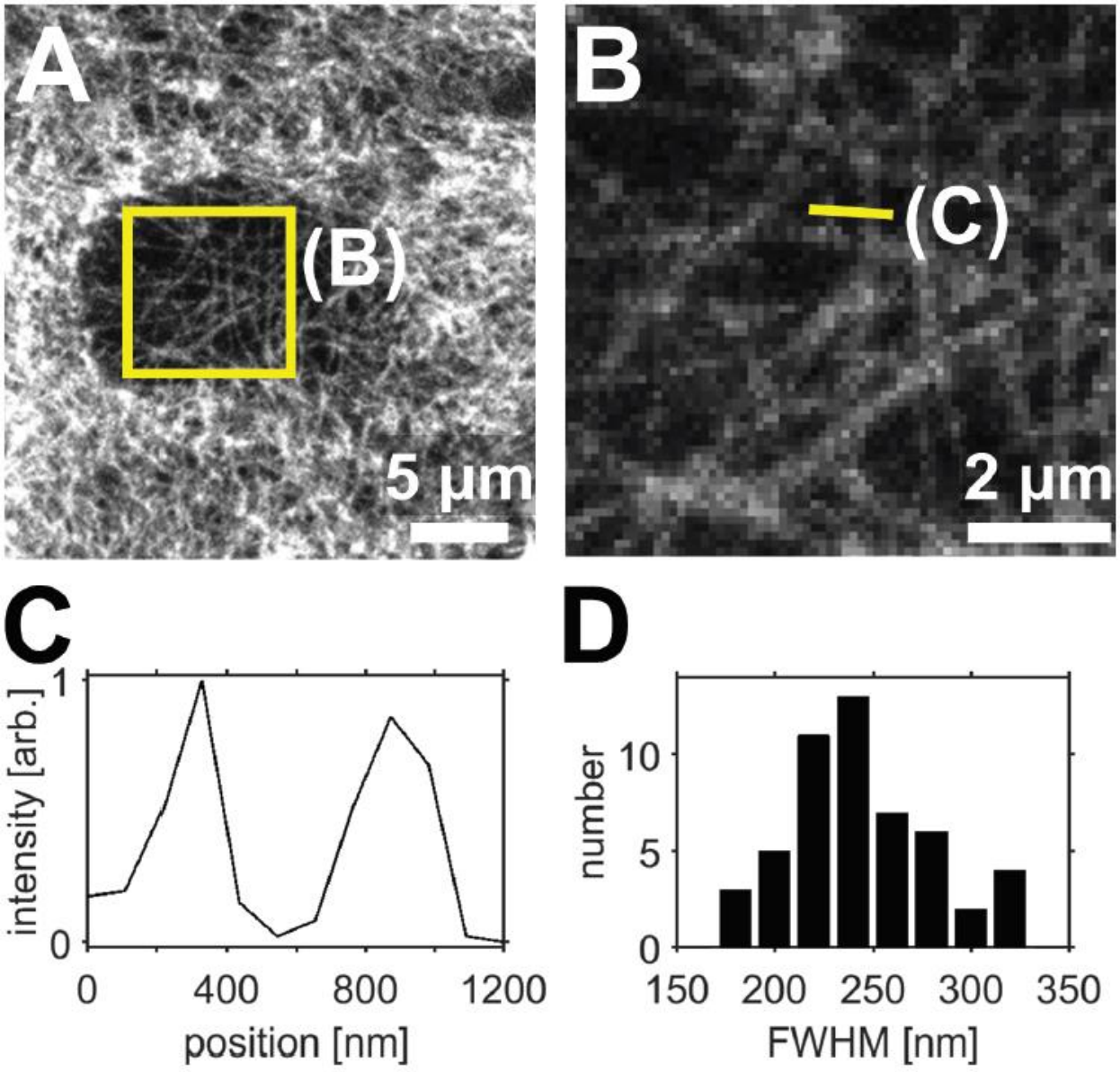

Supplementary Fig. 3.3 | Related to **Fig. 3.2**. (**A-B**) Maximum intensity projections of epithelial cells immunostained for acetylated tubulin (acTub) in unexpanded third instar larval body walls. (**B**) Zoomed-in view of single focal plane image corresponding to boxed regions in (**A**). (**C**) Line profile from **B** (arb., arbitrary units). (**D**) Analysis of microtubule widths.

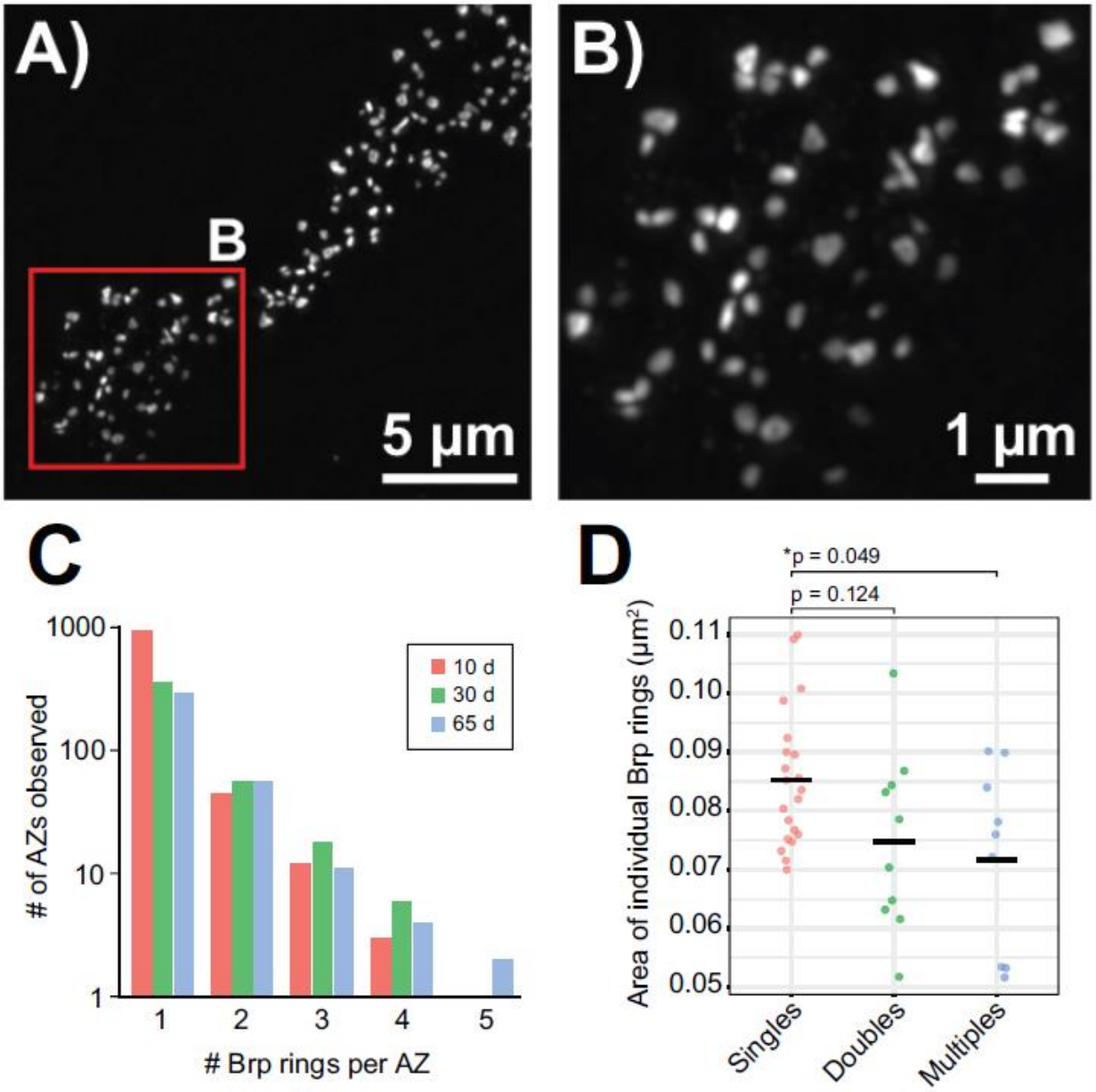

Supplementary Fig. 3.4 | Related to **Fig. 3.3**. (**A-B**) Representative structured illumination microscopy (SIM) images of unexpanded Brp-labeled active zones in fillet preparation of third instar larval body wall (**A**) and zoomed-in view (**B**). The resolution achieved by SIM, which was performed on a Nikon N-SIM microscope, was intermediate between that of confocal microscopy and confocal microscopy of expanded specimens. (**C-D**) Characterization of multiple Brp ring-containing active zones at the adult CM9 neuromuscular junction (NMJ). (**C**) Distribution of multiple Brp ring-containing active zones in 10-day, 30-day, and 65-day adult CM9 NMJs stained with an anti-Brp antibody and imaged using ExM. (**D**) Scatter plot showing the size of individual Brp rings in 65-day adult active zones containing one (singles), two (doubles), or three to five (multiples) Brp rings. Points mark individual measurements and bars mark mean values. *p<0.05, one-way ANOVA with a post-hoc Dunnett's test.

Supplementary Table 3.1 | Staining conditions for each sample in this work. After staining and before gelation, each sample below as treated with 1 mM MA-NHS for 1 hour at room temperature in PBS.

Sample	Fixation	Washing and blocking	Primary antibodies	Incubation time	Secondary antibodies	Incubation time
embryos	Dechorionate 4 min in 50% bleach Fix in 1:1 Heptane:4% PFA 15 min Devitellinize in MeOH	wash with PBST block with 5% NGS in PBST	Mouse anti-Futsch, clone 22c10 (DSHB, 1:100)	4°C overnight	Alexa Fluor 488 (Goat anti-Mouse, Thermofisher A31561, 1:100)	20-25°C 6 h
larval VNC	4% PFA 30 min	wash with PBST block with 5% NGS in PBST	1D4 (Mouse, DSHB, 1:20)	4°C overnight	Alexa488 (Goat anti-Mouse, Thermofisher A31561, 1:100)	20-25°C 6 h
larval VNC	4% PFA 30 min	wash with PBST block with 5% NGS in PBST	Rabbit anti-dsRed (Clonetech #632496, 1:50)	4°C overnight	ATTO 565 (Donkey anti-Rabbit, Vaughan lab, 1:10)	20-25°C 6 h
larval body wall: C4da neurons	4% PFA 30 min	wash with PBST block with 5% NGS in PBST	Mouse anti-GFP, clone 3E6 (Invitrogen #A11120, 1:100)	4°C overnight	Alexa Fluor 488 (Goat anti-Mouse, Thermo Fisher A31561, 1:100)	20-25°C 2-4 h
larval body wall: mitochondria	4% PFA 30 min	wash with PBST block with 5% NGS in PBST	Mouse anti-GFP, clone 3E6 (Invitrogen #A11120, 1:100)	4°C overnight	Alexa Fluor 488 (Goat anti-Mouse, Thermofisher A31561, 1:100)	20-25°C 2-4 h
larval body wall: microtubules	PEM/0.5% Triton X-100, 30 s PEM/4% PFA + 0.5% Triton X-100, 15 min PEM/0.5% Triton X-100, 30 s	wash with PBST block with 5% NGS in PBST	Mouse anti-acetylated-tubulin, clone 6-11B-1 (Sigma #T7451, 1:200)	4°C overnight	Alexa Fluor 488 (Goat anti-Mouse, Thermo Fisher A31561, 1:100)	20-25°C 2-4 h
larval body wall: nuclei	4% PFA 30 min	wash with PBST block with 5% NGS in PBST			Hoechst 33258 (Thermo Fisher, 1:1000)	20-25°C 2-4 h
larval/adult body wall: NMJ active zones	4% PFA 15 min	wash with PBST block with 5% NGS in PBST	Mouse anti-Bruchpilot (Brp), clone nc82 (DSHB, 1:50)	4°C overnight	Alexa Fluor 488 (Goat anti-Mouse, Thermo Fisher A31561, 1:100)	20-25°C 6 h
larval body wall: ECM	4% PFA 30 min	wash with PBST block with 5% NGS in PBST	Rabbit anti-Perlecan (courtesy of Stefan Baumgartner,1:1000)	4°C overnight	ATTO 565 (Donkey anti-Rabbit, Vaughan lab, 1:10)	20-25°C 2-4 h

Abbreviations:ECM, extracellular matrix; MA-NHS, methacrylic acid N-hydroxysuccinimidyl ester; NGS, Normal Goat Serum (Jackson Labs); NMJ, neuromuscular junction; PBST, PBS + 0.3% Triton X-100; PEM, 80 mM PIPES pH 6.9, 2 mM MgCl2 and 0.5 mM EGTA; PFA, EM-grade Paraformaldehyde (EMS); VNC, ventral nerve cord.

3.9 Supplementary Protocol

BACKGROUND: This protocol is based off of methods used in the publication "Super-resolution Imaging of *Drosophila* Tissues Using Expansion Microscopy" and is adapted from the protocol used in "Expansion microscopy with conventional antibodies and fluorescent proteins"[106]. **The following is meant for brain, embryo, and larval *Drosophila* tissues only.** Figures are provided to aid in visualizing the key steps in the procedure.

REAGENTS OR SUPPLIES TO OBTAIN OR PREPARE AHEAD OF TIME (see Supplementary Table 3.1 below for a list of vendors and item numbers):

1. Sylgard 184 Silicone Elastomer Kit (For dissection pads and Polydimethylsiloxane (PDMS) wells)
    a. Sylgard 184 Silicone Elastomer Base
    b. Sylgard 184 Silicone Elastomer Curing Agent
    c. Store at RT
2. Grape juice agar plates (for embryo collection)
    a. Store at 4 °C
3. Dissection tools: Minutien insect pins, forceps, vannas scissors
4. 50% bleach
5. Paraformaldehyde solution (4% in PBS; methanol-free)
6. N-heptane (for embryos)
7. Methanol (for embryos)
8. Poly-L-lysine Solution (0.1% (w/v) in water)
9. Ammonium Persulfate (APS is a salt and initiates polymerization)
    a. Store at 4 °C
10. Tetramethylethylenediamine (TEMED is a liquid and catalyzes polymerization)
    a. Store at 4 °C
11. 2,2,6,6-tetramethylpiperidine 1-oxyl (TEMPO is a solid and inhibits polymerization so that gelation starts after reagents permeate sample)
    a. Store at 4 °C
12. Methacrylic Acid-NHS (MA-NHS is a solid and is used to link proteins to the gel)
    a. Store the powder at 4 °C. KEEP AWAY FROM WATER.
    b. As with all water-sensitive reagents stored below room temperature, allow bottle to warm to room temperature before opening to avoid condensation of water.
13. 40% Acrylamide (w/v) (Acrylamide is a liquid solution and is a monomer of the hydrogel.)
    a. Store at 4 °C
14. 2% Bisacrylamide (w/v) (Bisacrylamide is a liquid solution and is a hydrogel crosslinker.)
    a. Store at 4 °C
15. Sodium Acrylate (SA is an ionic monomer for the hydrogel.)
    a. Store in desiccator at RT.
16. Sodium Chloride (Salt)

17. 1x PBS Buffer pH 7.0
    a. Prepared by diluting 10x PBS Buffer pH 7.0 with deionized water.
18. 1x PBS buffer pH ~6
    a. Made by dissolving 86.8 mol% KH_2PO_4 and 13.2 mol% K_2HPO_4 in deionized water.
19. 10x TAE Buffer (Tris base, acetic acid, and EDTA)
20. 8M Guanidine-HCl (component of proteinase digestion buffer)
21. 1x HBSS with 0.01M $CaCl_2$ and 0.01M $MgCl_2$ (used as collagenase digestion buffer)
    a. Add 0.01M $CaCl_2$ and 0.01M $MgCl_2$ to 1x HBSS w/o calcium, magnesium, and phenol red to make this buffer solution.
22. Proteinase K (Digestion enzyme, 600-800 Units/mL in 50% glycerol.)
    a. Store at -20 °C
23. Chitinase (Enzyme digestion of chitin-rich cuticle, 25 Units.)
    a. Store at -20 °C
24. Collagenase Type I (Digestion enzyme for collagen, 1 g.)
    a. Store at 2-8 °C
25. #1.5 Coverglass (24mm x 50 mm) is convenient to be used as a substrate. Coverglass is convenient as a substrate for two reasons. First, it is useful for performing pre-expansion imaging with short-working-distance microscope objective lenses. Second, excess coverglass can be removed by cutting the coverglass with a diamond knife so it may be digested in a small well that conserves reagents.
26. 8mm Disposable Biopsy Punch
27. Multiwell plate or similar for digestion. 12-well plates are convenient.

STOCK SOLUTIONS

1. Formaldehyde: 4% in PBS
    a. Prepare from 8% stock sealed under inert gas
    b. Store at 4 °C for 1-2 days
2. APS: 10% (w/w) in water
    a. Store at -20 °C for up to 1 week
3. TEMED: 10% (v/v) in water
    a. Store at -20 °C for up to 1 week
4. TEMPO: 1% (w/w) in water
    a. Prepare freshly, within a few hours of use
5. MA-NHS: 1 M in anhydrous DMSO
    a. Store at -20 °C
    b. Keep away from water
6. Monomer Solution. Final concentrations are listed. Recipe achieves ~4x expansion. Bolded quantities in brackets, below, are for 10 mL of monomer solution.
    a. 2 M NaCl **[1.17 g]**
    b. 8.625% (w/v) Sodium Acrylate **[0.863 g]**
    c. 2.5% (w/v) Acrylamide **[0.625 mL]**
    d. 0.15% (w/v) Bisacrylamide **[0.75 mL]**

e. 10× PBS (concentrated PBS stock), pH 7.4 **[1 mL]**
f. Add sufficient water to reach a final volume of 10 mL.
g. Store at 4 °C for up to two weeks.

7. Proteinase digestion Buffer. Bolded quantities in brackets, below, are for 10 mL of solution.
    a. 10x TAE Buffer **[1 mL]**
    b. 0.8 M Guanidine-HCl **[1 mL]**
    c. 0.5% Triton **[0.25 mL]**
    d. Add sufficient deionized water to reach a final volume of 10 mL.
    e. Store at 4 °C. Solution should be stable but we usually consume within a week.
8. Chitinase stock solution: 5 Units/mL in PBS pH 6.0
    a. Aliquot 200 μL of stock solution into 1.5 mL Eppendorf tubes.
    b. Freeze and store aliquots at -20 °C. Frozen aliquots should be stable for at least 1 month.
9. Collagenase stock solution: 5 mg/mL in 1x HBSS with 0.01M $CaCl_2$ and 0.01M $MgCl_2$
    a. Aliquot 200 μL of stock solution into 1.5mL Eppendorf tubes.
    b. Freeze and store aliquots at -20 °C. Frozen aliquots should be stable for at least 1 month.
10. Grape juice agar plates: quantities listed are for 1 L of grape juice agar
    a. 750 mL water
    b. 250 mL grape juice
    c. 30 g agar
    d. 10 g sucrose
    e. 20 mL EtOH
    f. 10 mL Acetic Acid
    g. Dissolve agar in water/grape juice mixture by heating, add remaining ingredients, mix and dispense to petri dishes.
    h. Prior to use, score the surface of the plates with forces and add a dollop of yeast paste to facilitate egg laying.
11. Embryo fixative
12. Tissue Fixative

PRE-EXPANSION PREPARATION

1. Tissue isolation/fixation
    a. Embryos.
        i. Collect *Drosophila* embryos on a yeasted grape juice agar plate for the appropriate length of time and age as needed.
        ii. Harvest embryos, dechorionate in 50% bleach for ~2 minutes, and rinse thoroughly with water
        iii. Using a paintbrush or spatula, transfer embryos to a glass vial containing embryo fixative (equal volumes of heptane and 4% formaldehyde). Fix with vigorous shaking at room temperature for 10-15 minutes.

iv. Allow heptane/formaldehyde phases to separate (embryos will settle at the interface) remove the upper phase (formaldehyde) and add one volume of methanol.
v. Devitellinize embryos by shaking the methanol/heptane mixture for ~30 seconds. Remove heptane phase, rinse embryos in methanol, and transfer embryos to a 1.7 mL tube using a Pasteur pipette.
vi. Wash embryos 3 x in 1 mL PBS + 0.1% Triton-X100 and proceed with immunostaining.

b. Larval/Adult tissue
i. Dissect larvae/adults. "Butterfly" preparations are compatible with staining of body wall tissue or removal of other tissues of interest. Pin larvae (or adult abdomen) at head and tail in a Sylgard dish filled with PBS, fillet along the long axis using vannas scissors, and pin tissue flaps. Remove excess tissue as needed. For more details on fillet preparations see [53].
ii. Fix tissue with 4% Formaldehyde (or other fixative; see supplemental table 1 for details) in PBS with gentle shaking for 15-30 minutes.
iii. Remove fixative and rinse tissue extensively with PBS.
iv. Transfer tissue to 1.7 mL eppendorf tube, wash 3x with PBS (5 min each) to remove residual fixative, and proceed with immunostaining.

2. Immunostaining. Details of immunostaining protocols are available in the materials and methods section of the main text and the accompanying **Supplementary Table 3.1**, **section 3.9**.
3. Prepare a lysine-coated coverglass by applying 10 μL of the stock poly-L-lysine solution to a clean, sterilized 24 mm x 50 mm coverglass and spread out the liquid to cover the region of the surface to be used. Allow the lysine solution to air dry. The lysine-coated coverglass is used to ensure the tissue stays intact on the coverglass.
    a. Apply the poly-L-lysine solution to the coverglass by pipetting 10 μL and spreading it evenly throughout the coverglass.
    b. If different size of coverglass is used, adjust the volume so that the poly-L-lysine solution thoroughly covers the surface of the coverglass.
4. Prepare PDMS (polydimethylsiloxane) wells for convenient solution exchange during post-stain treatment and gelation step. Quantities in brackets, below, are for 10 g. (See **Supplementary Protocol Fig. 3.1**)
    a. Mix 91% Sylgard Silicone Elastomer Base **[9.1 g]** and 9% Sylgard Silicone Elastomer Curing Agent **[0.9 g]** in a 50 mL Falcon centrifuge tube. Make sure the ingredients are thoroughly mixed.
    b. Centrifuge the mixed solution at about 500 g for 3 min.
    c. Pour the PDMS solution into a 3.5'' diameter petri dish. Place the petri dish on a 55 °C hot plate and allow the PDMS to solidify overnight.
        i. If small bubbles form during the process, remove them by gently blowing air with an air hose.

    d. Cut off a rectangular piece using a razor blade and punch out 1-3 holes (roughly matched to the size of the rectangular piece) using an 8 mm biopsy punch or similar. Make sure that the bottom of the PDMS is clean and kept untouched.
    e. This procedure produces ~1 mm thick wells. (See **Supplementary Protocol Fig. 3.1**)
5. Place the cut-out PDMS wells onto the lysine-coated coverglass. If necessary, press on the PDMS wells to make sure there are no bubbles or gaps between them and the coverglass.
6. Place the tissues inside each PDMS well as shown in **Supplementary Protocol Fig. 3.2**. Make sure the tissues are flat on the surface of the coverglass.
    a. For **brain and embryo tissues**
        i. Transfer the tissue with forceps or glass pipets to the center of the well.
    b. For **larval tissues**
        i. Transfer the tissue to the coverglass with the cuticle side facing down. This step is **important** because it allows for more efficient cuticle (chitin) digestion.
    c. Remove excess water with Kim wipe and allow the tissue to "stick" to the coverglass.

POST-STAIN TREATMENT

1. After preparing and immunostaining the sample (or after expression of FP), treat with 1 mM MA-NHS in PBS (freshly diluted from the concentrated DMSO stock). Because NHS groups can rapidly hydrolyze in aqueous solutions, do not make the NHS solution in PBS until just before you are ready to treat your sample.
    a. Depending on how your tissue was fixed, you may need to alter the concentration of MA-NHS.
2. Allow the sample to react for 1 h at room temperature.
3. Wash the sample 2-3 times with several volumes of PBS. Make sure not to disturb the sample.

GELATION

1. Incubate the tissue in monomer solution for 30-45 min at 4 °C prior to gelation to allow monomer to penetrate the whole tissue. **NOTE: the monomer solution here DOES NOT contain APS, TEMED, or TEMPO.**
2. Remove excess monomer solution using a micropipette. Ensure tissue is flat against the glass and not disturbed during the process.
3. Prepare the gelation solution in a separate tube. Quantities in brackets, below, are for a 50 µL volume which is well-suited to 8 mm PDMS wells. Note that APS should always be added last to the gelation solution tube, right before adding the solution to the specimen.
    a. 0.2% TEMED **[1 µL of 10% solution]**

b. 0.01% TEMPO **[0.5 µL of 1% solution]**
c. 95% monomer solution **[~48 µL of monomer stock]**
d. 0.2% APS **[1 µL of 10% solution]**

4. Cover the tissue with the gelation solution without disturbing it. Avoid letting the tissue fold over or float up into the gel.
5. Place a drop of leftover gelation solution on top of the coverglass as a "test" gel to see when the polymerization is complete.
6. Allow the sample to gel at 37 °C for 1.5-2 h.

DIGESTION

1. Remove the PDMS wells without lifting the gel off the coverglass (**Supplementary Protocol Fig. 3.2**). Do not remove the gels from the coverglass at this stage because they may tear.
    a. Note: the sample will slightly expand if it is gelled for too long. While this is fine in most cases, try to avoid this.
2. Cut away excess gel from around the tissue (Your sample will be cleared after expansion and will be difficult to find in a lot of excess gel.) Use a diamond knife or razor blade to score the bottom coverglass near to the tissue and then break away excess coverglass so that the coverglass and gel will fit into the digestion buffer well. (**Supplementary Protocol Fig. 3.4.2**).
3. Place the gel sitting on the coverglass in a suitably sized well, e.g., a well of a 12-well plate.
    a. Keep in mind that the gels will expand slightly (~1.5x) during digestion so make sure the well is a large enough to accommodate the slightly expanded gel.
4. Different digestion steps are required depending on the type of the tissue:
    a. For **brain and embryo tissues**
        i. Add proteinase digestion buffer with ~8 Units/mL of proteinase K to the sample. Make sure to cover the sample completely and allow to digest for 1 h at 37 °C.
    b. For **larval tissues**
        i. Dilute chitinase stock solution to 1 Unit/mL in 1x PBS 6.0 and add to the sample. Make sure to cover the sample completely and allow to digest for ~ 4 days at 37 °C.
        ii. Wash the sample 2-3 times with several volumes of PBS.
        iii. (**For ECM/larval body wall samples only**) Dilute collagenase stock solution to 1 mg/mL with 1x HBSS (w/ 0.01 M $CaCl_2$ and 0.01 M $MgCl_2$) and add to the sample. Digest the sample overnight at 37 °C.
            1. Then wash the sample 2-3 times with PBS.
        iv. Digest the gel with Proteinase K by following the procedure in (a).

EXPANSION

1. Remove the gel from digestion buffer and place in DI water to expand. Anticipate the size of the expanded gel (~32 mm for 8 mm PDMS wells) and use a suitably sized container such as a 3.5” petri dish.
2. Exchange water as needed until fully expanded (typically 2-3 exchanges). The refractive index of the gel is nearly identical to that of water so you will not easily see the gel. Be careful not to pour out or aspirate the gel. Typical expansion times are 1-2 hours, total, with exchanges every ~30 min. The specimen should expand ~4× compared to the initial sample before gelation. If desired, the expansion factor can be tuned by adding more or less bisacrylamide crosslinker, where more bisacrylamide leads to less expansion and vice versa.
3. Thinner gels will expand relatively quickly and may only need one water exchange.

SAMPLE HANDLING TIPS

- Removing expanded gels from petri dishes (or handling them in general) can be difficult. A large rectangular coverglass (~1” x 2”) is probably the best tool to use but other flat objects or spatulas may also work well. Place the coverglass short edge against the petri dish surface and tilt the dish to allow the gel to gently slide onto the coverglass. Cut away excess gel if necessary and remove as much water as possible before picking up the gel. (**Supplementary Protocol Fig. 3.3**)
- Try to gently wick away excess water before imaging using a Kim wipe. The gels will otherwise slide around during imaging. Be sure not to touch the side where the sample is facing (usually the bottom) as doing so would disturb the sample.
- If the gels fold over onto themselves after removing excess water, try to use a fine tip paintbrush and gently poke the edges of the gel back until the sample is back in its original shape.
- Illuminating the specimen from below with a flashlight and observing against a dark background are helpful when trying to locate your tissue within the gel. Look for a small amount of scattering.
- It is highly recommended to use a poly-L-lysine coated coverglass for post-ExM imaging because it will firmly hold the gel in place and reduce sample drift during acquisition. If there are bubbles present underneath the gel, pop them by simply pressing down the gel.

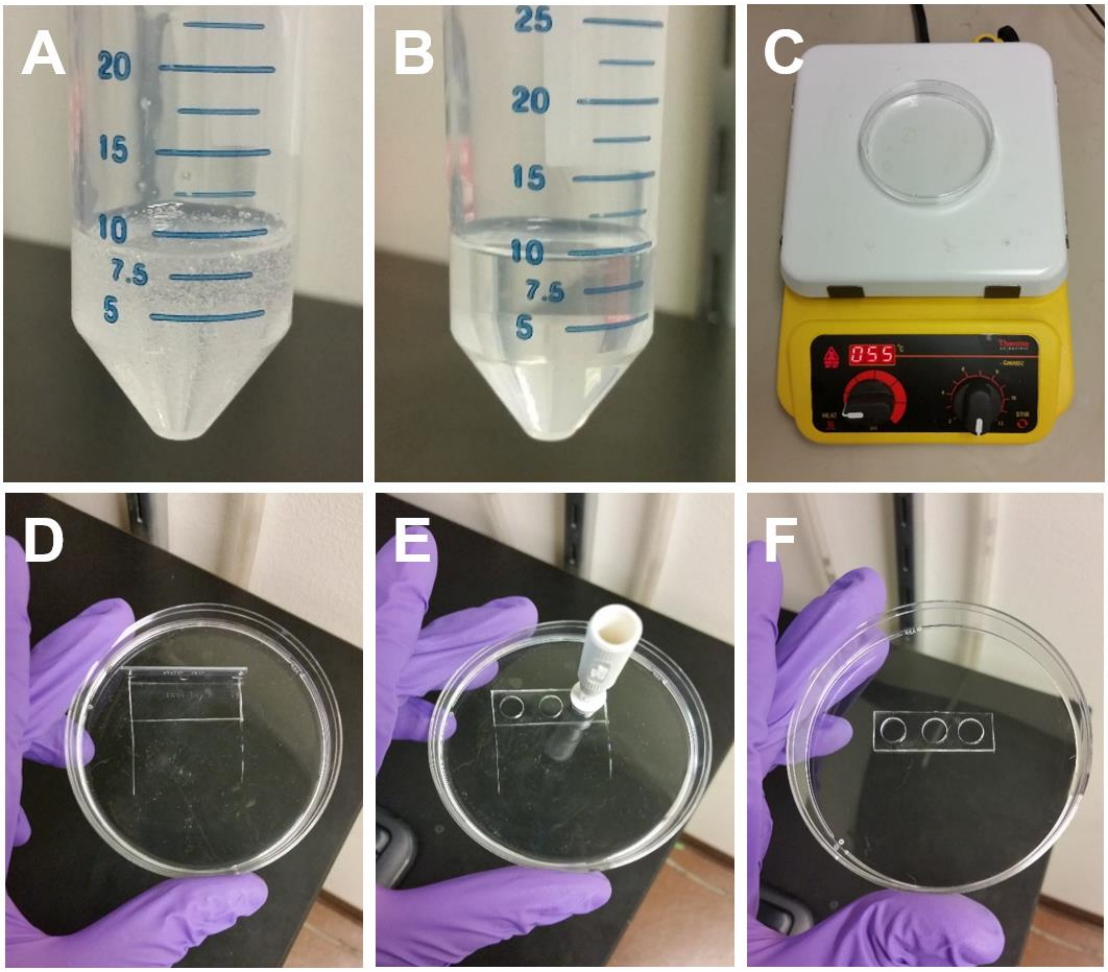

Supplementary Protocol Figure 3.1 | Preparation of PDMS wells. Sylgard silicone elastomer base and curing agent mixture (**a**) before and (**b**) after centrifugation to remove bubbles. (**c**) PDMS solution poured into a 3.5” diameter petri dish and placed on a 55 °C hot plate. (**d**) Rectangular PDMS block cut out with a razor blade. (**e**) 8 mm wells created in rectangular PMDS block using disposable 8mm biopsy punch. (**f**) PDMS wells are detached and stored in a clean petri dish until use.

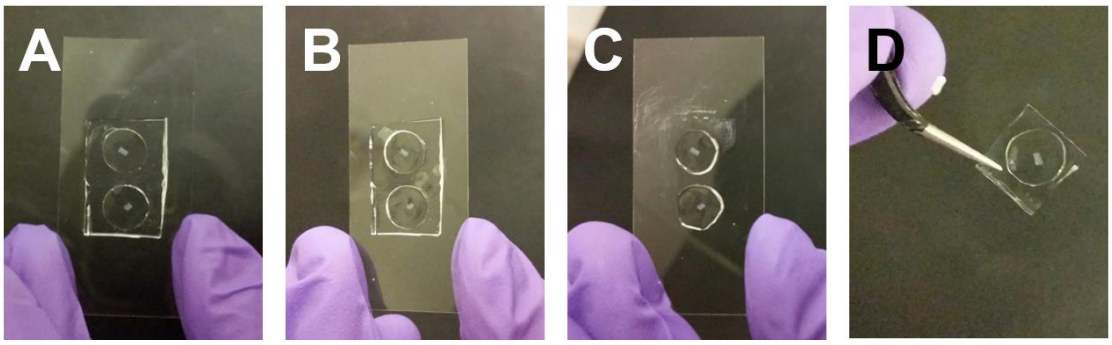

Supplementary Protocol Figure 3.2 | (**a**) Mounted *Drosophila* larval tissues (small opaque rectangle) inside 8 mm PDMS wells. Specimen (**b**) after polymerizing hydrogel within the PDMS wells and (**c**) after removal of PDMS well, leaving behind 8 mm hydrogel "pucks" containing *Drosophila* tissues. (**d**) Individual hydrogel puck after trimming coverglass substrate with glass cutter or razor blade.

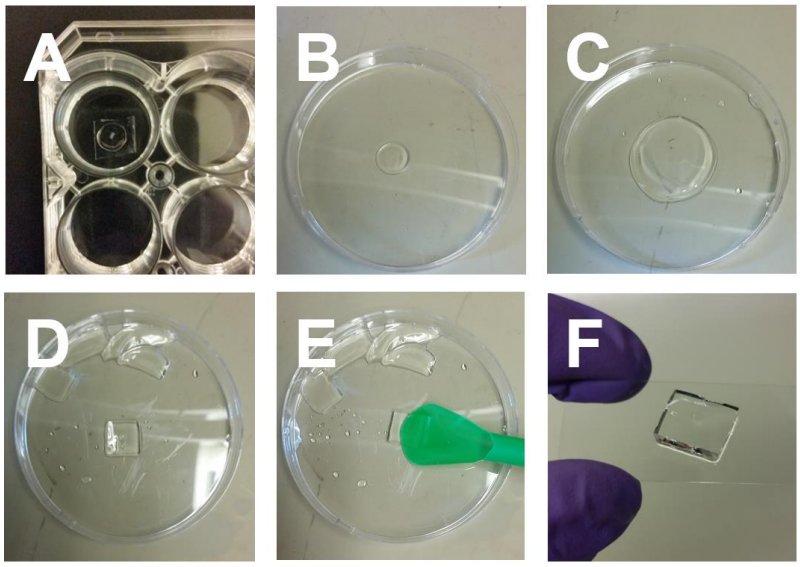

Supplementary Protocol Figure 3.3 | (**a**) Trimmed coverglass specimen is placed in a well of a 12-well plate and digested. (**b**) Specimen after digestion. (**c**) Specimen after expansion. (**d**) Excess hydrogel is trimmed away from the specimen. (**e**) Removal of expanded, trimmed specimen using a disposable spatula. (**f**) Mounted specimen on poly-L-lysine coated coverglass.

Sources for reagents used in this protocol

Reagent	Vendor	Product #
Sylgard 184 Silicone Elastomer Kit	Dow Corning	N/A
Minutien Insect Pins	Fine Science Tools	26002-10
Vannas Scissors	World Precision Instruments	501778
8% paraformaldehyde solution	Electron Microscopy Sciences	157-8
n-heptane	Thermo Scientific	BP1115500
methanol	Thermo Scientific	BP1105
Poly-L-lysine Solution (0.1% (w/v) in water)	Sigma-Aldrich	P8920
Ammonium Persulfate	Thermo Scientific	17874
Tetramethylethylenediamine	Bio-Rad	1610800
2,2,6,6-Tetramethylpiperidine-1-oxyl	Sigma-Aldrich	176141
Methacrylic Acid-NHS	Sigma-Aldrich	730300
40% Acrylamide (w/v)	Bio-Rad	1610140
2% Bisacrylamide (w/v)	Bio-Rad	1610142
Sodium Acrylate	Sigma-Aldrich	408220
Sodium Chloride, Granular	Avantor	7713
10x PBS pH 7.0	Thermo Scientific	BP39920
Potassium Phosphate Monobasic	Thermo Scientific	P285500
Potassium Phosphate Dibasic	Thermo Scientific	P290500
10x TAE Buffer	Thermo Scientific	148698
Guanidine-HCl	MP-Bio	101905
1x HBSS w/o Calcium, Magnesium, and Phenol Red	Corning	16115011
Proteinase K	Thermo Scientific	EO0491
Chitinase	Sigma-Aldrich	C6137
Collagenase Type I	Gibco	17100017
#1.5 Microscope Cover Glass	Thermo Scientific	12-544E
8mm Disposable Biopsy Punch	Acuderm	P850
12-Well Plate with Lid	CytoOne	CC7672-7512

Chapter 4

Volumetric, Nanoscale Optical Imaging of Mouse and Human Kidney via Expansion Microscopy

4.1 Preface

Again, seeking to extend the utility of ExM to a broader range of sample types, we next established the goal of expanding kidney tissue due to its clinical importance. Recent studies report that approximately 1 in 7 adults in the United States (approximately 30 million people) suffer from kidney disease and that >90% of those with kidney damage or reduced kidney function are unaware of their condition due to a lack of symptoms in the early stages of kidney disease.[108,109] Diagnosis of certain kidney conditions requires visual confirmation of nanoscale phenotypes and is traditionally performed using electron microscopy because of its superior spatial resolution[110,111]; however, it suffers from some of the same limitations associated with instrument-based super-resolution microscopy techniques (high cost, limited accessibility, non-trivial volumetric data acquisition, etc.). As shown in the previous chapters, ExM is well-suited to overcome these challenges and thus has the potential to be an inexpensive and effective compliment to electron microscopy in the visual diagnosis of kidney diseases.

Just as before, the expansion of new tissue types requires careful method adaptation, optimization, and validation. Kidney is known to have large quantities of connective tissues such as collagen and elastin[42] and, as it will be shown in the following sections, additional digestion enzymes must be incorporated into the protocol to achieve low-distortion expansion of mouse and human kidney tissue. Additionally, because expanded specimens are rendered optically transparent and have a refractive index nearly identical to that of water, volumetric images of kidney tissues can be obtained using water immersion objectives without depth-dependent resolution degradation (**section 1.3.1**). Large, volumetric data sets such as these are not easily obtained with electron microscopy and, thanks to the molecular specificity of

immunofluorescence, also contain information about the spatial distributions of various molecular species.

Around the same time that the manuscript described in this chapter was submitted, another research article demonstrating super-resolution imaging of kidney tissue via sample expansion was published. However, as will be discussed later, the authors used a separate protocol that utilizes a different strategy for linking proteins to the hydrogel matrix and a non-enzymatic homogenization step.[43,112] This alternative method as well as many others in the literature demonstrate the growing popularity of ExM and highlight the need for robust protocol development so that potential users are well-informed when choosing a particular variation to implement.

I was highly involved with and contributed to all aspects of this project. Chenyi Mao and I co-authored the protocol provided with this work (**section 4.9**), which is based on my protocols from **section 2.10**. This work was carried out in collaboration with members from the laboratories of Dr. Charles E. Alpers, Dr. Stuart J. Shankland, and Dr. Behzad Najafian who provided mouse and human kidney tissue. All authors contributed to editing the manuscript. Supplemental figures as well as a supplementary protocol are provided in addition to the main text.

4.2 Abstract

Although light microscopy is a powerful tool for the assessment of kidney physiology and pathology, it has traditionally been unable to resolve structures separated by less than the ~250 nm diffraction limit of visible light. Here, we report on the optimization, validation, and application of a recently developed super-resolution fluorescence microscopy method, called expansion microscopy (ExM), for volumetric interrogation of mouse and human kidney tissue with 70-75 nm lateral and ~250 nm axial spatial resolution. Using ExM with a standard confocal microscope, we resolve fine details of structures that have traditionally required visualization by electron microscopy, including podocyte foot processes, the glomerular basement membrane, and the cytoskeleton. This inexpensive and accessible approach to volumetric, nanoscale imaging enables visualization of fine structural details of kidney tissues that were previously difficult or impossible to measure by conventional methodologies.

4.3 Introduction

The kidney glomerulus is a compact network of capillaries, supporting tissue, and resident cells. A critical structure of the glomerulus is the three-layered glomerular filtration barrier (GFB) that filters waste products from the blood space to the urinary space and is comprised of innermost fenestrated glomerular endothelial cells, glomerular basement membrane (GBM), and outermost interdigitated epithelial cells called podocytes. A major limitation in imaging the GFB is that many of the structures of the GFB are too small and too densely packed to be resolvable by the ~250 nm resolution of traditional diffraction-limited light microscopy. To date, the analysis of fine structural details of the GFB has primarily relied on electron microscopy (EM). Although extremely powerful, EM is typically limited to thin sections (<100 nm) and has a poor ability to report on distributions of specific protein molecules. Advanced EM methods such as serial block face scanning electron microscopy (SEM) or focused ion beam SEM can produce high-resolution volumetric image stacks that are on the order of 100 µm thick, although the instruments are not yet widely available and the data acquisition process is timeconsuming.[114] Correlative light and electron microscopy is technically demanding and requires use of sophisticated instruments

and/or workflow, and typically lacks high-resolution volumetric information.[115] There is thus a strong need for new, accessible tools to interrogate kidney tissue with high spatial resolution, practical volumetric imaging capability, and molecular specificity.

A range of established super-resolution fluorescence microscopy methods are capable of analyzing 3D molecular distributions at length scales below 250 nm and have recently been applied to the study of kidney. Single molecule localization microscopy (SMLM), stimulated emission depletion (STED) microscopy, and structured illumination microscopy (SIM) have been used to study separate components of the GFB such as GBM composition[116], slit diaphragm structure[33], and podocyte effacement in diseased tissue[117], respectively. Unfortunately, each of these methods currently suffers from certain limitations which still hinder widespread implementation. SMLM and STED have strict requirements for fluorophore properties, which create challenges for multicolor imaging. Additionally, SMLM, and to a lesser extent SIM (in its most common, commercial implementations) typically have poor resolution beyond a few micrometers from a coverglass substrate. Moreover, all of these methods require expensive, specialized instruments, and substantial technical and interpretive expertise.

Here, we report on the optimization, validation, and application of a recently developed super-resolution fluorescence microscopy method, called expansion microscopy (ExM), for volumetric nanoscale interrogation of mouse and human kidney tissue using a conventional fluorescence microscope. In ExM, fluorescent labels on fixed specimens are linked to a swellable polymer hydrogel that is grown within the specimen, after which the specimen is homogenized to facilitate uniform expansion and then swollen through incubation with deionized water (**Fig. 4.1a**).[35,43,49,118] The physical magnification of the specimen in ExM allows features closer than the diffraction limit of light (~250 nm) to become resolvable in the expanded state. Additionally, the procedure renders samples optically clear with little scattering, facilitating deep volumetric imaging. With ~4× expansion per dimension, we achieve 70-75 nm lateral and ~250 nm axial spatial resolution at substantial depths, enabling nanoscale analysis of volumetric data sets as well as digital reorientation to ensure *en face* or orthogonal views. Additionally, because imaging is performed with a confocal microscope, multichannel data collection is straightforward.

4.4 Results

4.4.1 Expansion of Mouse Kidney Tissue

Faithful expansion of a biological specimen using ExM requires the specimen to be homogenized after hydrogel embedding in order to avoid non-uniform expansion or tearing during the expansion process. Our initial results showed that homogenization procedures previously established for cultured cells and brain tissue using the broad-specificity protease proteinase K[35,49,118] was unable to successfully homogenize fresh 100 µm mouse kidney sections embedded in hydrogel and led to gross distortions of the tissue (**Supplementary Fig. 4.1**). To test the hypothesis that the kidney's collagen-rich extracellular matrix hindered homogenization, a collagenase digestion step was added and led to robust expansion with high fidelity (**Fig. 4.1b-g**, **Supplementary Fig. 4.1**). It should be noted that treatment with heat and detergent, which is used in the magnified analysis of the proteome (MAP) protocol under different fixation and hydrogel embedding conditions[43,112], did not successfully homogenize the specimen (**Supplementary Fig. 4.1**). Interdigitated podocyte foot processes that were separated by <250 nm were clearly evident in the post-expansion images but were unobservable pre-expansion (**Fig. 4.1e-f, h-j**). A comparison of pre-expansion and post-expansion images of the same regions revealed that expansion-induced distortions were relatively minor, with 2-4% distortions for length scales up to ~150 µm and <2% for larger length scales (**Fig. 4.1d, g**; see also **Supplementary Fig. 4.2**). Based on the measured cross-sectional profiles of microtubules in expanded kidney tissue, we estimate our resolution to be ~70-75 nm (**Supplementary Fig. 4.3**). Note that all distances and scale bars for expanded specimens have been divided by their respective, measured expansion factors of ~4× and therefore refer to pre-expansion dimensions.

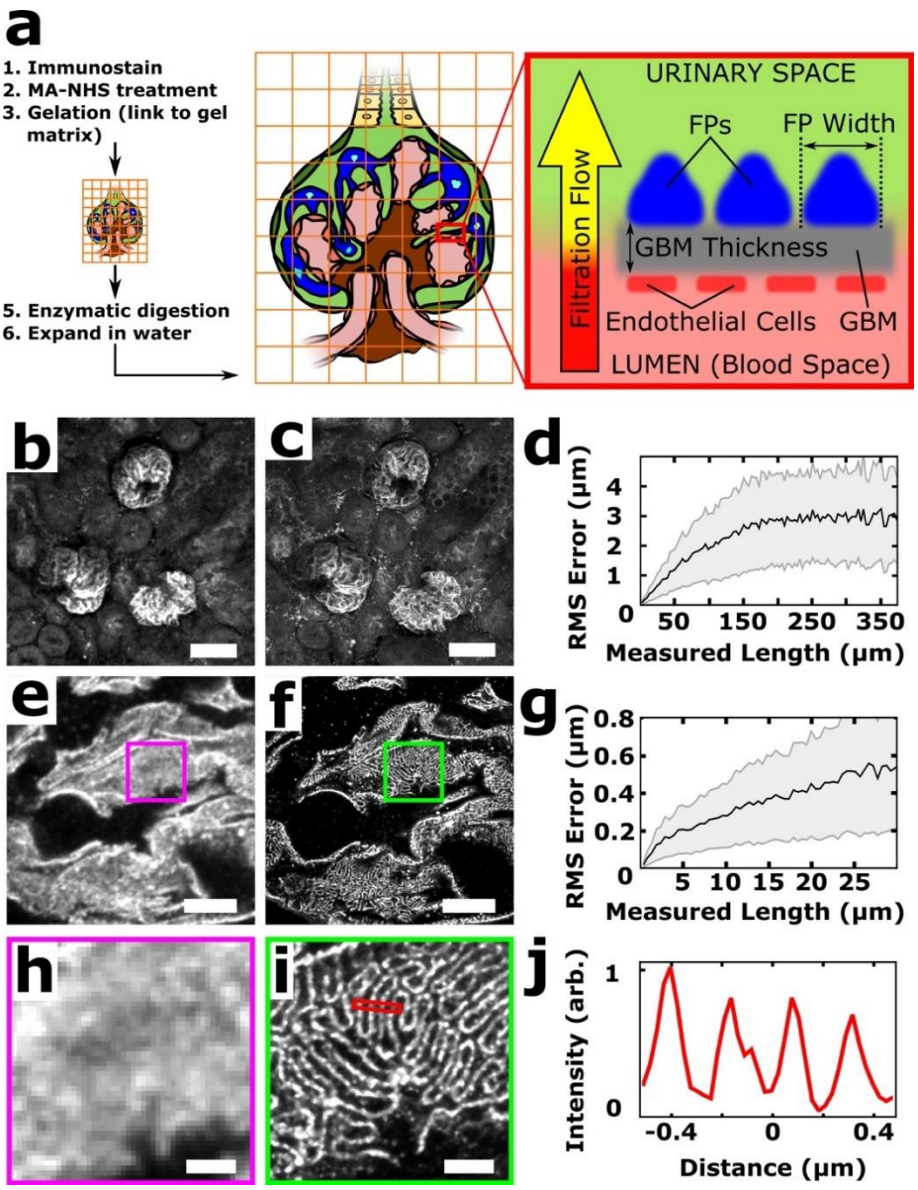

Figure 4.1 | **ExM schematic and validation in mouse kidney.** (**a**) Fixed tissue is immunostained, treated with methacrylic acid *N*-hydroxy succinimidyl ester (MA-NHS) to covalently link antibody labels and proteins to the hydrogel during gelation, homogenized by enzymatic digestion, and then expanded ~4× along all dimensions by incubation with deionized water. (**b-c**) 100 µm thick mouse kidney section immunostained for podocin and imaged before (**b**) and after (**c**) expansion using a 10× 0.4 numerical aperture (NA) air objective lens. (**d**) Quantification of expansion-induced distortions for panels **b** and **c** showing root mean square (RMS) error as a function of distance. (**e-f**) Mouse kidney section immunostained for podocin and imaged before (**e**) and after (**f**) expansion using a 63× 1.2 NA water immersion objective lens. (**g**) Quantification of expansion-induced distortions for panels **e** and **f**. (**h**, **i**) Zoomed-in views of boxed regions in **e** and **f**, showing that the expanded specimen successfully reveals interdigitated podocyte foot processes. (**j**) Cross-sectional profile of boxed region in **i.** All distances and scale bars are in pre-expansion units. Scale bars, 50 µm (**b**, **c**), 5 µm (**e**, **f**), 1 µm (**h**, **i**).

We next assessed fine structural details that were observable by expanding mouse kidney sections that had been labeled with a range of antibodies or fluorescent proteins. A triple immunostain for podocin (podocyte foot process junctions), agrin (glomerular basement membrane), and podocalyxin (podocyte apical surfaces and, more weakly, endothelial cells) clearly resolved the separate layers of the GFB, and demarcated podocyte foot processes (**Fig. 4.2a-d**). A triple immunostain for synaptopodin (body of podocyte secondary foot processes), acetylated tubulin (podocyte primary foot processes, generally), and podocin enabled the identification of primary and secondary foot processes, and revealed the expected interior/surface relationship of stains for synaptopodin and podocin (**Fig. 4.2e-h**). A triple immunostain for full-length collagen IV (basement membrane, mesangium, and Bowman's capsule), podocalyxin, and α smooth muscle actin (afferent and efferent arterioles and mesangium) showed larger-scale features of the glomerulus (**Fig. 4.2i-l**). Taking advantage of permanently lineage-tagged cells in reporter mice[119], we found that our procedure is also compatible with genetically-encoded fluorescent proteins (without post-fixation immunolabeling) by recording images of expanded mouse kidney sections derived from a Podocin-confetti mouse (**Fig. 4.2m-r**). The expression of GFP, YFP, and RFP within different podocytes allowed them to be clearly identified as distinct cells over relatively large regions. Altogether, the expansion of kidney tissues was robust and versatile, with the ability to report on key glomerular structures and distributions of proteins using genetically encoded or exogenous fluorescent labels.

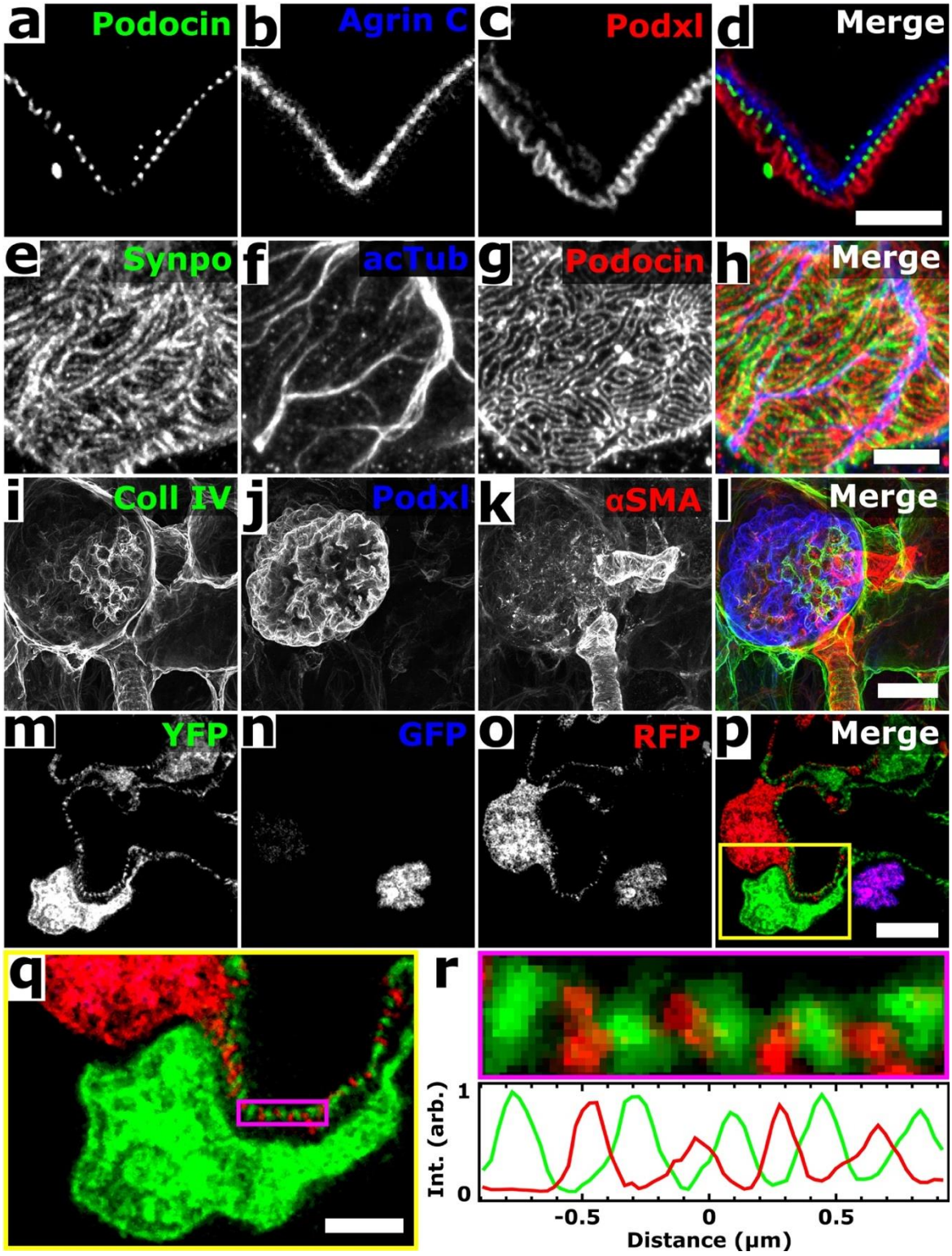

Figure 4.2 | Confocal ExM images of mouse kidney labeled with antibodies or fluorescent proteins. (**a-c**) Single focal plane of glomerulus immunostained for podocin (**a**), agrin (**b**), podocalyxin (Podxl **c**), and merge (**d**) of **a-c**. (**e-g**) Confocal maximum intensity projections of

glomerulus immunostained for synaptopodin (Synpo, **e**), acetylated tubulin (acTub, **f**), podocin (**g**) highlighting secondary FPs, primary FPs, and slit diaphragms/FP boundaries, respectively. (**h**) Merge of **e-h**. (**i-k**) Confocal maximum intensity projections of glomerulus immunostained for collagen IV (Coll IV, **i**), podocalyxin (Podxl, **j**), and α smooth muscle actin (αSMA, **k**) and highlighting Bowman's capsule and the mesangium, podocytes, and arterioles and the mesangium, respectively. (**l**) Merge of **i-k**. (**m-p**) Single focal plane of glomerulus showing native fluorescence from confetti mouse expressing YFP (**m**) and RFP (**o**) in separate podocyte cell bodies and FPs as well as GFP (**n**) in various podocyte nuclei. (**p**) Merge of **m-o**. (**q**) Zoomed-in view of region highlighted in **p**. (**r**) Further zoomed-in view (top) and cross-sectional profile (bottom) of boxed region highlighted in **q**. All distances and scale bars are in pre-expansion units. Scale bars, 2 μm (**a-h**, **q**), 25 μm (**i-l**), 5 μm (**m-p**).

In order to further validate this approach, we measured quantitative features of the GFB such as foot process width and GBM thickness, which are metrics that are of clinical use and are typically obtained via transmission EM (TEM). Unlike TEM, however, which is typically measured in two dimensions on thin tissue sections, volumetric data sets are easily obtained with ExM (**Fig. 4.3a**, **Supplementary Video 4.1** and **4.2**) and enable the viewing of images *en face* or orthogonally. This approach therefore avoids sectioning artifacts that commonly occur when imaging thin sections that can, for instance, lead to overestimation of foot process width or GBM thickness.[120,121] An immunostain for podocin was used to measure the average foot process width (FPW) in three different ways (**Fig. 4.3c-h**). First, an analysis of many cross-sectional profiles *en face* revealed an average peak-to-peak separation of 247 ± 29 nm (mean ± standard deviation (SD)), which was taken to be the average FPW (**Fig. 4.3c-e**). Second, the length of a cross-sectional profile drawn across an orthogonal view of podocin signal was divided by the number of foot processes (troughs) along it, giving an average FPW of ~250 nm (**Fig. 4.3g, h**). Third, a stereological approach originally developed for two-dimensional TEM[122,123] was used to calculate the average FPW by dividing the area of a region of GFB by the total length of podocin signal within that area (red trace in **Fig. 4.3c**), again giving a similar value of 240 ± 46 nm (mean ± SD) (**Fig. 4.3f**). Previous studies utilizing different fixation and hydrogel-embedding methods[33,112] from those used here have resolved the slit diaphragm and reported its width to be ~80 nm, close to our estimated spatial resolution of 70-75 nm. Next, the distribution of three GBM proteins were measured for regions of the GBM that were oriented perpendicular to the plane; agrin

exhibited an average full width at half maximum (FWHM) of 178 ± 36 nm while vimentin and collagen IV stains in the same mouse revealed average GBM thicknesses of 192 ± 36 nm and 147 ± 26 nm (mean ± SD) (**Supplementary Figure 4.4**), respectively, in agreement with previously measured GBM thicknesses measured by SMLM in ultracryomicrotome sections.[116] Nanoscale features could be resolved in these specimens at relatively large depths (up to ~120 µm in expanded specimens, or ~30 µm in pre-expansion units) and were limited here simply by the working distance of the objective lens available on our microscope **Supplementary Fig. 4.3, 4.5**).

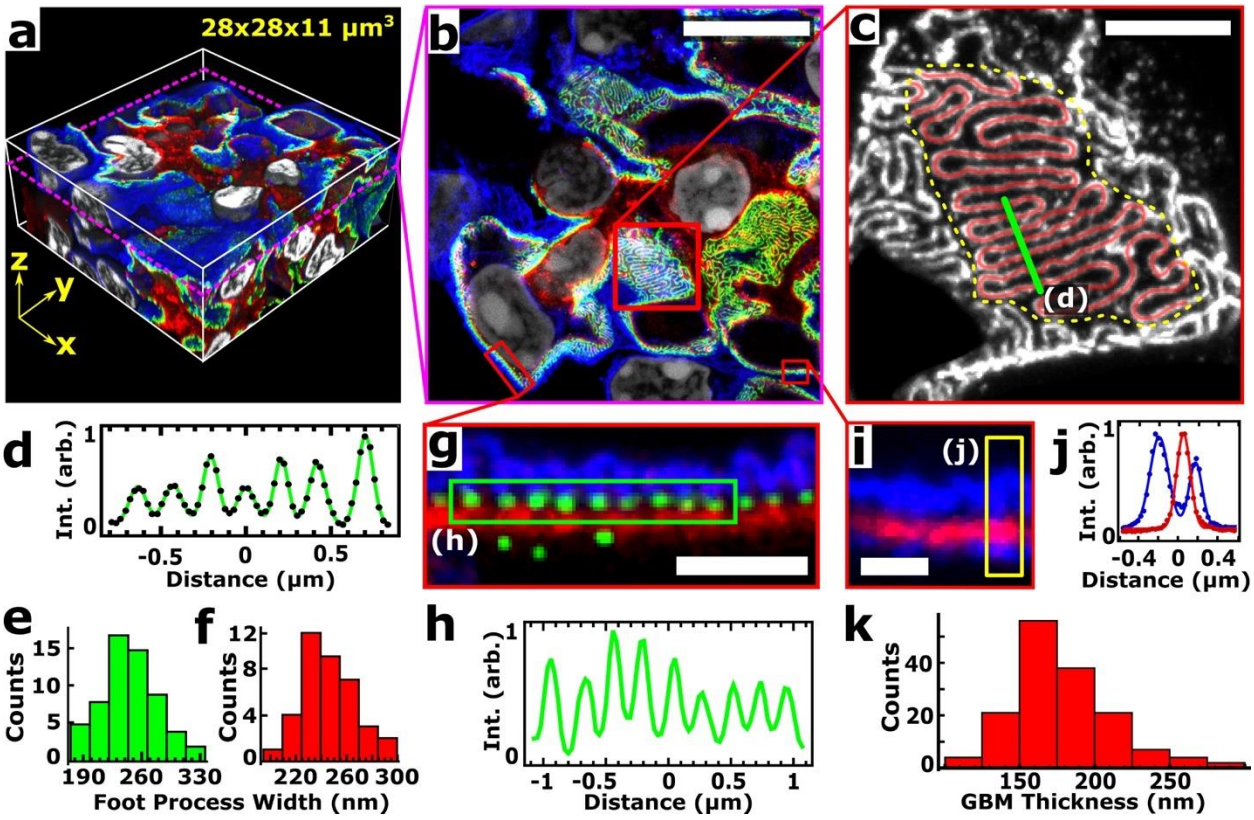

Figure 4.3 | **Quantification of GBM thickness and FP width.** (**a**) Volume perspective rendering of expanded mouse kidney immunostained for podocin (green), agrin (red), podocalyxin (blue), and stained for DNA with Hoechst (white), highlighting podocyte foot process (FP) boundaries, glomerular basement membrane (GBM), endothelial cells, the apical side of FPs, and nuclei, respectively. See **Supplementary Video 4.1** for an animation of this volume. (**b**) A single confocal image plane from data shown in **a**. (**c**) Zoomed-in view of podocin channel from boxed region in **b** showing two methods for FP width (FPW) analysis. (**d**) Line profile (Int., signal intensity) of line in **c** (arb., arbitrary units) including a fit of the profile (black dots) with several Gaussians (green line) for determining positions of FPs. (**e**) Histogram of FPW determined by measuring peak-to-

peak distances in **d** (data from 2 kidney samples, 7 glomeruli, and 61 profiles). (**f**) Histogram of average FPWs (data from 2 kidney samples, 7 glomeruli, and 39 profiles) determined by dividing the area within a flat region of the glomerulus (yellow dashed line) by the length of the podocin signal within that area (red lines in **c**). (**g**) Zoomed-in view of boxed region in **b** where the basement membrane and FPs are approximately perpendicular to the image plane (nuclear channel omitted for clarity). (**h**) Cross-sectional profile of the (green) podocin channel in the boxed region of **g**. (**i**) Zoomed-in view of the podocalyxin (blue) and agrin (red) channels from the boxed region in **b**. (**j**) Cross-sectional profile (points) of the boxed region in **i** together with Gaussian fits (lines). (**k**) Histogram of GBM thicknesses measured as the full width at half maximum of multiple agrin profiles (data from 3 kidney samples, 4 glomeruli, and 154 profiles). All distances and scale bars are in pre-expansion units. Scale bars, 8 μm (**b**), 2 μm (**c**), 1 μm (**g**), and 500 nm (**i**).

4.4.2 Expansion of Human Kidney Tissue

We next sought to use the kidney ExM procedure described above on fresh human (nephrectomy) kidney tissue. Unfortunately, digestion with proteinase K and collagenase was insufficient for homogenization, and human kidney specimens expanded poorly (**Supplementary Fig. 4.6**). Based on our previous results showing that collagenase is necessary for mouse kidney digestion, we hypothesized that the poor homogenization was caused by the presence of one or more additional proteins in the extracellular matrix of human kidney which are more abundant than their counterparts in mouse kidney. We considered elastin as a candidate due to its abundance in human tissue.[42,124,125] Following the incorporation of an additional, initial digestion step with the enzyme elastase, in addition to the proteinase K and collagenase digestion steps, reliable expansion of fixed 100 μm human kidney sections was successfully achieved (**Fig. 4.4a**). Quantitative correlative analysis of pre- and post-expansion images of the same region of human kidney stained for podocin showed distortions of 1-3% over a range of length scales (**Supplementary Fig. 4.7**). Measurements showed foot process widths of ~418 ± 61 nm using a series of cross-sectional profiles (**Fig. 4.4c**) and ~426 ± 31 nm (mean ± SD) using areas divided by the length of the podocin signal (**Fig. 4.4d**), consistent with values reported in the literature.[122,123] In some instances, this methodology resolved two closely-spaced features within the podocin signal with a separation of 113 ± 13 nm (mean ± SD) (**Supplementary Fig. 4.8**) that likely represent expression of podocin within adjacent foot processes.

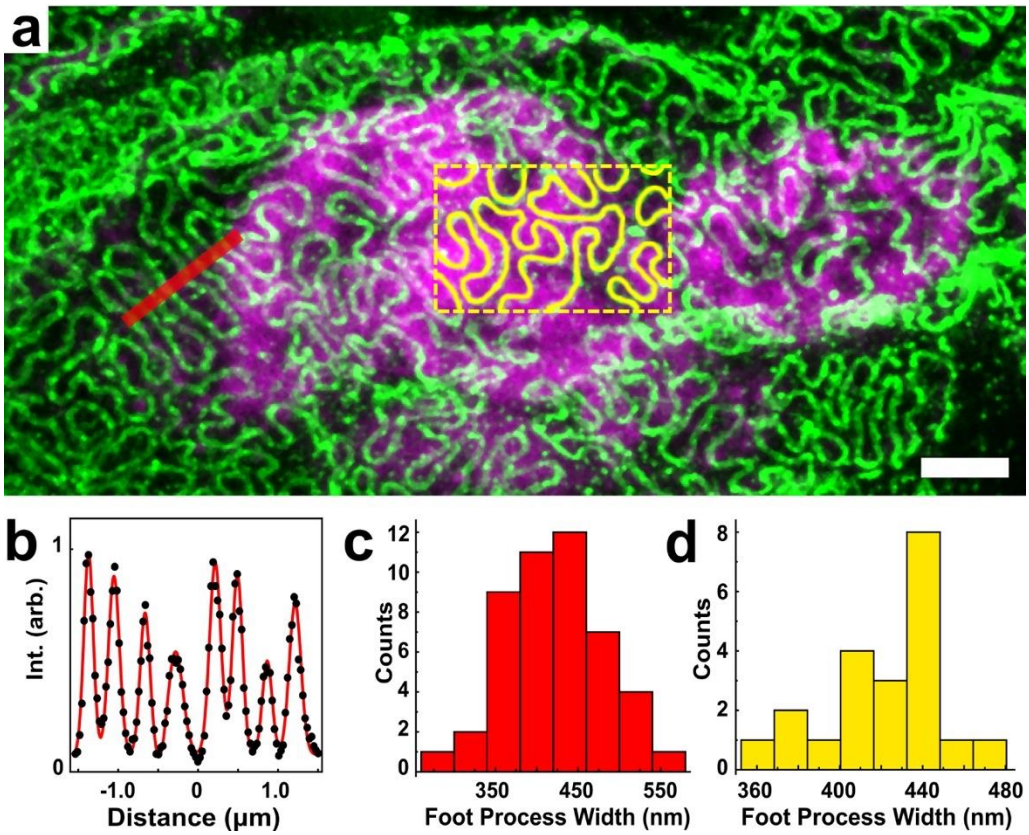

Figure 4.4 | **Confocal ExM images of expanded human kidney tissue.** (**a**) Human kidney immunostained for podocin (green) with nuclei stained by Hoechst (magenta). (**b**) Cross-sectional profile along the red line in **a** and fitted with multiple Gaussian functions (black dots are data, and red curve is result of Gaussian fitting). (**c**) Histogram of foot process widths determined by a set of peak-to-peak distances in **a**. (**d**) Histogram of foot process widths measuring by tracing podocin signal within a given area as in the yellow boxed region in **a**, as described in the text. All distances and scale bars are in pre-expansion units. Scale bar, 2 μm (**a**).

4.5 Discussion

Our results show the optimization and validation of new ExM protocols which enables volumetric, nanoscale imaging of mouse and human kidney tissue using a standard confocal microscope. Importantly, the procedures utilize new homogenization strategies to enzymatically digest the extracellular matrix of mouse and human kidney tissue with minimal distortion upon expansion (1-4%). These or other tissue-optimized digestion procedures may also be useful for ExM with other tissues whose substantial extracellular matrix or other components may also

resist enzymatic digestion. While electron microscopy has vastly superior spatial resolution compared to ExM, the 70-75 nm resolution demonstrated here is sufficient to resolve key nanoscale structures important for understanding kidney function in the laboratory or clinic while also providing the ability to measure 3D distributions of multiple, specific molecules. These 3D data sets allow users to identify areas of interest with a desired orientation (i.e. *en face*, orthogonal, etc.) which helps to avoid sectioning artifacts and thereby simplifies analysis and interpretation. Additionally, the simplicity and reduced cost of ExM compared to EM or other optical super-resolution techniques, makes the technique accessible to a wide range of potential practitioners.

Three recent studies have also applied expansion methodology to the kidney. Zhao et al. applied ExM to the study of ~5 μm thick formalin-fixed paraffin-embedded (FFPE) tissue sections and was limited to two-dimensional imaging.[126] The FFPE kidney sections expanded with low distortion in the Zhao et al. study[126] using only proteinase K digestion, perhaps due to some combination of a low amount of connective tissue in the very thin specimens and/or structural changes to the specimen due to FFPE sample processing (e.g., dehydration or treatment with organic solvents, etc.).[127] Ku et al. demonstrated expansion of multiple, perfusion-fixed whole mouse organs including kidney but only imaged and quantitatively validated the procedure with brain and cultured cells.[43] During the final stages of this work, a similar procedure to that of Ku et al., but different from ours, was reported by Unnersjö-Jess et al.[112] for expansion of rat and mouse kidney, and the authors demonstrated the nanoscale, volumetric imaging of rat and mouse glomeruli using specimen expansion with confocal microscopy.

We note a number of key differences between the Unnersjö-Jess et al. study and ours, which we believe are complementary studies. First, we performed careful imaging of kidney tissues both before and after expansion in order to quantify the amount of distortion introduced by expansion, and we used this to show quantitatively that our procedures induce minimal distortion over a range of length scales for both mouse and human kidney tissues. In contrast, Unnersjö-Jess et al. compared two average feature sizes from different samples before and after expansion, although their results were strong on a qualitative level and no obvious distortions were apparent. Second, while our immunolabeling was performed prior to gelation, the

procedure of Unnersjö-Jess et al. used immunolabeling after expansion. Thus, pre-expansion and post-expansion labeling may have different abilities to detect epitopes, and there is precedence for some epitopes being masked due to hydrogel polymerization and others that are revealed upon denaturation.[43] Additionally, post-expansion staining may cause less antibody-induced broadening since pre-expansion labeling leads to expansion of the antibody labels while post-expansion labeling does not.[49] Third, our procedures enabled us to image intrinsic signal from fluorescent proteins in kidney in reporter mice, including ones which are not antigenically distinct (i.e., GFP, YFP, etc.), while the Unnersjö-Jess et al. protocol did not. Fourth, using five-fold expansion together with deconvolution confocal or STED microscopy, Unnersjö-Jess et al. were able to achieve higher spatial resolution than we achieved here with four-fold expansion and standard confocal microscopy, although these techniques could in principle also be implemented with our procedures to similarly improve the spatial resolution. Lastly, we have provided extensive documentation of our procedures for ExM of mouse and human kidney tissue in a detailed experimental protocol to help accelerate the dissemination of these methods for a range of applications from the research laboratory to the clinic.

4.6 Materials and Methods

4.6.1 Reagents and Reagent Preparation

Unconjugated **s**econdary antibodies were obtained from Jackson Immunoresearch (West Grove, PA, USA) and included donkey anti-mouse (715-005-151), donkey anti-rabbit (711-005-152), donkey anti-goat (705-005-147), donkey anti-rat (712-545-150), and donkey anti-guinea pig (706-005-148). Primary antibodies were purchased as follows: Rabbit anti-podocin (P0372, Sigma-Aldrich, St. Louis, MO, USA), goat anti-podocalyxin (AF1556, R&D Systems Inc., Minneapolis, MN, USA), mouse anti-agrin (6D2, DSHB, Iowa City, IA, USA), rabbit anti-collagen IV (ab6586, Abcam, Cambridge, MA, USA), mouse anti-acetylated tubulin (T7451, Sigma-Aldrich), mouse anti-alpha smooth muscle actin (904601, BioLegend, San Diego, CA, USA), guinea pig anti-synaptopodin (internal N-terminus) (GP94-IN, Progen Biotechnik, Heidelberg, Germany), mouse anti-vimentin (18-0052, Thermo Fisher Scientific/Invitrogen, Waltham, MA, USA), and rat anti-alpha tubulin (Thermo Fisher Scientific). NHS-functionalized dyes were purchased from Sigma-

Aldrich (ATTO 488 and ATTO 647N) and Thermo Fisher Scientific (Alexa Fluor 488 and Alexa Fluor 568). NHS-functionalized dyes were received in 1 mg aliquots and were dissolved at a concentration of 100 mg/mL in anhydrous DMSO, further diluted into subaliquots of 1-10 mg/mL, and were stored at -20 ˚C. Hoechst 33342 was purchased from Life Technologies (Carlsbad, CA, USA) and was used according to manufacturer's instructions. NAP-5 size-exclusion chromatography columns were purchased from GE Healthcare (Little Chalfont, Buckinghamshire, United Kingdom). Methacrylic acid N-hydroxy succinimidyl ester (MA-NHS) was purchased from Sigma-Aldrich and was dissolved in anhydrous DMSO in 1 M aliquots which were stored at -20 ˚C. Paraformaldehyde (32%) was obtained from Electron Microscopy Sciences (Hatfield, PA, USA). Tetramethylethylenediamine (TEMED, 17919) and ammonium persulfate (APS, 17874) were obtained from Thermo Fisher Scientific. 4-hydroxy-2,2,6,6-tetramethylpiperadin-1-oxyl (TEMPO, 97%, 176141) and sodium acrylate (97%, 408220) were purchased from Sigma Aldrich. 40% acrylamide (1610140) and 2% bis-acrylamide (1410142) were obtained from Bio-Rad Laboratories (Herculues, CA, USA). Proteinase K was purchased from Thermo Fisher Scientific (EO0491), collagenase (F type blend, C7926) from Sigma-Aldrich, and elastase (16-19-051200-porcine) from Athens Research & Technology (Athens, GA, USA). 10x phosphate buffered saline (70011044) and 10x Tris-acetate-EDTA (TAE, 15558042) buffers were purchased from Thermo Scientific. Hank's Balanced Salt Solution (HBSS, 1x) buffer was purchased from Corning (Manassas, VA, USA). Bovine serum albumin (BSA) was obtained from Santa Cruz Biotechnology (Santa Cruz, CA, USA).

4.6.2 Preparation of Fluorophore-labeled Secondary Antibodies

Fluorescent dyes were coupled to secondary antibodies in-house by first mixing ~40 µL of unconjugated antibody (~1.3 mg/mL), 5 µL of 1 M sodium bicarbonate (pH ~8.3), and 1-2 µL of NHS dye (stocks made in DMSO at 1-10 mg/mL depending on the dye). The reaction was allowed to proceed at room temperature for 30 min. For purification, a NAP-5 size exclusion column was equilibrated by flowing through 10-20 mL PBS. The entire reaction mixture was then loaded onto the column followed by 650 µL of PBS which was discarded after elution. Another 300 µL was then added and the eluent was collected. Characterization of the dye-to-IgG ratio was performed

with UV/Vis absorption spectroscopy and the results can be found in **Supplementary Table 4.1** in **section 4.9**.

4.6.3 Fluorescence Microscopes

Conventional epifluorescence microscopy was performed with an inverted Nikon Ti-S microscope fitted with a 4× 0.2 NA air objective lens (Nikon, Melvill, NY, USA), a 10× 0.25 NA air objective lens (Nikon), or a 20× 0.45 NA air objective lens (Nikon). Illumination was achieved using a four-channel light emitting diode (LED4D120, Thorlabs, Newton, NJ, USA) with a multiband filter set LF405/488/532/635-A-000, Semrock, Rochester, NY, USA) and images were captured using a Zyla 5.5 sCMOS camera (Andor, Windsor, CT, USA). Confocal microscopy was performed on a Leica SP5 inverted confocal point scanning microscope at the UW Biology Imaging Core using a 10× 0.4 NA air objective lens (Leica, Nussloch, Germany), 20× 0.7 NA air objective (Leica), and a 63× 1.2 NA water immersion objective (Leica).

4.6.4 Mouse Kidney Dissection and Preparation

All experimental protocols and methods in this work involving animals were approved by and conducted in accordance with all guidelines and regulations set forth by the Institutional Animal Care and Use Committee at the University of Washington. At approximately 2 months old, female mice (strain C57BL/6) were sacrificed by suffocation with CO_2 followed by cervical dislocation. Kidneys were immediately removed and the renal capsule was stripped off. The kidneys were then halved longitudinally and immersed in 4% PFA in PBS for 1 hour at room temperature. They were then washed with PBS and sliced to 100 µm thickness using a vibratome. The slices were stored in PBS at 4 ˚C until staining.

4.6.5 Confetti-mouse Kidney Dissection and Preparation

All experimental protocols and methods in this work involving animals were approved by and conducted in accordance with all guidelines and regulations set forth by the Institutional Animal Care and Use Committee at the University of Washington. NPHS2Cre/R26R-ConfettiTG/WT (podocin/cre recombinase/confetti) mice were used to provide permanent and stochastic expression of one of four fluorescent colored reporters in podocytes. These colors

were cytoplasmic targeted red fluorescent protein (cRFP), membrane targeted cyan fluorescent protein (mCFP), nuclear targeted green fluorescent protein (nGFP) or cytoplasmic targeted yellow fluorescent protein (cYFP). Mice were sacrificed with an overdose of Ketamine/Xylazine, cardiac perfused with 10-15 mL of ice cold phosphate buffered saline (PBS) at 25 inches of gravity pressure (47 mmHg or 63 mbar) through a 21G butterfly infusion set (UW IACUC 2968-04). Kidneys were placed into 4% paraformaldehyde in PBS (PFA, Affymetrix, Santa Clara, CA) for 45 minutes, washed briefly in PBS, placed in 30% sucrose in PBS (Sigma-Aldrich, St Louis, MO) overnight, blotted dry, embedded in Tissue-Tek® O.C.T. Compound (VWR, Radnor, PA), and frozen in a 100% ethanol/dry ice bath. Kidney slices (50 µm thickness) were obtained using a Leica CM1850 cryostat, placed into 24-well culture dish and stored at -80 ˚C until staining. Tissue slices were fixed for 1 h in 3% PFA in PBS at room temperature for 1 h and then washed with PBS prior to immunostaining.

4.6.6 Human Kidney Tissue Preparation

De-identified non-tumoral human kidney tissue samples from individuals undergoing nephrectomy for a kidney tumor and no history of other kidney disease were obtained from NW Biotrust under a protocol approved by the University of Washington Institutional Review Board with informed patient consent. All experimental protocols and methods involving human tissue were performed in accordance with the guidelines and regulations set forth by the University of Washington Institutional Review Board. The samples were cut to be ~1 mm^3 and immersed in 4% PFA in PBS for 1 h at room temperature. The tissue was then washed with PBS and sliced to 100 µm thickness using a vibratome. The slices were stored in PBS at 4 ˚C until staining.

4.6.7 Tissue Immunostaining and Pre-expansion MA-NHS Treatment

Both human and mouse kidneys were stained using the following protocol. 100-µm-thick kidney slices were first incubated in blocking/permeabilization buffer (3% BSA and 0.1% Triton X-100 in PBS) for at 6-12 h at 4 ˚C. The slices were then incubated with primary antibody diluted in blocking/permeabilization buffer (see **Supplementary Table 4.1** for dilutions) for 18-24 h at 4 ˚C and were then washed with blocking/permeabilization buffer three times at room temperature (15 min each). The tissues were then incubated in fluorescently labeled secondary antibodies

diluted in blocking/permeabilization buffer for 18-24 h at 4 ˚C. The slices were then washed three times with PBS at room temperature (15 min each). Nuclear staining was performed with Hoechst 33342 according to manufacturer instructions. Tissues were then incubated in 1 mM MA-NHS in PBS (diluted freshly from a 1 M stock in DMSO) for 1 h at room temperature followed by three washes with PBS.

4.6.8 Tissue Gelation

After immunostaining and treatment with MA-NHS, the tissue slices were incubated in monomer solution (1× PBS, 2 M NaCl, 2.5% (wt/wt) acrylamide, 0.15% (wt/wt) N,N'-methylenebisacrylamide, 8.625% (wt/wt) sodium acrylate) for at least 1 h at 4 ˚C. The tissues were then placed on a clean #1.5 coverglass and the excess liquid was removed from the sample. A concentrated stock of TEMPO at 1% (wt/wt) in water was diluted in monomer solution to a final concentration of 0.01% (wt/wt). TEMPO acts as an inhibitor to the gelation reaction to allow complete diffusion of the monomers through the tissue. Concentrated stocks of APS and TEMED at 10% (wt/wt) in water were also diluted alongside the TEMPO in monomer solution to final concentrations of 0.2% (wt/wt) with APS added last. The gelation solution was gently applied to the tissue so that the sample did not leave the surface of the glass. Two stacked small pieces of #1.5 coverglass were placed on either side of the sample and another whole coverglass was placed on top to create a tissue gelation chamber. Tissues were incubated in a humidified environment at 37 ˚C for 1.5-2.5 h. The chambers were disassembled leaving the gelled sample on one piece of coverglass. The excess gel and glass around the sample was cut and removed for digestion.

4.6.9 Mouse Kidney Digestion, Expansion, and Nuclear Restaining

Gelled mouse kidney samples were transferred to at least 1 mL of proteinase digestion buffer (1× TAE buffer, 0.5% Triton X-100, 0.8 M guanidine HCL) containing 8 units mL^{-1} proteinase K and were digested at 37 ˚C overnight. The gels were then washed in PBS and transferred to collagenase buffer (1× HBSS + 0.7 mM $CaCl_2$) with 5 mg mL^{-1} collagenase (at least 1 mL total volume). Next, the samples were digested overnight at 37 ˚C. After digestion, the samples were placed in DI water to expand (typically 30 min with 1-2 water exchanges). Nuclear staining with

Hoechst 33342 was performed again (using water as a solvent) at this stage as well. It should be noted that larger samples may require larger volumes of digestion solutions for complete homogenization.

4.6.10 Human Kidney Digestion, Expansion, and Nuclear Restaining

Gelled human kidney samples were transferred to at least 1 mL of 200 mM Tris buffer (pH 8) containing 1 mg mL^{-1} elastase and were allowed to digest at 37 ˚C overnight. The samples were washed with PBS and transferred to proteinase digestion buffer containing 8 units mL^{-1} proteinase K. The samples were digested at ~65 ˚C overnight. The digestion buffer and proteinase were removed and refreshed the next day and the samples were allowed to again digest overnight at 65 ˚C. After washing with PBS, the samples were digested overnight at 37 ˚C in collagenase buffer with 5 mg mL^{-1} collagenase. The samples were then transferred to DI water for expansion. Nuclear staining with Hoechst 33342 was performed again (using water as a solvent) at this stage as well.

4.6.11 Expanded Sample Handling

The gels were immobilized on glass as follows. Rectangular #1.5 coverglasses were plasma cleaned and coated with poly lysine by spreading an aqueous solution of poly lysine over their surface and allowing them to air dry. Gels were cut to fit on the rectangular coverglass and the excess water was removed by wicking it away from the edges with tissue paper. The gels were then gently placed onto the poly lysine glass by sliding the gel off an untreated piece of glass using a low contact angle with respect to the treated glass to avoid sample bending. The immobilized gels were then immediately imaged.

4.6.12 Image Visualization

Fiji and Imaris (Bitplane) were used for visualization of all images acquired in this study.

4.6.13 Correlative Image Analysis

Quantitative distortion analysis was performed as described previously.[118] Briefly, pre- and post-expansion images of the same region were first aligned using a rigid transformation

(similarity, linear) to roughly align the images and determine the expansion factor. Next, a non-rigid (B-spline, non-linear) transformation was applied to the post-expansion image so that it matched the pre-expansion image (see also **Supplementary Fig. 4.2**).

4.6.14 Foot Process Width Measurement by Tracing Method

Areas of expanded, podocin-stained tissue samples were first isolated based on their flatness in the image plane. Areas that remained within a thickness of 0.75 µm (distance in pre-expansion units) were chosen for further analysis while others were rejected to avoid projection artifacts. The podocin signal in the maximum intensity projections of the selected areas were then traced in ImageJ and the length of the traces was recorded. Dividing the area of analysis by the length of trace it contained gave the average foot process width.

4.6.15 Foot Process Width Measurement by Cross-sectional Profiles

Using the above method to ensure the area of interest was oriented flat with respect to the image plane, we obtained line profiles in the podocin channel of expanded kidney specimens. Line profiles that were perpendicular to the foot processes were chosen for analysis. The adjacent peak-to-peak distance was measured after fitting the profiles with Gaussian functions to obtain foot process width values.

4.6.16 Glomerular Basement Membrane Thickness Measurement

Expanded specimens stained for podocalyxin and a GBM marker (agrin, collagen IV, or vimentin) were used for this analysis. Orthogonal image sections were chosen using the podocalyxin channel. Podocalyxin stains both the apical side of foot processes as well as endothelial cells, and we used the lack of lateral movement of these features when scrolling through confocal image stacks to visually confirm the area of interest was perpendicular to the image plane in order to avoid projection artifacts. A line profile perpendicular to the GBM and spanning its entire thickness was drawn and the cross-sectional profile obtained from the GBM marker channel (either agrin, collagen IV, or vimentin) was fitted with a Gaussian function whose full width at half maximum was taken to be the GBM thickness.

4.7 Acknowledgements

This work was supported by: the University of Washington, a Burroughs-Wellcome Career Award at the Scientific Interface, NIH grant R01 MH115767 (J.C.V.); NIDDK Diabetic Complications Consortium grants DK076169 and DK115255 (J.C.V., B.N., C.E.A.); NSF Graduate Research Fellowship DGE-1256082 (T.J.C.); NIH NIDDK: R01 DK097598-01A1, NIH NIA: R01 AG046231-01A1 (S.J.S.). NW BioTrust, a core service for patient consenting, and NWBioSpecimen, a core service for procurement and annotation of research biospecimens, are supported by National Cancer Institute grant P30 CA015704 (G. Gilliland, principal investigator [PI]), Institute of Translational Health Sciences grant UL1 TR000423 (M. Disis, PI), the University of Washington School of Medicine and Department of Pathology, and Fred Hutchinson Cancer Research Center. The authors would like to thank H. Y. Kueh and M. Wither (University of Washington, Seattle, WA) for providing whole mouse kidneys, K. Oda (University of Washington, Seattle, WA) for help with vibratome sectioning, A. Glaser and J. Liu (University of Washington, Seattle, WA) for the use of Imaris software for rendering 3D animations, and the Biology Imaging Facility at the University of Washington for imaging assistance.

4.8 Supplementary Information

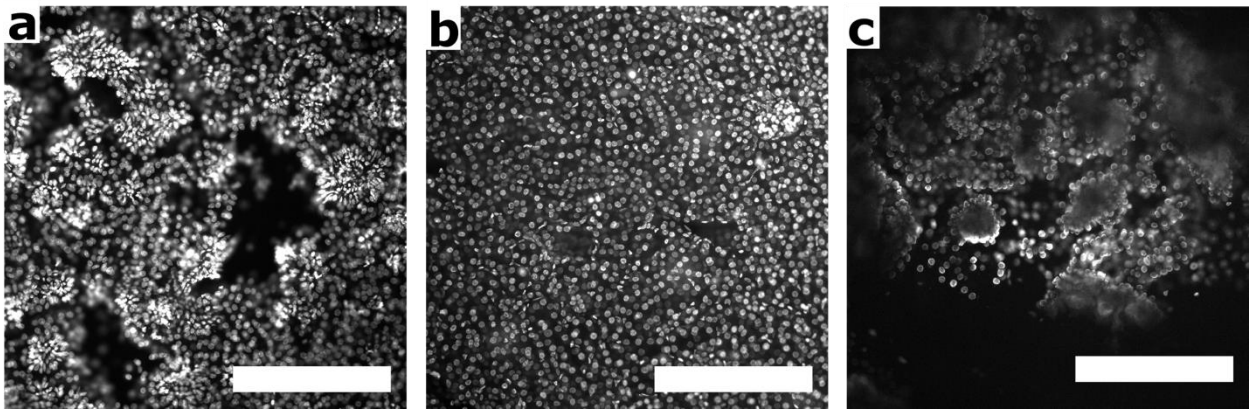

Supplementary Figure 4.1 | Epifluorescence images of expanded 100 µm thick sections of mouse kidney stained for DNA with Hoechst and processed using different digestion protocols. (**a**) Mouse kidney tissue treated with MA-NHS for linkage of proteins to the hydrogel and digested with proteinase K alone leads to abundant tears (empty areas) and under-expanded regions exhibiting relatively small or stretched nuclei. (**b**) MA-NHS-treated tissue that was digested with proteinase K followed by collagenase leads to uniform sample homogenization and lacks obvious distortions. (**c**) MA-NHS-treated tissue that is later homogenized with detergent and heat (MAP homogenization) leads to obvious tearing and distortions of the expanded specimen. All scale bars are in pre-expansion units. Scale bars: 200 µm.

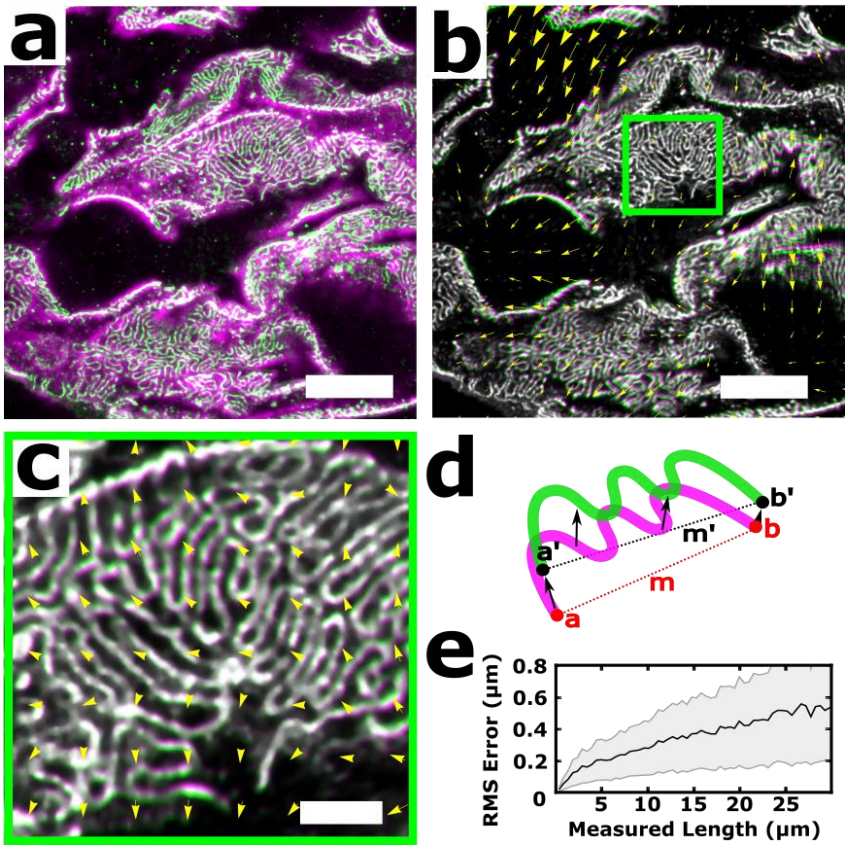

Supplementary Figure 4.2 | Comparison of pre- and post-expansion confocal images of expanded mouse kidney tissue stained for podocin (data from **Fig. 1**). (**a**) Overlay of pre-expansion (magenta) and post-expansion (green) images after registration by similarity transform (a rigid transformation including scaling, rotation, and translation). A Gaussian blurring filter was applied to the post-expansion image prior to registration in order for the pre- and post-expansion images to have similar "resolution". (**b**) Overlay of post-expansion image before (magenta) and after (green) the application of a B-Spline registration (non-rigid transformation) to warp the post-expansion image so that it aligns to the pre-expansion image (considered to be ground truth data). Yellow arrows show the direction and relative magnitude (scaled up by a factor of 8 for visibility) of the local transformation required to align the post-expansion image to the pre-expansion image. (**c**) Zoomed view of the boxed region in **b**. Note that in both **b** and **c** the white color indicates that the magenta and green channels overlap. (**d**) Schematic of correlation analysis procedure. For a detailed distortion analysis protocol, see Chozinski *et al.* 2016.[118] Briefly, post-expansion images before and after B-spline registration are binarized to create "skeletons" (green and magenta lines in **d**). 50,000 points are then randomly chosen from each skeleton and the distance between all points in each image is calculated. The value *m* represents the distance between points *a* and *b* in the pre-B-Spline-registration image (magenta) while *m'* is the distance between *a'* and *b'* in the post-B-Spline-registration image (green). RMS error plots (**e**) were generated by calculating the difference between *m* and *m'* as a function of distance *m* for 25,000 sets of points throughout the image (shaded areas represent plus or minus the standard deviation). Note that **e** was calculated by performing the distortion analysis in three dimensions. All distances and scale bars are in pre-expansion units. Scale bars: 5 µm (**a, b**) and 1 µm (**c**).

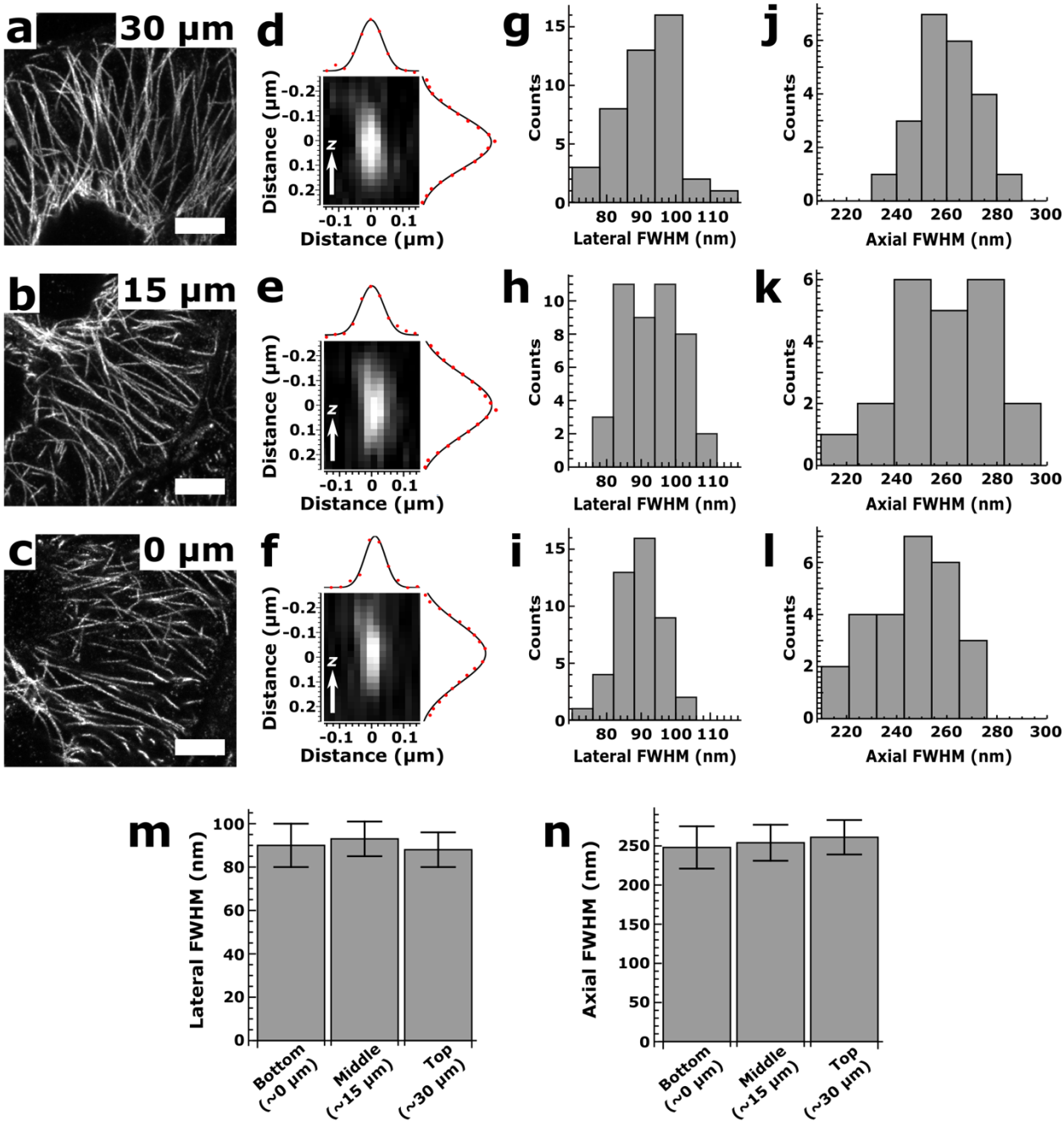

Supplementary Figure 4.3 | Estimation of resolution using cross-sectional profiles of microtubules in expanded mouse kidney. (**a-c**) Confocal fluorescence images (representative ~500 nm thick projections taken from 5 µm stacks) of expanded mouse kidney immunostained for tyrosinated tubulin taken at 0, 15, and 30 µm depths (which corresponds to 0 µm, 60 µm, and 120 µm in post-expansion dimensions and is near the limit of the objective lens's working distance). (**d-f**) Representative cross-sections of individual microtubules at the same depths corresponding to **a**, **b**, and **c** including cross-sectional profiles with Gaussian fits (lateral, top; axial, right). (**g-l**) Histograms of full width at half-maximum (FWHM) values of cross-sectional profiles of single microtubules fitted with Gaussian functions in lateral (**g-i**) and axial (**j-l**) dimensions. (**m**)

Summary of histograms in **g**, **h**, and **i** showing average lateral FWHM values of **g** 88 ± 8 nm (mean ± SD, 47 profiles), **h** 93 ± 8 nm (mean ± SD, 44 profiles), and **i** 90 ± 10 nm (mean ± SD, 45 profiles). Using our previous study[118] where the convolution of a double-peaked cross-sectional profile of indirectly immunostained microtubules measured by localization microscopy (at ~20 nm resolution) with a ~65 nm Guassian point spread function (the estimated resolution) yielded an observed microtubule FWHM of ~80 nm, we estimate our lateral resolution here to be 70-75 nm. (**n**) Summary of histograms in **j**, **k**, and **l** showing average axial FWHM values of **j** 261 ± 13 nm (mean ± SD, 47 profiles), **h** 254 ± 23 nm (mean ± SD, 23 profiles), and **i** 248 ± 19 nm (mean ± SD, 27 profiles). From this data, we estimate our axial resolution to be ~250 nm. The expansion protocol effectively clears the tissue and the hydrogel changes the sample's refractive index to that of water. By using a water immersion objective lens, spherical aberration due to refractive index mismatch is minimized and, as shown here, the resolution is preserved throughout the thickness of the sample. All distances and scale bars correspond to pre-expansion dimensions. Scale bars: 3 μm.

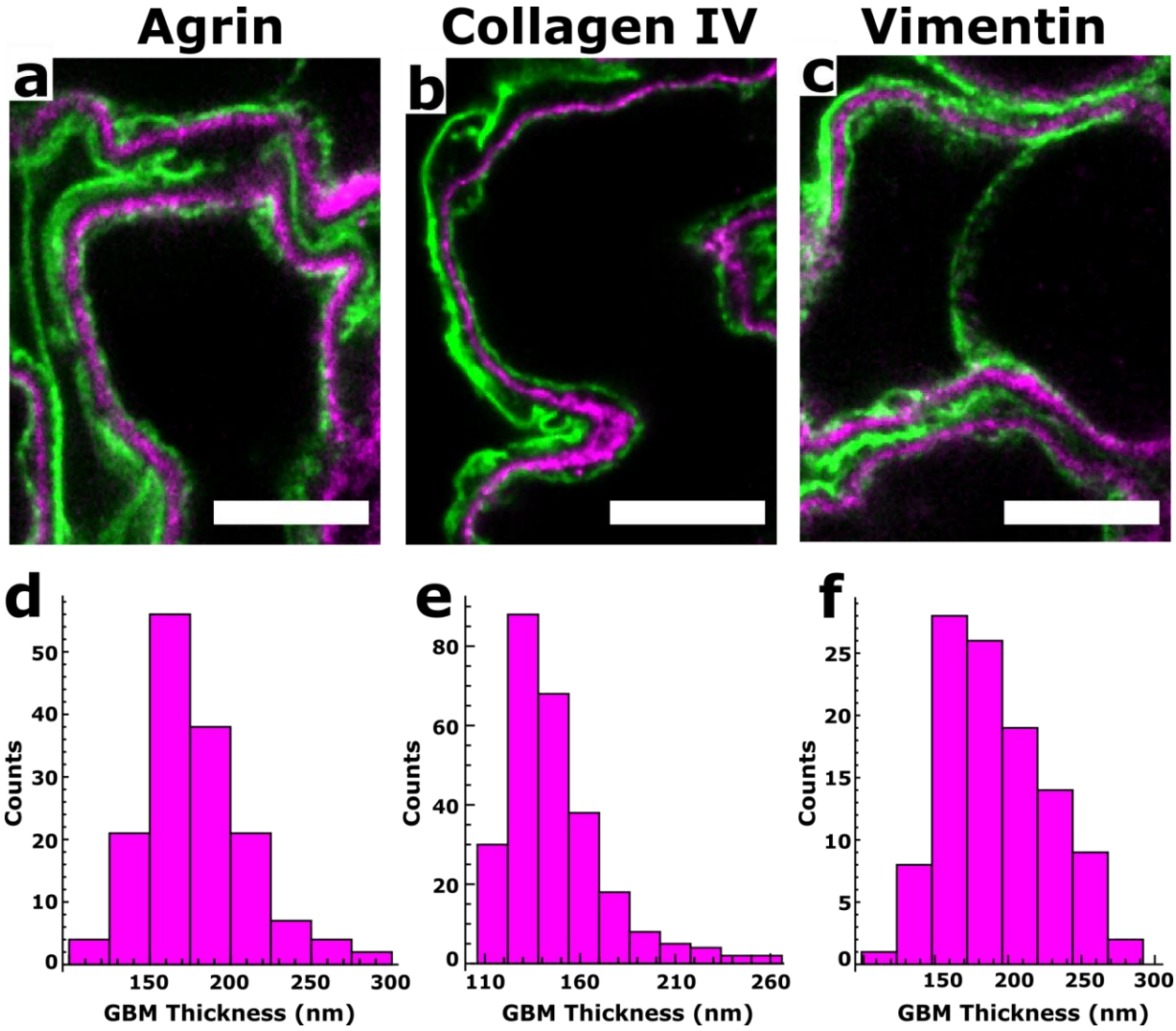

Supplementary Figure 4.4 | Glomerular basement membrane (GBM) markers and GBM thickness measurements from confocal microscopy (orthogonal sections) of expanded 100 µm thick slices of mouse kidney. (**a**-**c**) Immunostaining of podocalyxin (green) and various GBM markers (magenta): agrin (**a**), collagen IV (**b**), and vimentin (**c**). (**d**-**f**) Distributions of GBM thicknesses measured in agrin (**a**), collagen IV (**b**), and vimentin (**c**) with average values of 178 ± 34 nm, 147 ± 26 nm, and 192 ± 36 nm, respectively (mean ± SD). The number of samples used in each case is as follows: agrin (3 kidney samples, 4 glomeruli, 154 cross-sectional profiles), collagen IV (3 kidney samples, 7 glomeruli, 263 cross-sectional profiles), and vimentin (3 kidney samples, 3 glomeruli, 107 cross-sectional profiles). All distances and scale bars are in pre-expansion units. Scale bars: 3 µm.

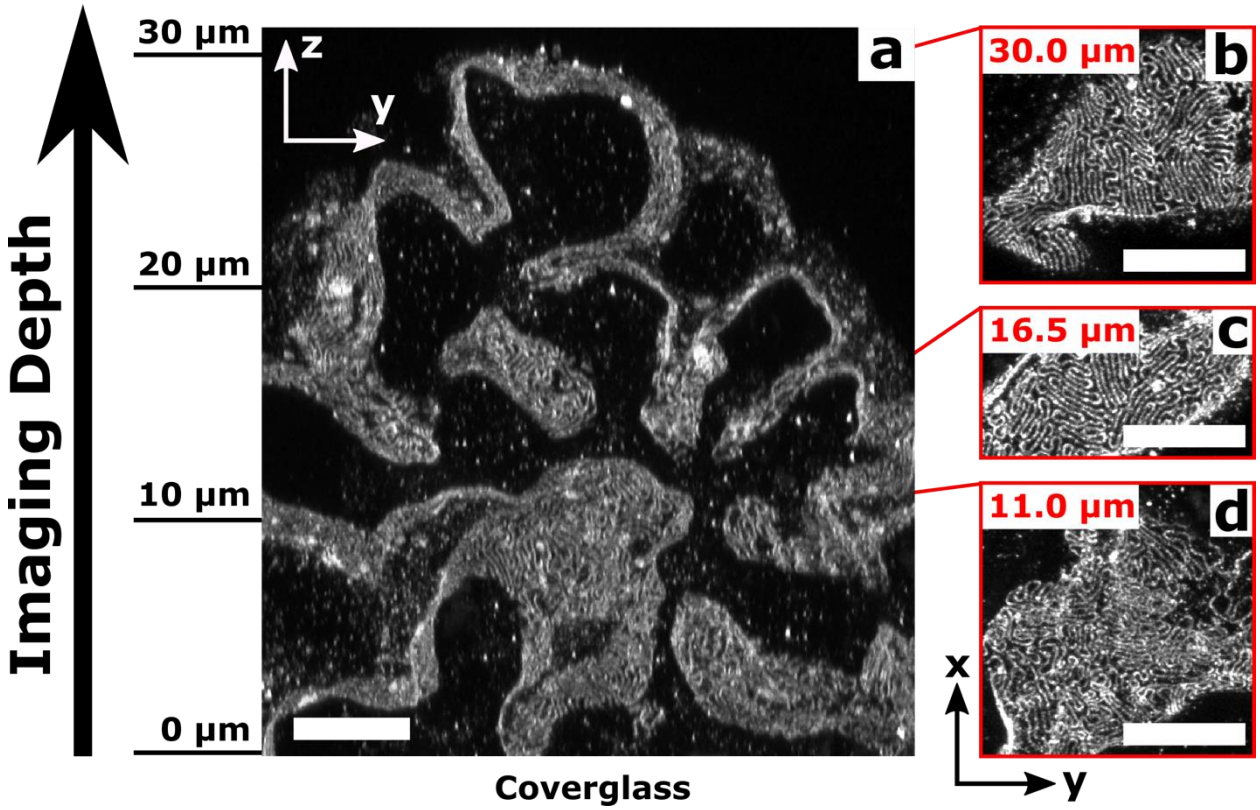

Supplementary Figure 4.5 | Confocal images of expanded mouse kidney stained for podocin. (**a**) Confocal maximum intensity projection of 2.5 µm thick section in the YZ plane showing an imaging depth of ~30 µm (which corresponds to ~120 µm in post-expansion dimensions and is near the limit of the objective lens's working distance). Note that foot process boundaries are still clearly resolvable in the *z*-dimension throughout the entire imaging depth. (**b**-**d**) Confocal maximum intensity projections of 1.4 µm (**b**), 1.3 µm (**c**), and 1.8 µm (**d**) thick sections in the XY plane at various imaging depths. All distances and scale bars are in pre-expansion units. Scale bars: 5 µm. See also **Supplementary Video 4.2** for an animation of this volume.

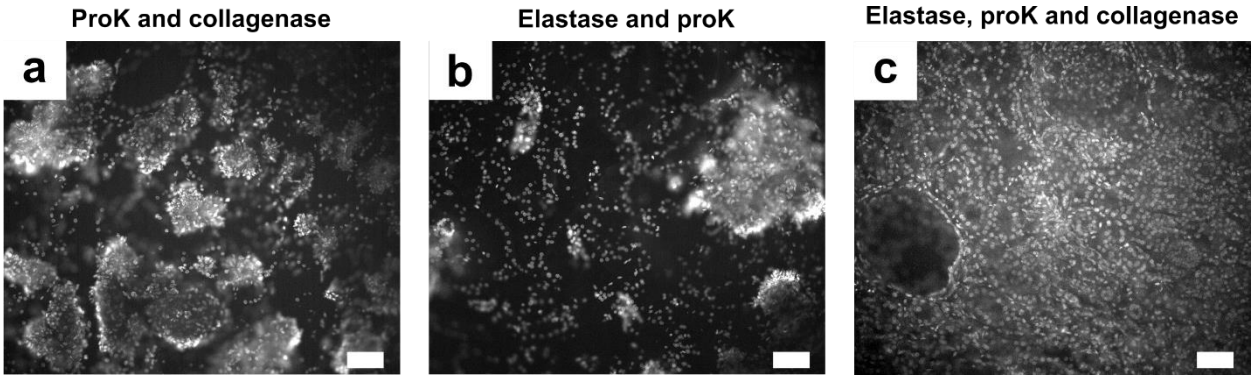

Supplementary Figure 4.6 | Epifluorescence images of expanded 100 µm thick sections of human kidney stained for DNA with Hoechst and processed for expansion using different enzymatic treatments to homogenize the tissue. Enzymatic digestion with proteinase K and collagenase (**a**) or elastase and proteinase K (**b**) leads to an incomplete digestion with obvious tears and tissue loss, whereas digestion with elastase, proteinase K, and collagenase (**c**) enables uniform expansion. Scale bars are all 100 µm and are in pre-expansion dimensions.

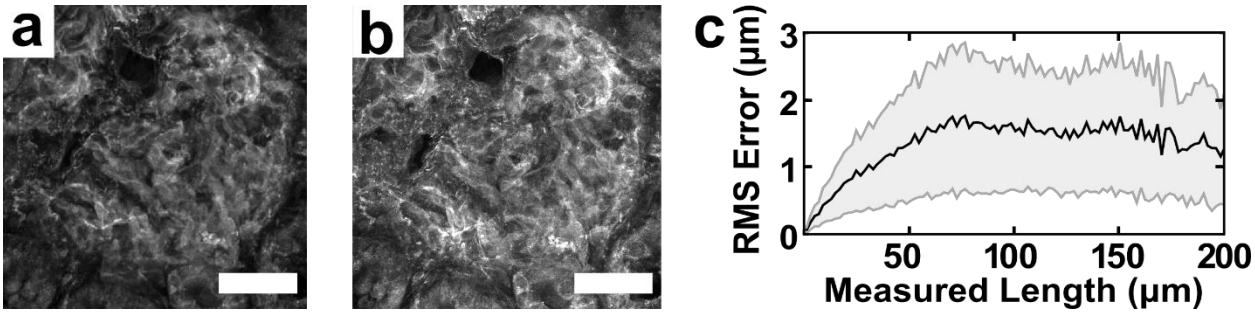

Supplementary Figure 4.7 | Comparison of pre-expansion **(a)** and post-expansion **(b)** images of human kidney tissue taken by confocal fluorescence microscopy for a whole glomerulus immunostained for podocin. (**c**) Quantification of root mean square (RMS) error of pre- versus post- expansion confocal images of the human kidney tissue. All distances and scale bars are in pre-expansion units. Scale bars are 50 µm.

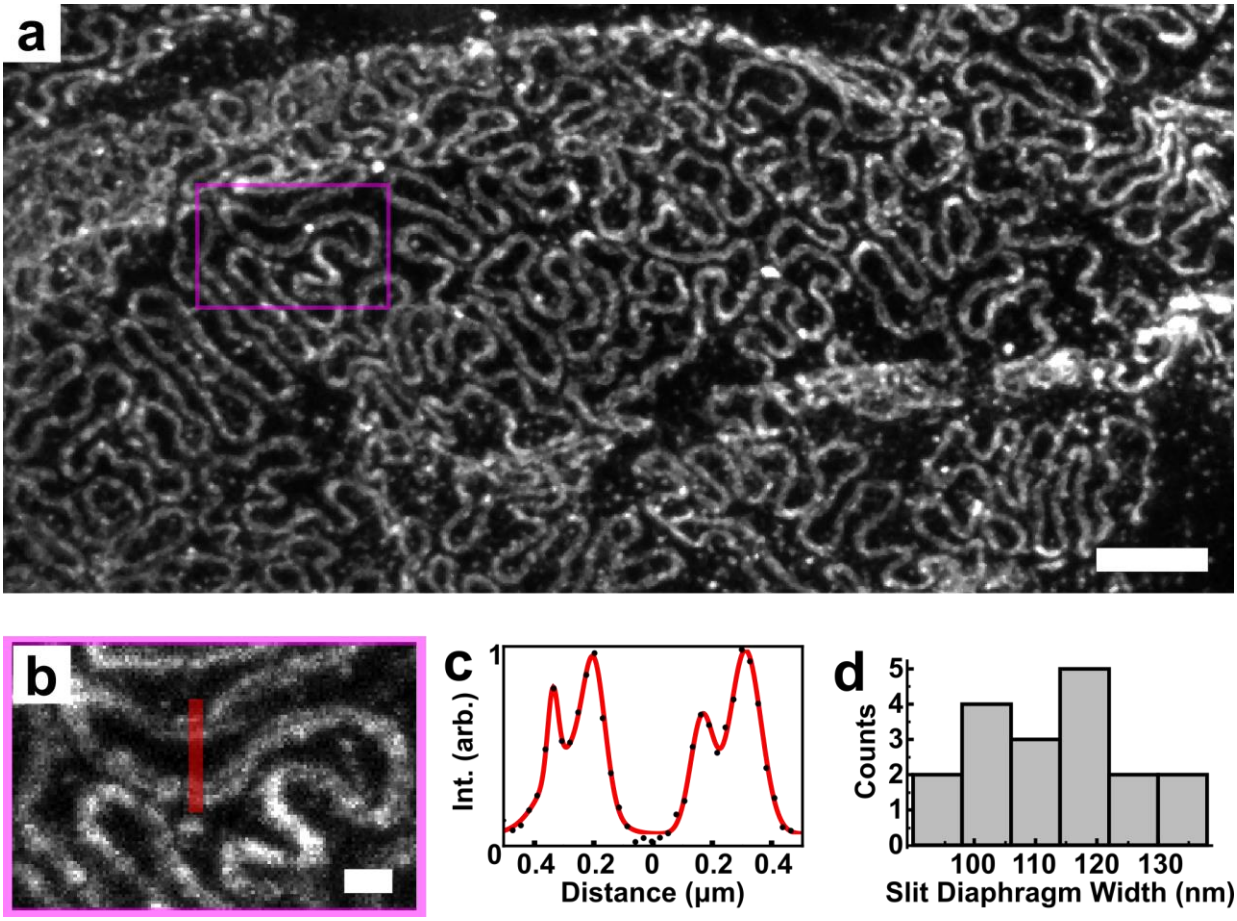

Supplementary Figure 4.8 | Confocal fluorescence images of expanded human kidney tissue. (**a**) Human kidney immunostained for podocin using the conventional antibody. (**b**) zoomed-in view of the boxed area in **a**, showing resolvable gap between adjacent podocytes. (**c**) Cross-sectional profile of red line in **b** fitted with multiple Gaussian functions. (**d**) Histogram of measured width between adjacent podocin signals (taken to be the slit diaphragm) in **a**. Scale bars are 2 µm (**a**) and 500 nm (**b**) and are all in pre-expansion dimensions.

Supplementary Video 4.1 | Animated rendering of data from **Fig. 4.3a** showing a 28×28×11 μm^3 volume (tick marks spaced by 420 nm) of mouse kidney tissue immunostained for podocin (green), agrin (red), podocalyxin (blue), and stained for DNA with Hoechst (white). All distances and units are in pre-expansion units.

Supplementary Video 4.2 | Animated rendering of data from **Supplementary Fig. 4.4** showing a 28×28×31 μm^3 volume (tick marks spaced by 550 nm) of mouse kidney tissue immunostained for podocin. All distances and units are in pre-expansion units.

Supplementary Table 4.1 | Summary of sample preparation and imaging conditions. All primary antibody incubations were 18-24 hours at 25 °C at a concentration of 1-2 µg/mL and all secondary antibodies were incubated for 18-24 hours at 25 °C at a concentration of 2.5-5 µg/mL. The dye-to-IgG ratios for secondary antibodies were as follows: Alexa 488, 8-10 dyes/IgG; Alexa 568, 5-7 dyes/IgG; Atto 647N, 2-3 dyes/IgG.

Fig.	Specimen Info	1° Ab	2° Ab, etc.	Digestion†	Imaging Info *Distances in pre-expansion units
4.2.1b-c, e-f,h-i, S4.3.2	C57/BL6 mouse, drop-fixed in 4% PFA for 1 hr, 100 µm vibratome section	Rb x Podocin	D x Rb Alexa 488	ProK overnight, coll overnight	Confocal: **b-c**) 10x 0.4NA, 40µm thick max projections; **e,h,S4.3.2**) 63x 1.2NA,~500nm single plane; **f**,**i**,**S4.3.2**) 63x 1.2NA, ~130nm single plane
4.2.2a-d, 4.2.3a-c,g,l, Supp. Video 4.1	C57/BL6 mouse, drop-fixed in 4% PFA for 1 hr, 100 µm vibratome section	Rb x Podocin Ms x Agrin G x Podocalyxin	D x Rb Alexa 488 D x Ms Alexa 568 D x G Atto 647N	ProK overnight, coll overnight	Confocal 63x 1.2 NA; **4.2.2a-d**) ~130 nm single confocal plane; **4.2.3a**) 11 µm thick (in *z*) 3D rendering; **4.2.3b-c**) ~700 nm max projection; **4.2.3g,i**) ~130 nm single plane
4.2.2e-h	C57/BL6 mouse, drop-fixed in 4% PFA for 1 hr, 100 µm vibratome section	GP x Synaptopodin Ms x acet. Tubulin Rb x Podocin	D x GP Atto 647N D x Ms Alexa 568 D x Rb Alexa 488	ProK overnight, coll overnight	Confocal 63x 1.2 NA, 1.4 µm max projections
4.2.2i-l	C57/BL6 mouse, drop-fixed in 4% PFA for 1 hr, 100 µm vibratome section	Rb x Collagen IV G x Podocalyxin Ms x α SMA	D x Rb Alexa 488 D x G Atto 647N D x Ms Alexa 568	ProK overnight, coll overnight	Confocal 20x 0.7 NA, ~30 µm max projections
4.2.2m-r	Podocyte-confetti mouse, fresh frozen in OCT, 40 µm cryosection drop fixed in 4% PFA for 1 h	No stains; only fluorescent proteins were used (GFP, YFP, and RFP)	None	ProK overnight, coll overnight	Confocal 63x 1.2 NA: ~130 nm single plane
4.2.4, S4.3.7, S4.3.8	Human nephrectomy tissue, drop-fixed in 4% PFA for 1 hr, 100 µm vibratome section	Rb x Podocin	D x Rb Atto 488 Hoechst	Elast overnight, proK two days at 65°C, and coll overnight	Confocal: **4.2.4**) 63x 1.2 NA, ~1.15 µm max projection; **S4.3.6**) 20x 0.7 NA, ~9.1 µm max projection; **S4.3.7**)
S4.3.6	Human nephrectomy tissue, drop-fixed in 4% PFA for 1 hr, 100 µm vibratome section	None	Hoechst (nuclei)	**a**) ProK 2 days at 65 °C, coll overnight **b**) Elast overnight, proK 2 days at 65 °C **c**) Elast overnight, proK 2 days at 65 °C, coll overnight	Widefield epifluorescence image, 4× 0.2 NA air objective
S4.3.1a-c	C57/BL6 mouse, drop-fixed in 4% PFA for 1 hr, 100 µm vibratome section	None	Hoechst (nuclei)	**a**) ProK overnight **b**) ProK overnight, coll overnight **c**) 200 mM SDS, 200mM NaCl, 50mM tris pH 9, 24 h at 70 °C then 24 h at 90 °C	Widefield epifluorescence image, 4× 0.2 NA air objective
S4.3.3	C57/BL6 mouse, drop-fixed in 4% PFA for 1 hr, 100 µm vibratome section	Rat x Tubulin	D x Rat Atto 488	ProK overnight, coll overnight	Confocal: 63x 1.2 NA, ~500 nm max projections
S4.3.4	C57/BL6 mouse, drop-fixed in 4% PFA for 1 hr, 100 µm vibratome section	**a-c**) G x Podocalyxin **a**) Ms x Agrin **b**) Rb x Collagen IV **c**) Ms x Vimentin	**a-c**) D x G Atto647N **a**) D x Ms Alexa 568 **b**) D x Rb Atto 488 **c**) D x Ms Alexa 568	ProK overnight, coll overnight	Confocal: 63x 1.2 NA, ~130 nm single confocal plane
S4.3.5, Supp. Video 4.2	C57/BL6 mouse, drop-fixed in 4% PFA for 1 h, 100 µm vibratome section	Rb x Podocin	D x Rb Atto 488	ProK overnight,coll overnight	Confocal, 63x 1.2 NA, max projections with thicknesses in µm of: **a**) 2.5; **b**) 1.4; **c**) 1.3; **d**) 1.8.

† Enzymatic digestion steps performed at 37 °C except as indicated otherwise; proK, coll, and elast are short for proteinase K, collagenase, and elastase, respectively

4.9 Supplementary Protocol

BACKGROUND: This protocol is based on methods described in the publication "Expansion microscopy with conventional antibodies and fluorescent proteins" (DOI: 10.1030/nmeth.3833); however, it has been adapted for expansion of mouse and human kidney tissue that has been fixed for 1 h in 4% paraformaldehyde. Other tissues or fixation conditions may require a different procedure. In general, it is best to start with bright, robust stains to assess effectiveness of expansion, and to use relatively small specimens (e.g., ~1-2 mm^2 × 100 µm thick). It is also important to assess possible distortions by imaging the same specimen before and after expansion (with both high and low magnification). A detailed procedure for analyzing distortions in pairs of pre-expansion/post-expansion images is described in the publication listed above.

REAGENTS:

1. Ammonium Persulfate (APS is a salt and initiates polymerization)
    a. Store at 4 °C
2. Tetramethylethylenediamine (TEMED is a liquid and catalyzes polymerization)
    a. Store at 4 °C
3. 2,2,6,6-tetramethylpiperidine 1-oxyl (TEMPO is a solid and inhibits polymerization so that gelation starts after reagents permeate sample)
    a. Store at 4 ^{0}C
4. Methacrylic Acid-NHS (MA-NHS is a solid and is used to link proteins to the gel)
    a. Store the powder at 4 °C, KEEP AWAY FROM WATER
    b. Allow to warm to room temperature before opening to avoid condensation.
5. 40% Acrylamide (w/v) (Acrylamide is a liquid solution and is a monomer of the hydrogel)
    a. Store at 4 °C
6. 2% Bisacrylamide (w/v) (Bisacrylamide is a liquid solution and is a hydrogel crosslinker)
    a. Store at 4 °C
7. Sodium Acrylate (SA is an ionic monomer for the hydrogel)
    a. Store at room temperature, dry
8. Sodium Chloride (Salt)
9. 10x PBS Buffer
10. 10x TAE Buffer (Tris base, acetic acid, and EDTA)
11. 8 M Guanidine-HCl (component of digestion buffer)
12. Proteinase K (digestion enzyme, 600-800 Units/mL in glycerol. We typically purchase stocks from NEB.)
    a. Store at -20 °C
13. Collagenase (digestion enzyme, ≤10 units/mg solid. Sigma-Aldrich Blend Type F)
    a. Store at -20 °C

STOCKS

1. APS: 10% (w/w) in water
    a. Store at -20 °C for up to 1 week
2. TEMED: 10% (v/v) in water
    a. Store at -20 °C for up to 1 week
3. TEMPO: 1% (w/w) in water
    a. Prepare freshly, within a few hours of use
4. MA-NHS: 1 M in anhydrous DMSO
    a. Store at -20 °C
    b. Keep away from water
5. Monomer Solution. Final concentrations are listed. Recipe achieves ~4x expansion. Bolded quantities in brackets, below, are for 10 mL of monomer solution.
    a. 1x PBS **[1 mL]**
    b. 2 M NaCl **[1.17 g]**
    c. 8.625% (w/v) Sodium Acrylate **[0.863 g]**
    d. 2.5% (w/v) Acrylamide **[0.625 mL]**
    e. 0.15% (w/v) Bisacrylamide **[0.75 mL]**
    f. Store at 4 °C for up to 1 month
6. Proteinase K digestion buffer. Bolded quantities in brackets, below, are for 10 mL of solution.
    a. 1x TAE Buffer **[1 mL]**
    b. 0.8 M Guanidine-HCl **[1 mL]**
    c. 0.5% Triton **[0.25 mL]**
    d. Store at 4 °C. Solution should be stable but we usually consume within a week.
7. Collagenase digestion buffer. Bolded quantities in brackets, below, are for 10mL of solution.
    a. 1M $CaCl_2$ **[7 µL]**
    b. 1X HBSS **[10 mL]**
    c. Store at 4 °C. Solution should be stable but we usually consume within a week.

POST-STAIN TREATMENT

1. After immunostaining the sample (or after expression of FP, **Supplementary Protocol Fig. 4.1a**), treat with 1 mM MA-NHS in PBS (diluted from your DMSO stock). Because NHS compounds rapidly hydrolyze in water, do not make the NHS solution in PBS until you are ready to treat your sample.
    a. Depending on how your tissue was fixed, you may need to alter the concentration of MA-NHS.
2. Allow the sample to react for 1 h at room temperature.
3. Wash the sample 2-3 times with several volumes of PBS.

GELATION

1. Incubate the tissue in monomer solution for 30-45 min at 4 °C prior to gelation to allow monomer to penetrate the whole tissue. **NOTE: the monomer here DOES NOT contain APS, TEMED, or TEMPO.**
2. Place tissue on #1.5 coverglass and remove excess monomer (wick away with Kim wipe). Ensure tissue is flat against the glass.
3. Prepare the gelation solution. Quantities in brackets, below, are for a 100 µL volume. Note that APS should always be added last, right before adding to the specimen.
    a. 0.2% TEMED **[2 µL of 10% solution]**
    b. 0.01% TEMPO **[1 µL of 1% solution]**
    c. 95% monomer solution **[95 µL of monomer stock]**
    d. 0.2% APS **[2 µL of 10% solution]**
4. Cover the tissue with the gelation solution without disturbing it. Avoid letting the tissue fold over or float up into the gel (**Supplementary Protocol Fig. 4.1b**).
5. Place two pieces of #1.5 coverglass stacked on either side of the tissue and cover with another #1.5 coverglass. Place a drop of leftover gelation solution on top of the coverglass as a "tester" gel to see when the polymerization is complete.
    a. We use 2 pieces of coverglass to make the resulting gel thicker so it's easier to handle. You can alter the number of pieces or use thinner glass for thinner gels. You'll figure out what works best when you try to image the expanded sample and find out your needs based on the working distance of your objective lens.
    b. If you're using a thick piece of tissue you may need to use thicker coverglass spacers to ensure the whole sample is incorporated into the gel.
6. Allow the sample to gel at 37 °C for 1.5-2 h.

DIGESTION

1. As described, below, the digestion of mouse kidney tissue sections consists of digestion with proteinase K and collagenase, while the digestion of human kidney tissue sections consists of digestion with elastase, proteinase K, and collagenase.
2. Remove top piece of coverglass as well as spacers. Cut away excess gel from around the tissue (Your sample will be cleared after expansion and will be difficult to find in a lot of excess gel.) Use a diamond knife or razor blade to score the bottom coverglass near to the tissue and then break away excess coverglass so that the coverglass and gel will fit into the digestion buffer well. Do not try to remove the gels from the coverglass because they may tear (**Supplementary Protocol Fig. 4.1c**).
3. Place the gel sitting on the coverglass in a suitably sized well, e.g., a well of a 12-well plate (**Supplementary Protocol Fig. 4.2a**).
    a. Keep in mind that the gels will expand slightly (~1.5x) during digestion so make sure the well is a bit larger than the gel.
4. **For mouse kidney section digestion**, use the following protocol for digestion.

a. Add proteinase K digestion buffer with ~8 Units/mL of proteinase K to the sample. Make sure to cover the sample completely and allow to digest at 37 °C for 12-18 hours (typically done overnight).
b. Wash the digested specimen three times with several volumes of PBS. Then add collagenase digestion buffer containing 5 mg/mL collagenase and incubate at 37 °C for 12-18 hours (typically done overnight).

5. **For human kidney section digestion**, use the following protocol for digestion.
    a. Digest in 1mg/mL elastase in 200mM Tris buffer (pH 8) at 37 ˚C for 12-18 hours (typically done overnight).
    b. Digest in ~8 Units/mL of proteinase K for two days at ~65 ˚C. Replace the digestion solution (digestion buffer and proteinase K) after the first day.
    c. Wash the digested specimen three times with several volumes of PBS. Then add collagenase digestion buffer containing 5 mg/mL collagenase and incubate at 37 °C for 12-18 hours (typically done overnight).

EXPANSION

1. Remove gels from collagenase digestion buffer and place in DI water to expand. Anticipate the size of the expanded gel and use a suitably sized container (we often use a 3.5” petri dish).
2. Exchange water as needed until fully expanded (typically 2-3 exchanges). The refractive index of the gel is nearly identical to that of water so you will not easily see the gel. Be careful not to pour out or aspirate the gel. Typical expansion times are 1-2 hours, total, with exchanges every 30 min (**Supplementary Protocol Fig. 4.2b-c**).
3. Thinner gels will expand relatively quickly and may only need one water exchange.

SAMPLE HANDLING TIPS

- Removing expanded gels from petri dishes (or handling them in general) can be difficult. A large rectangular coverglass (~1” x 2”) is probably the best tool to use but other flat objects or spatulas may also work well. Place the coverglass short edge against the petri dish surface and tilt the dish to allow the gel to gently slide onto the coverglass.
- Try to gently wick away excess water before imaging using a Kim wipe. The gels will otherwise slide around during imaging.
- If the gels fold over onto themselves after removing excess water, try to use a fine-tipped paintbrush and gently poke the edges of the gel back until the sample is back in its original shape.
- A flashlight (illuminating from below) and a dark background are helpful when trying to locate your tissue within the gel. Look for a small amount of scattering.
- To prevent gels from sliding during imaging, mount them on poly-lysine-coated coverglass. Do this by sliding the gel from a spatula (or whatever tool was used to pick up the gel) onto the coated glass until the first edge sticks down. Continue sliding the spatula

out from under the gel allowing it to slowly sit down on the coated glass so that the gel does not bend.

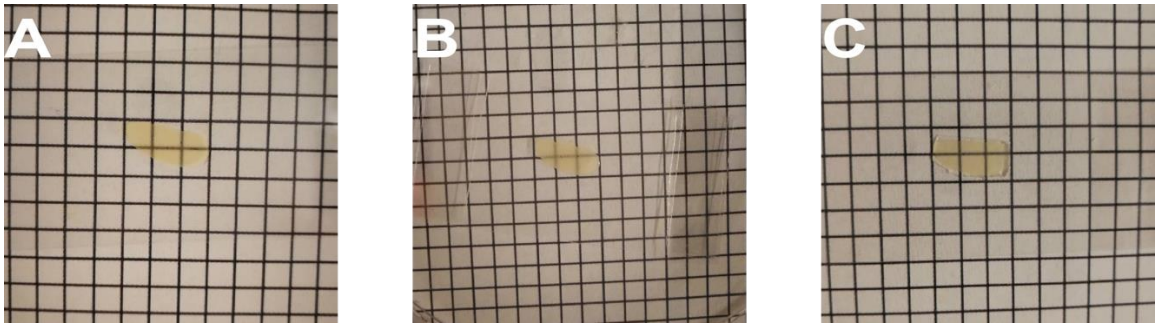

Supplementary Protocol Fig. 4.1 | (**a**) A flat, 100 µm mouse kidney section, after immunostaining, was mounted on a coverglass. (**b**) The MA-NHS treated section was polymerized in a home-built chamber consisting of two coverglasses with a spacer as described in the text. **C**) After polymerization, the excess gel around the specimen was trimmed with a razor blade. The coverglass substrate was also trimmed with a glass cutter or razor blade to enable it to fit in a 12-well plate for digestion. The grid lines are separated by ~4mm.

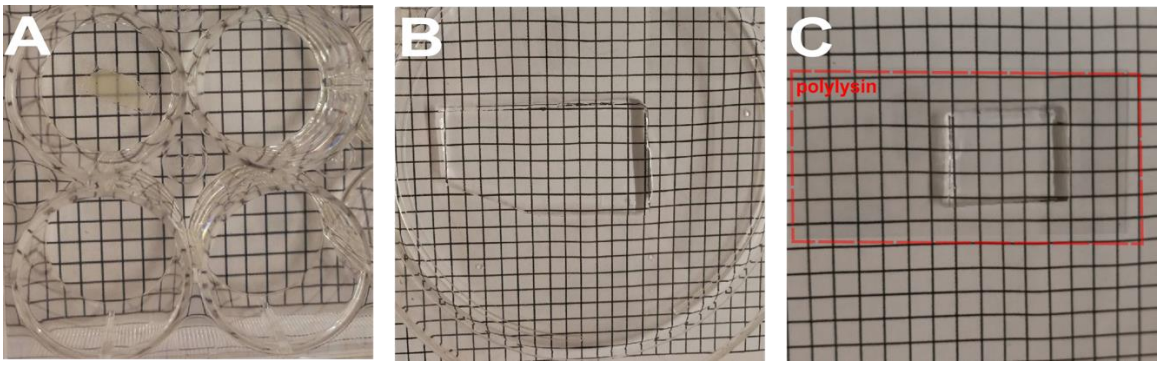

Supplementary Protocol Fig. 4.2 | (**a**) Trimmed hydrogel specimen was placed in a well of a 12-well plate to digest. (**b**) Specimen after expansion. (**c**). Portion of expanded hydrogel mounted on a polylysine-coated coverglass. The grid lines are separated by ~4 mm.

References

1. Chozinski, T. J., Gagnon, L. A. & Vaughan, J. C. Twinkle, twinkle little star: Photoswitchable fluorophores for super-resolution imaging. *FEBS Lett.* **588,** 3603–3612 (2014).
2. Halpern, A. R., Alas, G. C. M., Chozinski, T. J., Paredez, A. R. & Vaughan, J. C. Hybrid Structured Illumination Expansion Microscopy Reveals Microbial Cytoskeleton Organization. *ACS Nano* (2017). doi:10.1021/acsnano.7b07200
3. Betzig, E. Nobel Lecture: Single molecules, cells, and super-resolution optics. *Rev. Mod. Phys.* **87,** 1153–1168 (2015).
4. Hell, S. W. Nobel Lecture: Nanoscopy with freely propagating light. *Rev. Mod. Phys.* **87,** 1169–1181 (2015).
5. Moerner, W. E. (William E. . Nobel Lecture: Single-molecule spectroscopy, imaging, and photocontrol: Foundations for super-resolution microscopy. *Rev. Mod. Phys.* **87,** 1183–1212 (2015).
6. Hell, S. W. & Wichmann, J. Breaking the diffraction resolution limit by stimulated emission: stimulated-emission-depletion fluorescence microscopy. *Opt. Lett.* **19,** 780–782 (1994).
7. Dyba, M. & Hell, S. W. Focal Spots of Size λ / 23 Open Up Far-Field Florescence Microscopy at 33 nm Axial Resolution. *Phys. Rev. Lett.* **88,** (2002).
8. Wildanger, D., Rittweger, E., Kastrup, L. & Hell, S. W. STED microscopy with a supercontinuum laser source. *Opt. Express* **16,** 9614–9621 (2008).
9. Göttfert, F. *et al.* Coaligned Dual-Channel STED Nanoscopy and Molecular Diffusion Analysis at 20 nm Resolution. *Biophys. J.* **105,** L01–L03 (2013).
10. Donnert, G. *et al.* Two-Color Far-Field Fluorescence Nanoscopy. *Biophys. J.* **92,** L67–L69 (2007).
11. Vaughan, J. C., Jia, S. & Zhuang, X. Ultrabright photoactivatable fluorophores created by reductive caging. *Nat Methods* **9,** 1181–1184 (2012).

12. Vaughan, J. C., Dempsey, G. T., Sun, E. & Zhuang, X. Phosphine quenching of cyanine dyes as a versatile tool for fluorescence microscopy. *J. Am. Chem. Soc.* **135,** 1197–1200 (2013).

13. Dempsey, G. T. *et al.* Photoswitching Mechanism of Cyanine Dyes. *J. Am. Chem. Soc.* **131,** 18192–18193 (2009).

14. Betzig, E. Proposed method for molecular optical imaging. *Opt. Lett.* **20,** 237–239 (1995).

15. Betzig, E. *et al.* Imaging intracellular fluorescent proteins at nanometer resolution. *Science* **313,** 1642–1645 (2006).

16. Hess, S. T., Girirajan, T. P. K. & Mason, M. D. Ultra-high resolution imaging by fluorescence photoactivation localization microscopy. *Biophys. J.* **91,** 4258–4272 (2006).

17. Rust, M. J., Bates, M. & Zhuang, X. Sub-diffraction-limit imaging by stochastic optical reconstruction microscopy (STORM). *Nat. Methods* **3,** 793–796 (2006).

18. Sigal, Y. M., Speer, C. M., Babcock, H. P. & Zhuang, X. Mapping Synaptic Input Fields of Neurons with Super-Resolution Imaging. *Cell* **163,** 493–505 (2015).

19. Gustafsson, M. G. Surpassing the lateral resolution limit by a factor of two using structured illumination microscopy. *J. Microsc.* **198,** 82–87 (2000).

20. Gustafsson, M. G., Agard, D. A. & Sedat, J. W. Doubling the lateral resolution of wide-field fluorescence microscopy using structured illumination. in *BiOS 2000 The International Symposium on Biomedical Optics* 141–150 (2000).

21. Gustafsson, M. G. L. *et al.* Three-Dimensional Resolution Doubling in Wide-Field Fluorescence Microscopy by Structured Illumination. *Biophys. J.* **94,** 4957–4970 (2008).

22. Rego, E. H. *et al.* Nonlinear structured-illumination microscopy with a photoswitchable protein reveals cellular structures at 50-nm resolution. *Proc. Natl. Acad. Sci.* **109,** E135–E143 (2012).

23. Gustafsson, M. G. . Nonlinear structured-illumination microscopy: wide-field fluorescence imaging with theoretically unlimited resolution. *Proc. Natl. Acad. Sci. U. S. A.* **102,** 13081 (2005).

24. Nixon-Abell, J. *et al.* Increased spatiotemporal resolution reveals highly dynamic dense tubular matrices in the peripheral ER. *Science* **354,** aaf3928 (2016).

25. Schermelleh, L., Heintzmann, R. & Leonhardt, H. A guide to super-resolution fluorescence microscopy. *J. Cell Biol.* **190,** 165–175 (2010).

26. Kempf, C. *et al.* Tissue Multicolor STED Nanoscopy of Presynaptic Proteins in the Calyx of Held. *PLoS ONE* **8,** e62893 (2013).

27. Bates, M., Dempsey, G. T., Chen, K. H. & Zhuang, X. Multicolor Super-Resolution Fluorescence Imaging via Multi-Parameter Fluorophore Detection. *ChemPhysChem* **13,** 99–107 (2012).

28. Bates, M., Huang, B., Dempsey, G. T. & Zhuang, X. Multicolor super-resolution imaging with photo-switchable fluorescent probes. *Science* **317,** 1749–1753 (2007).

29. Shim, S. H. *et al.* Super-resolution fluorescence imaging of organelles in live cells with photoswitchable membrane probes. *Proc. Natl. Acad. Sci.* **109,** 13978–13983 (2012).

30. Butkevich, A. N. *et al.* Fluorescent Rhodamines and Fluorogenic Carbopyronines for Super-Resolution STED Microscopy in Living Cells. *Angew. Chem. Int. Ed.* **55,** 3290–3294 (2016).

31. Barna, L. *et al.* Correlated confocal and super-resolution imaging by VividSTORM. *Nat. Protoc.* **11,** 163–183 (2015).

32. Huang, F. *et al.* Ultra-High Resolution 3D Imaging of Whole Cells. *Cell* **166,** 1028–1040 (2016).

33. Unnersjö-Jess, D., Scott, L., Blom, H. & Brismar, H. Super-resolution stimulated emission depletion imaging of slit diaphragm proteins in optically cleared kidney tissue. *Kidney Int.* **89,** 243–247 (2016).

34. Demmerle, J. *et al.* Strategic and practical guidelines for successful structured illumination microscopy. *Nat. Protoc.* **12,** 988–1010 (2017).

35. Chen, F., Tillberg, P. W. & Boyden, E. S. Expansion microscopy. *Science* **347,** 543–548 (2015).

36. Ohmine, I. Salt effects on the phase transition of ionic gels. *J. Chem. Phys.* **77,** 5725 (1982).

37. Ricka, J. & Tanaka, T. Swelling of ionic gels: quantitative performance of the Donnan theory. *Macromolecules* **17,** 2916–2921 (1984).

38. Ganji, F., Vasheghani-Farahani, S. & Vasheghani-Farahani, E. Theoretical Description of Hydrogel Swelling: A Review. 25

39. Rosenblum, G. *et al.* Direct Visualization of Protease Action on Collagen Triple Helical Structure. *PLoS ONE* **5,** e11043 (2010).

40. Mecham, R. P. *et al.* Elastin Degradation by Matrix Metalloproteinases: CLEAVAGE SITE SPECIFICITY AND MECHANISMS OF ELASTOLYSIS. *J. Biol. Chem.* **272,** 18071–18076 (1997).

41. Kramer, K. J. & Koga, D. Insect Chitin: Physical State, Synthesis, Degredation, and Metabolic Regulation. *Insect Biochem.* **16,** 851–877 (1986).

42. Neuman, R. E. & Logan, M. A. The determination of collagen and elastin in tissues. *J. Biol. Chem.* **186,** 549–556 (1950).

43. Ku, T. *et al.* Multiplexed and scalable super-resolution imaging of three-dimensional protein localization in size-adjustable tissues. *Nat. Biotechnol.* **34,** 973–981 (2016).

44. Chang, J.-B. *et al.* Iterative expansion microscopy. *Nat. Methods* **14,** 593–599 (2017).

45. Cahoon, C. K. *et al.* Superresolution expansion microscopy reveals the three-dimensional organization of the *Drosophila* synaptonemal complex. *Proc. Natl. Acad. Sci.* **114,** E6857–E6866 (2017).

46. Chen, F. *et al.* Nanoscale imaging of RNA with expansion microscopy. *Nat. Methods* (2016). doi:10.1038/nmeth.3899

47. Wang, G., Moffitt, J. R. & Zhuang, X. Multiplexed imaging of high-density libraries of RNAs with MERFISH and expansion microscopy. *Sci. Rep.* **8,** (2018).

48. Boyden, E. S. Expansion Microscopy Website. *http://www.expansionmicroscopy.org/* (2017). Available at: c. (Accessed: 15th November 2017)

49. Tillberg, P. W. *et al.* Protein-retention expansion microscopy of cells and tissues labeled using standard fluorescent proteins and antibodies. *Nat. Biotechnol.* **34,** 987–992 (2016).

50. Chung Lab Resources. *Chung Lab Resources* Available at: http://www.chunglabresources.com/. (Accessed: 30th April 2018)

51. 2015 Seattle Super-Resolution Microscopy Workshop. Available at: https://sites.google.com/a/uw.edu/ssmw2015/. (Accessed: 30th April 2018)

52. Neurofutures 2017 University of British Columbia. Available at: http://www.neuroscience.ubc.ca/Neurofutures/BrainClearing.html. (Accessed: 30th April 2018)

53. Expansion Microscopy Workshop | Janelia Research Campus. Available at: https://www.janelia.org/you-janelia/conferences/expansion-microscopy-workshop. (Accessed: 30th April 2018)

54. Geertsema, H. & Ewers, H. Expansion microscopy passes its first test. *Nat. Methods* **13,** 481–482 (2016).

55. Huang, B., Babcock, H. & Zhuang, X. Breaking the diffraction barrier: super-resolution imaging of cells. *Cell* **143,** 1047–1058 (2010).

56. Hell, S. W. Far-field optical nanoscopy. *Science* **316,** 1153 (2007).

57. Hern, D. L. & Hubbell, J. A. Incorporation of adhesion peptides into nonadhesive hydrogels useful for tissue resurfacing. *J. Biomed. Mater. Res.* **39,** 266–276 (1998).

58. Dempsey, G. T., Vaughan, J. C., Chen, K. H., Bates, M. & Zhuang, X. Evaluation of fluorophores for optimal performance in localization-based super-resolution imaging. *Nat. Methods* **8,** 1027–1036 (2011).

59. Olivier, N., Keller, D., Gönczy, P. & Manley, S. Resolution Doubling in 3D-STORM Imaging through Improved Buffers. *PLoS ONE* **8,** e69004 (2013).

60. Weston, P. D. & Avrameas, S. Proteins coupled to polyacrylamide beads using glutaraldehyde. *Biochem. Biophys. Res. Commun.* **45,** 1574–1580 (1971).

61. Lee, K., Choi, S., Yang, C., Wu, H.-C. & Yu, J. Autofluorescence generation and elimination: a lesson from glutaraldehyde. *Chem. Commun.* **49,** 3028 (2013).

62. Chung, K. *et al.* Structural and molecular interrogation of intact biological systems. *Nature* **497,** 332–337 (2013).

63. Yang, B. *et al.* Single-Cell Phenotyping within Transparent Intact Tissue through Whole-Body Clearing. *Cell* **158,** 945–958 (2014).

64. Migneault, I., Dartiguenave, C., Bertrand, M. J. & Waldron, K. C. Glutaraldehyde: behavior in aqueous solution, reaction with proteins, and application to enzyme crosslinking. *Biotechniques* **37,** 790–806 (2004).

65. Kim, D. & Park, K. Swelling and mechanical properties of superporous hydrogels of poly(acrylamide-co-acrylic acid)/polyethylenimine interpenetrating polymer networks. *Polymer* **45,** 189–196 (2004).

66. Klein, S., Staring, M., Murphy, K., Viergever, M. A. & Pluim, J. elastix: A Toolbox for Intensity-Based Medical Image Registration. *IEEE Trans. Med. Imaging* **29,** 196–205 (2010).

67. Schindelin, J. *et al.* Fiji: an open-source platform for biological-image analysis. *Nat. Methods* **9,** 676–682 (2012).

68. Jiang, N. *et al.* Super-resolution imaging of Drosophila tissues using expansion microscopy. *Press Mol. Biol. Cell* (2018).

69. Huang, B., Babcock, H. & Zhuang, X. Breaking the diffraction barrier: super-resolution imaging of cells. *Cell* **143,** 1047–1058 (2010).

70. Chen, F., Tillberg, P. W. & Boyden, E. S. Expansion microscopy. *Science* **347,** 543–548 (2015).

71. Chozinski, T. J. *et al.* Expansion microscopy with conventional antibodies and fluorescent proteins. *Nat. Methods* **13,** 485–488 (2016).

72. Ku, T. *et al.* Multiplexed and scalable super-resolution imaging of three-dimensional protein localization in size-adjustable tissues. *Nat. Biotechnol.* **34,** 973–981 (2016).

73. Tillberg, P. W. *et al.* Protein-retention expansion microscopy of cells and tissues labeled using standard fluorescent proteins and antibodies. *Nat. Biotechnol.* **34,** 987–992 (2016).

74. Cahoon, C. K. *et al.* Superresolution expansion microscopy reveals the three-dimensional organization of the Drosophila synaptonemal complex. *Proc. Natl. Acad. Sci. U. S. A.* **114,** E6857–E6866 (2017).

75. Mosca, T. J., Luginbuhl, D. J., Wang, I. E. & Luo, L. Presynaptic LRP4 promotes synapse number and function of excitatory CNS neurons. *eLife* **6,** (2017).

76. Hummel, T., Krukkert, K., Roos, J., Davis, G. & Klämbt, C. Drosophila Futsch/22C10 is a MAP1B-like protein required for dendritic and axonal development. *Neuron* **26,** 357–370 (2000).

77. Pernas, L. & Scorrano, L. Mito-Morphosis: Mitochondrial Fusion, Fission, and Cristae Remodeling as Key Mediators of Cellular Function. *Annu. Rev. Physiol.* **78,** 505–531 (2016).

78. Kittel, R. J. *et al.* Bruchpilot promotes active zone assembly, Ca2+ channel clustering, and vesicle release. *Science* **312,** 1051–1054 (2006).

79. Wagh, D. A. *et al.* Bruchpilot, a protein with homology to ELKS/CAST, is required for structural integrity and function of synaptic active zones in Drosophila. *Neuron* **49,** 833–844 (2006).

80. Ehmann, N. *et al.* Quantitative super-resolution imaging of Bruchpilot distinguishes active zone states. *Nat. Commun.* **5,** 4650 (2014).

81. Fouquet, W. *et al.* Maturation of active zone assembly by Drosophila Bruchpilot. *J. Cell Biol.* **186,** 129–145 (2009).

82. Matkovic, T. *et al.* The Bruchpilot cytomatrix determines the size of the readily releasable pool of synaptic vesicles. *J. Cell Biol.* **202,** 667–683 (2013).

83. Jepson, J. E. C. *et al.* Regulation of synaptic development and function by the Drosophila PDZ protein Dyschronic. *Development* **141,** 4548–4557 (2014).

84. Lepicard, S., Franco, B., de Bock, F. & Parmentier, M.-L. A presynaptic role of microtubule-associated protein 1/Futsch in Drosophila: regulation of active zone number and neurotransmitter release. *J. Neurosci. Off. J. Soc. Neurosci.* **34,** 6759–6771 (2014).

85. Weyhersmüller, A., Hallermann, S., Wagner, N. & Eilers, J. Rapid active zone remodeling during synaptic plasticity. *J. Neurosci. Off. J. Soc. Neurosci.* **31,** 6041–6052 (2011).

86. Mahoney, R. E., Rawson, J. M. & Eaton, B. A. An age-dependent change in the set point of synaptic homeostasis. *J. Neurosci. Off. J. Soc. Neurosci.* **34,** 2111–2119 (2014).

87. Propst, J. W. & Ko, C. P. Correlations between active zone ultrastructure and synaptic function studied with freeze-fracture of physiologically identified neuromuscular junctions. *J. Neurosci. Off. J. Soc. Neurosci.* **7,** 3654–3664 (1987).

88. Holderith, N. *et al.* Release probability of hippocampal glutamatergic terminals scales with the size of the active zone. *Nat. Neurosci.* **15,** 988–997 (2012).

89. Südhof, T. C. The presynaptic active zone. *Neuron* **75,** 11–25 (2012).

90. Gupta, V. K. *et al.* Spermidine Suppresses Age-Associated Memory Impairment by Preventing Adverse Increase of Presynaptic Active Zone Size and Release. *PLoS Biol.* **14,** e1002563 (2016).

91. Cooper, R. L., Winslow, J. L., Govind, C. K. & Atwood, H. L. Synaptic structural complexity as a factor enhancing probability of calcium-mediated transmitter release. *J. Neurophysiol.* **75,** 2451–2466 (1996).

92. O'Brien, G. S. *et al.* Coordinate development of skin cells and cutaneous sensory axons in zebrafish. *J. Comp. Neurol.* **520,** 816–831 (2012).

93. Han, C. *et al.* Integrins Regulate Repulsion-Mediated Dendritic Patterning of Drosophila Sensory Neurons by Restricting Dendrites in a 2D Space. *Neuron* **73,** 64–78 (2012).

94. Kim, M. E., Shrestha, B. R., Blazeski, R., Mason, C. A. & Grueber, W. B. Integrins establish dendrite-substrate relationships that promote dendritic self-avoidance and patterning in drosophila sensory neurons. *Neuron* **73,** 79–91 (2012).

95. Chalfie, M. & Sulston, J. Developmental genetics of the mechanosensory neurons of Caenorhabditis elegans. *Dev. Biol.* **82,** 358–370 (1981).

96. Jiang, N., Soba, P., Parker, E., Kim, C. C. & Parrish, J. Z. The microRNA bantam regulates a developmental transition in epithelial cells that restricts sensory dendrite growth. *Dev. Camb. Engl.* **141,** 2657–2668 (2014).

97. Cauna, N. The free penicillate nerve endings of the human hairy skin. *J. Anat.* **115,** 277–288 (1973).

98. Weis, J. *et al.* Small-fiber neuropathy in patients with ALS. *Neurology* **76,** 2024–2029 (2011).

99. Üçeyler, N. *et al.* Small fibre pathology in patients with fibromyalgia syndrome. *Brain J. Neurol.* **136,** 1857–1867 (2013).

100. Feinberg, E. H. *et al.* GFP Reconstitution Across Synaptic Partners (GRASP) defines cell contacts and synapses in living nervous systems. *Neuron* **57,** 353–363 (2008).

101. Morell, M. *et al.* Monitoring the interference of protein-protein interactions in vivo by bimolecular fluorescence complementation: the DnaK case. *Proteomics* **8,** 3433–3442 (2008).

102. Eichler, K. *et al.* The complete connectome of a learning and memory centre in an insect brain. *Nature* **548,** 175–182 (2017).

103. Chen, F. *et al.* Nanoscale imaging of RNA with expansion microscopy. *Nat. Methods* **13,** 679–684 (2016).

104. Chang, J.-B. *et al.* Iterative expansion microscopy. *Nat. Methods* **14,** 593–599 (2017).

105. Han, C. *et al.* Integrins Regulate Repulsion-mediated Dendritic Patterning of Drosophila Sensory Neurons by Restricting Dendrites in a Two-dimensional Space. *Neuron* **73,** 64–78 (2012).

106. Chozinski, T. J. *et al.* Expansion microscopy with conventional antibodies and fluorescent proteins. *Nat. Methods* **13,** 485–488 (2016).

107. Parton, R. M., Vallés, A. M., Dobbie, I. M. & Davis, I. Drosophila larval fillet preparation and imaging of neurons. *Cold Spring Harb. Protoc.* **2010,** pdb.prot5405 (2010).

108. National Chronic Kidney Disease Fact Sheet, 2017. 4

109. Kidney Disease Statistics for the United States | NIDDK. *National Institute of Diabetes and Digestive and Kidney Diseases* Available at: https://www.niddk.nih.gov/health-information/health-statistics/kidney-disease. (Accessed: 17th May 2018)

110. Darouich, S. *et al.* Value of Electron Microscopy in the Diagnosis of Glomerular Diseases. *Ultrastruct. Pathol.* **34,** 49–61 (2010).

111. Hogan, J., Mohan, P. & Appel, G. B. Diagnostic Tests and Treatment Options in Glomerular Disease: 2014 Update. *Am. J. Kidney Dis.* **63,** 656–666 (2014).

112. Unnersjö-Jess, D. *et al.* Confocal super-resolution imaging of the glomeruluar filtration barrier enables by tissue expansion. *Kidney Int.* (2017). doi:https://doi.org/10.1016/ j.kint.2017.09.019

113. Chozinski, T. J. *et al.* Volumetric, Nanoscale Optical Imaging of Mouse and Human Kidney via Expansion Microscopy. *Rev. Sci. Rep.* (2018).

114. Hughes, L., Hawes, C., Monteith, S. & Vaughan, S. Serial block face scanning electron microscopy—the future of cell ultrastructure imaging. *Protoplasma* **251,** 395–401 (2014).

115. Plitzko, J. M., Rigort, A. & Leis, A. Correlative cryo-light microscopy and cryo-electron tomography: from cellular territories to molecular landscapes. *Curr. Opin. Biotechnol.* **20,** 83–89 (2009).

116. Suleiman, H. *et al.* Nanoscale protein architecture of the kidney glomerular basement membrane. *Elife* **2,** e01149 (2013).

117. Pullman, J. M. *et al.* Visualization of podocyte substructure with structured illumination microscopy (SIM): a new approach to nephrotic disease. *Biomed. Opt. Express* **7,** 302 (2016).

118. Chozinski, T. J. *et al.* Expansion microscopy with conventional antibodies and fluorescent proteins. *Nat. Methods* **13,** 485–488 (2016).

119. Kaverina, N. V., Eng, D. G., Schneider, R. R. S., Pippin, J. W. & Shankland, S. J. Partial podocyte replenishment in experimental FSGS derives from nonpodocyte sources. *Am. J. Physiol.-Ren. Physiol.* **310,** F1397–F1413 (2016).

120. Ramage, I. J. *et al.* Glomerular basement membrane thickness in children: a stereologic assessment. *Kidney Int.* **62,** 895–900 (2002).

121. Jensen, E., Gunderson, H. & Østerby, R. Determination of membrane thickness distribution from orthogonal intercepts. *J. Microsc.* **115,** 19–33 (1979).

122. Bjørn, S. F. *et al.* Glomerular epithelial foot processes and filtration slits in IDDM patients. *Diabetologia* **38,** 1197–1204 (1995).

123. Toyoda, M., Najafian, B., Kim, Y., Caramori, M. L. & Mauer, M. Podocyte Detachment and Reduced Glomerular Capillary Endothelial Fenestration in Human Type 1 Diabetic Nephropathy. *Diabetes* **56,** 2155–2160 (2007).

124. Thongboonkerd V. alternations in renal elastin-elastase system in type 1 diabetic nephropathy identified by proteomic analysis. *J Am Soc Nephrol* **15,** 650–662 (2004).

125. Sterzel, R. B. *et al.* Elastic fiber proteins in the glomerular mesangium in vivo and in cell culture. *Kidney Int.* **58,** 1588–1602 (2000).

126. Zhao, Y. *et al.* Nanoscale imaging of clinical specimens using pathology-optimized expansion microscopy. *Nat. Biotechnol.* (2017). doi:10.1038/nbt.3892

127. Puchtler, H. & Meloan, S. N. On the chemistry of formaldehyde fixation and its effects on immunohistochemical reactions. *Histochem. Cell Biol.* **82,** 201–204 (1985).

Vita

Tyler Joseph Chozinski

Education

PhD in Analytical Chemistry, *University of Washington, Seattle, WA* **2018**
BS in Chemistry with a minor in Mathematics, *University of Arizona, Tucson, AZ* **2013**

Research and Professional Development

Graduate Research Assistant/NSF Graduate Fellow, Mentor: Dr. Joshua C. Vaughan **2013-2018**
University of Washington, Seattle, WA
Undergraduate Researcher, Mentors: Dr. Jeanne. E. Pemberton and Dr. Katrina Miranda **2010-2013**
University of Arizona, Tucson, AZ

Selected Scientific Communication Experience

Invited Speaker, University of Arizona, Analytical Division Seminar **February 2018**
University of Arizona, Tucson, AZ
Neurofutures Conference and Expansion Microscopy Workshop **July 2017**
University of British Columbia, Vancouver, BC
Seattle Super-Resolution Microscopy Workshop **September**
University of Washington, Seattle, WA **2014 and 2015**

Mentor Experience and Community Outreach

Mentor to Undergraduate and Graduate Researchers, Vaughan Lab **2013-2018**
University of Washington, Seattle, WA
Graduate Teaching Assistant **2013-2014**
University of Washington, Seattle, WA
Undergraduate Teaching Assistant and Tutor **2012-2013**
University of Arizona, Tucson, AZ
Chemistry Camp for Children with Autism **2012-2013**
University of Arizona, Tucson, AZ
Biannual University of Arizona Chemistry Magic Show **2011-2013**
University of Arizona, Tucson, AZ

Selected Awards, Honors, and Scholarships

University of Washington, Seattle, WA
NSF Graduate Research Fellowship **2014-2018**
UW Alma Mater Travel Grant **2018**
Expansion Microscopy work featured on cover of Nature Methods June **2016**
2016 Issue **2013**
Excellence in Chemistry Graduate Research Fellowship **2013**
Early Bird Research Assistantship
University of Arizona, Tucson, AZ **2013**
Galileo Scholarship **2011-2013**
Undergraduate Biology Research Program (UBRP) **2009-2013**
Wildcat Excellence Scholarship

Selected Publications

"Volumetric, Nanoscale Optical Imaging of Mouse and Human Kidney via Expansion Microscopy", **T.J. Chozinski**, C. Mao, A.R. Halpern, S.S. Shankland, C.E. Alpers, B. Najafian, J.C. Vaughan. In Review.

"Hybrid Super-Resolution Microscopy via Specimen Expansion and Structured Illumination Reveals Nanoscale Organization of Microbial Cytoskeleton", A.R. Halpern, G.C. M. Alas, **T.J. Chozinski**, A.R. Paredez, J.C. Vaughan. *ACS Nano*, 11 (12): 12677-12686 (2017).

"Super-resolution imaging of *Drosophila* tissues using expansion microscopy", N. Jiang, H.J. Kim, **T.J. Chozinski**, J.E. Azpurua, B.A. Eaton, J.C. Vaughan, J.Z. Parrish. Accepted, *MBoC* (2017).

"Expansion microscopy with conventional antibodies and fluorescent proteins", **T.J. Chozinski***, A.R. Halpern*, H. Okawa, H.J. Kim, G.J. Tremel, R.O.L. Wong, J.C. Vaughan. *Nature Methods*, 13: 485-488 (2016). *Indicates equal contributions.

"Twinkle, twinkle little star: Photoswitchable fluorophores for super-resolution imaging", **T.J. Chozinski***, L.A. Gagnon*, J.C. Vaughan. FEBS Letters, 19: 3603-3612 (2014). *Indicates equal contributions.

"Glutathione sulfonamide serves as a selective, endogenous biomarker for nitroxyl after exposure to therapeutic levels of donors", G.M. Johnson, **T.J. Chozinski**, E.S. Gallagher, C.A. Aspinwall, K.M. Miranda. *Free Radic Biol Med*, 76: 299-307 (2014).

"Quantitative Detection of Nitroxyl Upon Trapping with Glutathione and Labeling with a Specific Fluorogenic Reagent", G.M. Johnson, **T.J. Chozinski**, D.J. Salmon, A.D. Moghaddam, H.C. Chen, K.M. Miranda. *Free Radic Biol Med*, 63: 476-484 (2013).

Patents

"Expansion Microscopy Methods and Kits", **T.J. Chozinski**, A.R. Halpern, H.J. Kim, J.C. Vaughan. Patent Application US 47585.03US2, filed March 22, 2017.